Dear Co-Editor Dr. Jason Surratt and Referees,

We highly appreciate the detailed valuable comments of the three referees on our manuscript of "‘acp-2017-115". The suggestions are quite helpful for us. We have incorporated them in the revised manuscript to improve the quality of our paper. Please see the detailed point-by-point response below and the changes marked blue in the revised manuscript.

Thank you very much!

Best regards,

Min Hu

On behalf of co-authors

Point-by-Point Response to Reviewers′ Comments:

Referee #1

General comments

This study presents high time resolution chemical characterization of ambient submicron aerosols measured in Beijing between March 2012 and March 2013 using HR-ToF-AMS. Seasonal comparison of the chemical composition shows that organic aerosol (OA) and inorganic species (i.e. sulfate, nitrate, and ammonium) contributes equally towards total PM_1 mass. The chemical component composition and diurnal trend were impacted by atmospheric conditions of each season. Relationship between the atmospheric conditions to PM_1 composition need to be further discussed and/or clarified as outlined in the specific comments.

Additionally, sources of OA fraction in Beijing were identified using PMF. Primary OA (i.e. HOA and COA) and secondary OA sources were observed in all seasons, whereas BBOA and CCOA were only observed in autumn and winter, respectively. It is interesting that CCOA factor was resolved in winter dataset indicating significant contribution of coal combustion from domestic heating to ambient submicron aerosol. There seems to be an unresolved factor in winter dataset that could be a BBOA factor. Residual mass spectra should be added as supplementary information for evaluating the PMF solution.

Overall, this study falls within the scope of Atmospheric Chemistry and Physics journal. The results contribute to long-term and seasonal evaluation of air quality and can support air pollution prevention policy in Beijing. The manuscript is written pretty well with only some minor issues as outlined in the technical comments. I support publication of this manuscript after minor revisions.

Response: Thank you very much for your helpful comments and kind encouragement. According to the specific comments, we strengthened the content on the relationship between the atmospheric conditions and PM_1 compositions. The supplementary information for evaluating the PMF solution was added. Please see the detailed response below and the changes marked blue in the revised manuscript.

Specific comments

1. PM_1 mass concentration is estimated as a sum of NR-PM_1 measured by AMS and BC measured by Aethalometer. However, cutoff size of the AMS's inlet (PM_1) is different from the

Aethalometer ($PM_{2.5}$). How did you consider the cutoff size when summing the measurements? This information can be added into the experimental section.

Response: Ambient BC particles are largely found in the Aitken and accumulation modes (i.e., in the submicron range) because of their formation mechanism (Bond et al., 2013; Huang et al., 2012a; Rose et al., 2006). The sum of non-refractory species measured by the HR-ToF-AMS and BC measured by instruments such as MAAP or aethalometer with the cut-size of 2.5 μm is often treated as total PM_1 in previous studies (Huang et al., 2010, 2012b, 2013; He et al., 2011; Hu et al., 2013, 2016). Herein we thought this match has little influence on PM_1.

In the revision, "***Atmospheric black carbon (BC) particles are mostly in the submicron range because of their formation mechanisms (Bond et al., 2013)***" was added in Line 11, Page 6.

"***(non-refractory species measured by the AMS and BC by the aethalometer or MAAP)***" was added to clarify "*main chemical components in PM_1*" in Line 12, Page 6.

2. Pg 6 Lns 9-11: What are considered in the certain atmospheric conditions? How do these conditions relate to the current study?

Response: Wang et al. (2016) showed that the aqueous oxidation of SO_2 by NO_2 is key to efficient sulfate formation but is only feasible under two atmospheric conditions: on fine aerosols with high relative humidity and NH_3 neutralization or under cloud conditions. Similarly, Cheng et al. (2016) found that high reaction rates of SO_2 oxidized by NO_2 to form sulfate are sustained by the high neutralizing capacity of the atmosphere in northern China. This mechanism is self-amplifying because higher aerosol mass concentration corresponds to higher aerosol water content, resulting in faster sulfate production and more severe haze pollution. In summary, the certain atmospheric conditions represent the fine aerosols with high aerosol water content and NH_3 neutralization or under cloud conditions. These two studies included field observations conducted in urban area of Beijing.

In the revision, "*Wang et al. (2016) and Cheng et al. (2016) found that high levels of sulfate and fine PM can be explained by reactive aqueous oxidation of SO_2 by NO_2 under certain atmospheric conditions*" was changed to "***Recently it was found that high levels of sulfate and fine PM in northern China can be explained by reactive aqueous oxidation of SO_2 by NO_2 under certain atmospheric conditions, i.e., on the fine aerosols with high aerosol water content and NH_3 neutralization or under cloud conditions (Cheng et al., 2016; Wang et al., 2016)***".

3. Pg 8 Lns 8-10: "Affected by different meteorological conditions, e.g., solar radiation, temperature, RH, boundary layer, and mountain-valley breeze in summer (Fig. S7), as well as different emission sources, the chemical compositions in PM_1 showed distinct diurnal patterns in four seasons." The beginning of sentence implies that the meteorological conditions specific for summer, whereas the ending suggests the distinctive diurnal patterns in four seasons. I think meteorological conditions in four seasons, not only summer, will affect the chemical composition and diurnal patterns in each season. This needs to be clarified.

Response: "*mountain-valley breeze in summer*" means that mountain-valley breeze is the most common in summer in Beijing. In the revision, "*in summer*" was deleted.

4. Pg 8 Ln 19: "Flatter diurnal cycles of sulfate were observed in four seasons, …". What does "flatter" here compare with? Does it compare with OA diurnal pattern? Also, add discussion about the diurnal patterns in spring and summer. Sulfate in spring showed small peaks around 13:00 and 20:00, whereas in summer, it peaked at evening only. What could possibly drive changes in sulfate diurnal patterns?

Response: In the revision, "***Compared with OA diurnal patterns,***" was added in Line 15, Page 9. "*In the summer of Beijing, the formation of sulfate is mainly attributed to in-cloud/aqueous-phase reactions (70–80%), and also arises from photochemical oxidation of SO_2 (Guo et al., 2010). In this study, sulfate enhanced gradually from morning to late afternoon in summer.*" was changed to "***In spring, sulfate showed small peaks around 13:00 and 20:00. In the daytime, both active photochemical production and more favorable dispersion conditions due to higher planetary boundary layer (PBL) possibly caused such a diurnal pattern of sulfate. In summer, sulfate enhanced gradually from morning to evening and peaked in the evening only, indicating that the photochemical production of sulfate might be significant. In addition to the gas-phase processes, the formation of sulfate is mainly attributed to aqueous-phase reactions in clouds and/or wet aerosols (70–80%) in the summer of Beijing (Guo et al., 2010).***"

5. Pg 9 Lns 9-11: I think nitrate diurnal pattern in autumn is still significant; nitrate increased in the morning and then later in the evening. Also, what is the evidence of combined effect of sulfate and nitrate to ammonium diurnal pattern? Maybe you can correlate the diurnal variations and provide the coefficient of determination.

Response: In the revision, "*The diurnal variation of nitrate in spring and autumn was insignificant.*" was changed to "***In autumn, nitrate increased in the morning and then later in***

the evening, primarily driving by the photochemical production. The diurnal variation of nitrate in spring was insignificant."

Because ammonium is usually in the forms of ammonium sulfate and ammonium nitrate, so the diurnal pattern of ammonium should be a combined effect of sulfate and nitrate. The coefficients of determination between the diurnal variations of sulfate and ammonium are calculated as 0.503 (p<0.05), 0.191, 0.802 (p<0.01) and 0.914 (p<0.01) in four seasons, respectively. The coefficients of determination between the diurnal variations of nitrate and ammonium are calculated as 0.803 (p<0.01), 0.549 (p<0.01), 0.855 (p<0.01) and 0.976 (p<0.01) (p<0.05), respectively.

In the revision, "***In summer, the diurnal variation of ammonium correlated better (r=0.55, p<0.01) with that of nitrate than sulfate (r=0.19, p>0.05). In other seasons, the diurnal variations of ammonium showed good correlations with those of both sulfate and nitrate (r=0.50–0.98, p<0.01 or 0.05).***" was added in Line 11, Page 10.

6. Pg 10 Ln 3: The size distribution of NH_4 is pretty similar to NO_3 in all four seasons. The size difference is not obvious in Fig. 4. To help comparison, you can consider increasing the size of the figure (panel for each season), or providing a summary table of size distribution in the SI section.

Response: Figure 4 is re-illustrated as follows.

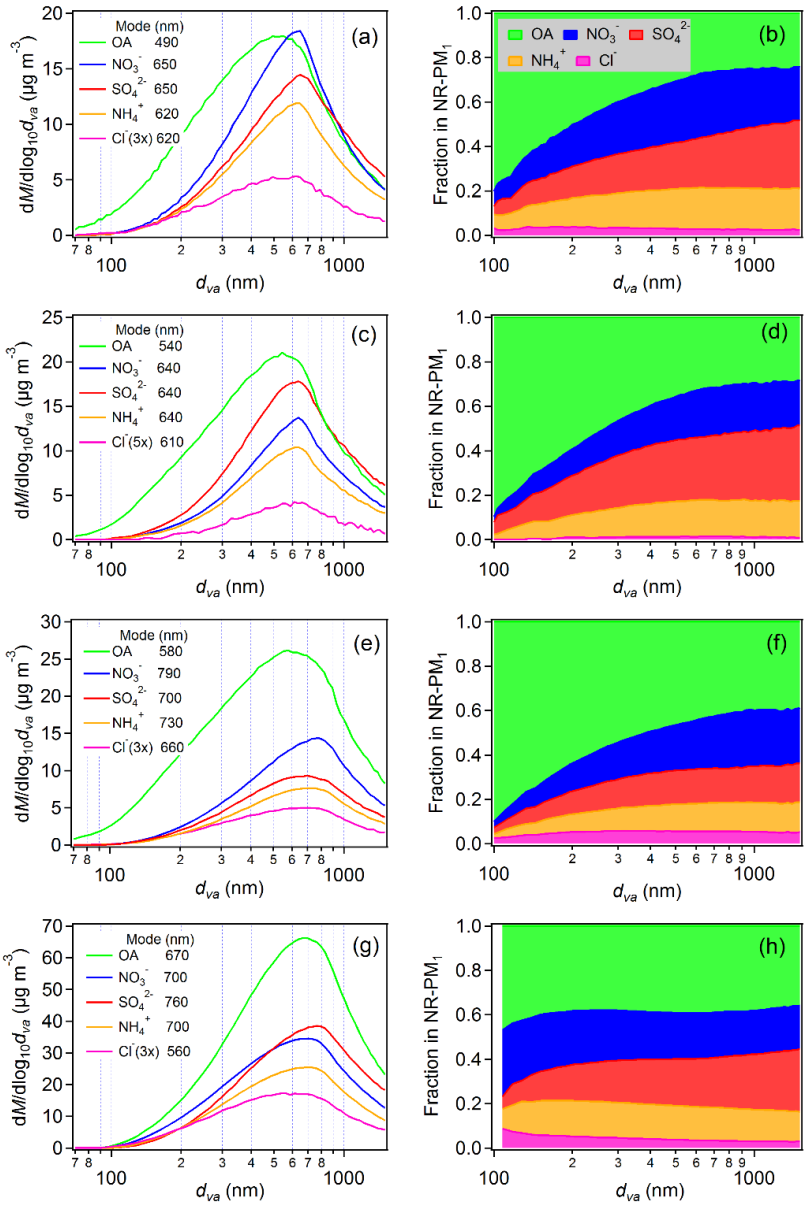

Figure 4. Mass size distributions of chemical compositions in NR-PM_1 during the spring (a, b), summer (c, d), autumn (e, f) and winter (g, h) observations.

In the revision, "*The size distribution of ammonium was more consistent with that of nitrate in autumn and winter. Nitrate likely mainly existed in the form of NH_4NO_3, resulted from the condensation of gaseous HNO_3 and NH_3 on the surfaces of atmospheric particles (Liu et al., 2008).*" was changed to "***The size distribution of ammonium was more consistent with that of nitrate than sulfate in winter. More nitrate likely existed in the form of NH_4NO_3, formed by the reaction of gaseous HNO_3 and NH_3 condensed on atmospheric particles (Weimer et al., 2006).***"

7. Pg 11 Lns 23-24: Provide reference(s) that show the role of emission reduction of gaseous precursors to SOA formation. For example: Pye, et al. Epoxide pathways improve model predictions of isoprene markers and reveal key role of acidity in aerosol formation. Environ. Sci. Technol. 2013, 47, 11056-11064.

Response: In the revision, "***(Guo et al., 2014; Pye, et al., 2013)***" was added.

8. Pg 14 Lns 18-20: Are you implying that there is a factor (BBOA) that is not resolved by PMF in the winter dataset? What may cause PMF can't resolve BBOA factor in winter? Is the residual still showing important mass spectrum (e.g. m/z 60, 73) and time series features? Diagnostic plots of PMF winter dataset analysis (see Zhang et al. 2011) will be useful for readers to understand the analysis process. These diagnostic plots can be added in the SI section and referred in the main text. In addition to winter, diagnostics for other season should be provided in the SI section to help reader understand the PMF analysis process.

Response: There might be relatively limited BBOA contribution to the OA in winter, so the BBOA factor cannot be resolved in our dataset by free PMF. In recently published papers (Sun et al., 2013, 2014; Zhang et al., 2014), there were also no BBOA factor resolved by PMF analysis in urban Beijing during the similar periods of 2012 and 2013.

The mass spectrum of the residual doesn't show obvious feature of characteristic ion fragments.

In the revised manuscript, "***The optimum solutions were selected following the steps as described in Zhang et al. (2011). The key diagnostic plots of the PMF analysis are shown in Sect. S5 in the supplement.***" was added in Line 5, Page 6.

The PMF diagnostic plots and related tables are added in Sect. S5 in the supplement as follows.

Factor number from 1 to 10 and the different seeds (0-50) were selected to run in the PMF model. For the spring observation, diagnostic plots of the PMF analysis are shown in Fig. S16. When OA was separated into four fractions, it included more oxidized (MO-OOA) and less oxidized OOA (LO-OOA), cooking OA (COA) and hydrocarbon-like OA (HOA). The performances of spectra and time series of the four factors at different f_{peak} are shown in Fig. S17. When OA was separated into five fractions, OOA was also split into two factors, but more information on the OA sources (BBOA) could be provided. When more than five factors, OOA decomposed into three or more factors. After comparing the performances of MS spectra and

time series of five factors at different f_{peak}, the five factors, f_{Peak}=1 solution is chosen as the optimal solution for this PMF analysis because the signal of the characteristic ion fragment m/z is more obvious in one factor. In the five-factor solution, the mass spectra of two OOA factors are similar (r= 0.955), and the elemental ratios and OA/OC ratios (O/C: 0.99, 1.00; H/C: 1.50, 1.26; OA/OC: 2.51, 2.47) are close. It is unclear if the two OOA components represent distinct sources or chemical types. Thus, two OOA factors were combined into total OOA for further analysis (Hayes et al., 2013). Finally, four factors of OA were obtained, i.e., oxygenated OA (OOA), cooking OA (COA), hydrocarbon-like OA (HOA), and biomass burning OA(BBOA), as shown in Fig. S28. The detailed information on how to select the optimum PMF solution is available in Table S4.

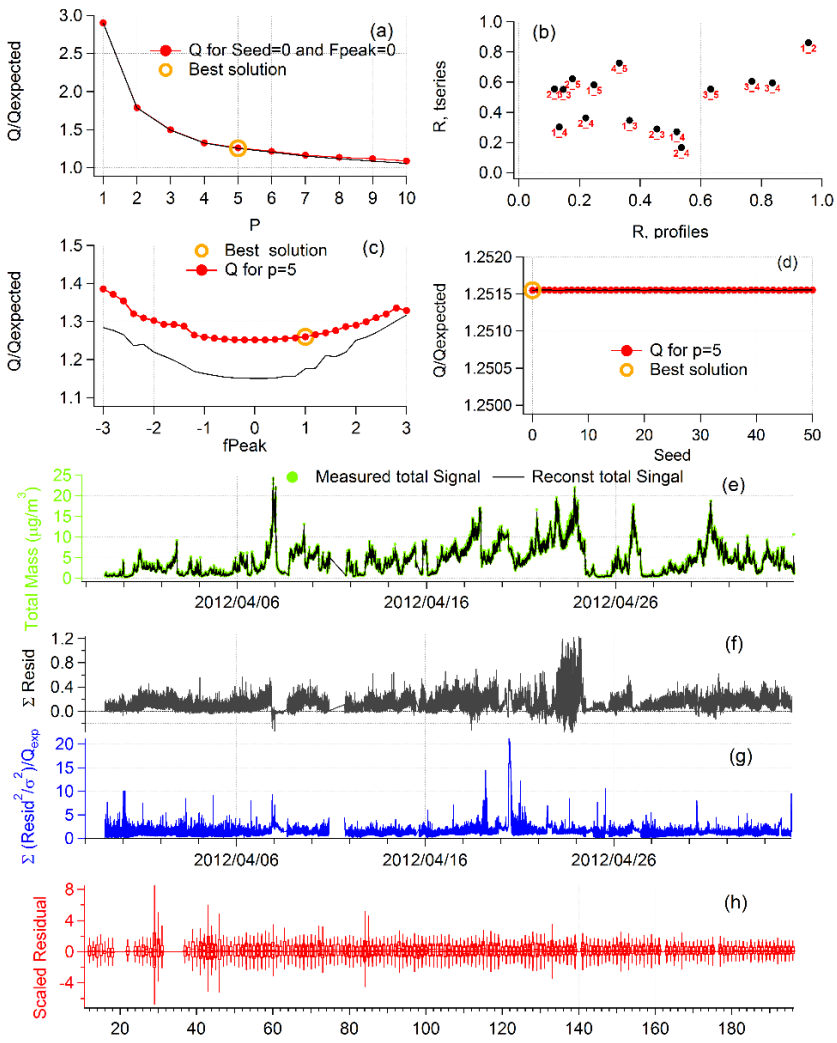

Figure S16. Diagnostic plots of the PMF analysis on OA mass spectral matrix for the spring observation.

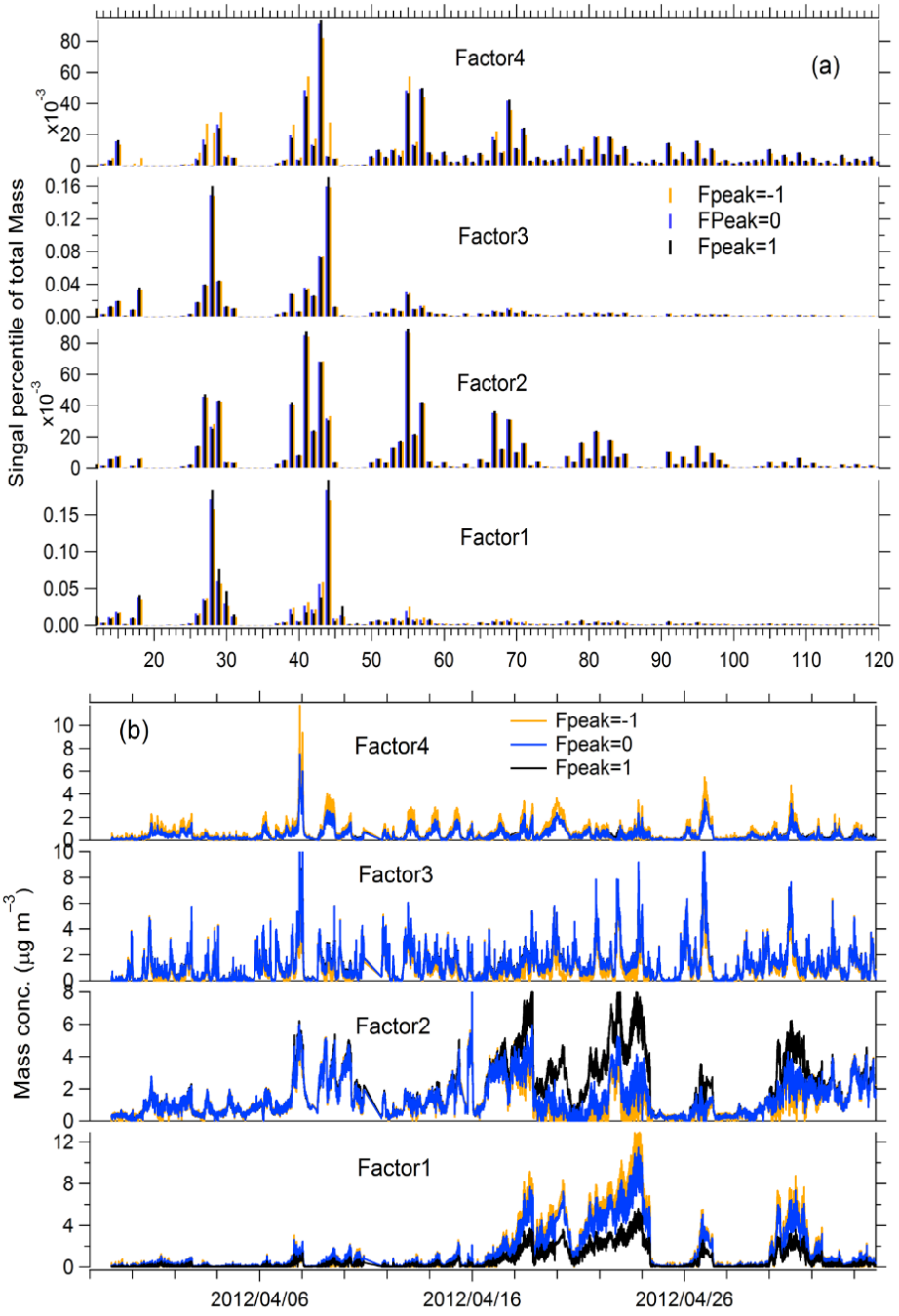

Figure S17. The spectra and time series of 4-factor solution at different f_{peak} values for the spring observation.

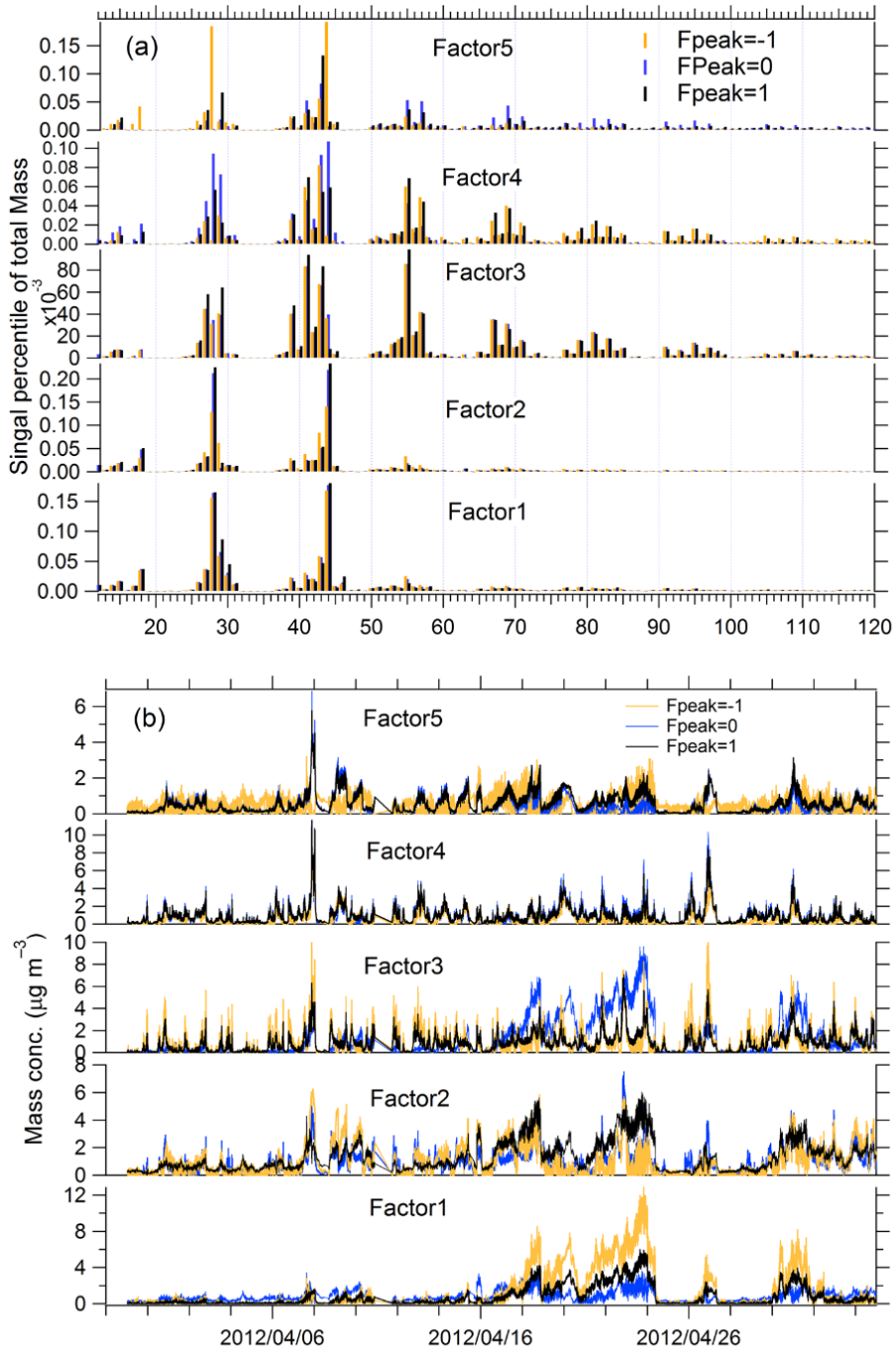

Figure S18. The spectra and time series of 5-factor solution at different f_{peak} values for the spring observation.

Table S4 Descriptions of PMF solutions for the spring observation in Beijing.

Factor number	**F_{peak}**	**Seed**	**Q/Q_{exp}**	**Solution Description**
1	0	0	2.90	Too few factors, large residuals at time periods and key *m/z*'s
2	0	0	1.79	Too few factors, large residuals at time periods and key *m/z*'s
3	0	0	1.49	Too few factors (OOA, HOA and COA). The Q/Q_{exp} at different seeds (0-50) are very unstable. Factors are mixed to some extent based on the time series and spectra.
4	0	0	1.32	OA factors could be identified as MO-OOA, LO-OOA, COA and HOA. Time series and diurnal variations of OA factors are consistent with the external tracers. But, the signal of characteristic ion *m/z* 60 biomass burning is strong in HOA factor.
5	**1**	**0**	**1.25**	**Final choice for the PMF solution. Two OOA factors, COA, HOA and BBOA are identified. Two similar OOA factors are combined for further analysis. Time series and diurnal variations of OA factors are consistent with the external tracers.**
6-10	0	0	1.20-1.06	Factor split. OOA was split into three or more factors with similar spectra, however, different time series.
5	-3 to 3	0	1.25-1.39	In f_{peak} range from −1.0 to 1.0, factor MS of OOA and COA are nearly identical, but there is a shift between HOA and BBOA for some ion fragments. The time series of OOA and HOA are nearly identical, but the other show some changes.

For the summer observation, the 4-factor, f_{peak}=0 solution was selected as the optimum solution. Four OA factors are more oxidized (MO-OOA) and less oxidized OOA (LO-OOA), cooking OA (COA) and hydrocarbon-like OA (HOA). The performances of spectra and time series of the four factors at different f_{peak} were also investigated. The detailed information on how to select the optimum PMF solution can be found in Figure S19-S21 and Table S5.

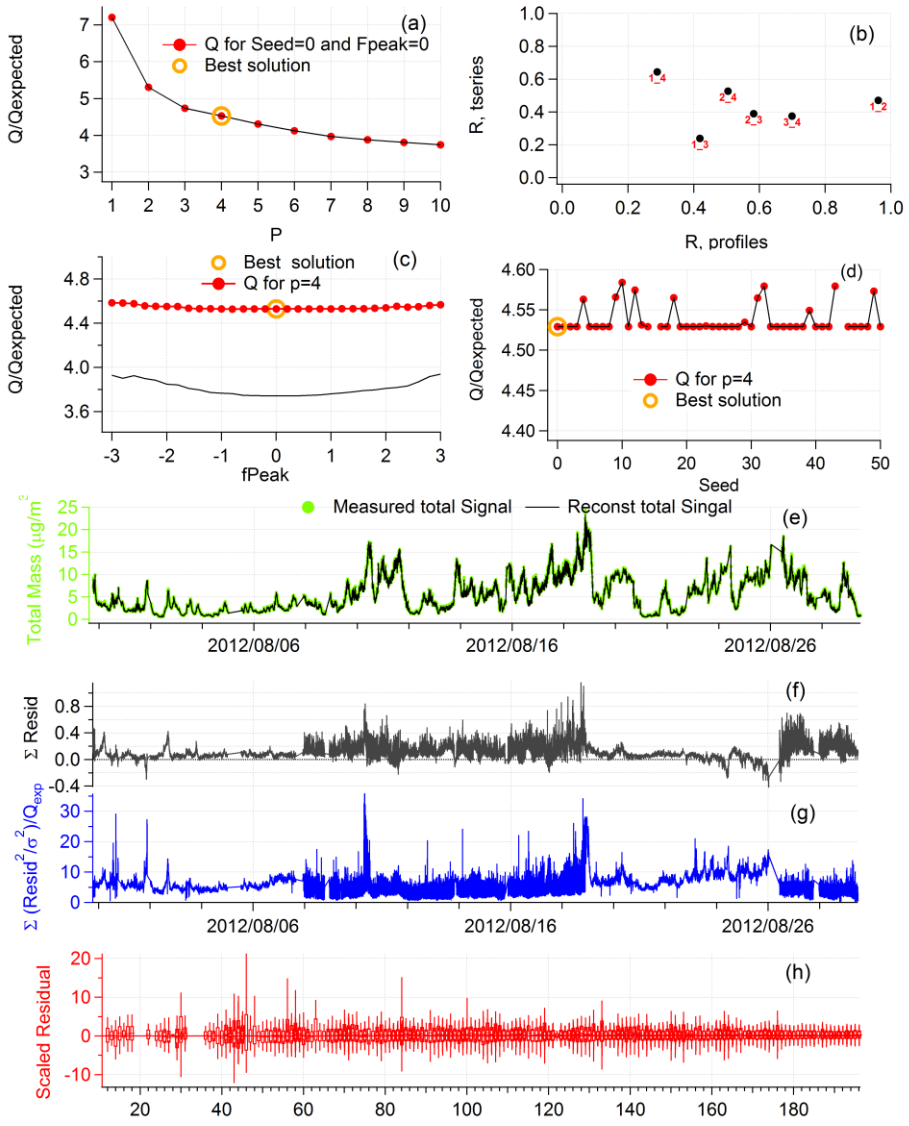

Figure S19. Diagnostic plots of the PMF analysis on OA mass spectral matrix for the summer observation.

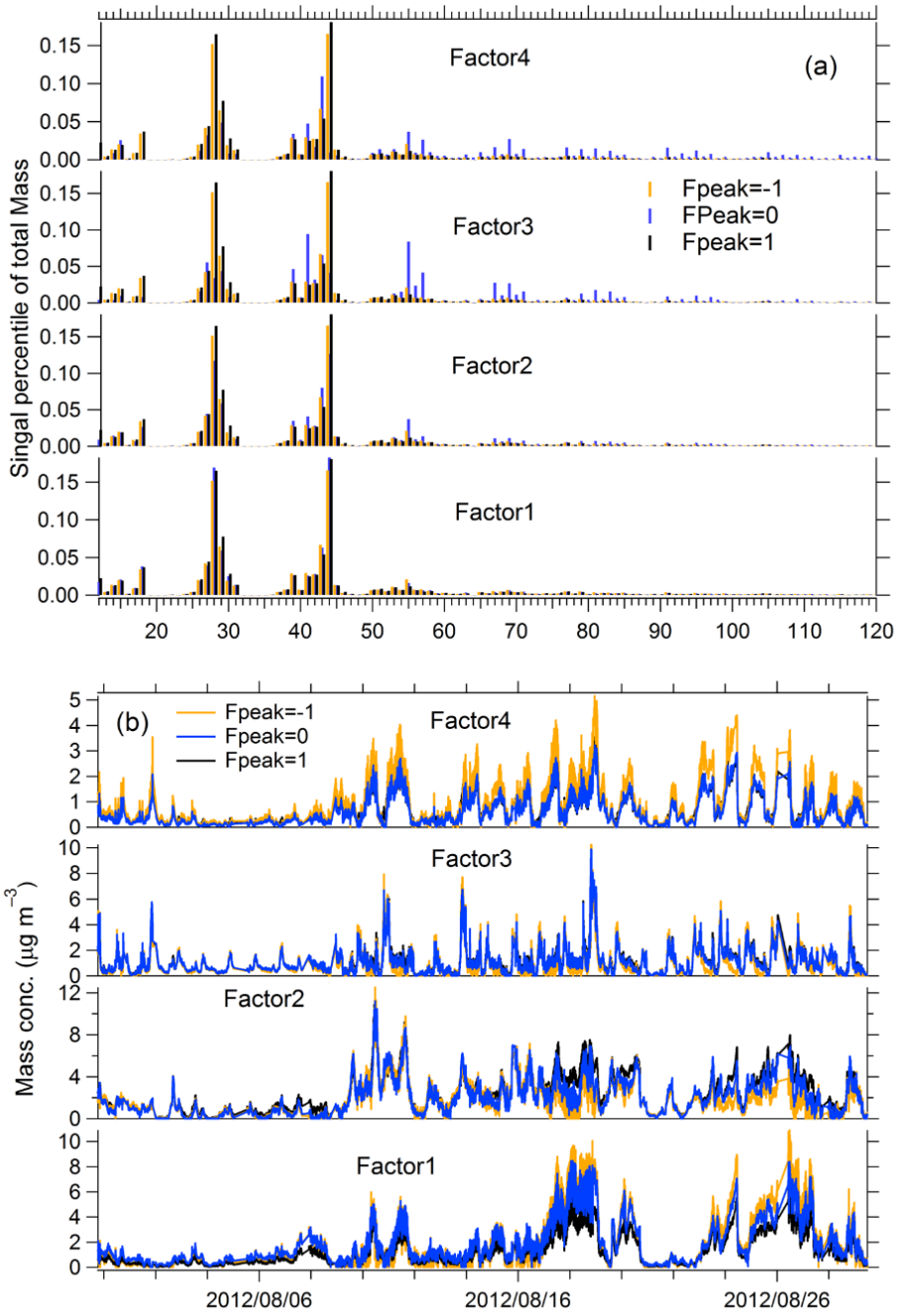

Figure S20. The spectra and time series of 4-factor solution at different f_{peak} values for the summer observation.

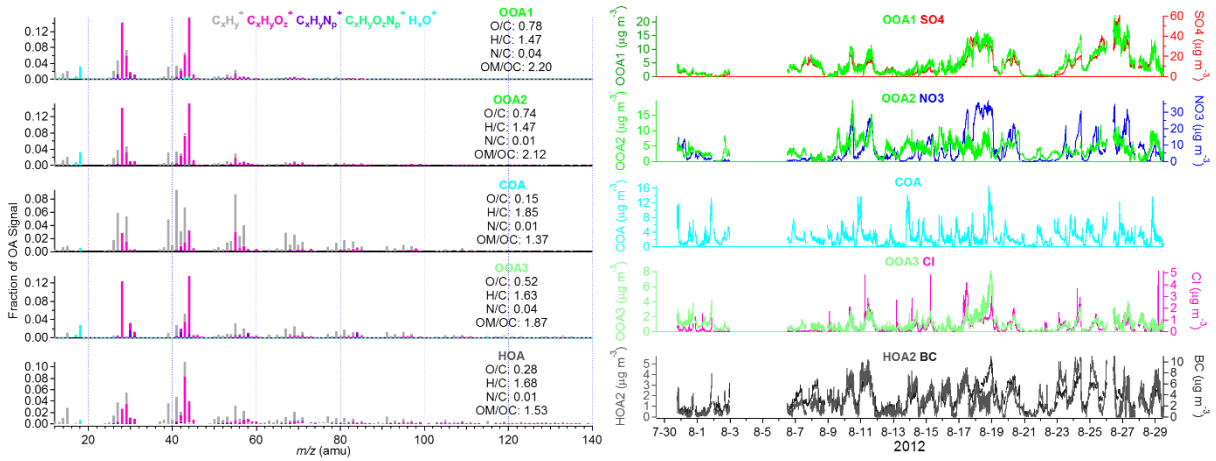

Figure S21. Unit mass spectra and time series of OA factors for 5-factor solution. The factors are marked as OOA1, OOA2, COA, OOA3 and HOA, respectively. OOA1, OOA2 and OOA3 show similar MS features (r=0.87–0.90). It is unclear if these OOA components represent distinct sources or chemical types. The elemental ratios and OA/OC ratios of each component are added.

Table S5 Descriptions of PMF solutions for the summer observation in Beijing.

Factor number	**Fpeak**	**Seed**	**Q/Q$_{exp}$**	**Solution Description**
1	0	0	7.20	Too few factors, large residuals at time periods and key *m/z*'s
2	0	0	5.31	Too few factors, large residuals at time periods and key *m/z*'s
3	0	0	4.73	Too few factors (OOA, HOA and COA). Factors are mixed to some extent based on the time series and spectra.
4	**0**	**0**	**4.53**	**Optimum solution for the PMF analysis (MO-OOA, LO-OOA, COA and HOA). Time series and diurnal variations of OA factors are consistent with the external tracers. The spectra of four factors are consistent with the source spectra in AMS spectra database.**
5-10	0	0	4.30-3.74	Factor split. Take 5 factor number solution as an example, OOA is likely split into three factors with similar mass spectra and different time series. However, it is difficult to explain if they represent distinct sources or chemical types.
4	-3 to 3	0	4.53-4.58	In f_{peak} range from −1.0 to 1.0, factor MS and time series are nearly identical.

The solution of the PMF analysis for the autumn observation is similar to that for the spring observation. When OA was separated into five fractions, OOA was also split into two factors, but a BBOA factor of distinct characteristics (f_{60}=1.3%) could be identified. When more than five factors, OOA decomposed into three or more factors. The performances of spectra and time series of the four factors at different f_{peak} are nearly identical. The five factors, f_{Peak}=0 and seed=0 solution is chosen as the optimal solution for this PMF analysis. In the five-factor solution, two OOA factors have similar MS characteristics (r= 0.976) and the elemental ratios and OA/OC ratios (O/C: 0.85–0.91; H/C: 1.24–1.40; OA/OC: 2.24–2.37) are close. It is unclear if the two OOA components represent distinct sources or chemical types. Thus, two OOA factors were combined into total OOA for further analysis (Hayes et al., 2013). Finally, four factors of OA were obtained, i.e., oxygenated OA (OOA), cooking OA (COA), hydrocarbon-like OA (HOA), and biomass burning OA(BBOA), as shown in Fig. S30. The detailed information on how to select the optimum PMF solution are given as Figs. S22-S24 and Table S6.

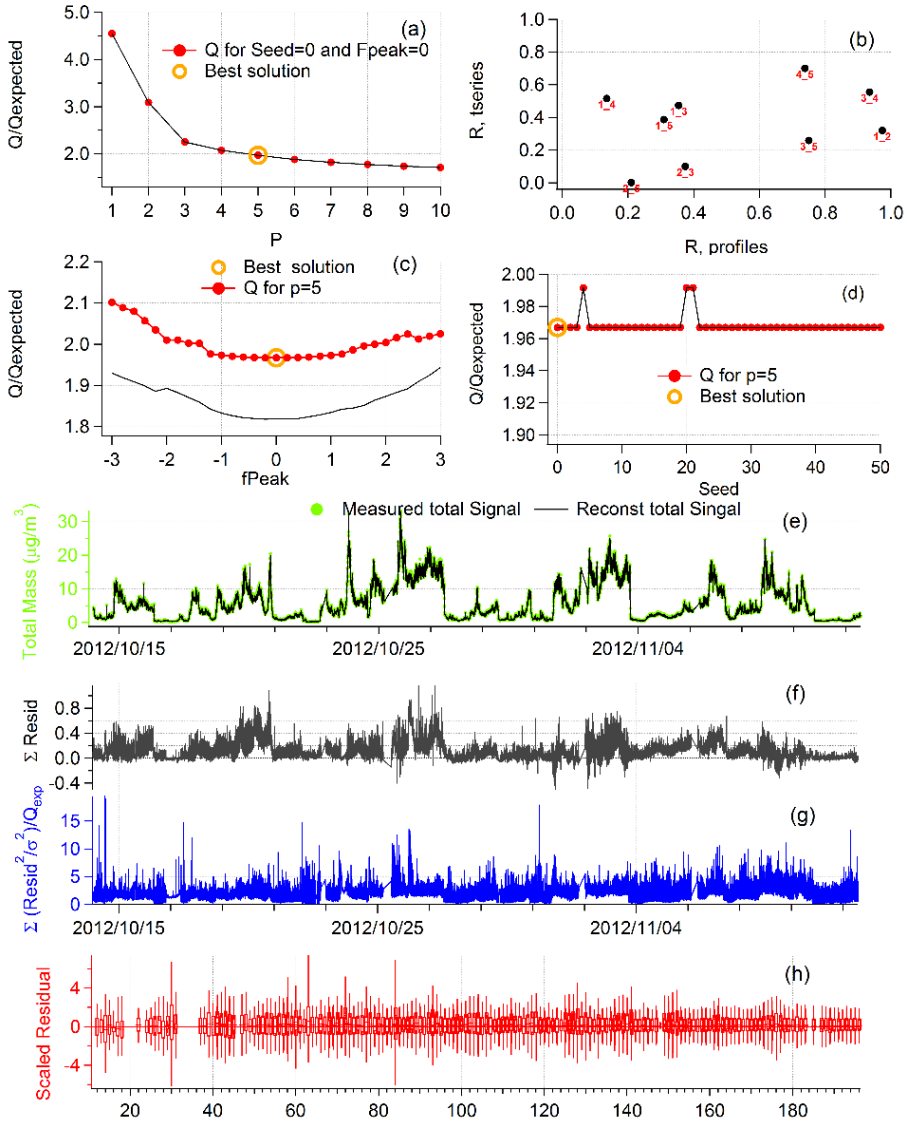

Figure S22. Diagnostic plots of the PMF analysis on OA mass spectral matrix for the autumn observation.

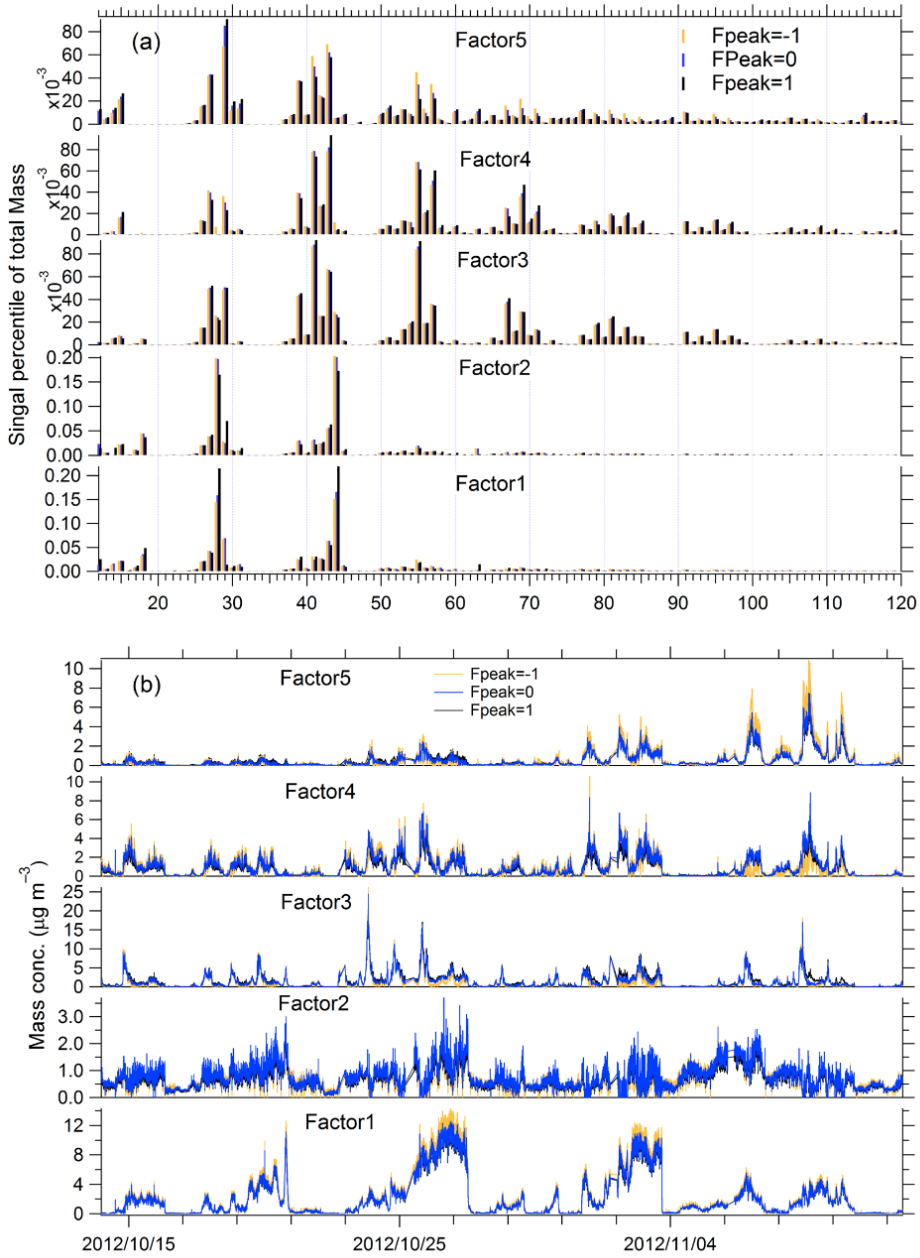

Figure S23. The spectra and time series of 5-factor solution at different f_{peak} values for the autumn observation.

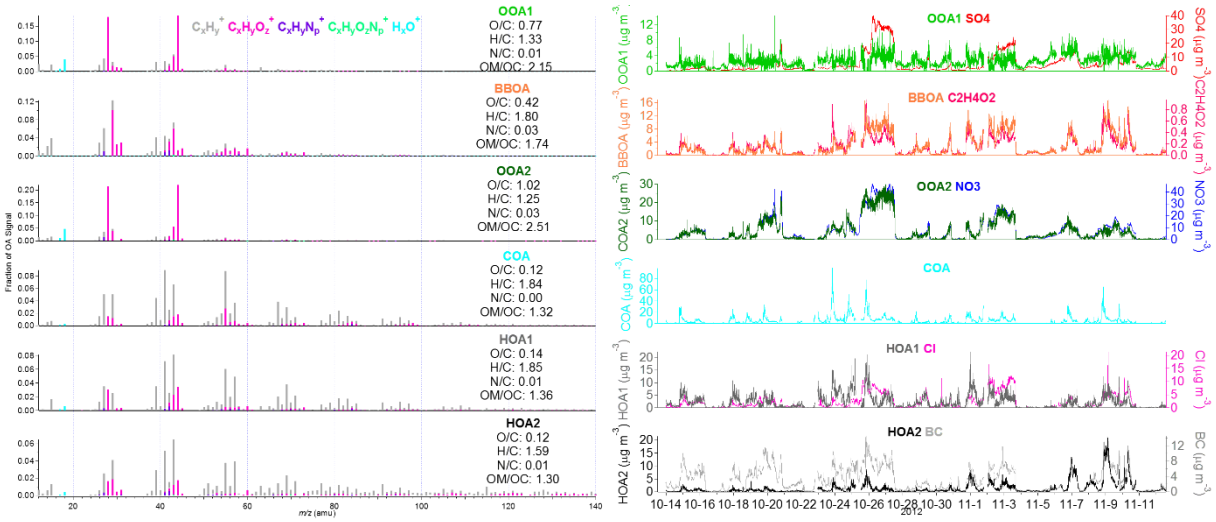

Figure S24. Unit mass spectra and time series of OA factors for 6-factor solution. The factors are marked as OOA1, BBOA, OOA2, COA, HOA1 and HOA2, respectively. The time series of BBOA and OOA2 trend well (r=0.78). HOA1 and HOA2 have similar MS (r=0.94) and diurnal variations (r=0.93). These factors appear mixed with each other.

Table S6 Descriptions of PMF solutions for the autumn observation in Beijing.

Factor number	**Fpeak**	**Seed**	**Q/Q$_{exp}$**	**Solution Description**
1	0	0	4.55	Too few factors, large residuals at time periods and key *m/z*'s
2	0	0	3.09	Too few factors, large residuals at time periods and key *m/z*'s
3	0	0	2.25	Too few factors (OOA, COA and HOA). The Q/Q$_{exp}$ at different seeds (0-50) are very unstable. The HOA factor contain high abundance (1.0%) of *m/z* 60.
4	0	0	2.07	Four factors include two similar OOA factors, COA and HOA. The HOA factor contain high abundance (1.1%) of *m/z* 60.
5	**0**	**0**	**1.97**	**Optimum solution for the PMF analysis (two OOA factor, COA, HOA and BBOA). Two similar OOA factors are combined for further analysis. Time series and diurnal variations of OA factors are consistent with the external tracers.**
6-10	0	0	1.88-1.71	Factor split. Some of the split factors have time series and MS that appear mixed.
5	-3 to 3	0	1.97-2.10	In f_{peak} range from −1.0 to 1.0, factor MS and time series are nearly identical.

For the winter observation, a 5-factor, f_{peak}=0 solution was selected as the optimum solution. Five OA factors are more oxidized (MO-OOA) and less oxidized OOA (LO-OOA), cooking OA (COA), coal combustion OA (CCOA) and hydrocarbon-like OA (HOA), respectively. The performances of spectra and time series of the five factors at different f_{peak} were also investigated. The detailed information on how to select the optimum PMF solution can be found in Figs. S25-S27 and Table S7.

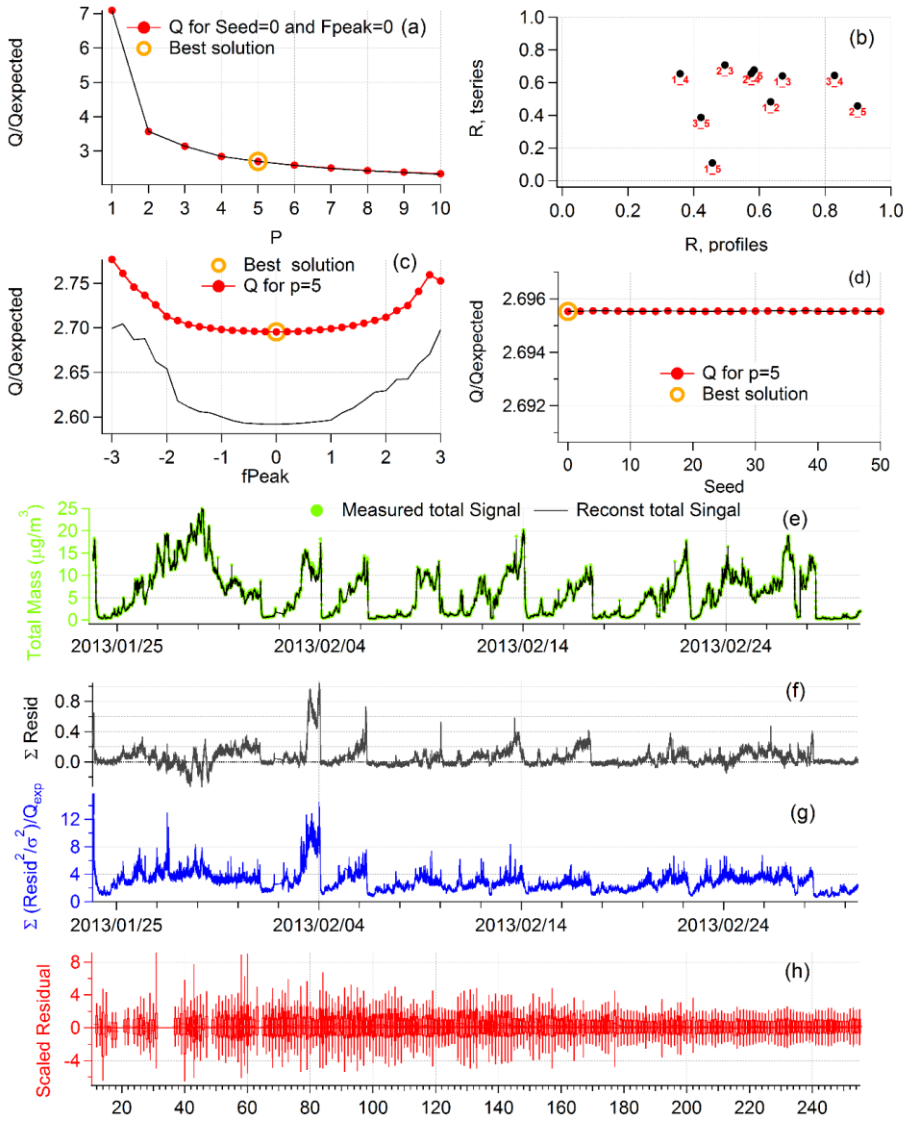

Figure S25. Diagnostic plots of the PMF analysis on OA mass spectral matrix for the winter observation.

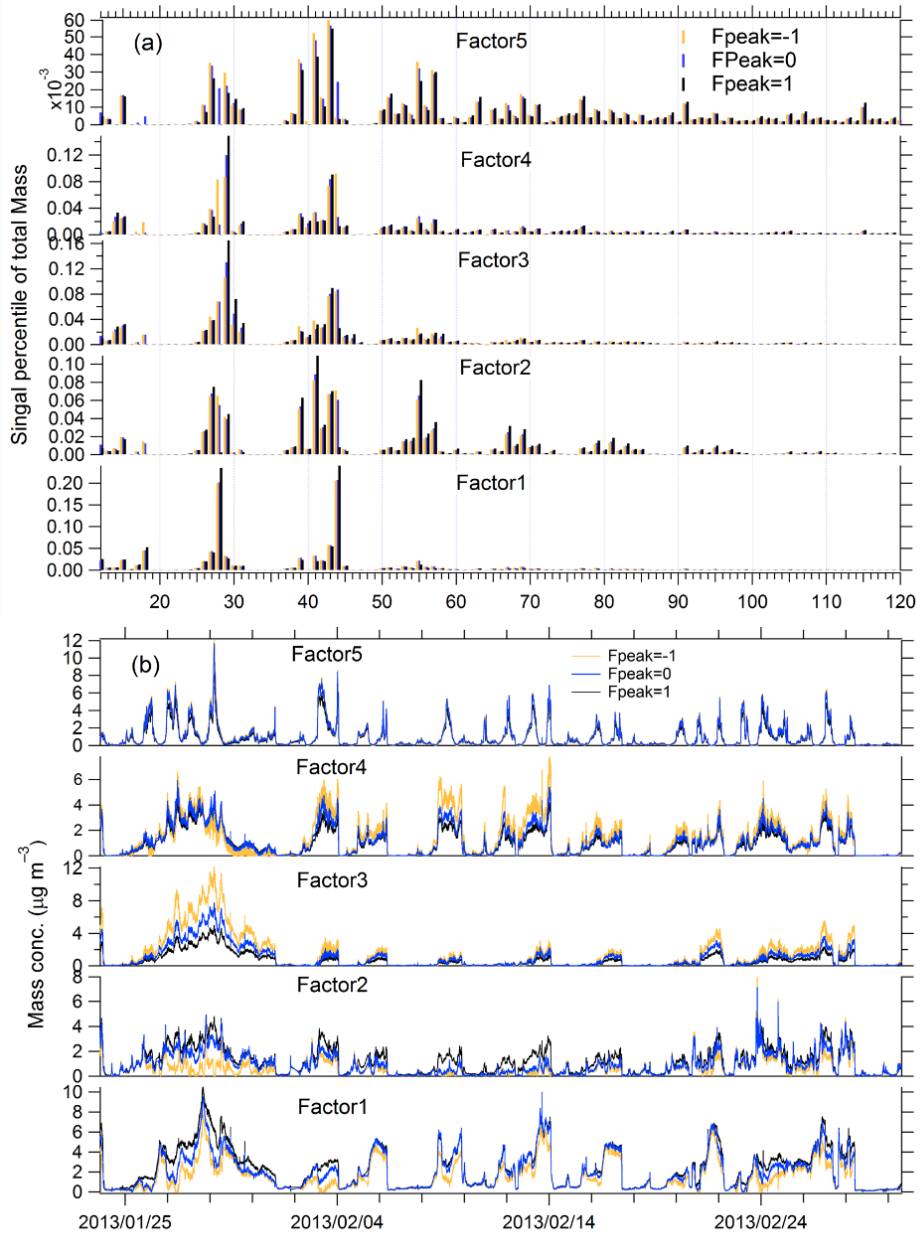

Figure S26. The spectra and time series of 5-factor solution at different f_{peak} values for the winter observation.

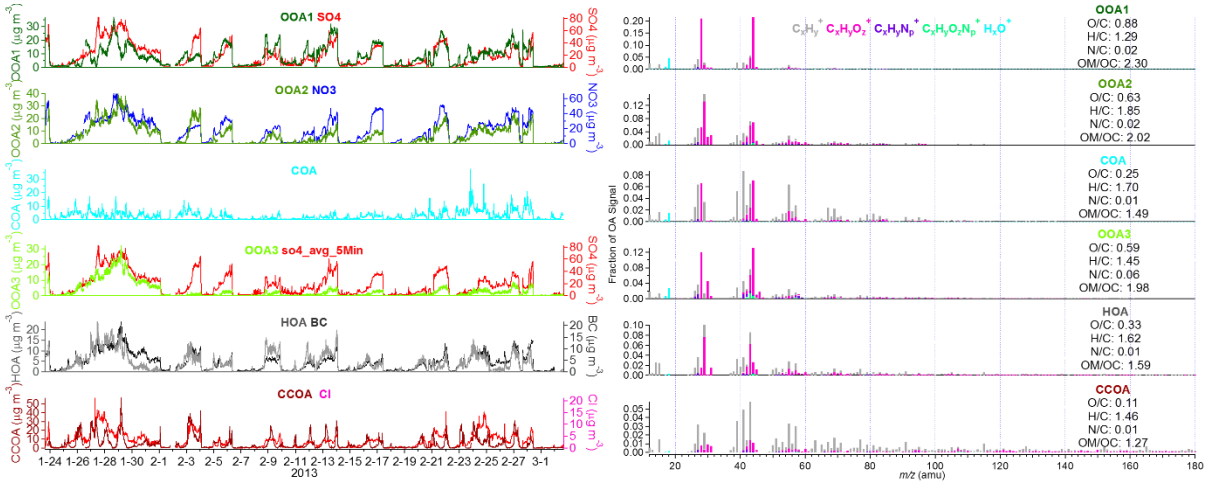

Figure S27. Unit mass spectra and time series of OA factors for 6-factor solution. The factors are marked as OOA1, OOA2, COA, OOA3, HOA and CCOA, respectively. OOA1, OOA2 and OOA3 show similar time series or MS features (r=0.56–0.95). The characteristics of OOA3 factor is not obvious. It is unclear if these factors represent distinct sources or chemical types.

Table S7 Descriptions of PMF solutions for the winter observation in Beijing.

Factor number	**Fpeak**	**Seed**	**Q/Q$_{exp}$**	**Solution Description**
1	0	0	7.09	Too few factors, large residuals at time periods and key *m/z*'s
2	0	0	3.57	Too few factors, large residuals at time periods and key *m/z*'s
3	0	0	3.14	Too few factors (OOA-, HOA- and COA-like). The Q/Q$_{exp}$ at different seeds (0-50) are very unstable. Factors are mixed to some extent based on the time series and spectra.
4	0	0	2.84	OA is split to two OOA factors, COA and HOA. It seems that HOA mixed with CCOA.
5	**0**	**0**	**2.70**	**Optimum choice for PMF factors (MO-OOA, LO-OOA, COA, HOA and CCOA). Time series and diurnal variations of OA factors are consistent with the external tracers. The spectra of four factors are consistent with the source spectra in AMS spectra database.**
6-10	0	0	2.59-2.33	Factor split. Take 6 factor number solution as an example, OOA was split into three factors with similar spectra and/or time series.
5	-3 to 3	0	2.70-2.78	In f_{peak} range from −1.0 to 1, factor MS and time series are nearly identical, but there is likely a shift of the time series for LO-OOA and COA during the heavy-pollution episodes.

9. Pg 17 Lns 7-8: It is interesting that the LO- and MO-OOA fractions slightly increased around 100 μg m^{-3} only. What influence the increase of OOA factors during particular OA mass concentration?

Response: It has been found that a substantial fraction (50–75%) of POA is semivolatile, evaporates when the plume becomes more dilute, and is then available in the gas phase to take part in photochemical reactions (Shrivastava et al., 2006; Robinson et al., 2007). This material has the physicochemical properties of SOA. Murphy and Pandis (2009) define that fresh POA is emitted in the particulate phase and has not undergone chemical processing, while oxidized POA (OPOA) refers to POA compounds that evaporate and undergo oxidation in the gas phase, which allows them to reduce their volatility and re-condense back to the particulate phase. SOA produced from the oxidation of intermediate-volatility compounds (IVOCs) was also included in OPOA mainly because the IVOC emissions were calculated based on the POA emissions (Fountoukis et al., 2014). Intermediate-volatility organic compounds (IVOCs) have been proposed to be an important source of SOA (Zhao et al., 2014).

SOA chemistry is complex and the contribution of different pathways is not well understood. More work is needed to accurately identify the volatility and aging of primary emissions, and to quantify the contributions of SOA from different sources and formation mechanisms.

In this study, we have no strong evidence to elaborate the mechanisms or pathways. We only give our hypothesis in this sentences.

In the revision, "*In both autumn and winter, the fractions of OOA slightly increased around 100 μg m^{-3}, implying that POA probably transformed to SOA more effectively within this range*" was changed to "***In both autumn and winter, the fractions of OOA slightly increased around 100 μg m^{-3}. More work is needed to accurately clarify the cause of the OOA increase within this range.***"

10. Pg 18 Lns 27-28: The VK diagram in winter does not show any correlation (r^2 = 0.02) between H/C and O/C. The slope is nearly zero (0.08; not broad). This suggests that hydroxylation and/or peroxidation processes were likely to occur in Beijing during winter. On the other hand, carboxylation process might be unlikely to occur since the slope is higher than -0.5. Please elaborate or clarify the discussion.

Response: Currently, there is no substantial progress on explicating specific oxidation pathways for OA evolution (Chen et al., 2015; Heald et al., 2010). In winter, CCOA was resolved by the PMF analysis, which was different from other seasons. This is a possible reason

the VK Diagram in winter was different from those in other seasons.

In the revision, "*However, in winter, the correlation was not good (r^2 = 0.02), with a fitted slope -0.08, exhibiting a "broader" range in the VK Diagram than in other seasons (Fig. 8 and Fig. S21)*" was changed to "***However, the VK diagram in winter (Fig. 8 and Fig. S39) does not show any correlation (r^2 = 0.02) between H/C and O/C. The slope is nearly zero (-0.08). This is possibly caused by the more complex sources of OA in winter, e.g., CCOA was only resolved in winter***" in Line 25, Page 19.

"*In winter, the scatterplot of H/C vs. O/C ratios in the VK Diagram showed "broader" slopes, hinting the more complex sources and evolution processes of OA. The scatterplot indicated that OA in winter mainly evolved between the hydroxylation or peroxidation reactions (slope = 0) and carboxyl groups addition with fragmentation (slope = -0.5).*" was changed to "***In winter, the nearly zero slope of the VK Diagram suggests that hydroxylation and/or peroxidation processes (slope = 0) were likely to occur in Beijing during winter. On the other hand, carboxylation process might be unlikely to occur since the slope is higher than -0.5.***" in Line 5, Page 20.

Technical comments

1. Pg 1 Ln 14: If PM_1 here is NR-PM1+BC, it needs to be specified in the sentence.

Response: "*An Aerodyne high resolution time-of-flight aerosol mass spectrometry (HR-ToF-AMS) and other relevant instrumentations for gaseous and particulate pollutants were deployed. The average mass concentrations of submicron particulate matter (PM_1)…*" was changed into "***An Aerodyne high resolution time-of-flight aerosol mass spectrometry (HR-ToF-AMS) was deployed to measure non-refractory chemical components of submicron particulate matter (NR-PM_1). The average mass concentrations of PM_1 (NR-PM_1+black carbon)***…".

2. Pg 2 Lns 26-27: Is SNA important only for the urban area or in general? Clarify the sentence and add reference.

Response: "***in urban regions (Guo et al., 2014; Huang et al., 2014; Lee, 2015)***" was added.

3. Pg 5 Lns 7: ..., the last well calibrated…

Response: "*last well calibrated*" was corrected into "***the last well calibrated***".

4. Pg 5 Lns 8-9: Do you mean "the size distribution calibration"? Please clarify.

Response: "*the size distribution*" was corrected into "***the size distribution calibration***".

5. Pg 7 Lns 1-2: Do you mean "…PM_1 in winter was higher than previous studies in Beijing…"? Also please clarify what does "close periods" mean.

Response: "*PM_1 in winter was higher than before, and equivalent to those in close periods (Zhang et al., 2014; Sun et al., 2014)*" was revised into "*PM_1 in winter was higher than* ***the previous results in Beijing before 2013****, and equivalent to those in close periods* ***from January to February 2013 (Fig. 1;*** *Zhang et al., 2014; Sun et al., 2014).*"

6. Pg 7 Ln 13: Figures S6 and S8 don't display fire points as mentioned in the sentence.

Response: The maps of fire points from satellites were added in the supplementary material as follows.

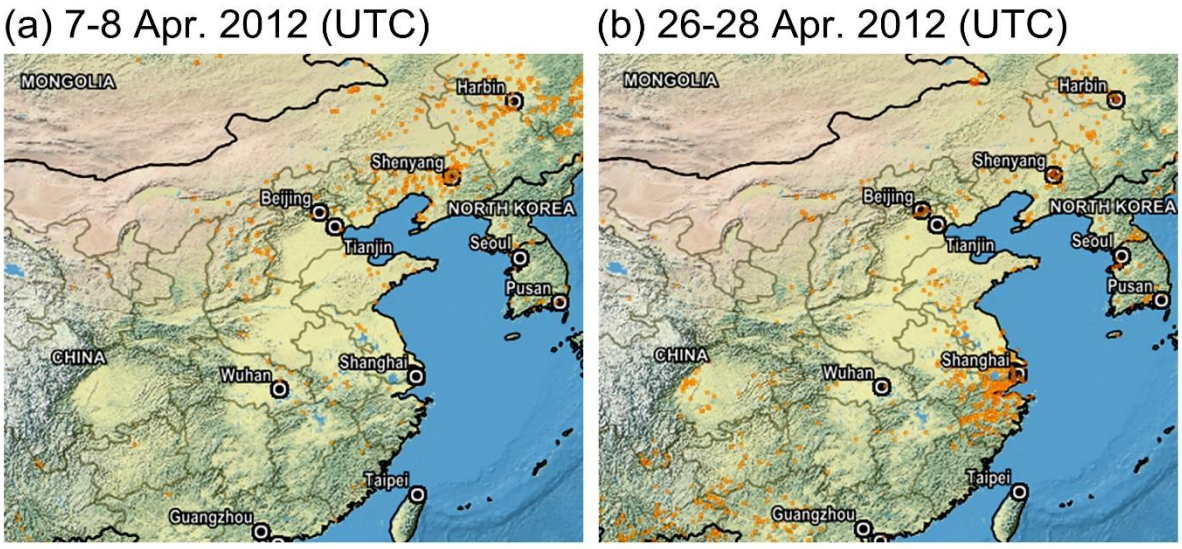

Fig. S10. Fire points observed by satellites (https://firms.modaps.eosdis.nasa.gov/firemap) in Beijing and surrounding areas during 7–8 (a) and 26–28 (b) Apr. 2012.

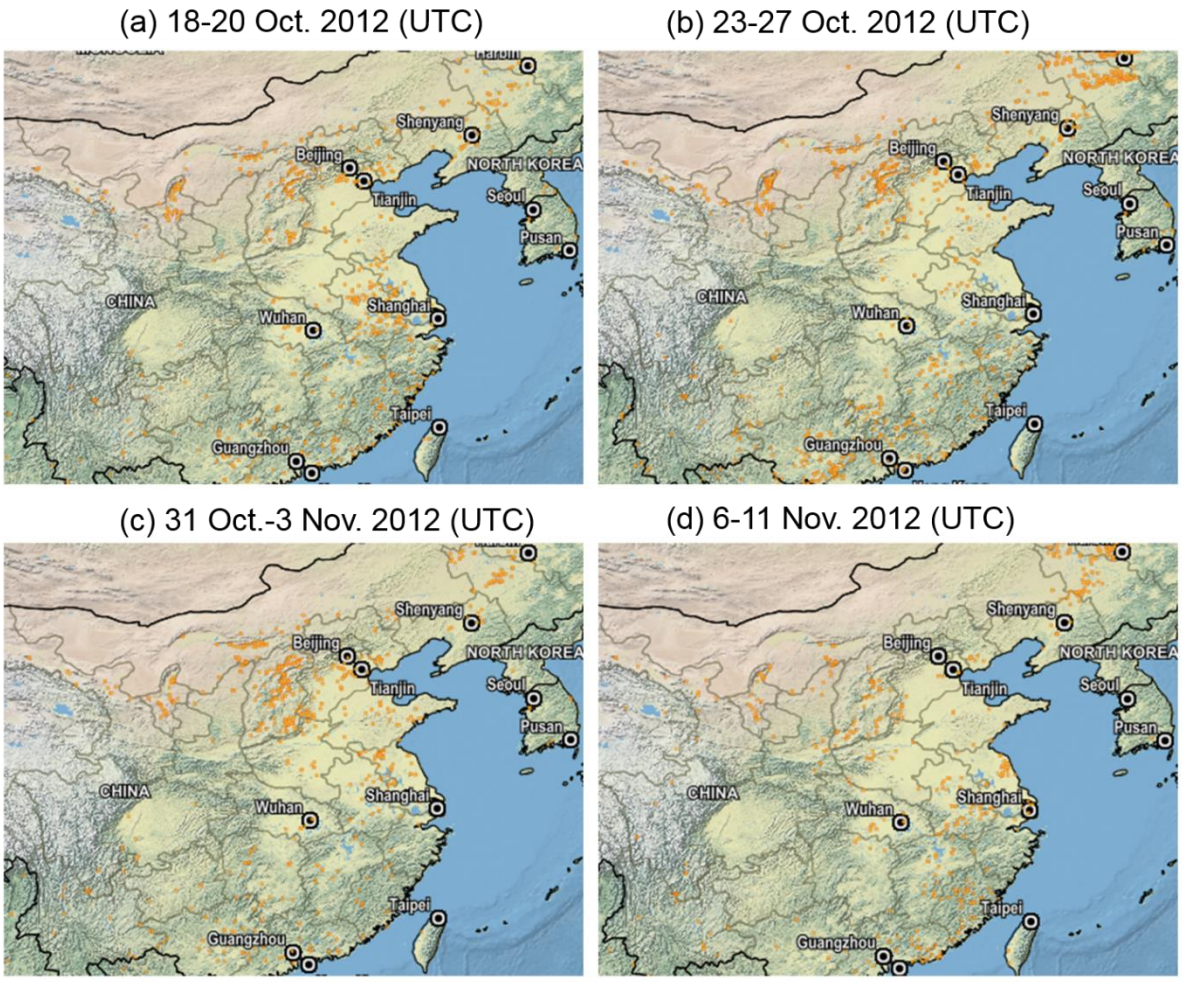

Fig. S11. Fire points observed by satellites (https://firms.modaps.eosdis.nasa.gov/firemap) in Beijing and surrounding areas during the autumn observation.

7. Pg 9 Ln 27: …the internally mixed states…

Response: "*the internal mixed states*" was changed into "***the internally mixed states***".

8. Pg 11 Ln 8: The term "freshly secondary formation" is ambiguous. Consider "new SOA formation".

Response: This sentence was removed because it is arguable (Comment 8 of Reviewer#2).

9. Pg 12 Ln 26: Provide the coefficient of determination for any statement about correlation.

Response: Here the uncentered coefficient (UC) represents the cosine of the angle between a

pair of mass spectra (MS) or time series (TS) as vectors, such that

$UC = \cos\theta = (x \cdot y)/(|x| \cdot |y|)$

where x and y denote a pair of MS or TS as vectors. The uncentered correlation is very similar to the well-known Pearson coefficient (R) for mass spectra, and quite correlated with Pearson's R for time series (Ulbrich et al., 2009). Whereas, it is a value of cosine and has no the coefficient of determination.

The coefficients of determination for Pearson correlations were checked in the whole text.

10. Pg 15 Lns 24-27: Insert respectively after on average. Breaking this sentence into two will be better as it is pretty long at the current state.

Response: "***respectively***" was added. The original sentence was broken into two sentences, that is "***The concentrations of COA factors at the noon peak (about 12:00–14:00) were 3.1, 2.5, 4.0 and 4.4 μg m^{-3} on average, respectively. COA reached the highest concentrations in the evening (18:00–21:00), as 5.6, 6.2, 14.0 and 7.5 μg m^{-3} on average, respectively.***"

11. Pg 18 Ln 2: …, 1.52-1.63, …

Response: Corrected.

12. Pg 18 Ln 18: What does "shallower" mean? Do you mean flatter slope?

Response: "*shallower*" was changed into "***flatter***".

13. Pg 20 Ln 7: …(i.e. lower H/C ratio, and higher O/C ratio and ***OSC***)….

Response: Corrected.

14. Pg 20 Ln 28: What does "higher" compare to? Is it higher than "stable level". What does stable level mean here?

Response: The content was addressed in the text above, "*In laboratory and field studies on OA aging under strong oxidizing conditions, it was found that the OA/ΔCO ratios remain relatively*

stable at high O/C ratios with the increase of O/C ratios because organics obtain oxygen atoms but loss carbon atoms in the oxidation processes (DeCarlo et al., 2008, 2010).” “*Higher*” is compared to the results we obtained. The *“stable level”* means *“OA/ΔCO ratios remain relatively stable at high O/C ratios with the increase of O/C ratios*”.

In the revision, “*get higher*” was changed to “***reach higher values***”.

15. Pg 21 Ln 28: Provide indicator (value) of the low aging degrees of air masses.

Response: “***(-log (NO_x/NO_y) < 0.05)***” was added.

16. Fig 3: Need label (Hours of Day) for the X-axis.

Response: “Hour of day” was added as X-axis label.

17. Figs 5-8: Colors for MO-OOA and OOA are difficult to distinguish on print.

Response: The difference between the colors for MO-OOA and OOA was largened in these figures. Please see these figures in the manuscript.

18. Figs 6-7: The legends for these figures are not consistent. OOA is missing from Fig. 7.

Response: The legend of OOA was added in Fig. 7.

19. Fig. S13: … LV-OOA, MO-OOA…

Response: The figure caption was corrected.

References

Pye, H. O. T. Epoxide pathways improve model predictions of isoprene markers and reveal key role of acidity in aerosol formation. Environ. Sci. Technol., 47, 11056-11064, 2013.

Zhang, Q. Q. Understanding atmospheric organic aerosols via factor analysis of aerosol mass spectrometry: a review, Analyt. Bioanalyt. Chem., 401, 3045-3067, 2011.

Thank you very much for your comments and suggestions. Your any further comments and suggestions are appreciated.

Referee #2

The manuscript investigates the seasonal variations of compositions, sources, and evolution for atmospheric aerosols in the megacity of Beijing. While field measurements have been carried out by other groups in this city, this work provides a more comprehensive exploration of organic aerosol composition and evolution. Generally, the paper is quite well written. The methodology and results are presented clearly. The measurements provide sufficiently new data that the manuscript may merit publication. However, the qualitative interpretation of the results may limit the application and impacts of this work. This calls for a more detailed data analysis, explaining the mechanisms behind the observations. I suggest the authors respond to the following suggestions before the paper is accepted to publication.

Response: Thank you very much for your helpful comments and kind encouragement. We responded the specific suggestions of the reviewer, and revised the manuscript correspondingly to improve the quality of this manuscript. Please see the detailed response below and the changes marked blue in the revised manuscript.

Major Comment:

My main question is that as mentioned by the authors, the characteristics and evolution of aerosol pollution are multifactorial (e.g. meteorological conditions, regional transport, and local sources). These factors can have distinct patterns in different seasons, thus the formation, transformation and removal of pollutants are affected. The authors have provided nice discussions on the sources and evolution of ambient atmospheric aerosols under the influence of different meteorological conditions and sources. However, what would be the impacts of regional or long range transport on the composition, formation and evolution of atmospheric aerosols in different seasons in Beijing? For example, the authors mentioned that regional transport can play a role in the sulfate concentration in the winter season. While regional transport impacts have briefly discussed or mentioned in various sections or paragraphs, it would be nice to have a more coherent, quantitative discussion on the role of regional (or long range) transport in the concentration and evolution of different inorganic and organic components in different seasons.

Response: Ideally, regional transport may be evaluated using chemical transport models that interactively consider emissions, chemistry, meteorology, and removal (Zhang et al., 2015b). There have been several studies on the contribution of regional/long-distance transport to atmospheric aerosols in Beijing. Hu et al. (2015) applied a source-oriented Community Multi-

scale Air Quality (CMAQ) simulation to determine source sector/region contributions to primary aerosols. They found that local residential/transportation emissions and residential/industrial emissions from Heibei contributed predominately to primary aerosols in the spring of Beijing. In summer and fall, local industrial emissions were the largest contributor. In winter, local/regional residential/industrial sources contributed to over 90% of primary aerosols in Beijing. Wu et al. (2011) investigated the impact of local and regional sources on the air pollutants in Beijing with an online air pollutant tagged module in the Nested Air Quality Prediction Model System (NAQPMS), and estimated the air pollutant contributions from local and regional sources to the surface layer (about 30 m) and the upper layer (about 1.1 km) in the summer of 2006 in Beijing. The contribution of local sources to PM_{10} at the surface layer in Beijing was dominated (75%). Comparatively, the contribution of the surrounding regions (e.g., southern Beijing) was large (more than 50%) to PM_{10} at the 1.1 km layer. Lin et al. (2015) extended the Comprehensive Air Quality Model with Extensions (CAMX) v 5.4, and found that in August 2007, the local source contributions to anthropogenic and biogenic SOA in Beijing were 23.8% and 16.6%, respectively; regional/long-distance transport dominated for both anthropogenic and biogenic SOA in Beijing. Zhang et al. (2015a) quantified the source contributions to surface $PM_{2.5}$ pollution over North China from January 2013 to 2015 using the GEOS-Chem transport model and its improved adjoint, and attributed about half of the $PM_{2.5}$ pollution in Beijing to sources outside of the city.

Other than chemical transport models, Jia et al. (2008) describe a novel technique for quantifying regional aerosol solely from a series of fast-response aerosol measurements at a single site. Based on the strong asymmetric "sawtooth cycles" of aerosol in Beijing, they suggest the regional component averages about 50% and can range from 10%–20% during northwesterly flow to 70% or so during southerly flow. The uncertainties of the concentrations of regional aerosol can be up to 50% for one day but <10% when totaled over a sawtooth. Using data from two sites, Guo et al. (2010) give a rough estimation that 87% of the $PM_{1.8}$ in the summer of urban Beijing were regional contributions. The regional contributions to sulfate, ammonium and oxalate in $PM_{1.8}$ were 90%, 87% and 95%, respectively. Nitrate formation was locally dominant.

Li et al. (2015) report the results of the hybrid receptor modeling with observations at 10 sites in Beijing and cluster analysis of the 48-h air mass back trajectories for the same study periods. They show that the source areas leading to high $PM_{2.5}$ in Beijing were primarily located in the southwest and south of Beijing. However, Zhang et al. (2015b) considered the back trajectory analysis is unsuitable for urban-scale studies because it employs large-scale wind fields with coarse resolutions and does not consider the complex urban canopies.

The contribution of regional (long-distance) transport to aerosol pollution is important for reducing regional air pollution under a joint control policy. The contributions of local/regional transport are difficult to quantify, however, even with transport models (Jia et al., 2008). In this study, this issue will not be focused on.

Here for reference, the results of backward trajectories of air parcels calculated with the NOAA's HYSPLIT4 trajectory model (http://www.arl.noaa.gov/hysplit.html) are shown in Fig. S43 in the supplementary, to give an insight into the impacts of regional/long-distance on the composition, formation and evolution of atmospheric aerosols in different seasons in Beijing.

The following texts were added in the manuscript and the supplementary, respectively.
In the manuscript, "***To give an insight into the impacts of regional/long-distance transport on atmospheric aerosols in Beijing, the backward trajectories of air parcels during the observation periods were calculated with the NOAA's HYSPLIT4 trajectory model (http://www.arl.noaa.gov/hysplit.html). A new 3-day backward trajectory was traced from the observation site at an altitude of 500 m above ground level every hour. Cluster analyses of backward trajectories were applied to reveal the major pathways during different campaigns (Sect. S11 in the supplement).***" was added in Sect. 2.1.

In the supplementary, the following contents "***During the seasonal observations in Beijing, the pathways of dominant air masses are different. Both long-distance transported and regional/local air masses influenced Beijing. In summer, the transport distance of long-distance transported air masses was shorter than in other seasons. In general, with the decrease of transport distance, the concentration of PM_1 gradually increased. When Beijing was dominated by regional/local air masses, the fractions of secondary inorganic species (SNA) increased, while the contributions of carbonaceous components (OA+BC) decreased, which is consistent with the previous results in Beijing (Sun et al., 2010; Huang et al., 2010; Zhang et al., 2014). Higher concentrations of SNA and PM_1 under the control of regional/local air masses reflected the great contribution of secondary formation from the gaseous precursors (e.g., NO_x and SO_2) emitted by vehicles and coal combustion in urban areas.***"

"***During the observations in spring, summer and autumn, the contributions of OOA (MO-OOA+LO-OOA) increased when Beijing was dominated by regional or local air masses. In summer, the fractions of LO-OOA in OA were high (29–48%) regardless of the different trajectories, signifying that the secondary formation from photochemical oxidations probably***

made an important contribution to OA. During the winter observation, POA and OOA contributed equally to OA in most cases due to the long-lasting stable weather conditions, indicating that both primary pollutants and regional secondary formation made important contributions to OA. When Beijing was dominated by long-distance transported air masses from north polar regions in winter, OOA contributed more significantly to OA, implying that organic aerosols were fully aged during long-distance transport." was added.

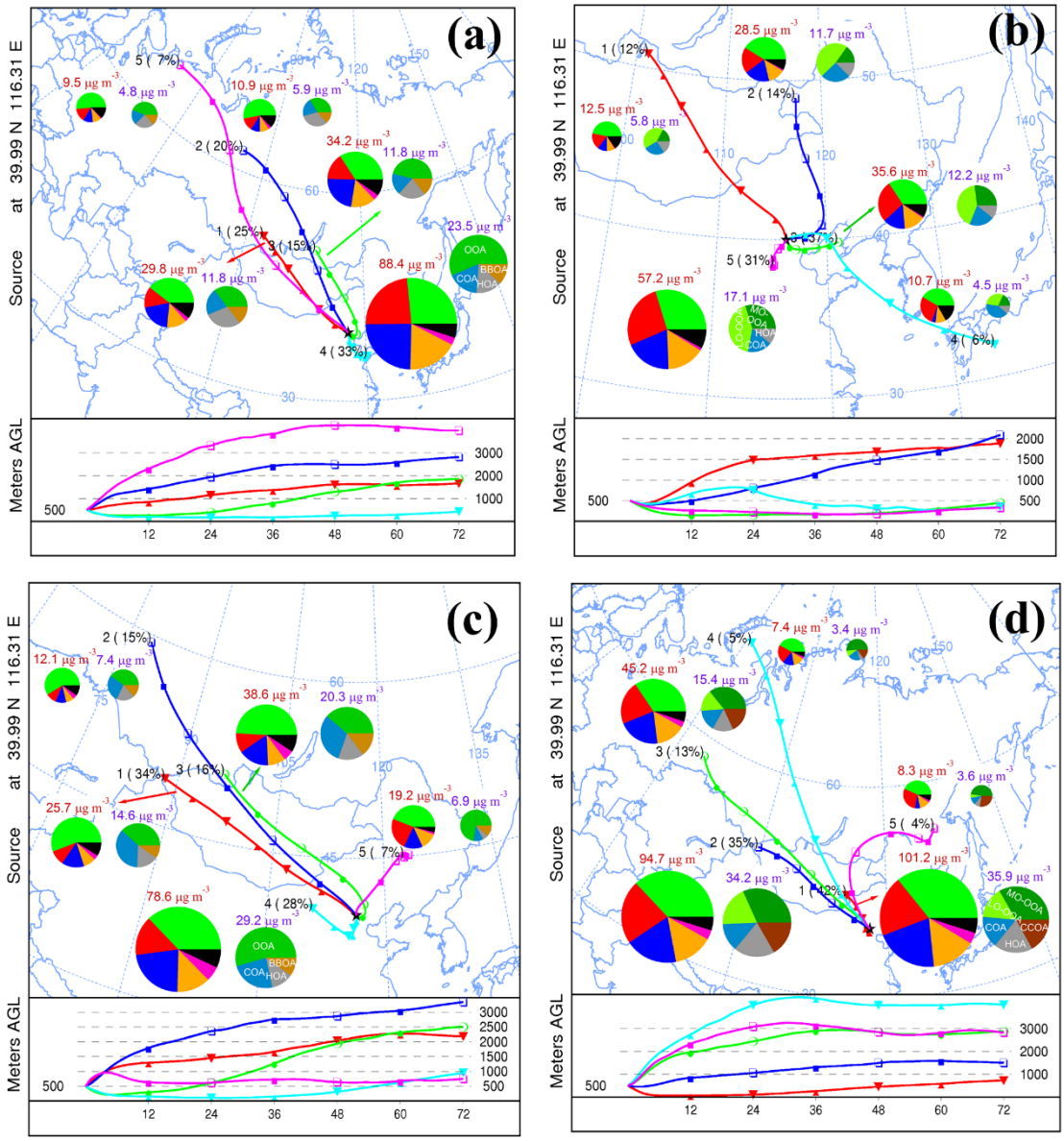

Figure S43. Back trajectories for each of the identified clusters and corresponding average main components of PM_1 and OA in PM_1 during the seasonal campaigns. (a) spring; (b)summer; (c) autumn and (d) winter. The filling color of main chemical species in PM_1 is the same with other figures.

Minor comments:

1. Abstract, "The evolution process of OA in different seasons was investigated with multiple metrics and tools. The average carbon oxidation states and other metrics show that the oxidation state of OA was the highest in summer, probably due to both strong photochemical and aqueous-phase oxidations." Any evidence supports the contribution of aqueous-phase oxidation to OA? What is the relative contribution of photochemical vs. aqueous-phase oxidation to the concentration and evolution of OA?

Response: Frankly, the contributions of different formation pathways have not been quantified yet, and it is difficult to give a quantitative result for the relative contribution of photochemical vs. aqueous-phase oxidation to the secondary formation based on field observation data only. Further studies including laboratory experiments, field observations and model simulations are needed to close the gaps in the current understanding of SOA formation pathways (Ervens et al., 2011).

Based on laboratory experiments and simulations, Ervens et al. (2011) suggest that SOA formed in cloud and aerosol water (aqSOA) might contribute almost as much mass as SOA formed in the gas phase to the SOA budget, with highest contributions from biogenic emissions of VOCs in the presence of anthropogenic pollutants (i.e., NO_x) at high RH and cloudiness. Xu et al. (2017) show that aqueous-phase processes have a dominant impact on the formation of MO-OOA, and the contribution of MO-OOA to OA increases substantially as a function of RH or liquid water content (LWC) in aerosols. In contrast, photochemical processing plays a major role in the formation of LO-OOA, as indicated by the strong correlations between LO-OOA and odd oxygen (O_x=O_3+NO_2) during periods of photochemical production.

Here the LWC in aerosols in this study was roughly estimated with the ISORROPIAII model. The input data were the four species (sulfate, nitrate, ammonium and chloride) measured by the AMS, RH and temperature. The reverse mode and the metastable state of aerosols were selected. According to the results, the ambient aerosols were generally in aqueous phase. The average values of aerosol LWC in four seasons were 17.3±28.5, 18.8±24.9, 12.8±27.3 and 25.2±32.8 μg m^{-3}, respectively. During the heavy-polluted episodes, the LWC was frequently higher than 100 μg m^{-3}.

Table S14 shows the correlation coefficients between OOA and some indicators (RH, LWC, O_3 and O_x). The good correlations between OOA and RH and/or LWC indicate that aqueous-phase reactions play a more significant role in OOA formation. The slope of OOA against O_x steepened with the increase of RH and LWC (Figs. S41 and S42), also implying that the

aqueous-phase oxidation was an important pathway of the OOA formation. The strong correlations between total oxidant (O_x) and LO-OOA in summer, and between O_x and OOA in autumn and winter, suggesting photochemical processes contributed substantially to OOA, especially LO-OOA, in these seasons.

Table S14. Pearson correlation coefficients between secondary organic and inorganic species and some indicators (RH, LWC, O_3 and O_x). Coefficients greater than 0.5 are in bold. Correlation is significant at the 0.01 level (2-tailed) except for those marked by $^{\#}$.

		RH	LWC	O_3	O_x
Spring	OOA	**.661**	**.754**	-.199	.345
	SO_4^{2-}	**.764**	**.901**	-.207	.186
	NO_3^-	**.705**	**.827**	-.318	.254
Summer	MO-OOA	.176	**.751**	.131	.264
	LO-OOA	.005$^{\#}$	.469	.360	**.527**
	SO_4^{2-}	.114	**.686**	.262	.359
	NO_3^-	.335	**.873**	-.123	.000$^{\#}$
Autumn	OOA	.483	**.803**	-.433	**.571**
	SO_4^{2-}	**.552**	**.919**	-.340	.338
	NO_3^-	.489	**.854**	-.379	**.548**
Winter	MO-OOA	**.624**	**.647**	-.504	**.640**
	LO-OOA	**.692**	**.840**	-.534	**.726**
	SO_4^{2-}	**.801**	**.899**	-.613	**.597**
	NO_3^-	**.785**	**.819**	-.637	**.655**

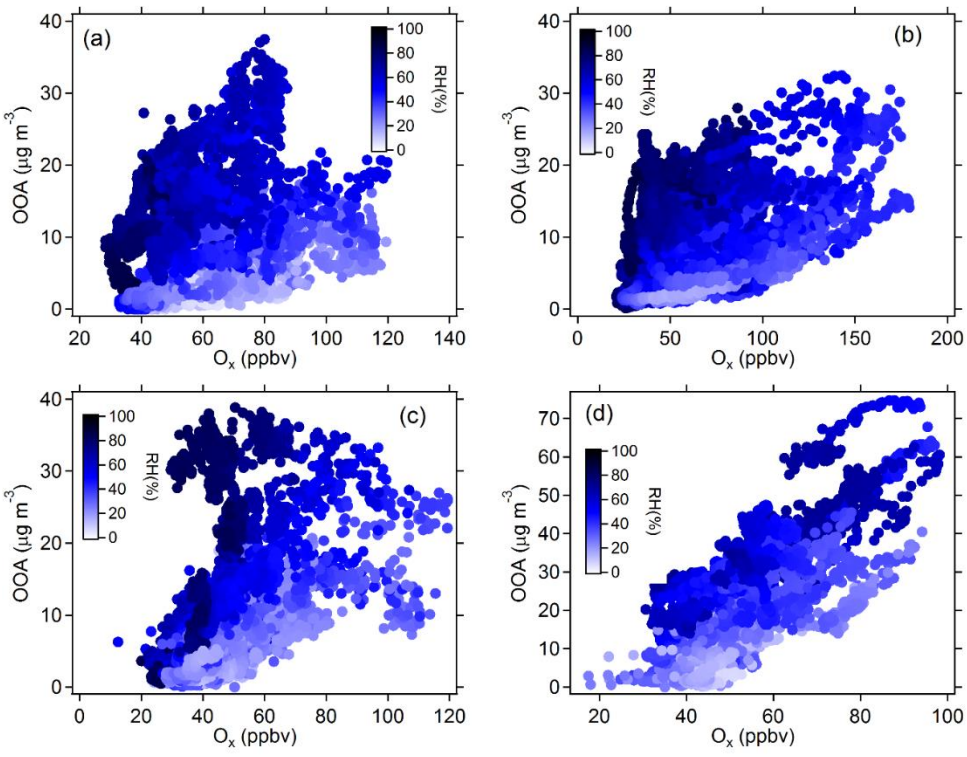

Figure S41. Scattering plots of OOA mass concentrations against O_x concentrations. (a)

spring; (b) summer; (c) autumn and (d) winter. Data points are color coded by RH.

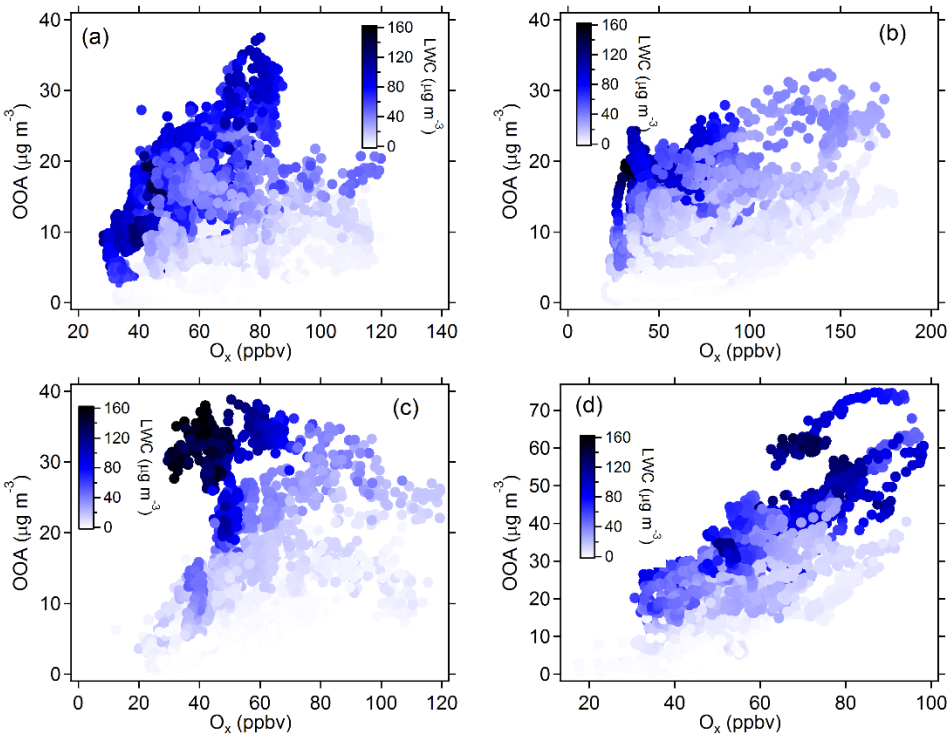

Figure S42. The same as above. Data points are color coded by estimated LWC in aerosols.

In the revision, the related content above is added in Sect. S5 in the Supplement.

In the abstract, "***It was indicated by the good correlations (Pearson correlation coefficients r=0.53–0.75, p<0.01) between LO-OOA and odd oxygen (O_x=O_3+NO_2), and between MO-OOA and liquid water content in aerosols.***" was added.

In the manuscript, "***OOA had strong correlations with RH and/or LWC (Table S14), indicating that aqueous-phase reactions play a dominant role in OOA formation. The slope of OOA against O_x steepened with the increase of RH and LWC (Figs. S41 and S42), also implying that the aqueous-phase oxidation was an important pathway of the OOA formation. The good correlations (r=0.53–0.73, p<0.01) between O_x and LO-OOA in summer, and between O_x and OOA in autumn and winter, suggesting photochemical processes also contributed substantially to SOA, especially LO-OOA, in these seasons.***" was added in Line 17, Page 16.

2. Page 6, "In spring, summer and winter, SNA accounted for about 60% in PM_1 due to the secondary aerosol formation through strong photochemical and aqueous-phase reactions." Like OA, what is the relative contribution of photochemical vs. aqueous-phase oxidation to the

concentration and evolution of SNA?

Response: As mentioned in the response to comment 1, the contributions of photochemical and aqueous-phase oxidation to the concentration and evolution of SNA have not been quantified yet.

It is well known that most of aerosol sulfate are formed from heterogeneous or aqueous-phase/cloud processes (Kulmala et al., 2016). On a global scale, about 80% of the sulfate formation occurs within clouds. Ambient aerosol populations often show two distinct submicron modes (<0.2 μm and 0.5–1 μm) where the larger (droplet) mode is formed from the smaller (condensation) mode through volume-phase reactions in clouds and wet aerosols (Ervens et al., 2011). Based on this assumption, Guo et al. (2010) found that the gas-to-particle condensation process was important for aerosol pollution in the summer of Beijing. In urban Beijing, the formation of sulfate was mainly attributed to in-cloud or aerosol droplet process (80%) and gas condensation process (14%).

As shown in Table S14, sulfate and nitrate correlated well with RH and/or LWC in four seasons, indicating that the aqueous-phase reactions in aerosols played an important role in secondary inorganic formation in Beijing. The contributions of photochemical processes to sulfate and nitrate in four seasons were probably less than those of aqueous-phase reactions according to the weaker correlations between secondary inorganics and O_x. Especially, in summer nitrate showed no correlation with O_x.

As shown in Fig. S40, when RH was higher than 40% (or 30% in winter), aqueous-phase processed likely played a dominant role in secondary inorganic formation.

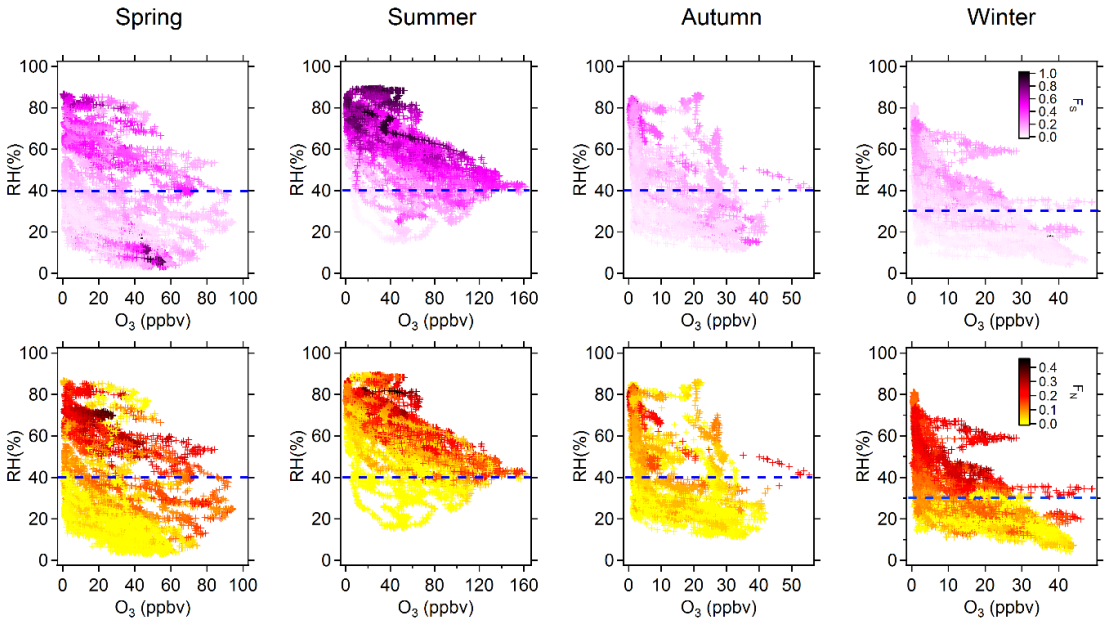

Figure S40. Influences of RH and O_3 concentrations on sulfate and nitrate formation.

Conversion ratios for sulfur and nitrogen (F_S and F_N) were calculated as follows:

$$F_S = \boldsymbol{n} - SO_4^{2-}/(\boldsymbol{n} - SO_4^{2-} + \boldsymbol{n} - SO_2) \quad (3)$$

$$F_N = \boldsymbol{n} - NO_3^{-}/(\boldsymbol{n} - NO_3^{-} + \boldsymbol{n} - NO_2) \quad (4)$$

where *n* means the amount of substance of the gaseous and particulate pollutants, mol m^{-3}.

Table S15 Pearson correlation coefficients between F_S and F_N with RH, LWC, O_3, O_x and NH_4^+.

	Spring		Summer		Autumn		Winter	
	F_S	F_N	F_S	F_N	F_S	F_N	F_S	F_N
RH	.339	**.722**	**.639**	.393	.432	**.574**	**.531**	**.744**
LWC	.475	**.816**	.464	**.816**	**.647**	**.874**	**.583**	**.676**
O_3	.024*	-.146	-.100	.024*	.035	-.321	-.268	-.518
O_x	-.166	.277	-.096	.052	-.122	.359	.342	.368
NH_4^+	.324	**.924**	.353	**.822**	.495	**.938**	**.598**	**.855**

Note: Coefficients greater than 0.5 are in bold. Correlation is significant at the 0.01 level (2-tailed) except for those marked with *.

The good correlation between F_N/F_S and RH/LWC also support that aqueous-phase reactions in aqueous aerosols and/or clouds could contribute to secondary inorganic formation remarkably in highly humid air.

In the revision, the related content above is added in Sect. S10 in the Supplement.

In the manuscript, "*In spring, summer and winter, SNA accounted for about 60% in PM_1 due to the secondary aerosol formation through strong photochemical and aqueous-phase reactions.*" was changed to "***In four seasons, SNA accounted for about 40–60% in PM_1. Secondary inorganics (sulfate and nitrate) correlated well with RH and/or LWC (Table S14), indicating that aqueous-phase reactions in aerosols played an important role in secondary inorganic formation in Beijing. The contribution of photochemical processes to secondary inorganics was likely less than those of aqueous-phase reactions according to the weaker correlations between secondary inorganics and odd oxygen (O_x=O_3+NO_2). Especially, nitrate did not correlate with O_x in summer (Table S14).***"

3. Page 6, "Wang et al. (2016) and Cheng et al. (2016) found that high levels of sulfate and fine PM can be explained by reactive aqueous oxidation of SO_2 by NO_2 under certain atmospheric conditions." Please elaborate what the meaning of "certain atmospheric conditions". How frequent these atmospheric conditions occur during the field campaign?

Response: Wang et al. (2016) showed that the aqueous oxidation of SO_2 by NO_2 is key to

efficient sulfate formation but is only feasible under two atmospheric conditions: on fine aerosols with high relative humidity and NH_3 neutralization or under cloud conditions. Similarly, Cheng et al. (2016) found that high reaction rates of SO_2 oxidized by NO_2 to form sulfate are sustained by the high neutralizing capacity of the atmosphere in northern China. This mechanism is self-amplifying because higher aerosol mass concentration corresponds to higher aerosol water content, resulting in faster sulfate production and more severe haze pollution. In summary, the certain atmospheric conditions represent the fine aerosols with high aerosol water content and NH_3 neutralization or under cloud conditions. These two studies included field observations conducted in urban area of Beijing. The PM pollution episodes exhibit a periodic cycle of several days (Guo et al., 2014; Fig. S6–S9), i.e., these atmospheric conditions occur quite often during the field campaigns.

In the revision, "*Wang et al. (2016) and Cheng et al. (2016) found that high levels of sulfate and fine PM can be explained by reactive aqueous oxidation of SO_2 by NO_2 under certain atmospheric conditions*" was changed to "***Recently it was found that high levels of sulfate and fine PM in northern China can be explained by reactive aqueous oxidation of SO_2 by NO_2 under certain atmospheric conditions, i.e., on the fine aerosols with high aerosol water content and NH_3 neutralization or under cloud conditions (Cheng et al., 2016; Wang et al., 2016)***".

4. Page 6, "Compared with the previous results in Beijing (Fig. 1), PM_1 in summer was lower than before, which likely resulted from the more effective rainout (Fig. S7) and lower concentrations of gaseous precursors (Table 1)." What are the frequency of precipitation/rainout and the concentration of gaseous precursors reported in previous studies?

Response: The time series of meteorological conditions and submicron aerosol species during 9 to 21 July 2006 (Sun et al., 2010) and 26 June to 28 August 2011 (Sun et al., 2012) are copied as follows. It is likely that the concentration of submicron aerosols was reduced litter by washout in some rain events (e.g., 13 and 18 Jul. 2006). So, we hypothesized that "*PM_1 in summer was lower than before, which **likely** resulted from the more effective **washout** (Fig. S7)*".

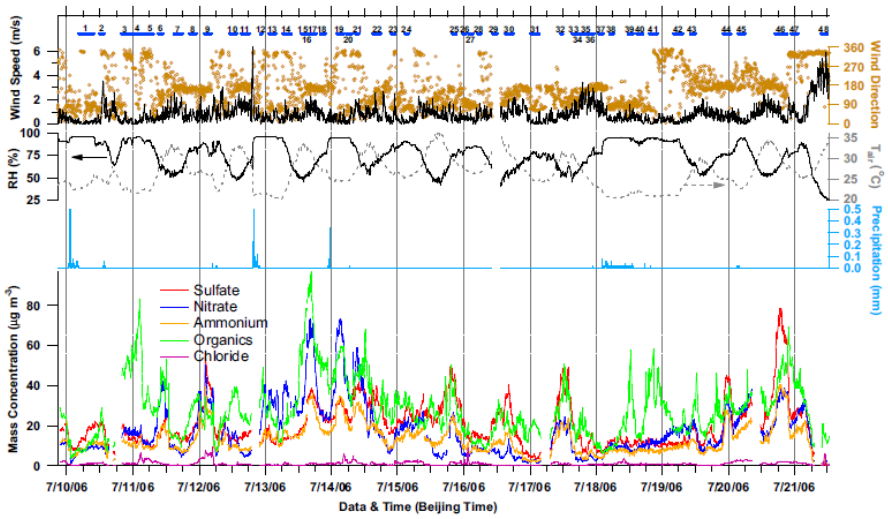

Figure R1. Time series of meteorological conditions and submicron aerosol species during 9 to 21 July 2006 (Sun et al., 2010).

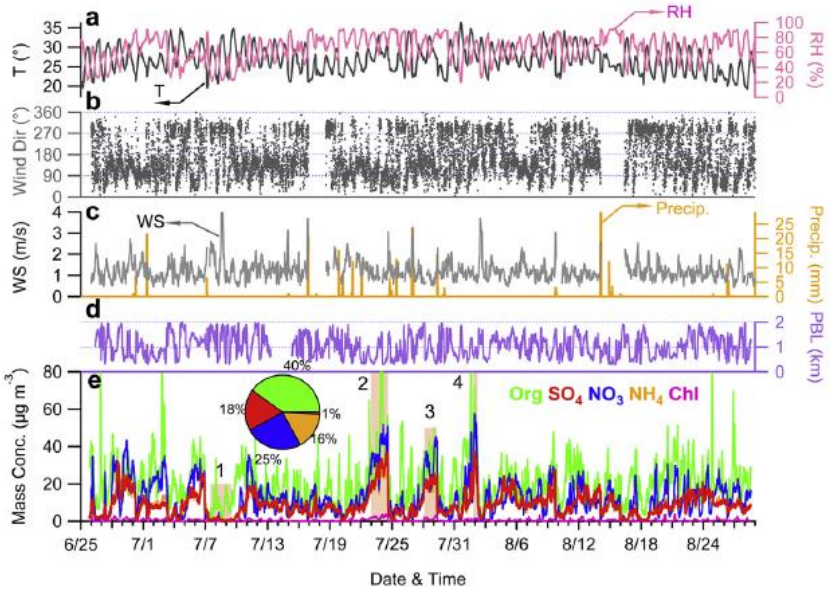

Figure R2. Time series of meteorological conditions and submicron aerosol species during 26 June to 28 August 2011 (Sun et al., 2012).

Compared with the previous results of gaseous precursors (SO_2 and NO_x) during July-August 2011 and June 2012 (Sun et al., 2015), the concentrations in this study were lower (Table R1).

In the revision, "*rainout*" was corrected to "***washout***"; "*(Table 1)*" was changed to "***(Table 1 and Table 1 in Sun et al. (2015))***".

Table R1. Comparison of the concentrations of gaseous pollutants during July-August 2011 and June 2012 (Sun et al., 2015), Aug.–Sept. 2011(Hu et al., 2016) and Jul. 29–Aug. 29 2012 (this study).

	Jul.-Aug. 2011, Jun. 2012	Aug.–Sept. 2011	Jul. –Aug. 2012
SO_2 (ppb)	5.4±0.8	4.4±2.6	3.1±3.3
CO (ppm)	1.8±1.3	0.9±0.5	0.7±0.3
NO (ppb)	7.8±10.8	8.0±14.5	3.5±6.6
NO_y (ppb)	35.6±17.9	35.6±21.6 (NO_2)	30.1±17.5
O_3 (ppb)	33.3±29.1	63.2±30.6	41.6±34.7

5. Page 7, "While, PM_1 ranged much more broadly, with the highest concentrations of over 200 or 300 μg m^{-3}, resulting from accumulated pollutants under extremely unfavorable meteorological conditions or strong primary emissions." What is "the extremely unfavorable meteorological conditions"?

Response: "*extremely unfavorable meteorological conditions or strong primary emissions*" was changed to "***strong primary emissions coupled with extremely unfavorable meteorological conditions, e.g., long-lasting stagnant weather, high humidity, and temperature inversion.***"

6. Page 7, "The proportions of nitrate increased more significantly, and the nitrate concentration increased rapidly under higher RH (Fig. 2; Pearson correlation coefficients r=0.71, 0.34, 0.49 and 0.79, $p<0.01$). These results indicate that the aqueous reactions could contribute to nitrate remarkably in highly humid and static air." What are the aqueous reactions referring to? Aerosol phase reactions, in-cloud reactions or both? Ambient RH is a good proxy for indicting the occurrence and importance of aqueous phase reactions. However, what the physical state of the ambient aerosols (e.g. aqueous or solid)? What is the aerosol water content inferred or predicted from the aerosol speciation data and meteorological conditions? Will the water content and physical state of the aerosols play a role in the aqueous phase reactions and nitrate formation? If the aqueous phase reactions involve in-cloud reactions, any data (e.g. cloud coverage) can be used to support the importance of in-cloud reactions to the formation of nitrate and organic compounds during the campaign?

Response: Aqueous-phase uptake (in clouds or aqueous aerosols) of nitric acid and condensation onto preexisting particles are two possible pathways to form fine mode nitrates (Guo et al., 2010). In this study, whether the aqueous-phase reactions were aerosol phase

reactions, in-cloud reactions or both was not considered.

As mentioned in the response to Comment 1 and 2, the liquid water content (LWC) in aerosols was roughly estimated with the ISORROPIAII model. According to the results, the ambient aerosols were generally in aqueous phase. The Pearson correlation coefficients between nitrate and LWC in four seasons were 0.827, 0.873, 0.854 and 0.819 (p<0.01), respectively, indicating that the aqueous-phase reactions in aerosols played an important role in nitrate formation in Beijing. The good correlation between F_N and RH/LWC also support that aqueous-phase reactions in aqueous aerosols and/or clouds could contribute to nitrate remarkably in highly humid air.

In the revision, the average LWC was added in Table 1.

"*The proportions of nitrate increased more significantly, and the nitrate concentration increased rapidly under higher RH (Fig. 2; Pearson correlation coefficients r=0.71, 0.34, 0.49 and 0.79, p<0.01). These results indicate that the aqueous reactions could contribute to nitrate remarkably in highly humid and static air.*" was changed to "***The proportions of nitrate increased significantly, and the nitrate concentration increased rapidly under higher RH (Fig. 2 and Fig. S6–S9). Nitrate showed good correlations with RH (Pearson correlation coefficients r=0.34–0.79, p<0.01) and the LWC in aerosols (r=0.82–0.87, p<0.01). These results indicate that the aqueous-phase reactions in wet aerosols and/or clouds could substantially contribute to nitrate formation.***"

7. Page 8, "The peak concentration of OA in the evening in autumn was about two times higher than in spring and summer, consistent with the results in Oct.-Nov. 2011 (Sun et al., 2015), possibly because of the more intense cooking activities." Please elaborate why there is more instance cooking activity in the evening in autumn, but not in other seasons?

Response: In contrast to other seasons (including spring, summer and winter), the weather conditions in autumn are more moderate and pleasant (Table 1). As mentioned in the manuscript, "*In autumn charcoal-grilling or barbecuing has become one of the most popular outdoor recreational activities in urban Beijing and surrounding areas.*"

In the revision, "***In autumn, charcoal-grilling or barbecuing has become one of the most popular outdoor recreational activities in urban Beijing and surrounding areas, due to more moderate and pleasant weather conditions than in other seasons (Table 1).***" was moved from Page 17 to Page 9.

Page 18, "*in autumn charcoal-grilling or barbecuing has become one of the most popular outdoor recreational activities in urban Beijing and surrounding areas, which could be an important source of COA.*" was changed to "***in autumn intensive barbecue activities in urban Beijing and surrounding areas could be an important source of COA as mentioned above.***"

8. Page 11, "LO-OOA dominated OA in summer (44%) due to the freshly secondary formation from strong photochemical oxidations; whereas, MO-OOA was dominant in OA in winter (33%), maybe because the air masses were more aged on heavy-polluted days." Please elaborate why the air masses are more aged on the heavy-polluted days in winter, but not in other seasons?

Response: After deeper discussion among coauthors, we think this comparison is arguable because the oxidation degrees of LO-OOA and MO-OOA during summer and winter were different. So, in the revision, we **removed** these contents.

9. Page 13, "Fewer cooking activities during and around the Chinese New Year holiday (7-19 Feb.; Fig. S17), as well as the lower evaporation rate of oil, led to the lower concentration and proportion of COA in winter." This argument is interesting. How does the evaporate rate of oil depend on the temperature? What the contribution of this evaporation process to the total volatile organic compounds generated/originated from the cooking activities?

Response: In China, both vegetable oils and animal fats are commonly used as cooking oils. In China, village residents use homemade vegetable oils and animal fats in cooking, and store them in the kitchens for several months even longer than one year. The edible oils partially evaporate very slowly over months to years leaving a sticky varnish on the inner wall of the container. The odors of stored cooking oils can be more obviously smelt in summer than in winter. Thus, the evaporation process of cooking oils is much slower and significantly less visible in winter.

Vegetable oils and animal fats used in cooking contain saturated and unsaturated fatty acid esters of glycerol. The Clausius–Clapeyron relation for a system consisting of vapor and liquid of a pure substance is in applicable to cooking oils. Several previous studies (e.g., Ndiaye et al., 2005; Murata et al., 1993) measured the vapor pressures of some kinds of edible oils at different temperatures. For vegetable oils, vapor pressure values varied in the range of 0.19–2.16 kPa, whereas for fatty acid ethyl ester (FAEE) mixtures a maximum value of 4.85 kPa was found (Ndiaye et al., 2005).

The vapor pressures of edible oils at different temperatures measured by Ndiaye et al. (2005) are listed as follows:

Table R2. Experimental vapor pressure data for soybean oil, castor oil, and their FAEE derivatives.

soybean oil			castor oil			FAEE from soybean oil			FAEE from castor oil		
	p/kPa			*p*/kPa			*p*/kPa			*p*/kPa	
T/K	measured	σ	*T*/K	measured	σ	*T*/K	measured	σ	*T*/K	measured	σ
294.1	0.354	0.019	299.1	0.192	0.023	290.4	0.437	0.035	290.7	0.259	0.006
299.5	0.453	0.015	304.2	0.258	0.009	294.6	0.549	0.018	293.7	0.323	0.017
304.0	0.543	0.043	308.9	0.328	0.003	299.5	0.718	0.014	298.0	0.427	0.053
309.3	0.661	0.075	313.6	0.416	0.021	304.7	0.916	0.033	303.8	0.577	0.084
313.8	0.753	0.083	319.1	0.529	0.032	309.0	1.144	0.077	308.9	0.753	0.126
318.8	0.892	0.114	323.5	0.647	0.049	314.5	1.447	0.086	313.7	0.951	0.167
323.5	1.033	0.140	329.2	0.806	0.048	319.5	1.781	0.086	318.5	1.198	0.214
328.7	1.195	0.151	334.0	0.979	0.053	324.3	2.196	0.104	323.4	1.505	0.267
333.9	1.364	0.146	339.2	1.182	0.031	328.9	2.652	0.091	328.0	1.857	0.315
338.7	1.513	0.111	344.2	1.402	0.020	334.4	3.228	0.025	333.2	2.301	0.337
344.0	1.717	0.073	348.2	1.648	0.031	338.9	3.958	0.014	338.6	2.806	0.273
348.9	1.962	0.063	354.0	1.950	0.185	344.3	4.658	0.165	343.5	3.415	0.224
353.2	2.155	0.006							348.5	4.000	0.044
									354.6	4.848	0.540

Because edible oils have significantly lower evaporation rates than isoviscous hydrocarbon and synthetic base fluids at room temperatures, the contribution of the evaporation process to the total VOCs generated/originated from the cooking activities might be insignificant. Further studies are essential to confirm it.

In the revision, "*as well as the lower evaporation rate of oil*" was changed to "***and the lower evaporation rates of cooking oils (Ndiaye et al., 2005)***".

10. Page 16" In summer, OOA showed obvious diurnal variations: MO-OOA peaked in the morning and afternoon; LO-OOA showed two pronounced peaks at noon and at night, which was likely influenced by the photochemical oxidations and aqueous-phase formation from POA." It is not clear why the formation of LO-OOA is likely influenced by the photochemical oxidations and aqueous-phase formation from POA. Any other processes that can be contributed to the formation and transformation of LO-OOA?

Response: LO-OOA is usually considered to be fresh SOA. Traditionally, SOA is formed from gas-phase oxidation, heterogeneous reactions on aerosol surfaces, and multiphase chemistry of gas-phase organic compounds (Kroll et al., 2005; Hallquist et al., 2009). It has been recognized that a substantial fraction (50–75%) of POA is semivolatile. This fraction of POA evaporates when the plume becomes more dilute, and is then available in the gas phase to take part in photochemical reactions, producing SOA far exceeding that from traditional precursors (Robinson et al., 2007; Shrivastava et al., 2006). Murphy and Pandis (2009) define that oxidized

POA (OPOA) refers to POA compounds that evaporate and undergo oxidation in the gas phase, which allows them to reduce their volatility and re-condense back to the particulate phase. SOA produced from the oxidation of intermediate-volatility compounds (IVOCs) was also included in OPOA mainly because the IVOC emissions were calculated based on the POA emissions (Fountoukis et al., 2014).

In addition to SOA formation in the gas phase (gasSOA), SOA (aqSOA) forms in the aqueous phase of cloud/fog and aerosol water through complex chemical reactions. Based on model studies, Ervens et al. (2011) compared aqSOA and gasSOA yields and mass predictions for selected conditions, and suggest that aqSOA might contribute almost as much mass as gasSOA to the SOA budget.

As mentioned above in the response to Comment 1, in summer, LO-OOA correlated well with O_x (r=0.53, p<0.01) and LWC (r=0.47, p<0.01).

In the revision, "*In summer, OOA showed obvious diurnal variations: MO-OOA peaked in the morning and afternoon; LO-OOA showed two pronounced peaks at noon and at night, which was likely influenced by the photochemical oxidations and aqueous-phase formation from POA.*" was changed to "***In summer, OOA showed obvious diurnal variations: MO-OOA peaked in the morning and afternoon; LO-OOA showed two pronounced peaks at noon and at night. This was likely the co-effect of SOA formation via gas-phase photochemical reactions in the daytime and aqueous chemistry in humid air at night (Ervens et al., 2011; Lim et al., 2010).***"

11. Page 16, "the concentration and proportion of LO-OOA increased significantly in the afternoon (12:00-16:00), up to 7 ug m^{-3} and 50%, respectively (Fig. 6b), suggesting that LO-OOA was a strong local/regional photochemical product despite the much higher PBL in the daytime (Hu et al., 2016a)" What is the contribution of regional transport to LO-OOA (and other components)?

Response: The contribution of regional (long-distance) transport to aerosol pollution is important for reducing regional air pollution under a joint control policy. The contributions of local/regional transport are difficult to quantify, however, even with transport models (Jia et al., 2008). In this study, this issue will not be focused on.

Please refer to the response to general comments for details.

In the revision, "***Regardless of the air mass history (local, regional and long-distance transported), LO-OOA dominated OOA, accounting for 29–48% of OA (Fig. S43).***" was

added in Line 20, Page 17.

12. Page 17, "In both autumn and winter, the fractions of OOA slightly increased around 100 ug m^{-3}, implying that POA probably transformed to SOA more effectively within this range." Please elaborate why the POA is more likely transformed to SOA under these conditions. What mechanisms or pathways?

Response: As mentioned in the response to Comment 10, it has been found that a substantial fraction (50–75%) of POA is semivolatile, evaporates when the plume becomes more dilute, and is then available in the gas phase to take part in photochemical reactions (Shrivastava et al., 2006; Robinson et al., 2007). This material has the physicochemical properties of SOA. Murphy and Pandis (2009) define that fresh POA is emitted in the particulate phase and has not undergone chemical processing, while oxidized POA (OPOA) refers to POA compounds that evaporate and undergo oxidation in the gas phase, which allows them to reduce their volatility and re-condense back to the particulate phase. SOA produced from the oxidation of intermediate-volatility compounds (IVOCs) was also included in OPOA mainly because the IVOC emissions were calculated based on the POA emissions (Fountoukis et al., 2014). Intermediate-volatility organic compounds (IVOCs) have been proposed to be an important source of SOA (Zhao et al., 2014).

SOA chemistry is complex and the contribution of different pathways is not well understood. More work is needed to accurately identify the volatility and aging of primary emissions, and to quantify the contributions of SOA from different sources and formation mechanisms.

In this study, we have no strong evidence to elaborate the mechanisms or pathways. We only give our hypothesis in this sentences.

In the revision, "*In both autumn and winter, the fractions of OOA slightly increased around 100 μg m^{-3}, implying that POA probably transformed to SOA more effectively within this range*" was changed to "***In both autumn and winter, the fractions of OOA slightly increased around 100 μg m^{-3}. More work is needed to accurately clarify the cause of the OOA increase within this range.***"

13. Page 18, "In spring, summer and autumn, the slopes fell between -1 (the addition of carboxyl functional groups without fragmentation or carbonyl and hydroxyl in different carbons) and -0.5 (carboxyl functionalization with fragmentation)." In addition to overall oxidation pathways,

what other information we could learn from the reported slopes between -1 and -0.5? Are these pathways consistent with the reactions we expected for the formation and chemical transformations of ambient aerosols in Beijing?

Response: We did not do chamber experiments to verify the consistency between measurements and simulation. Currently there is no substantial progress on the issue of specific oxidation pathways.

A large data set including surface, aircraft, and laboratory studies of the atomic O/C and H/C ratios of OA is synthesized by Heald et al. (2010) and Chen et al. (2015). The overall fit for ambient data characterizes measurements that span a wide range of OA oxidation, and the complex chemical evolution of OA in the atmosphere could be simply represented in models. Chen et al. (2015) show that laboratory OA including both source and aged types explains some of the key differences in OA observed across different environments. However, the comparisons also reveal significant gaps between ambient and laboratory measured OA composition.

More works are required to bridge the gaps. For instance, it is needed to characterize the yields and bulk composition of SOA produced by aqueous-phase reactions under atmospherically relevant conditions (Chen et al., 2015). In addition, a complete description of OA processing must link the compositional changes with key physical properties (e.g., volatility, hygroscopicity, light absorption) of the aerosol (Heald et al., 2010).

14. Page 19, "In winter, the scatterplot of H/C vs. O/C ratios in the VK Diagram showed "broader" slopes, hinting the more complex sources and evolution processes of OA. The scatterplot indicated that OA in winter mainly evolved between the hydroxylation or peroxidation reactions (slope = 0) and carboxyl groups addition with fragmentation (slope = -0.5)." Any hypothesis or explanation for the complex sources and evolution process of OA in the winter. Why these processes have not been observed or suggested in the other seasons?

Response: As mentioned above in the response to Comment 13, there is no substantial progress on explicating specific oxidation pathways for OA evolution. In winter, CCOA was resolved by the PMF analysis, which was different from other seasons. This is a possible reason these processes were not suggested in the other seasons.

In the revision, "*However, in winter, the correlation was not good (r^2 = 0.02), with a fitted slope -0.08, exhibiting a "broader" range in the VK Diagram than in other seasons (Fig. 8 and Fig. S21)*" was changed to "***However, the VK diagram in winter (Fig. 8 and Fig. S39) does not show any correlation (r^2 = 0.02) between H/C and O/C. The slope is nearly zero (-0.08). This***

is possibly caused by the more complex sources of OA in winter, e.g., CCOA was only resolved in winter" in Line 24, Page 19.

"*In winter, the scatterplot of H/C vs. O/C ratios in the VK Diagram showed "broader" slopes, hinting the more complex sources and evolution processes of OA. The scatterplot indicated that OA in winter mainly evolved between the hydroxylation or peroxidation reactions (slope = 0) and carboxyl groups addition with fragmentation (slope = -0.5).*" was changed to "***In winter, the nearly zero slope of the VK Diagram suggests that hydroxylation and/or peroxidation processes (slope = 0) were likely to occur in Beijing during winter. On the other hand, carboxylation process might be unlikely to occur since the slope is higher than -0.5.***" in Line 4, Page 20.

15. Page 19, "compared with the oxidation states of SV-OOA, OOA and LV-OOA summarized by Canagaratna et al. (2015), the oxidation states of OOA in Beijing were generally higher than in other areas, especially for LO-OOA (Fig. 8). The oxidation states of MO-OOA in Beijing were only lower than those in very aged air masses in Ziyang in the basin (Hu et al., 2016b), over Mexico City (DeCarlo et al., 2010) and in Barcelona (Mohr et al., 2012). The oxidation states of LO-OOA were only slightly lower than those of MO-OOA in Beijing, and were comparable to those of MO-OOA in other urban areas (Fig. 8)." It is nice to compare the data with those collected at different locations. However, without explaining the causes/reasons for the differences would not be useful for the readers to understand the formation and evolution of atmospheric aerosols.

Response: The possible reasons for relatively higher oxidation states of OA in Beijing could be the high hygroscopicity of aerosols and high OH radical concentration in air (Jimenez et al., 2009). As mentioned above, the average values of LWC in aerosols were 17.3±28.5, 18.8±24.9, 12.8±27.3 and 25.2±32.8 μg m^{-3} in four seasons, respectively. During the heavy-polluted episodes, the LWC was frequently higher than 100 μg m^{-3}. Sorooshian et al. (2010) found an important dual role of both ambient RH and hygroscopicity in leading to an enrichment of oxygenated OA. Faust et al. (2017) found that 13% and 19% enhancements in relative SOA yield for the α-pinene and toluene systems, respectively, when ammonium sulfate seeds were deliquesced (~20 μg m^{-3} LWC) rather than effloresced (~0.2 μg m^{-3} LWC) effloresced. Wu et al. (2016) found that the organic hygroscopicity parameter (κ_{org}) showed a positive correlation with the O/C ratio in the summer of Beijing. Relationship between O:C and hygroscopicity (κ, or equivalently the particle growth factor at 95% relative humidity) of OA for several field data sets showed a robust trend of increasing hygroscopicity with increasing O/C (Jimenez et al.,

2009).

Lim et al. (2010) suggest that reactions with OH radicals tend to be faster and form more SOA than non-radical reactions. High daily maximum concentrations ($0.5–1.5\times10^7$ cm^{-3}) for OH were observed in the North China Plain (Lu et al., 2013; Tan et al., 2017). During daytime, OH reactivities (inverse OH lifetime) were generally high (10–30 s^{-1}).

In the revision, "***The possible reasons for relatively higher oxidation states of OA in Beijing could be the high hygroscopicity of aerosols and high OH radical concentration in air (Jimenez et al., 2009). The trend of increasing hygroscopicity with increasing O/C is robust based on field observations in Beijing and at several other sites (Jimenez et al., 2009; Wu et al., 2016). Xu et al. (2017) suggest a major role of aqueous-phase processes in increasing the oxidation degree of SOA in Beijing based on the consistency of higher O/C of SOA and higher RH. Lim et al. (2010) suggest that reactions with OH radicals tend to be faster and form more SOA than non-radical reactions. High daily maximum concentrations (0.4–1.7×10^7 cm^{-3}) for OH were observed in the North China Plain (Lu et al., 2013; Tan et al., 2017).***" was added in Line 24, Page 20.

Thank you very much for your comments and suggestions. Your any further comments and suggestions are appreciated.

Referee #3

This manuscript by Hu et al. presents a comprehensive study on chemical compositions, sources and evolution for atmospheric submicron aerosols in the megacity Beijing in four seasons. Following typical AMS analysis, the source and evolution process of aerosol, especially OA in different seasons are discussed. The contributions of primary and secondary PM are also examined. With the wealth of AMS and ACSM studies in many locations including Beijing city, I was hoping for some unique discussions or scientific insights that were not available in the literature already. In particular, there are a lot of ACSM studies in Beijing in the literature that provide very similar analyses and results of the current paper. The additional analysis of OSc etc with the HR data is very similar to what has been published by many others. While the paper is well written and generally clear, the paper needs to be improved in emphasizing more on new science and insights of the work beyond our current understanding of PM in Beijing.

Response: Thank the reviewer very much for the helpful comments. In previous studies, the studies conducted in spring and autumn are relatively lacking, this study might be a supplementary of previous studies. As the general comment of Reviewer#2 said, "While field measurements have been carried out by other groups in this city, this work provides a more comprehensive exploration of organic aerosol composition and evolution." "The measurements provide sufficiently new data…" After response to all the comments of three reviewers and revised the manuscript correspondingly, we hope the quality of this manuscript has been improved.

Some other comments below:

1. Page 7, Line 11-12, please show the satellites data in the supporting information.

Response: The maps of fire points from satellites were added in the supplementary material. Please refer to the response to Technical Comment 6 of Reviewer#1.

2. Page 7, Line 14-15, have the authors examined the contributions of organic nitrate to the high nitrate concentration associated with biomass burning?

Response: In this study, as the title shown, we mainly focused on "*Seasonal variations of high time-resolved chemical compositions, sources and evolution for atmospheric submicron aerosols in the megacity Beijing*". So, we did not mention the details of the contributions of organonitrate (ON) to the high nitrate concentration.

We tried to examine the contributions of organic nitrate during the autumn observation. The concentration of ON was estimated using the PMF analysis including the mass spectra of OA, NO^+ and NO_2^+ (Sun et al., 2012; Xu et al., 2015; Zhang et al., 2016). As the factor of nitrate inorganic aerosol (NIA) was resolved, it is considered that the NO^+ and NO_2^+ in other OA factors were from ON. The concentration of ON was estimated using the following equations:

$$NO_{org}^{+} = \sum([OA\ \ factor]_i \times f\ \ NO^{+}{}_i) \quad (1)$$

$$NO_{2,org}^{+} = \sum([OA\ \ factor]_i \times f\ \ NO_2^{+}{}_i) \quad (2)$$

The estimated results are shown in Fig. R3. The contributions of ON to OOA, BBOA and COA factors were 0.4, 0.3 and 0.1 μg m^{-3}. On average, ON accounted for about 10% of nitrate measured by the AMS. There are some limitations of the estimation method, such as the collinearity of ion fragments and the PMF analysis lacking the knowledge of standard spectra of different sources, which may result in uncertainties. So, we omitted the related contents in the manuscript.

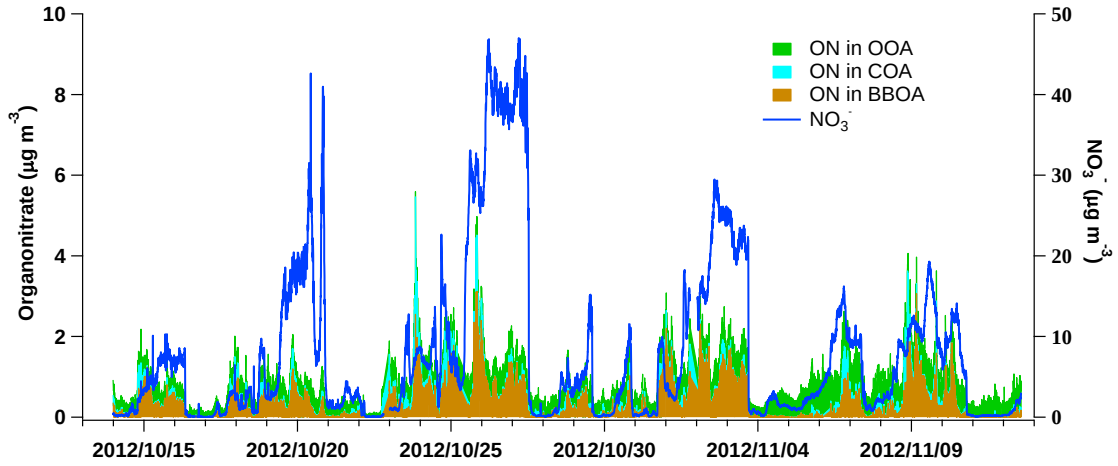

Figure R3. Estimated organonitrate concentrations in resolved OA factors and nitrate directly measured by the AMS.

3. Page 8, Line 1-3, it would be useful to show the correlations of nitrate with RH under high and low RH conditions in addressing the point that aqueous reactions could contribute to nitrate remarkably in highly humid and static air.

Response: Because under higher RH conditions (RH>60%), the ranges of the nitrate concentration are wide, the correlations between nitrate and RH were not good. Instead, we gave the Pearson correlation coefficients between the time series of nitrate and RH, as well as

Fig. 2 in the manuscript.

Conversion ratios for sulfur and nitrogen (F_S and F_N) were calculated as follows:

$$F_S = \boldsymbol{n} - SO_4^{2-}/(\boldsymbol{n} - SO_4^{2-} + \boldsymbol{n} - SO_2) \quad (3)$$

$$F_N = \boldsymbol{n} - NO_3^{-}/(\boldsymbol{n} - NO_3^{-} + \boldsymbol{n} - NO_2) \quad (4)$$

where *n* means the amount of substance of the gaseous and particulate pollutants, mol m^{-3}。

Table S15 Pearson correlation coefficients between F_S and F_N with RH, LWC, O_3, O_x and NH_4^+.

	Spring		Summer		Autumn		Winter	
	F_S	F_N	F_S	F_N	F_S	F_N	F_S	F_N
RH	.339	**.722**	**.639**	.393	.432	**.574**	**.531**	**.744**
LWC	.475	**.816**	.464	**.816**	**.647**	**.874**	**.583**	**.676**
O_3	.024*	-.146	-.100	.024*	.035	-.321	-.268	-.518
O_x	-.166	.277	-.096	.052	-.122	.359	.342	.368
NH_4^+	.324	**.924**	.353	**.822**	.495	**.938**	**.598**	**.855**

Note: Coefficients greater than 0.5 are in bold. Correlation is significant at the 0.01 level (2-tailed) except those marked with *.

The average values of LWC in aerosols in four seasons were 17.3±28.5, 18.8±24.9, 12.8±27.3 and 25.2±32.8 μg m^{-3}, respectively. The Pearson correlation coefficients between nitrate and LWC in four seasons were 0.827, 0.873, 0.854 and 0.819 (p<0.01), respectively, indicating that the aqueous-phase reactions in aerosols played an important role in nitrate formation in Beijing.

As listed in Table S15, the good correlations between F_N and RH/ LWC also support that aqueous-phase reactions in aqueous aerosols and/or clouds could contribute to nitrate remarkably in highly humid air.

In the revision, "***Nitrate showed good correlations with RH (Pearson correlation coefficients r=0.34–0.79, p<0.01) and the LWC in aerosols (r=0.82–0.87, p<0.01). These results indicate that the aqueous-phase reactions in wet aerosols and/or clouds could substantially contribute to nitrate formation.***" was added.

For more details, please refer to the response to Comment 6 of Referee#2.

4. Page 9 and Page 10, please clarify the calculation of the particle growth rate.

Response: We didn't e calculate the growth rates, and it is an inference. To avoid confusing, in the revision, this sentences was **removed**.

5. Have the authors tried more factors in PMF or using ME-2 to resolve a BBOA factor in spring and winter? In Page 22 and Figure 10, it seems that in both spring and autumn, a large number of data points affected by biomass burning. Further the author mentioned that in the satellites data, they identified some days with intense biomass burning activities in spring as well. In winter, it seems that HOA and CCOA spectra also bear some BBOA features.

Response: We tried more factors in PMF and didn't use ME-2 to resolve a BBOA factor in spring and winter. There were some episodes during the spring and winter observations affected by biomass burning. We are applying ME-2 to new datasets to look for minor sources in urban Beijing. In this study, we would like to keep using PMF analysis for OA factorization.

In the revision, after re-evaluation the PMF result, the five-factor solution is selected for the spring observation. Two similar OOA factors are combined. Finally, four components of OA were obtained, i.e., OOA, COA, HOA, and BBOA. However, the contributions of BBOA might be relatively limited during the winter campaign in Beijing, and the BBOA factor cannot be resolved in our dataset by free PMF. The resolved factors in winter were consistent with those in other studies (Fig. 5a). The processes of evaluating the PMF solution are available in the responses to Comment 8 of Reviewer#1.

The key diagnostic plots of the PMF analysis are shown in Sect. S5 in the supplement.

6. Page 16, Line 7-9, the authors state "the peaks of OOA (or LO-OOA) coincided with the peaks of primary emitted COA (spring, summer and autumn) and HOA (winter) in diurnal patterns, probably because strong primary emissions favored the partitioning of oxidized gas precursors to particulate phase" However, on Page 17, Line 7-8, the they also say "In both autumn and winter, the fractions of OOA slightly increased around 100 μg m^{-3}, implying that POA probably transformed to SOA more effectively within this range." Please clarify if it was POA transformed to SOA or primary emissions favored the partitioning of oxidized gas precursors to particulate phase for the increase of OOA.

Response: Traditionally, SOA is formed from gas-phase oxidation, heterogeneous reactions on aerosol surfaces, and multiphase chemistry of gas-phase organic compounds (Hallquist et al., 2009). It has also been recognized that a substantial fraction (50–75%) of POA is semivolatile, evaporates when the plume becomes more dilute, and is then available in the gas phase to take part in photochemical reactions (Shrivastava et al., 2006; Robinson et al., 2007). This material has the physicochemical properties of SOA. Murphy and Pandis (2009) define that fresh POA is emitted in the particulate phase and has not undergone chemical processing, while oxidized

POA (OPOA) refers to POA compounds that evaporate and undergo oxidation in the gas phase, which allows them to reduce their volatility and re-condense back to the particulate phase. SOA produced from the oxidation of intermediate-volatility compounds (IVOCs) was also included in OPOA mainly because the IVOC emissions were calculated based on the POA emissions (Fountoukis et al., 2014). Intermediate-volatility organic compounds (IVOCs) have been proposed to be an important source of SOA (Zhao et al., 2014).

Grieshop et al. (2009a, b) demonstrate that photooxidation of diluted wood combustion emissions in a smog chamber rapidly produced substantial SOA with a chemical character quite distinct from the primary emissions, and attribute the production of the unexplained OA to the oxidation of low-volatility organic vapors. The existence of these vapors is demonstrated by wood smoke POA evaporating upon isothermal dilution. However, some studies have only observed oxidation without production of new OA mass in fire plumes (Capes et al., 2008; Hoffer et al., 2006). Presto et al. (2014) conducted a series of smog chamber experiments to investigate the transformation of POA and formation of SOA during the photooxidation of dilute exhaust from mobile combustion sources. PMF deconvolved POA and/or SOA factors when substantial POA is present in the dilute exhaust.

SOA chemistry is complex and the contribution of different pathways is not well understood. More work is needed to accurately identify the volatility and aging of primary emissions, and to quantify the contributions of SOA from different sources and formation mechanisms.

In this study, we have no strong evidence to clarify whether it was POA transformed to SOA or primary emissions favored the partitioning of oxidized gas precursors to particulate phase for the increase of OOA. We only give our hypotheses in these two sentences.

In the revision, "*the peaks of OOA (or LO-OOA) coincided with the peaks of primary emitted COA (spring, summer and autumn) and HOA (winter) in diurnal patterns, probably because strong primary emissions favored the partitioning of oxidized gas precursors to particulate phase*." was changed to "***the peaks of OOA (or LO-OOA) coincided with the peaks of primary emitted COA (spring, summer and autumn) and HOA (autumn and winter) in diurnal patterns, probably because strong primary emissions favored SOA production. It has been found that primary emissions evaporate substantially upon dilution to ambient conditions and those vapors undergo photooxidation, which produces SOA efficiently (Robinson et al., 2007; Murphy and Pandis, 2009).***"

"*In both autumn and winter, the fractions of OOA slightly increased around 100 μg* m^{-3}*, implying that POA probably transformed to SOA more effectively within this range*" was

changed to "***In both autumn and winter, the fractions of OOA slightly increased around 100 μg m^{-3}. More work is needed to accurately clarify the cause of the OOA increase within this range.***"

7. Page 20, Line 12-19, please explain the use of OA/ΔCO ratio rather than ΔOA/ΔCO and ΔPOA/ΔCO used in the literature.

Response: Enhancement ratios of OA versus CO are denoted as ΔOA/ΔCO, where Δ indicates the excess amount over the background concentration. In practice, enhancement ratios are often calculated from correlation slopes between OA and CO (de Gouw et al., 2008; de Gouw, J., and Jimenez, 2009). Dzepina et al. (2009) summarized OA/ΔCO ratio from secondary formation during the several campaigns. DeCarlo et al. (2010) described the conceptual framework for the application of the OA/ΔCO method. Hu et al. (2013) studied the evolution of enhancement ratios OA/ΔCO) with the photochemical age at a regional receptor site.

In the revision, "***DeCarlo et al., 2010***" was added in Line 25, Page 21.

8. Figure 3, Please add the standard deviations in the diurnal plots.

Response: To avoid clutter, we added one panel of the diurnal plots for each season to show the ranges of diurnal variations (Fig. S12-S15) in the supplementary as follows. In the caption of Figure 3, "***The ranges of diurnal variations for each season are shown in Fig S12–S15***." was added.

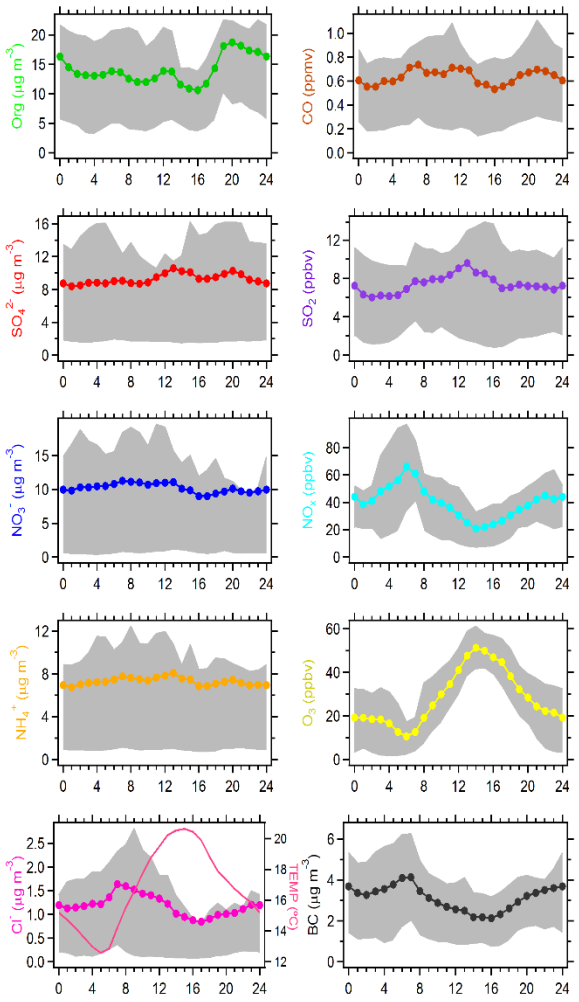

Figure S12. Diurnal patterns of chemical species of submicron particles and gaseous pollutants during the spring observation. The shaded area is between the 25% and 75% quantiles.

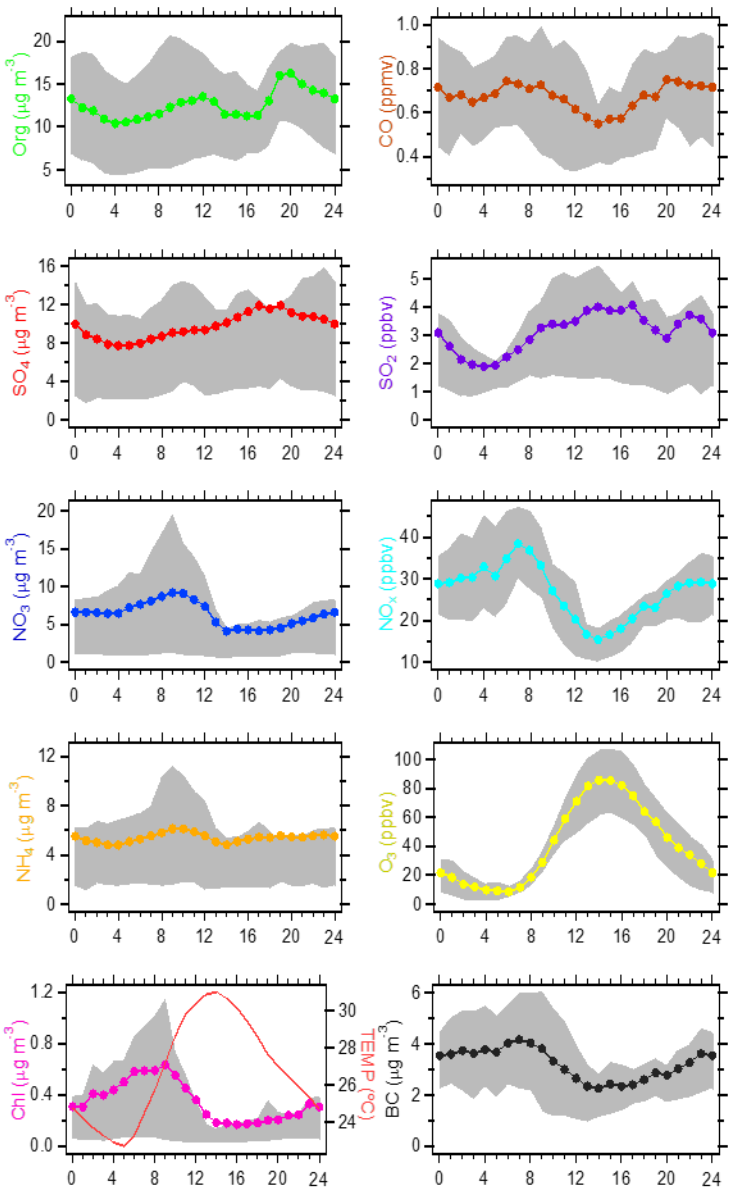

Figure S13. Diurnal patterns of chemical species of submicron particles and gaseous pollutants during the summer observation. The shaded area is between the 25% and 75% quantiles.

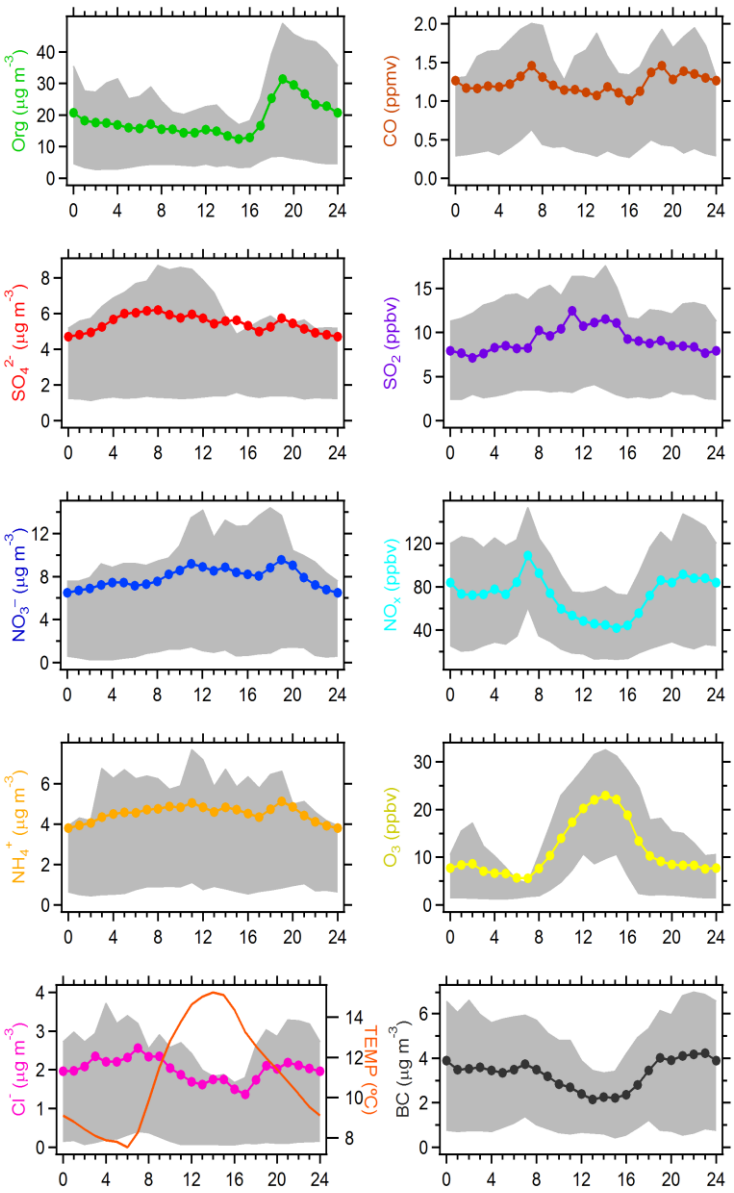

Figure S14. Diurnal patterns of chemical species of submicron particles and gaseous pollutants during the autumn observation. The shaded area is between the 25% and 75% quantiles.

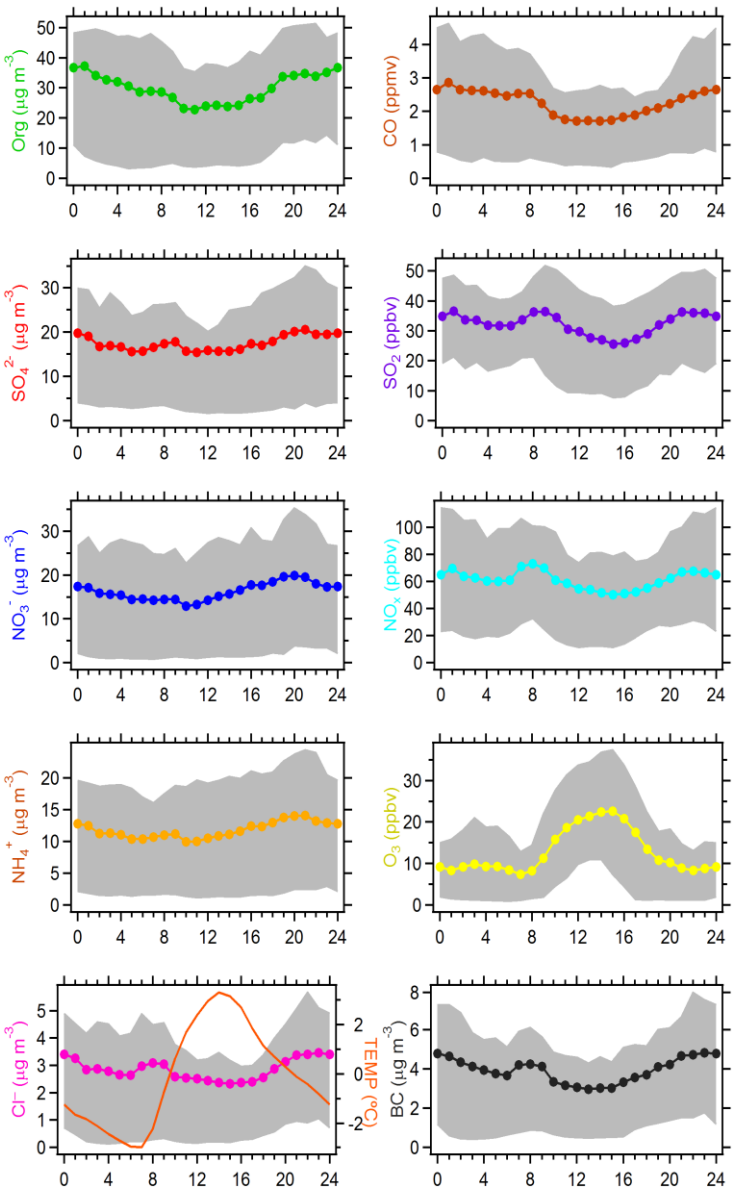

Figure S15. Diurnal patterns of chemical species of submicron particles and gaseous pollutants during the autumn observation. The shaded area is between the 25% and 75% quantiles.

9. Figure S5, I suggest making use of the OM:OC ratio in the AMS to convert OA to OC or OC to OA in the comparison with EC/OC analyzer.

Response: The OA/OC ratios measured by the AMS were used to convert OC measured by EC/OC analyzer to OA. The re-illustrated figure is as follows.

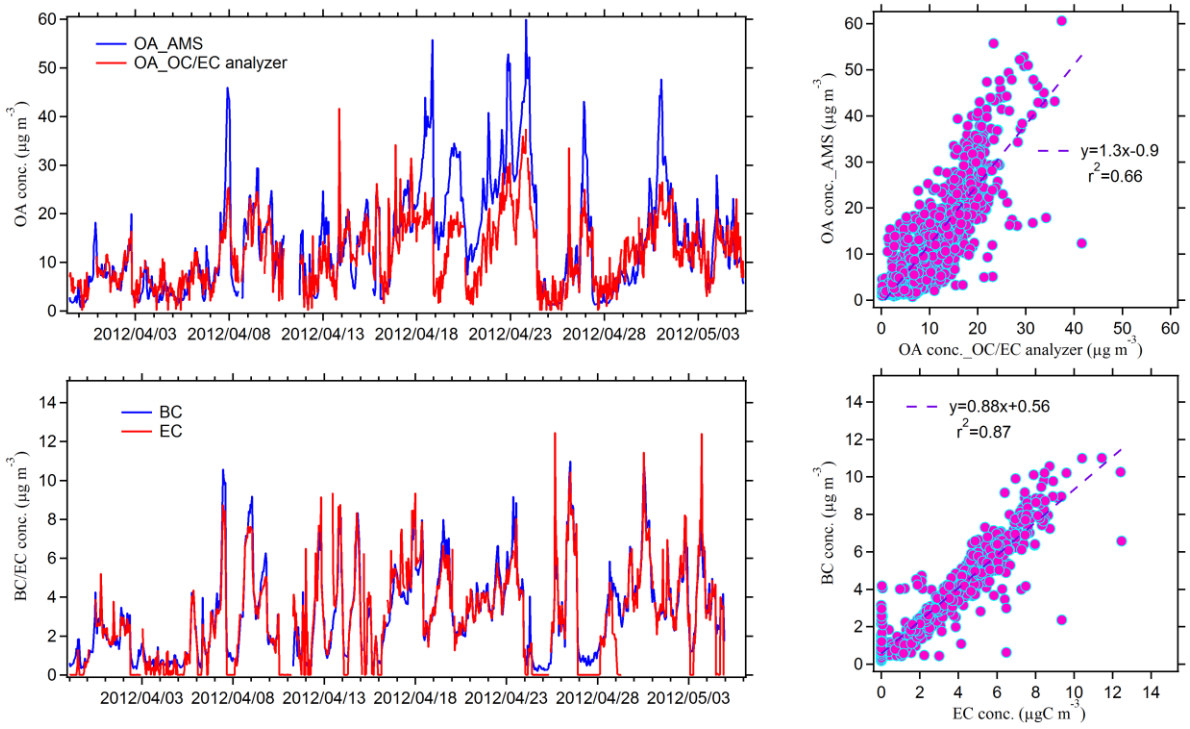

Figure S5. Time series and scatter plots of OA detected by the AMS vs. OA converted from OC measured by a semi-continuous OC/EC analyzer ($PM_{2.5}$ cutoff) using the OA/OC ratios measured by the AMS, and BC vs. EC during the spring observation.

To clarify the possible reasons causing the difference, "***OA concentrations measured by the AMS showed tight correlation with the OC concentrations measured by a Sunset OC/EC Analyzer (r^2 =0.61). The linear regression slope of 2.4 is comparable to or within the range (2.0–2.7) of the previous results (Sun et al., 2011; Hu et al., 2013; Lan et al., 2011; Weimer et al., 2006), but is higher than the average OA/OC ratio of 1.81 determined via elemental analysis of the AMS. When the OM were at high concentration levels, the OA converted from OC measured by the OC/EC analyzer, using the OA/OC ratios measured by the AMS, deviated more from the OA time-series trends, consistent with the result of Lan et al. (2011). Possible reasons for this discrepancy include: (1) evaporative losses of semi-volatile organic species due to striking the balance of gas-particle partition after passing the activated-carbon denuder (Grover et al., 2008), and during the carbon analysis (Sun et al., 2011); (2) "over-calibration" of the OC data using the blank filter values (Bae et al., 2006).***" was added.

Thank you very much for your comments and suggestions. Your any further comments and suggestions are appreciated.

References:

Bae, M.-S., Demerjian, K. L., and Schwab, J. J.: Seasonal estimation of organic mass to organic carbon in $PM_{2.5}$ at rural and urban locations in New York state, Atmos. Environ., 40, 7467–7479, 2006.

Bond, T. C., Doherty, S. J., Fahey, D. W., Forster, P. M., Berntsen, T., DeAngelo, B. J., Flanner, M. G., Ghan, S., Kärcher, B., Koch, D., Kinne, S., Kondo, Y., Quinn, P. K., Sarofim, M. C., Schultz, M. G., Schulz, M., Venkataraman, C., Zhang, H., Zhang, S., Bellouin, N., Guttikunda, S. K., Hopke, P. K., Jacobson, M. Z., Kaiser, J. W., Klimont, Z., Lohmann, U., Schwarz, J. P., Shindell, D., Storelvmo, T., Warren, S. G., and Zender, C. S.: Bounding the role of black carbon in the climate system: A scientific assessment, J. Geophys. Res. Atmos., 118, 5380-5552, doi:10.1002/jgrd.50171, 2013.

Chen, Q., Heald, C. L., Jimenez, J. L., Canagaratna, M. R., Zhang, Q., He, L.-Y., Huang, X.-F., Campuzano-Jost, P., Palm, B. B., Poulain, L., Kuwata, M., Martin, S. T., Abbatt, J. P. D., Lee, A. K. Y., and Liggio, J.: Elemental composition of organic aerosol: The gap between ambient and laboratory measurements, Geophys. Res. Lett., 42, 4182–4189, doi:10.1002/2015gl063693, 2015.

Ervens, B., Turpin, B. J., and Weber, R. J.: Secondary organic aerosol formation in cloud droplets and aqueous particles (aqSOA): a review of laboratory, field and model studies, Atmos. Chem. Phys., 11, 11069-11102, 10.5194/acp-11-11069-2011, 2011.

Faust, J. A., Wong, J. P., Lee, A. K., and Abbatt, J. P.: Role of Aerosol Liquid Water in Secondary Organic Aerosol Formation from Volatile Organic Compounds, Environ. Sci. Technol., 51, 1405-1413, 10.1021/acs.est.6b04700, 2017.

Fountoukis, C., Megaritis, A. G., Skyllakou, K., Charalampidis, P. E., Pilinis, C., Denier van der Gon, H. A. C., Crippa, M., Canonaco, F., Mohr, C., Prévôt, A. S. H., Allan, J. D., Poulain, L., Petäjä, T., Tiitta, P., Carbone, S., Kiendler-Scharr, A., Nemitz, E., O'Dowd, C., Swietlicki, E., and Pandis, S. N.: Organic aerosol concentration and composition over Europe: insights from comparison of regional model predictions with aerosol mass spectrometer factor analysis, Atmos. Chem. Phys., 14, 9061-9076, doi:10.5194/acp-14-9061-2014, 2014.

Grieshop, A., Donahue, N., and Robinson, A.: Laboratory investigation of photochemical oxidation of organic aerosol from wood fires 2: analysis of aerosol mass spectrometer data, Atmos. Chem. Phys., 9, 2227-2240, 2009a.

Grieshop, A., Logue, J., Donahue, N., and Robinson, A.: Laboratory investigation of photochemical oxidation of organic aerosol from wood fires 1: measurement and simulation of organic aerosol evolution, Atmos. Chem. Phys., 9, 1263-1277, 2009b.

Grover, B. D., Eatough, N. L., Woolwine, W. R., Cannon, J. P., Eatough, D. J., and Long, R. W.: Semi-continuous mass closure of the major components of fine particulate matter in Riverside, CA, Atmos. Environ., 42, 250-260, 2008.

Hallquist, M., Wenger, J., Baltensperger, U., Rudich, Y., Simpson, D., Claeys, M., Dommen, J., Donahue, N., George, C., and Goldstein, A.: The formation, properties and impact of secondary organic aerosol: current and emerging issues, Atmos. Chem. Phys., 9, 5155-5236, 2009.

Hayes, P. L., Ortega, A. M., Cubison, M. J., Froyd, K. D., Zhao, Y., Cliff, S. S., Hu, W. W., Toohey, D. W., Flynn, J. H., Lefer, B. L., Grossberg, N., Alvarez, S., Rappenglück, B., Taylor, J. W., Allan, J. D., Holloway, J. S., Gilman, J. B., Kuster, W. C., de Gouw, J. A., Massoli, P., Zhang, X., Liu, J., Weber, R. J., Corrigan, A. L., Russell, L. M., Isaacman, G., Worton, D. R., Kreisberg, N. M., Goldstein, A. H., Thalman, R., Waxman, E. M., Volkamer, R., Lin, Y. H., Surratt, J. D., Kleindienst, T. E., Offenberg, J. H., Dusanter, S., Griffith, S., Stevens, P. S., Brioude, J., Angevine, W. M., and Jimenez, J. L.: Organic aerosol composition and sources in Pasadena, California, during the 2010 CalNex campaign, J. Geophys. Res. Atmos., 118, 9233-9257, 2013.

He, L. Y., Huang, X. F., Xue, L., Hu, M., Lin, Y., Zheng, J., Zhang, R., and Zhang, Y. H.: Submicron aerosol analysis and organic source apportionment in an urban atmosphere in Pearl River Delta of China using high-resolution aerosol mass spectrometry, J. Geophys. Res. Atmos., 116, 2011.

He, L. Y., Lin, Y., Huang, X. F., Guo, S., Xue, L., Su, Q., Hu, M., Luan, S. J., and Zhang, Y. H.: Characterization of high-resolution aerosol mass spectra of primary organic aerosol emissions from Chinese cooking and biomass burning, Atmos. Chem. Phys., 10, 11535-11543, 2010.

Heald, C. L., Kroll, J. H., Jimenez, J. L., Docherty, K. S., DeCarlo, P. F., Aiken, A. C., Chen, Q., Martin, S. T., Farmer, D. K., and Artaxo, P.: A simplified description of the evolution of organic aerosol composition in the atmosphere, Geophys. Res. Lett., 37, doi:10.1029/2010gl042737, 2010.

Hu, J., Wu, L., Zheng, B., Zhang, Q., He, K., Chang, Q., Li, X., Yang, F., Ying, Q., and Zhang, H.: Source contributions and regional transport of primary particulate matter in China,

Environ. Pollut., 207, 31-42, 10.1016/j.envpol.2015.08.037, 2015.

Hu, W. W., Hu, M., Yuan, B., Jimenez, J. L., Tang, Q., Peng, J. F., Hu, W., Shao, M., Wang, M., Zeng, L. M., Wu, Y. S., Gong, Z. H., Huang, X. F., and He, L. Y.: Insights on organic aerosol aging and the influence of coal combustion at a regional receptor site of central eastern China, Atmos. Chem. Phys., 13, 10095-10112, 10.5194/acp-13-10095-2013, 2013.

Hu, W., Hu, M., Hu, W., Jimenez, J. L., Yuan, B., Chen, W., Wang, M., Wu, Y., Chen, C., Wang, Z., Peng, J., Zeng, L., and Shao, M.: Chemical composition, sources and aging process of sub-micron aerosols in Beijing: contrast between summer and winter, J. Geophys. Res. Atmos., 10.1002/2015JD024020, 2016.

Huang, X.-F., He, L.-Y., Hu, M., Canagaratna, M., Sun, Y., Zhang, Q., Zhu, T., Xue, L., Zeng, L.-W., and Liu, X.-G.: Highly time-resolved chemical characterization of atmospheric submicron particles during 2008 Beijing Olympic Games using an Aerodyne High-Resolution Aerosol Mass Spectrometer, Atmos. Chem. Phys., 10, 8933-8945, 2010.

Huang, X.-F., He, L.-Y., Xue, L., Sun, T.-L., Zeng, L.-W., Gong, Z.-H., Hu, M., and Zhu, T.: Highly time-resolved chemical characterization of atmospheric fine particles during 2010 Shanghai World Expo, Atmos. Chem. Phys., 12, 4897-4907, 2012a.

Huang, X.-F., Sun, T.-L., Zeng, L.-W., Yu, G.-H., and Luan, S.-J.: Black carbon aerosol characterization in a coastal city in South China using a single particle soot photometer, Atmos. Environ., 51, 21-28, 2012b.

Huang, X.-F., Xue, L., Tian, X.-D., Shao, W.-W., Sun, T.-L., Gong, Z.-H., Ju, W.-W., Jiang, B., Hu, M., and He, L.-Y.: Highly time-resolved carbonaceous aerosol characterization in Yangtze River Delta of China: Composition, mixing state and secondary formation, Atmos. Environ., 64, 200-207, 2013.

Jia, Y., Rahn, K. A., He, K., Wen, T., and Wang, Y.: A novel technique for quantifying the regional component of urban aerosol solely from its sawtooth cycles, J. Geophys. Res., 113, doi:10.1029/2008jd010389, 2008.

Jimenez, J. L., Canagaratna, M. R., Donahue, N. M., Prevot, A. S. H., Zhang, Q., Kroll, J. H., DeCarlo, P. F., Allan, J. D., Coe, H., Ng, N. L., Aiken, A. C., Docherty, K. S., Ulbrich, I. M., Grieshop, A. P., Robinson, A. L., Duplissy, J., Smith, J. D., Wilson, K. R., Lanz, V. A., Hueglin, C., Sun, Y. L., Tian, J., Laaksonen, A., Raatikainen, T., Rautiainen, J., Vaattovaara, P., Ehn, M., Kulmala, M., Tomlinson, J. M., Collins, D. R., Cubison, M. J., Dunlea, J., Huffman, J. A., Onasch, T. B., Alfarra, M. R., Williams, P. I., Bower, K., Kondo, Y.,

Schneider, J., Drewnick, F., Borrmann, S., Weimer, S., Demerjian, K., Salcedo, D., Cottrell, L., Griffin, R., Takami, A., Miyoshi, T., Hatakeyama, S., Shimono, A., Sun, J. Y., Zhang, Y. M., Dzepina, K., Kimmel, J. R., Sueper, D., Jayne, J. T., Herndon, S. C., Trimborn, A. M., Williams, L. R., Wood, E. C., Middlebrook, A. M., Kolb, C. E., Baltensperger, U., and Worsnop, D. R.: Evolution of Organic Aerosols in the Atmosphere, Science, 326, 1525-1529, 10.1126/science.1180353, 2009.

Kroll, J. H., Ng, N. L., Murphy, S. M., Varutbangkul, V., Flagan, R. C., and Seinfeld, J. H.: Chamber studies of secondary organic aerosol growth by reactive uptake of simple carbonyl compounds, J. Geophys. Res., 110, 10.1029/2005jd006004, 2005.

Kulmala, M., Petäjä, T., Kerminen, V.-M., Kujansuu, J., Ruuskanen, T., Ding, A., Nie, W., Hu, M., Wang, Z., Wu, Z., Wang, L., and Worsnop, D. R.: On secondary new particle formation in China, Front. Environ. Sci. Eng., 10, doi:10.1007/s11783-016-0850-1, 2016.

Lan, Z., Huang X., He, L., Hu, M., Xue, L., Sun, T., Hu, W., Lin, Y., Zhang Y. Comparison of measurement results of several online carbonaceous aerosol monitoring techniques. Acta Scientiarum Naturalium Universitatis Pekinensis, 47, 159-165, 2011.

Li, P., Yan, R., Yu, S., Wang, S., Liu, W., and Bao, H.: Reinstate regional transport of PM2.5 as a major cause of severe haze in Beijing, Proc. Natl. Acad. Sci. USA, 112, E2739-2740, 10.1073/pnas.1502596112, 2015.

Lim, Y. B., Tan, Y., Perri, M. J., Seitzinger, S. P., and Turpin, B. J.: Aqueous chemistry and its role in secondary organic aerosol (SOA) formation, Atmos. Chem. Phys., 10, 10521-10539, 10.5194/acp-10-10521-2010, 2010.

Lin, J., An, J., Qu, Y., Chen, Y., Li, Y., Tang, Y., Wang, F., and Xiang, W.: Local and distant source contributions to secondary organic aerosol in the Beijing urban area in summer, Atmos. Environ., 124, 176-185, 2016.

Lu, K. D., Hofzumahaus, A., Holland, F., Bohn, B., Brauers, T., Fuchs, H., Hu, M., Häseler, R., Kita, K., Kondo, Y., Li, X., Lou, S. R., Oebel, A., Shao, M., Zeng, L. M., Wahner, A., Zhu, T., Zhang, Y. H., and Rohrer, F.: Missing OH source in a suburban environment near Beijing: observed and modelled OH and HO_2 concentrations in summer 2006, Atmos. Chem. Phys., 13, 1057-1080, 10.5194/acp-13-1057-2013, 2013.

Murphy, B. N. and Pandis, S. N.: Simulating the formation of semivolatile primary and secondary organic aerosol in a regional chemical transport model, Environ. Sci. Technol., 43, 4722–4728, 2009.

Murata, S., Tanaka, F., and Tokunaga, J.: Measurement of Vapor Pressure of a Series of Edible Oils, Journal of the Faculty of Agriculture, Kyushu University, 38, 9-18, 1993.

Ndiaye, P. M., Tavares, F. W., Dalmolin, I., Dariva, C., Oliveira, D., and Oliveira, J. V.: Vapor Pressure Data of Soybean Oil, Castor Oil, and Their Fatty Acid Ethyl Ester Derivatives, J. Chem. Eng. Data, 50, 330-333, doi:10.1021/je049898o, 2005.

Presto, A. A., Gordon, T. D., and Robinson, A. L.: Primary to secondary organic aerosol: evolution of organic emissions from mobile combustion sources, Atmos. Chem. Phys., 14, 5015-5036, 10.5194/acp-14-5015-2014, 2014.

Robinson, A. L., Donahue, N. M., Shrivastava, M. K., Weitkamp, E. A., Sage, A. M., Grieshop, A. P., Lane, T. E., Pierce, J. R., and Pandis, S. N.: Rethinking organic aerosols: Semivolatile emissions and photochemical aging, Science, 315, 1259-1262, 2007.

Rose, D., Wehner, B., Ketzel, M., Engler, C., Voigtländer, J., Tuch, T., and Wiedensohler, A.: Atmospheric number size distributions of soot particles and estimation of emission factors, Atmos. Chem. Phys., 6, 1021-1031, 2006.

Shrivastava, M., Cappa, C. D., Fan, J., Goldstein, A. H., Guenther, A. B., Jimenez, J. L., Kuang, C., Laskin, A., Martin, S. T., Ng, N. L., Petaja, T., Pierce, J. R., Rasch, P. J., Roldin, P., Seinfeld, J. H., Shilling, J., Smith, J. N., Thornton, J. A., Volkamer, R., Wang, J., Worsnop, D. R., Zaveri, R. A., Zelenyuk, A., and Zhang, Q.: Recent advances in understanding secondary organic aerosol: Implications for global climate forcing, Rev. Geophys., doi:10.1002/2016rg000540, 2017.

Sorooshian, A., Murphy, S. M., Hersey, S., Bahreini, R., Jonsson, H., Flagan,R. C., Seinfeld, J. H.: Constraining the contribution of organic acids and AMS *m/z* 44 to the organic aerosol budget: On the importance of meteorology, aerosol hygroscopicity, and region. Geophys. Res. Lett., 37, L21807, 2010.

Sun, J., Zhang, Q., Canagaratna, M. R., Zhang, Y., Ng, N. L., Sun, Y., Jayne, J. T., Zhang, X., Zhang, X., and Worsnop, D. R.: Highly time- and size-resolved characterization of submicron aerosol particles in Beijing using an Aerodyne Aerosol Mass Spectrometer, Atmos. Environ., 44, 131-140, 2010.

Sun, Y., Jiang, Q., Wang, Z., Fu, P., Li, J., Yang, T., and Yin, Y.: Investigation of the sources and evolution processes of severe haze pollution in Beijing in January 2013, J. Geophys. Res. Atmos., 119, 4380-4398, 2014.

Sun, Y. L., Wang, Z. F., Fu, P. Q., Yang, T., Jiang, Q., Dong, H. B., Li, J., and Jia, J. J.: Aerosol

composition, sources and processes during wintertime in Beijing, China, Atmos. Chem. Phys., 13, 4577-4592, 2013.

Sun, Y. L., Zhang, Q., Schwab, J. J., Demerjian, K. L., Chen, W. N., Bae, M. S., Hung, H. M., Hogrefe, O., Frank, B., Rattigan, O. V., and Lin, Y. C.: Characterization of the sources and processes of organic and inorganic aerosols in New York city with a high-resolution time-of-flight aerosol mass apectrometer, Atmos. Chem. Phys., 11, 1581-1602, 10.5194/acp-11-1581-2011, 2011.

Sun, Y. L., Zhang, Q., Schwab, J. J., Yang, T., Ng, N. L., and Demerjian, K. L.: Factor analysis of combined organic and inorganic aerosol mass spectra from high resolution aerosol mass spectrometer measurements, Atmos. Chem. Phys., 12, 8537-8551, 10.5194/acp-12-8537-2012, 2012.

Tan, Z., Fuchs, H., Lu, K., Hofzumahaus, A., Bohn, B., Broch, S., Dong, H., Gomm, S., Häseler, R., He, L., Holland, F., Li, X., Liu, Y., Lu, S., Rohrer, F., Shao, M., Wang, B., Wang, M., Wu, Y., Zeng, L., Zhang, Y., Wahner, A., and Zhang, Y.: Radical chemistry at a rural site (Wangdu) in the North China Plain: observation and model calculations of OH, HO_2 and RO_2 radicals, Atmos. Chem. Phys., 17, 663-690, 10.5194/acp-17-663-2017, 2017.

Ulbrich, I. M., Canagaratna, M. R., Zhang, Q., Worsnop, D. R., and Jimenez, J. L.: Interpretation of organic components from Positive Matrix Factorization of aerosol mass spectrometric data, Atmos. Chem. Phys., 9, 2891–2918, 2009.

Weimer, S., Drewnick, F., Hogrefe, O., Schwab, J. J., Rhoads, K., Orsini, D., Canagaratna, M., Worsnop, D. R., and Demerjian, K. L.: Size-selective nonrefractory ambient aerosol measurements during the Particulate Matter Technology Assessment and Characterization Study–New York 2004 Winter Intensive in New York City, J. Geophys. Res., 111, D18305, doi:10.1029/2006JD007215, 2006.

Wu, Q. Z., Wang, Z. F., Gbaguidi, A., Gao, C., Li, L. N., and Wang, W.: A numerical study of contributions to air pollution in Beijing during CAREBeijing-2006, Atmos. Chem. Phys., 11, 5997-6011, doi:10.5194/acp-11-5997-2011, 2011.

Wu, Z. J., Zheng, J., Shang, D. J., Du, Z. F., Wu, Y. S., Zeng, L. M., Wiedensohler, A., and Hu, M.: Particle hygroscopicity and its link to chemical composition in the urban atmosphere of Beijing, China, during summertime, Atmos. Chem. Phys., 16, 1123-1138, 10.5194/acp-16-1123-2016, 2016.

Xu, L., Suresh, S., Guo, H., Weber, R. J., and Ng, N. L.: Aerosol characterization over the

southeastern United States using high-resolution aerosol mass spectrometry: spatial and seasonal variation of aerosol composition and sources with a focus on organic nitrates, Atmos. Chem. Phys., 15, 7307-7336, 10.5194/acp-15-7307-2015, 2015.

Xu, W., Han, T., Du, W., Wang, Q., Chen, C., Zhao, J., Zhang, Y., Li, J., Fu, P., Wang, Z., Worsnop, D. R., and Sun, Y.: Effects of Aqueous-Phase and Photochemical Processing on Secondary Organic Aerosol Formation and Evolution in Beijing, China, Environ. Sci. Technol., 51, 762-770, doi:10.1021/acs.est.6b04498, 2017.

Zhang, J. K., Cheng, M. T., Ji, D. S., Liu, Z. R., Hu, B., Sun, Y., and Wang, Y. S.: Characterization of submicron particles during biomass burning and coal combustion periods in Beijing, China, Sci. Total Environ., 562, 812-821, 10.1016/j.scitotenv.2016.04.015, 2016.

Zhang, J. K., Sun, Y., Liu, Z. R., Ji, D. S., Hu, B., Liu, Q., and Wang, Y. S.: Characterization of submicron aerosols during a month of serious pollution in Beijing, 2013, Atmos. Chem. Phys., 14, 2887-2903, doi:10.5194/acp-14-2887-2014, 2014.

Zhang, L., Liu, L., Zhao, Y., Gong, S., Zhang, X., Henze, D. K., Capps, S. L., Fu, T.-M., Zhang, Q., and Wang, Y.: Source attribution of particulate matter pollution over North China with the adjoint method, Environ. Res. Lett., 10, 084011, doi:10.1088/1748-9326/10/8/084011, 2015a.

Zhang, R., Guo, S., Levy Zamora, M., and Hu, M.: Reply to Li et al.: Insufficient evidence for the contribution of regional transport to severe haze formation in Beijing, Proc. Natl. Acad. Sci. USA, 112, E2741, doi:10.1073/pnas.1503855112, 2015b.

Zhao, Y., Hennigan, C. J., May, A. A., Tkacik, D. S., de Gouw, J. A., Gilman, J. B., Kuster, W. C., Borbon, A., and Robinson, A. L.: Intermediate-volatility organic compounds: a large source of secondary organic aerosol, Environ. Sci. Technol., 48, 13743-13750,doi:10.1021/es5035188, 2014.

Seasonal variations of high time-resolved chemical compositions, sources and evolution for atmospheric submicron aerosols in the megacity Beijing

Wei Hu, Min Hu*, Wei-Wei Hu, Jing Zheng, Chen Chen, Yusheng Wu, Song Guo

State Key Joint Laboratory of Environmental Simulation and Pollution Control, College of Environmental Sciences and Engineering, Peking University, Beijing 100871, China

*Corresponding author: minhu@pku.edu.cn

Abstract

Severe regional haze problem in the megacity Beijing and surrounding areas, caused by fast formation and growth of fine particles, has attracted much attention in recent years. In order to investigate the secondary formation and aging process of urban aerosols, four intensive campaigns were conducted in four seasons between March 2012 and March 2013 at an urban site in Beijing (116.31°E, 37.99°N). An Aerodyne high resolution time-of-flight aerosol mass spectrometry (HR-ToF-AMS) was deployed to measure non-refractory chemical components of submicron particulate matter (NR-PM_1). The average mass concentrations of PM_1 (NR-PM_1+black carbon) were 45.1±45.8, 37.5±31.0, 41.3±42.7, and 81.7±72.4 μg m^{-3} in spring, summer, autumn and winter, respectively. Organic aerosol (OA) was the most abundant component in PM_1, accounting for 31, 33, 44 and 36% seasonally, and secondary inorganic aerosol (SNA, sum of sulfate, nitrate and ammonium) accounted for 59, 57, 43, and 55% of PM_1 correspondingly. Based on the application of positive matrix factorization (PMF), the sources of OA were obtained, including the primary ones of hydrocarbon-like (HOA), cooking (COA), biomass burning OA (BBOA) and coal combustion OA (CCOA), and secondary component oxygenated OA (OOA). OOA, or split into more-oxidized (MO-OOA) and less-oxidized OOA (LO-OOA), accounted for 49, 69, 47 and 50% in four seasons, respectively. Totally, the fraction of secondary components (OOA+SNA) contributed about 60–80% to PM_1, suggesting that secondary formation played an important role in the PM pollution in Beijing, and primary sources were also non-negligible. The evolution process of OA in different seasons was investigated with multiple metrics and tools. The average carbon oxidation states and other metrics show that the oxidation state of OA was the highest in summer, probably due to both strong photochemical and aqueous-phase oxidations. It was indicated by the good correlations (r=0.53–0.75, p<0.01) between LO-OOA and odd oxygen (O_x=O_3+NO_2), and between MO-OOA and

liquid water content in aerosols. BBOA was resolved in spring and autumn, influenced by agricultural biomass burning (e.g., field preparation burnings, straw burning after the harvest). CCOA was only identified in winter due to domestic heating. These results signified that the comprehensive management for biomass burning and coal combustion emissions is needed. High concentrations of chemical components in PM_1 in Beijing, especially in winter or in adverse meteorological conditions, suggest that further strengthening the regional emission control of primary particulate and precursors of secondary species is expected.

Key words: PM_1, Secondary organic aerosol, AMS, PMF, Seasonal variations, Urban aerosols

1. Introduction

With rapid economic development and urbanization, air pollution stands in an increasingly serious situation in China. Severe regional air pollution, mostly characterized by high concentration of fine particulate matter ($PM_{2.5}$), happens frequently. Severe fine particle pollution can lead to visibility deterioration, damage ecosystems and human health, and affect climate change substantially, which has attracted widespread attention. Submicron particulate matter (PM_1) accounts for a large proportion of both mass and number concentrations in $PM_{2.5}$. Its physical and chemical properties can be greatly modified by dynamic and chemical conversion processes in the atmosphere (Buseck and Adachi, 2008). A full examination on the properties of chemical compositions, sources, and formation mechanisms of PM_1 will improve our abilities to understand, predict, and control its impacts.

Multiple observations have been conducted to investigate the concentrations and chemical compositions of non-refractory submicron particle (NR-PM_1) at diverse sites around the world (Jimenez et al., 2009 and references therein), and also in China (Hu et al., 2016a; Huang et al., 2014; Xu et al., 2014; Sun et al., 2010 and references therein). The PM_1 concentration in the megacity Beijing was 2–10 times higher than those in western cities, highlighting the severe situation of particulate pollution. Anthropogenic emissions due to a dense population, as well as the adverse meteorological and geographical conditions, can result in high PM pollution in Beijing (Hu et al., 2016a).

In urban atmospheres, aerosols can be directly emitted from complicated anthropogenic sources, such as coal and biomass burning, cooking, traffic-related and industrial emissions, or formed through gas to particle conversion and heterogeneous/aqueous-phase oxidations (Lee and Allen, 2012). Secondary inorganic aerosols (SNA, sum of

sulfate, nitrate and ammonium) are important in PM_1 in urban regions (Guo et al., 2014; Huang et al., 2014; Lee, 2015). Organic aerosol (OA) is the most complicated component in fine particles, with a high mass fraction of 20–90% (Turpin et al., 2000; Carlton et al., 2009). OA is constituted by hundreds of species, but only a small fraction (~10%) can be quantified by chemical analysis (Hallquist et al., 2009). A better understanding on OA properties is crucial for identifying the sources of OA.

The Aerodyne aerosol mass spectrometry (AMS) is currently one of the most popular technologies used to characterize the main species in NR-PM_1, and has been applied to many field and laboratory studies (Hallquist et al., 2009). By combining the time series of OA mass spectra (MS) from the AMS with source receptor models, different OA sources can be effectively distinguished. Analyzed with positive matrix factorization (PMF) model, several OA factors have been resolved (Hu et al., 2013; Jimenez et al., 2009; Ng et al., 2011). For instance, hydrocarbon-like (HOA), cooking (COA), biomass burning (BBOA) and coal combustion OA (CCOA), etc., are classified into primary organic aerosols (POA). Oxygenated OA (OOA) usually consists of low-volatility (LV-OOA) and semivolatile OOA (SV-OOA) based on their correlations with sulfate and nitrate, respectively, and inferred volatilities. OOA is also identified as more oxidized (MO-OOA) and less oxidized OOA (LO-OOA) because they show different O/C ratios but insignificantly different volatility (Hu et al., 2016a; Setyan et al., 2012). Based on the AMS measurement, the aging process of OA can also be characterized with some metrics, e.g., C/H/O atomic ratios, OA/OC, carbon oxidation state (OS_C), and the abundance of characteristic fragment ions (f_{44} and f_{43}). These results can help to quantify the contributions of primary emissions and secondary formations, and probe into secondary formation mechanisms and the aging process of OA (Ulbrich et al., 2009).

The characteristics and evolution of aerosol pollution are multifactorial, e.g., influenced by meteorological conditions, regional transport and local sources. Generally, these factors have quite distinct patterns in different seasons, thus the formation, transformation and removal of pollutants are affected. Some studies on the characteristics of submicron aerosol pollution in Beijing using the AMS were mainly carried out in summer and winter. The characterization of PM_1 in summer (e.g., Huang et al., 2010; Sun et al., 2010), and the comparisons of PM_1 characteristics between summer and winter (e.g., Hu et al., 2016a; Sun et al., 2012, 2013a), between the low and high humidity atmosphere (e.g., Sun et al., 2013b), and between the polluted and unpolluted days (e.g., Zhang et al., 2014), were conducted in Beijing. Yet the study comprehensively characterized the seasonal variations of PM_1 under different meteorological conditions and pollutant sources in Beijing is lacking, especially based on high mass-resolution measurements. Zhang et al. (2013) and Sun et al. (2015) investigated the seasonal variations of

PM_1 pollution in Beijing based on unit mass resolution (UMR), and there was no elemental information in these studies. High mass-resolution AMS can obtain elemental information, which can be used to more easily determine the oxidation state of OA and characterize the evolution of SOA. Therefore, to deeply explore the formation and evolution of SOA in urban atmosphere, the researches on PM_1 seasonality in Beijing based on field observations applying high mass-resolution AMS remain very necessary.

In this study, a high resolution time-of-flight AMS (HR-ToF-AMS) and other real-time online measurement instruments for gaseous and particulate pollutants were deployed at an urban site in Beijing from 2012 to 2013 to investigate the seasonal characteristics of PM_1. At first, the seasonal variations of chemical compositions in PM_1 were analyzed. Then the seasonal sources of OA were fully explored. Finally, we compared and discussed the evolution process of OA in different seasons. This study is of great significance to further understand complex air pollution, and to provide scientific support for model simulations of atmospheric aerosols, and also a theoretical basis for fine particulate pollution control.

2. Experiments

2.1 Sampling site and measurements

During the periods from March 2012 to March 2013, four intensive campaigns were carried out at the PeKing University Urban Atmosphere Environment MonitoRing Station (PKUERS, 39.99°N, 116.31°E), which is located on the roof of a building (approximately 20 m above ground level) on the campus (Fig. S1 in the supplement). The details about the observation site were described in several published papers (Wu et al., 2007; Huang et al., 2010). A HR-ToF-AMS (Aerodyne Research Inc., USA) was deployed to measure the mass concentrations and size distributions of submicron non-refractory species, including OA and inorganic aerosols (sulfate, nitrate, ammonium and chloride). In addition to the HR-ToF-AMS, multiple high time-resolution instruments for the measurements of meteorological conditions, and gaseous and particulate pollutants (as listed in Table S1) were also available in these campaigns.

The liquid water content (LWC) in aerosols was roughly estimated with the ISORROPIAII model. The input data included the concentrations of sulfate, nitrate, ammonium and chloride measured by the AMS, the relative humidity (RH) and temperature of ambient air. The reverse mode and the metastable state of aerosols were selected.

To give an insight into the impacts of regional/long-distance transport on atmospheric aerosols in Beijing, the

backward trajectories of air parcels during the observation periods were calculated with the NOAA's HYSPLIT4 trajectory model (http://www.arl.noaa.gov/hysplit.html). A new 3-day backward trajectory was traced from the observation site at an altitude of 500 m above ground level every hour. Cluster analyses of backward trajectories were applied to reveal the major pathways during different campaigns (Sect. S11 in the supplement).

2.2 HR-ToF-MS operation and data analysis

Ambient air was first introduced through a cutoff cyclone of $PM_{2.5}$ (1.5 m above the roof) and a copper tube (3/8 inch) at 10 L min^{-1}, then was sampled into the AMS at 0.09 L min^{-1}. A Nafion drier was set in front of the AMS inlet to keep the RH of ambient air sampled into the AMS below 30%. The time resolutions applied in all campaigns were 4 min, with 2 min in V-mode for concentrations and size distributions, and 2 min W mode to obtain the HR-MS data. Ionization efficiency (IE) calibrations were done every few days by sampling monodispersed 400 nm dried pure NH_4NO_3 particles into the AMS. Those particles were aerosolized by an aerosol atomizer (3076, TSI Inc., USA) and selected with a differential mobility analyzer (DMA, model 3081, TSI Inc., USA). IE values measured by the Brute-Force Single-Particle method (BFSP) were used. The ratio of IE to airbeam signal (=IE/AB, AB refers to N_2^+ detected by the AMS) of each calibration was applied for converting the instrument signals to actual mass concentrations. The IE/AB calibration values (Fig. S2) within the interval of two calibrations were obtained by linear interpreting IE/AB values before and after. Unless there was an instrument failure (e.g., turbo pump down and filament exchange), the last well calibrated IE/AB value was applied till the instrument failure time. The size distribution calibration of main species in NR-PM_1 was done in the beginning and ending of all campaigns by selecting pure NH_4NO_3 particles (stokes diameter 50–550 nm) with vacuum aerodynamic diameters (d_{va}) of 100–900 nm. The detected limits (V-mode) of organics, sulfate, nitrate, ammonium, and chloride during all campaigns were shown in Table S3. For the detailed operation and calibration procedures of the HR-ToF-AMS, refer to Hu et al. (2016a).

The data analysis procedures are similar to the method reported in Hu et al. (2016a). Middlebrook et al. (2012) created an algorithm estimating AMS collection efficiencies (CE) for field data based on the aerosol chemical compositions and sampling line RH. The chemical composition-based CEs (around 0.5) were applied to calculate the mass concentration of chemical compositions in PM_1. Good consistencies (Fig. S3–S5) of the results between the AMS and other instruments also prove the reliability of CE used here. Pieber et al. (2016) found that the CO_2^+ interference related to NH_4NO_3 sampling on the vaporizer showed a median of +3.4% relative to nitrate, and highly

varied between instruments and with operation history (percentiles $P_{10–90}$ = +0.4 to +10.2%). The effect of NH_4NO_3 on CO_2^+ ion signal was quite limited (about 1–2%) and not considered here. In this study, the "improved-ambient" correction (Canagaratna et al., 2015) was performed to calculate the elemental ratios of OA. The HR-MS data of OA in four seasons (*m/z* range 12–283 in winter campaign and 12–196 in other campaigns) were analyzed with PMF respectively, which follows the procedures described in Ulbrich et al. (2009). The optimum solutions were selected following the steps as described in Zhang et al. (2011). The key diagnostic plots of the PMF analysis are shown in Sect. S5 in the supplement.

3. Results and discussion

3.1 Dynamic variations of PM_1 pollution

3.1.1 Seasonality of chemical compositions in PM_1

Atmospheric black carbon (BC) particles are mostly in the submicron range because of their formation mechanisms (Bond et al., 2013). The average concentrations of main chemical components in PM_1 (non-refractory species measured by the AMS and BC by the aethalometer or MAAP) and gaseous pollutants, and meteorological conditions are listed in Table 1. The time series of meteorological parameters, including temperature, relative humidity (RH), atmospheric pressure, and wind speed and direction, can be found in Fig. S6-S9.

The average PM_1 concentrations showed little difference in spring, summer, and autumn, which were 45.1±45.8, 37.5±31.0, and 41.3±42.7 μg m^{-3}, respectively. The average PM_1 concentration of 81.7±72.4 μg m^{-3} in winter was the highest among the four seasons. OA was the most important component (31–44%) in PM_1, similar to previous studies (Fig. 1). In autumn, the contribution of the carbonaceous components (OA+BC) to PM_1 was over 50%. In four seasons, SNA accounted for about 40–60% in PM_1. Secondary inorganics (sulfate and nitrate) correlated well with RH and/or LWC (Table S14), indicating that aqueous-phase reactions in aerosols played an important role in secondary inorganic formation in Beijing. The contribution of photochemical processes to secondary inorganics was likely less than those of aqueous-phase reactions according to the weaker correlations between secondary inorganics and odd oxygen (O_x=O_3+NO_2). Especially, nitrate did not correlate with O_x in summer (Table S14). Recently it was found that high levels of sulfate and fine PM in northern China can be explained by reactive aqueous oxidation of SO_2 by NO_2 under certain atmospheric conditions, i.e., on the fine aerosols with high aerosol water content and NH_3 neutralization or under cloud conditions (Cheng et al., 2016;

Wang et al., 2016). Lower temperatures in winter, spring and autumn favored the partitioning to particulate nitrate and were partially related to higher concentrations of nitrate in PM_1 (Table 1).

Compared with the results obtained over the world, PM_1 and the concentrations of major chemical species in Beijing, especially in winter, were 2–10 times higher than those at American and European sites (Hu et al., 2016a). In China, PM_1 in urban Beijing in winter was much higher than those results (27–48 μg m^{-3}) obtained in the Yangtze River Delta (YRD) and Pearl River Delta (PRD) regions (Gong et al., 2012; He et al., 2011; Huang et al., 2011, 2012, 2013). While, PM_1 in other seasons was approximate to those obtained at the sites at Changdao Island, and in the YRD and PRD regions in the same seasons (Hu et al., 2013, 2016a and references therein). These results suggest that Beijing suffered from severe particulate pollution, especially in winter, which should be seriously taken into consideration.

Aerosol pollution in Beijing exhibited distinctive characteristics in four seasons, because of the significantly different meteorological conditions and emission sources of pollutants. Compared with the previous results in Beijing (Fig. 1), PM_1 in summer was lower than before, which likely resulted from the more effective washout (Fig. S7) and lower concentrations of gaseous precursors (Table 1 and Table 1 in Sun et al. (2015)). In summer, high temperature, strong solar radiation and high oxidant concentrations generally enhance the secondary aerosol formation from gaseous precursors (such as SO_2, NO_x and VOCs). As illustrated in Fig. 2, PM_1 in summer was mainly in the range of less than 50 μg m^{-3} (~80%), and skewed-normally distributed, with the highest frequency (~45%) in 15–35 μg m^{-3}. The probability distribution of PM_1 was similar to the previous results in Beijing in summer (Huang et al., 2010; Sun et al., 2010), but the range of PM_1 was narrower. In contrast, PM_1 in winter was higher than the previous results in Beijing before 2013, and equivalent to those in close periods from January to February 2013 (Fig. 1; Zhang et al., 2014; Sun et al., 2014). The heaviest particulate pollution in winter was the co-effect of the large amount of particles emitted from primary sources, prolonged control of weak weather system (i.e., low mixed layer and static air), as well as the rapid generation and accumulation of secondary particles from gaseous precursors (Hu et al., 2016a; Sun et al., 2013a).

In spring, autumn and winter, the passage of strong cold air parcels transported from Siberia and Mongolia through Beijing was usually accompanied by strong winds, thus atmospheric relative humidity decreased, pressure increased, which was conductive to the dispersal of pollutants (Fig. S6, S8 and S9). The heavy pollution processes were usually ended by the passages, demonstrating periodic cycles of aerosol pollution (Guo et al., 2014; Wu et al.,

2009). In spring and autumn, the biomass burning emissions in North China occurred often due to agricultural activities and traditional activities around Tomb-sweeping Day (early April). Dense fire points were observed by satellites (https://firms.modaps.eosdis.nasa.gov/firemap) in Beijing and surrounding areas, e.g., during 7–8, 26–28 Apr. 2012 (Fig. S10), and 18–20, 23–27 Oct. and 6–11 Nov. 2012 (Fig. S11). During these periods, the concentrations of OA and other pollutants increased substantially (Fig. S6 and S8). Higher nitrate concentrations in spring and autumn, likely caused by the secondary conversion of gaseous nitrogen oxides emitted from biomass burning (Fabian et al., 2005). The probability distributions of PM_1 in spring, autumn and winter were quite different from that in summer (Fig. 2), because the scavenging effect of strong wind was apparent due to the intrusion of long-range transported air masses. PM_1 mainly concentrated in the range of low levels (<20 μg m^{-3}), with frequencies of 40–60%. While, PM_1 ranged much more broadly, with the highest concentrations of over 200 or 300 μg m^{-3}, resulting from accumulated pollutants under strong primary emissions coupled with extremely unfavorable meteorological conditions, e.g., long-lasting stagnant weather, high humidity, and temperature inversion.

3.1.2 Contributions of chemical compositions to the increase of PM_1

The contributions of chemical components in atmospheric aerosols at different concentration levels can help better understand the origins of chemical components. The proportions of chemical compositions as a function of PM_1 are shown in Fig. 2.

In all seasons, at low PM_1, the contribution of carbonaceous components (OA+BC) was dominant, accounting for 50–80% of PM_1. With the increase of PM_1, the proportions of SNA in PM_1 increased gradually, indicating that the enhancement of SNA primarily contributed to the increase of PM_1, consistent with previous studies (Huang et al., 2010; Sun et al., 2010; Sun et al., 2012). The proportions of nitrate increased significantly, and the nitrate concentration increased rapidly under higher RH (Fig. 2 and Fig. S6–S9). Nitrate showed good correlations with RH (Pearson correlation coefficients r=0.34–0.79, p<0.01) and the LWC in aerosols (r=0.82–0.87, p<0.01). These results indicate that the aqueous-phase reactions in wet aerosols and/or clouds could substantially contribute to nitrate formation. It is worth noting that when PM_1 higher than 150 μg m^{-3}, carbonaceous aerosols dominated PM_1 again in autumn, mainly resulting from large amounts of primary emissions. The proportions of chemical components in PM_1 varied less significantly in winter, reflecting the characteristics of regional pollution over the North China under the control of static weather system.

3.1.3 Diurnal patterns of chemical compositions in PM_1

Affected by different meteorological conditions, e.g., solar radiation, temperature, RH, boundary layer, and mountain-valley breezes (Fig. S7), as well as different emission sources, the chemical compositions in PM_1 showed distinct diurnal patterns in four seasons. The diurnal patterns of gaseous and particulate pollutants during the seasonal observations are shown in Fig. 3.

Diurnal patterns of OA were similar in spring, summer and autumn. OA showed two obvious peaks around noon and in the evening. Similar peaks were also observed in winter, but were not as strong as in the other seasons. These two peaks corresponding to meal time were mainly caused by cooking emissions, which will be discussed later in Sect. 3.2.1. The peak concentration of OA in the evening in autumn was about two times higher than in spring and summer, consistent with the results in Oct.–Nov. 2011 (Sun et al., 2015), possibly because of the more intensive cooking activities. In autumn, charcoal-grilling or barbecue has become one of the most popular outdoor recreational activities in urban Beijing and surrounding areas, due to more moderate and pleasant weather conditions than in other seasons (Table 1). In winter study, OA increased at night due to extra primary emissions, e.g., coal combustion and biomass burning.

Compared with OA diurnal patterns, flatter diurnal cycles of sulfate were observed in four seasons, identifying the regional characteristics of sulfate formation (Sun et al., 2015). In spring, sulfate showed small peaks around 13:00 and 20:00. In the daytime, both active photochemical production and more favorable dispersion conditions due to higher planetary boundary layer (PBL) possibly caused such a diurnal pattern of sulfate. In summer, sulfate enhanced gradually from morning to evening and peaked in the evening only, indicating that the photochemical production of sulfate might be significant. In addition to the gas-phase processes, the formation of sulfate is mainly attributed to aqueous-phase reactions in clouds and/or wet aerosols (70–80%) in the summer of Beijing (Guo et al., 2010). The aqueous-phase formation of sulfate in summer should also be more intense than in spring and autumn due to high temperature and high humidity (Fig. 3k–l). In winter, sulfate showed two peaks in the morning (6:00–10:00) and evening (around 20:00), which was likely influenced by the secondary formation of primarily emitted SO_2 (Fig. 3f), and the lower sulfate concentration in the daytime was quite related to the dilution effect of the planetary boundary layer (PBL). The PBL height decreases at night, and the atmospheric stability increases, thus the pollutants are difficult to spread (Hu et al., 2016a).

Nitrate showed distinct diurnal patterns in four seasons. Heterogeneous/aqueous-phase reactions and gas-to-

particle condensation processes are the main pathways to form fine mode nitrate (Guo et al., 2010). Nitrate exhibited an obvious diurnal pattern in summer, with the concentrations gradually decreasing in the daytime, indicating that NH_4NO_3 evaporated due to high temperatures (Fig. 3k) and overcame the photochemical production of nitrate. The elevated PBL also plays a role in the low concentrations of nitrate in the daytime (Sun et al., 2015). In winter, nitrate increased gradually during 9:00–20:00, which did not appear in other seasons, suggesting that in addition to photochemical processes in the daytime, the partitioning of NH_4NO_3 into particulate nitrate was more significant due to low temperatures (<5°C; Fig. 3k). Similar diurnal patterns in summer and winter have been observed in previous studies (Sun et al., 2015). In autumn, nitrate increased in the morning and then later in the evening, primarily driving by the photochemical production. The diurnal variation of nitrate in spring was insignificant. Because ammonium mainly existed in the forms of $(NH_4)_2SO_4$ and NH_4NO_3, its diurnal patterns generally exhibited a combined effect of sulfate and nitrate formation mechanisms. In summer, the diurnal variation of ammonium correlated better ($r=0.55$, $p<0.01$) with that of nitrate than sulfate ($r=0.19$, $p>0.05$). In other seasons, the diurnal variations of ammonium showed good correlations with those of both sulfate and nitrate ($r=0.50$–0.98, $p<0.01$ or 0.05).

Chloride showed higher concentrations at night, with a peak in the morning, and then deceased in the daytime. Such a diurnal pattern was possibly caused by high primary emissions of chloride at night. It was also driven by the diurnal patterns of both temperatures and the PBL height, and controlled by the temperature-dependent gas-particle partitioning (Hu et al., 2016a; Sun et al., 2015). Chloride usually presents at semi-volatile state in the form of ammonium chloride in urban areas (Zhang et al., 2005), therefore the diurnal cycles of temperature and chloride trend oppositely. In winter, chloride was higher at night because of coal combustion and biomass burning emissions. Hu et al. (2016a) estimated that in winter over 50% of chloride in PM_1 existed as NH_4Cl, and part of chloride existed as KCl and NaCl. BC was mainly affected by the diurnal variation of the PBL height. BC showed a marked rise at night (around 21:00-0:00) and a small morning peak (7:00-8:00). Nocturnal heavy-duty vehicular exhausts (Lin et al., 2009; Hu et al., 2012), coal combustion and biomass burning emissions in the urban atmosphere also contributed to the high concentration of BC at night. The morning peak of BC was consistent with that of NO_x, probably due to vehicular emissions during rush hour.

3.1.4 Size distributions of chemical compositions in PM_1

The mass size distributions of chemical compositions in PM_1 during seasonal campaigns are shown in Fig. 4. The size distributions of SNA concentrated in accumulation mode, peaking at about 600–800 nm (d_{va}), indicating

the internally mixed states of submicron aerosols. The mode diameters of SNA in Beijing were higher than those (500–600 nm) in Hong Kong in four seasons (Li et al., 2015). The mode size (700 nm) of sulfate was smaller than that (790 nm) of nitrate in autumn, while the mode size of sulfate (760 nm) was larger than that (700 nm) of nitrate in winter. The size distribution of ammonium was more consistent with that of nitrate than sulfate in winter. More nitrate likely existed in the form of NH_4NO_3, formed by the reaction of gaseous HNO_3 and NH_3 condensed on atmospheric particles (Weimer et al., 2006).

During the winter, the peak size of OA was close to those of SNA; while in other seasons it was smaller than those of SNA, indicating a more aged state of OA in winter. The mass size distributions of chemical components in winter were also similar to those in the heavy-polluted episodes in other seasons, consistent with the severity of aerosol pollution in winter. In spring, summer and autumn, the size distributions of OA were wider than those of SNA. The OA concentrations were much higher than those of SNA in the range of small size (100–500 nm), similar to the results in other urban areas (Weimer et al., 2006; Aiken et al., 2009), probably caused by the contribution of POA (Huang et al., 2010; Hu et al., 2013). Especially, influenced by primary emissions, the concentration of OA at peak size was much higher than those of other species in autumn. During the spring, summer and autumn, the proportions of OA decreased, while those of SNA increased rapidly with the increase of particle size (>200 nm), indicating that SNA species were the main components contributed to the enhancement of PM_1, in accordance with that mentioned in Sect. 3.1.2. Different OA sources played different roles with the increase of particle size in winter, and the proportion of OA (about 40%) varied slightly. However, the proportions of sulfate rose with the increase of size, implying the significant contribution of regional transported sulfate.

3.2 Investigating OA sources with PMF

The sources of OA in four seasons were resolved by combining high-resolution OA mass spectra and PMF model respectively. The resolved fractions of OA during seasonal observations are shown in Fig. 5. The mass spectra and time series of OA components and some external tracers in each season are shown in Fig. S28-S31 and Fig. S32-S35, respectively.

In spring and autumn, four OA components, i.e., OOA, COA, BBOA and HOA, were identified. The fractions of POA (sum of HOA, COA and BBOA) was slightly higher than those of OOA because primary emissions, e.g., biomass burning, strongly influenced Beijing and surrounding areas. In autumn, the fraction of POA was close to that in the autumn of 2008 (Fig. 5b). OA was constituted by MO-OOA, LO-OOA, COA and HOA in summer.

OOA (MO-OOA+LO-OOA) dominated OA (69%), signifying the predominant contribution of SOA formation. Consistent with previous results, the contribution of SOA to OA is about 60–70% of OA in the summer of Beijing, which is quite stable in recent years (Fig. 5, and Guo et al., 2012, 2013). In winter, five components MO-OOA, LO-OOA, COA, HOA and CCOA were resolved. Secondary formations and primary emissions (e.g., biomass burning and fossil fuel combustion) contributed to OA equivalently. The fraction of SOA in OA in winter (50%) was much higher than those (20–30%) in previous studies, and comparable to the results in the same winter in Beijing (Fig. 5b and Table S5), which was related to effective SOA formation under the stable meteorological conditions during long-lasting severe haze episodes.

The comparison of seasonal variations of OA in PM_1 between this study and studies carried out at other sites is shown in Fig. 5c. The fractions of SOA during all seasons in Beijing were higher than or comparable to those at Mt. Tai (1534 m a.s.l.), North China (Zhang et al., 2014). Both in Beijing and at Mt. Tai, the fractions of SOA were higher in summer than in other seasons. The contribution of SOA to OA in Beijing was much lower than those in less-polluted atmospheres in Hong Kong (Li et al., 2015) and southeastern USA (Budisulistiorini et al., 2016). The fraction of SOA in OA was as high as 80–86% in Hong Kong in four seasons. At a downtown site in Atlanta, SOA accounted for over 80% in spring and summer, and 65 and 56% in autumn and winter. At a rural/forested site Look Rock, Great Smoky Mountains, even no POA sources were resolved except for BBOA in winter. Different from the two sites in southeastern USA, there were no isoprene-epoxydiols-derived SOA and a biogenic influenced factor characterized by distinct *m/z* 91 resolved in urban Beijing, the same as addressed in Hu et al. (2015).

Overall, the proportions of OOA in OA in this study were comparable to the average (58%) obtained at other urban sites around the world (Zhang et al., 2011). In total, secondary species (SNA+SOA) accounted for 74, 80, 64 and 73% of the total PM_1, respectively. The serious secondary pollution stresses the importance of control measures targeting the emission reduction of gaseous precursors, e.g., NO_x, SO_2 and VOCs (Guo et al., 2014; Pye, et al., 2013).

3.2.1 Primary OA sources

COA

COA refers to OA emitted from cooking activities (Allan et al., 2010). The knowledge on the transformation of COA in the atmosphere is limited (Dall′Osto et al., 2015). The reductive alkyl fragment ions are abundant in the MS of COA (Fig. S28-S31). The abundance of fragments *m/z* 55 and *m/z* 57 (f_{55} and f_{57}, mass fractions of *m/z* 55

and *m/z* 57) in the MS of COA were about 7–10% and 3–4%, respectively. Higher f_{55} and f_{57} are the most remarkable characteristic in the MS of identified COA factors, which are crucial to identify COA and HOA (Mohr et al., 2012). In this study, f_{55} in COA factors was significantly higher than in corresponding HOA factors, and f_{57} in COA factors were comparable to f_{57} in corresponding HOA factors (Fig. S28-S31). The oxidation state of COA was low, with low O/C (0.13–0.23) and OA/OC (1.33–1.46) ratios in this study.

As the edible oil is rich in oleic and linoleic acids (Dyer et al., 2008), the fragments *m/z* 55 and *m/z* 57 are not only contributed by the reductive alkyl fragments $C_4H_7^+$ and $C_4H_9^+$, but also by oxygenated fragments $C_3H_3O^+$ and $C_3H_5O^+$. The mass fractions of the later ones were about 1/3 of those of the reductive alkyl fragments with the same *m/z*. The ratios of oxygenated and reductive fragments *m/z* 55 and *m/z* 57 are used to identify the sources of OA. The ratio of $C_3H_3O^+$ to $C_3H_5O^+$ in COA is about 2, while in HOA about 1; the ratio of $C_4H_7^+$ and $C_4H_9^+$ in COA is about 2.5, in HOA approximate 1 (Mohr et al., 2012). In this study, the ratios of $C_3H_3O^+$ to $C_3H_5O^+$ in COA were 2.7, 3.4, 3.8 and 2.4, and in HOA were 4.1, 0.6, 0.0 and 1.3; the ratios of $C_4H_7^+$ and $C_4H_9^+$ in COA and HOA were 2.3, 1.8, 2.3 and 2.4, and 1.4, 1.6, 1.1 and 1.1 during four seasons, respectively.

The rationality of resolved COA factors was investigated through their concentrations, diurnal patterns, correlations of COA with external tracers, and the uncentered correlations (UC) of MS. The COA concentrations could be simply estimated with the formula provided by Mohr et al. (2012) based on the fragments *m/z* 55, *m/z* 57 and *m/z* 44. The estimated COA concentrations were 4.7, 4.4, 6.5 and 5.3 μg m^{-3} in four seasons, accounting for 33, 35, 35 and 18% of OA, respectively. Compared with the concentrations (2.6, 2.5, 5.2 and 4.3 μg m^{-3}) and proportions (19, 20, 28 and 15%) based on the AMS-PMF analysis (Fig. 5), the results were overestimated, especially in summer, which is likely related to the applicability of experience parameters in different regions and seasons. The COA factors showed apparent diurnal patterns during seasonal observations, which is a key feature in identifying COA (see Sect. 3.2.3).

COA correlated well with some gaseous and other particulate pollutants, e.g., NO_x and BC (Table S9-S12). Dall′Osto et al. (2015) considered that the COA factors at a rural site contained more sources other than cooking emissions, based on the good correlations between COA with HOA, BC, NO_x, nitrate, etc. The UC coefficients (Ulbrich et al., 2009) between the MS of resolved COA factors in this study and the average MS of COA in previous studies (Lanz et al., 2008; Mohr et al., 2009; Huang et al., 2010; He et al., 2010) were calculated. The UC coefficients were in the range of 0.910–0.990 (Table S13), confirming the good similarity and rationality of the

resolved COA factors.

In previous studies, it was reported that COA accounted for 14–25% (~20% on average) of the total OA in summer and winter in Beijing, with an average concentration (~6 μg m^{-3}), which is a relatively stable component of OA (Hu et al., 2016a; Wang et al., 2009). In this study, the concentrations and proportions of COA in OA during seasonal observations were in the range of 2.5–5.2 μg m^{-3} and 15–28%, respectively, comparable to previous results. The highest concentration and proportion of COA in autumn were likely caused by strong emissions from charcoal-grilling or barbecue activities, which are popular in Beijing and surrounding areas in autumn as mentioned above. Fewer cooking activities during and around the Chinese New Year holiday (7–19 Feb.) and the lower evaporation rates of cooking oils (Ndiaye et al., 2005) led to the lower concentration and proportion of COA in winter (Fig. S35). Overall, COA is an important non-fossil POA sources in all seasons, which should be taken into consideration, especially in autumn.

BBOA

The BBOA factors that were identified in spring and autumn accounted for 13% and 11% of OA, respectively. In summer and winter, the contributions of biomass burning to OA might be relatively low (probably<5%) and cannot be resolved in our dataset by PMF. Levoglucosan is a significant tracer of biomass burning emissions, the fragment of which, $C_2H_4O_2^+$ (*m/z* 60) is regarded as a tracer of BBOA (Alfarra et al., 2007; Cubison et al., 2011). The abundance of *m/z* 60 (~0.8–1.3%) in the MS of BBOA was much higher than the background abundance (0.3%) in the urban without biomass burning emissions, which is a primary feature in identifying BBOA factor. The O/C ratios (0.24–0.31) of BBOA factors were higher than those (0.07–0.18) of HOA, and comparable to those (0.2–0.4) in previous studies (Mohr et al., 2009; He et al., 2010, 2011). In spring, farmers start preparing fields and burn straw that was leftover on field. In autumn, burning crop straw randomly happened quite often during the harvest season for corn and other crops in North China. These phenomena result in serious atmospheric particulate pollution in Beijing and surrounding areas (Duan et al., 2004; Zheng et al., 2005).

BBOA tracked well (Tables S9 and S11) with chloride, BC, $C_2H_4O_2^+$ and acetonitrile, similar to the results of previous studies (DeCarlo et al., 2010; He et al., 2011; Gong et al., 2012). Particles emitted from biomass burning could contains a high proportion of chlorides (Silva et al., 1999). The diurnal variations of BBOA were similar with those of HOA, with higher concentrations at night and in the morning and lower ones in the daytime (see Sect. 3.2.3). They could be partially attributed to similar emission processes, such as residential burning activities.

CCOA

Coal accounts for two third of the total primary energy consumption and coal combustion is an important source of air pollution in China (You and Xu, 2010; Huang et al., 2014). CCOA was only resolved in winter, consistent with the domestic heating period, suggesting that this CCOA factor was dominated by residential burning with higher OA emission factors (Hu et al., 2016a). In addition to typical ion fragments from fossil fuel combustion, alkyl fragments ($C_nH_{2n+1}^+$ and $C_nH_{2n-1}^+$), the MS of CCOA also showed pronounced signals of polycyclic aromatic hydrocarbons (PAHs) ion fragments, e.g., $C_{10}H_8^+$ (*m/z* 128) from naphthalene and $C_{14}H_{10}^+$ (*m/z* 178) from anthracene (Fig. S31). The CCOA spectrum in winter is also similar to those in our previous studies at Changdao Island and in the winter of Beijing (Hu et al., 2013, 2016a). Compared to the average H/C ratios (1.76–1.96) in other POA factors (Canagaratna et al., 2015), H/C in CCOA (1.45) is lower. The O/C and OA/OC ratios in CCOA were 0.14 and 1.32, respectively. CCOA accounted for 17% of total OA on average, within the range of 10–33% reported in other studies in the winter of Beijing (Figure 5; Hu et al., 2016a).

HOA

HOA is the sum of unresolved reductive and primary OA except specific OA (e.g., COA, BBOA and CCOA), which is generally considered to be related to the emissions of fossil fuel combustion. The mass spectra (MS) features of HOA in this study are similar to those in previous studies (Huang et al., 2010; Hu et al., 2013 and references therein). Alkyl fragments ($C_nH_{2n+1}^+$ and $C_nH_{2n-1}^+$) are abundant in the spectra (Fig. S28-S31). During four observations, O/C and OA/OC ratios of HOA factors were 0.18, 0.19, 0.07 and 0.36, and 1.40, 1.41, 1.27 and 1.63 during four seasons, respectively. Compared with the corresponding ratios (O/C: 0.04–0.26; OA/OC: 1.21–1.50) of HOA in previous studies (Canagaratna et al., 2015), the higher values in winter were influenced by the contribution of BBOA. Absolutely independent sources cannot be identified by factor analysis (e.g. PMF model). Therefore, the typical MS features of OA from other primary sources can be found in the MS of HOA. In this study, the abundant fragment ions in the MS of POA factors, e.g., CCOA (*m/z* 67, 69, 91, etc.) and COA (*m/z* 55, 57, etc.) were also presented in the MS of HOA (He et al., 2011; Hu et al., 2013, 2016a). This can also be confirmed through the correlations between HOA and external tracers (See Table S9-S12). HOA tracked well (r=0.6–0.9, p<0.01) with traces of primary emissions (e.g., coal combustion and vehicular exhausts), such as chloride, NO_x, CO, BC and $C_2H_4O_2^+$, consistent with the primary sources of HOA.

3.2.2 Oxygenated OA sources

OOA, considered as a good alternative of SOA in most cases, has been extensively investigated in a large number of previous studies (Jimenez et al., 2009; Zhang et al., 2005; Ulbrich et al., 2009; Ng et al., 2011). During the seasonal observations, OOA was an important component of OA. In summer and winter, OOA was separated into MO-OOA and LO-OOA. Oxygenated fragments ($C_xH_yO_z^+$) are prominent in the MS of OOA. The abundance of $C_xH_yO_z^+$ in MO-OOA was higher than that in LO-OOA. For instance, the fragment of carboxylic acid CO_2^+ (*m/z* 44) accounted for 17–21% in MO-OOA, and 7–14% in LO-OOA. The average O/C ratios for SV-OOA, LV-OOA and OOA reported in some studies around the world were 0.53, 0.84 and 0.67, respectively (Canagaratna et al., 2015). In spring and autumn, the O/C ratios of OOA were 1.0 and 0.88, respectively. In summer and winter, the O/C ratios in resolved MO-OOA factors were about 0.91 and 0.84, higher than those of corresponding LO-OOA (0.67 and 0.77). In all four seasons, O/C ratios of OOA were higher than the average values mentioned above, indicating that OA was much more oxygenated and secondary formation contributed significantly to OA in urban Beijing.

Overall, OOA (MO-OOA+LO-OOA) correlated well (r=0.89–0.96, p<0.01) with secondary inorganics (sulfate and nitrate). MO-OOA, as extremely aged secondary species, exhibited good correlations with SNA (r=0.78–0.95, p<0.01). While, the correlation coefficients (r=0.63–0.89, p<0.01) between LO-OOA and SNA were slightly lower (Table S10 and S12). In summer, LO-OOA and nitrate trended well during most days; during the whole winter campaign, LO-OOA tracked well with nitrate. OOA had strong correlations with RH and/or LWC (Table S14), indicating that aqueous-phase reactions play a dominant role in OOA formation. The slope of OOA against O_x steepened with the increase of RH and LWC (Fig. S41–S42), also implying that the aqueous-phase oxidation was an important pathway of the OOA formation. The good correlations (r=0.53–0.73, p<0.01) between O_x and LO-OOA in summer, and between O_x and OOA in autumn and winter, suggesting photochemical processes also contributed substantially to SOA, especially LO-OOA, in these seasons (Xu et al., 2017). Note that gaseous pollutants and main chemical compositions in PM_1 displayed good correlations with each other in winter, which may be caused by regional pollution characteristics under weak weather system in heavy pollution days.

3.2.3 Diurnal variations of OA components

The diurnal patterns of OA components during seasonal observations are shown in Fig. 6. As mentioned above, the COA factors showed obvious diurnal patterns during all four campaigns, with two peaks at noon (about 13:00) and in the evening (about 20:00), in accordance with living habits of residents. The concentrations of COA factors

at the noon peak (about 12:00–14:00) were 3.1, 2.5, 4.0 and 4.4 μg m^{-3} on average, respectively. COA reached the highest concentrations in the evening (18:00–21:00), as 5.6, 6.2, 14.0 and 7.5 μg m^{-3} on average, respectively. HOA was lower in the daytime and higher at night. The nocturnal activities, such as heavy-duty diesel vehicles only permitted at night (Lin et al., 2009), biomass burning and coal combustion, could make more significant contributions to POA. In autumn, the OA concentrations began to raise in the evening, peaked at about 19:00, and kept higher at night (Fig. 2), reaching twice that in the daytime. As Fig. 6c shown, the anthropogenic emissions, e.g., biomass burning, coal combustion and especially cooking emissions, contributed significantly to OA. In winter, CCOA showed clear diurnal variations with high concentrations at night, consistent with the residential heating periods. The high concentration and (10 μg m^{-3}) and fraction (~30%) of CCOA in total OA points to strong coal combustion emissions at night in Beijing.

The peaks of OOA (or LO-OOA) coincided with the peaks of primary emitted COA (spring, summer and autumn) and HOA (winter) in diurnal patterns, probably because strong primary emissions favored SOA production. It has been found that primary emissions evaporate substantially upon dilution to ambient conditions and those vapors undergo photooxidation, which produces SOA efficiently (Robinson et al., 2007; Murphy and Pandis, 2009). In summer, OOA showed obvious diurnal variations: MO-OOA peaked in the morning and afternoon; LO-OOA showed two pronounced peaks at noon and at night. This was likely the co-effect of SOA formation via gas-phase photochemical reactions in the daytime and aqueous chemistry in humid air at night (Ervens et al., 2011; Lim et al., 2010). The concentration and proportion of LO-OOA increased significantly in the afternoon (12:00–16:00), up to 7 μg m^{-3} and 50%, respectively (Fig. 6b), suggesting that LO-OOA was a strong local/regional photochemical product despite the much higher PBL in the daytime (Hu et al., 2016a). Regardless of the air mass history (local, regional and long-distance transported), LO-OOA dominated OOA, accounting for 29–48% of OA (Fig. S43). In winter, despite the expanded PBL, MO-OOA increased gradually from noon, and peaked in the evening, implying that MO-OOA could form through photochemical oxidations in the daytime.

3.2.4 Source contributions to the OA increase

The probability distributions of OA and the fractions of OA components as a function of OA concentrations are illustrated in Fig. 7. In spring, autumn and winter, similar to the probability distributions of PM_1, the OA concentrations were frequently (about 50–80%) lower than 10 μg m^{-3}, due to the scavenging effect of strong wind accompanying long-range transported air parcels. In autumn and winter, primary emissions (e.g., cooking emission

and coal combustion) influenced strongly, resulting in the wide ranges of OA concentrations, up to 120 μg m^{-3} and 140 μg m^{-3}, respectively. In contrast, OA concentrations presented a skewed-normal distribution, mainly in the range of 5–20 μg m^{-3} in summer, similar to previous results (Huang et al., 2010; Hu et al., 2016a).

During the spring observation (Fig. 7a), as the OA concentration was less than 10 μg m^{-3}, OOA dominated OA (up to 55%), which was likely associated with the new particle formation in clean atmosphere (Wu et al., 2007). When the OA concentration was higher than 10 μg m^{-3}, OOA primarily contributed to the increase of OA. The fraction of OOA kept as about 50–60% as the OA concentration was over 25 μg m^{-3}. In summer, as the OA concentration was lower than 30 μg m^{-3}, OOA accounted for about 60–70% of OA (Fig. 7b). As mentioned above, LO-OOA formation was efficient due to both the strong photochemical and aqueous-phase processes under high RH and high temperature conditions (Xu et al., 2017). With the increase of OA, the fraction of MO-OOA enhanced gradually, implying that the aged MO-OOA contributed importantly to the OA increase. In autumn, with the increase of OA, the proportion of OOA decreased gradually (Fig. 7c). In winter, when the OA concentration was lower than 70 μg m^{-3}, OOA and POA contributed equally to OA, while the fraction of LO-OOA increased gradually (Fig. 7d). In both autumn and winter, the fractions of OOA slightly increased around 100 μg m^{-3}. More work is needed to accurately clarify the cause of the OOA increase within this range.

In spring, summer, and autumn, as the OA concentration was higher than 30 μg m^{-3}, the fraction of COA in OA increased to different extent, reaching 30–60%. In autumn, the contributions of BBOA and HOA to OA were relatively stable, while that of COA dramatically enhanced with OA increase, probably because that the static air during some intervals (e.g., 23-25 Oct.) was not conducive to the dispersal of heavy emissions from cooking activities (Fig. S8 and Fig. S34). Furthermore, in autumn intensive barbecue activities in urban Beijing and surrounding areas could be an important source of COA as mentioned above. These results indicate that strong cooking emissions were responsible for high OA concentrations partially in these seasons. In winter, when the OA concentration reached 100 μg m^{-3}, the fraction of CCOA dramatically increased, from 10% to about 40%, indicating that the strong emissions from coal combustion contributed predominately to high OA concentrations (Hu et al., 2016a). The O/C ratios of OA at different OA concentrations were dependent on the source contributions, showing lower values when the POA were dominant in all seasons (Fig. 7).

3.3 The aging process of OA

3.3.1 Elemental ratios, van Krevelen diagram and carbon oxidation state

Some important metrics or tools, such as elemental ratios, the van Krevelen (VK) diagram and carbon oxidation state (OS_C) of OA are used to investigate dynamic evolution and oxidation mechanisms for bulk organic aerosols.

The elemental compositions of OA are closely related to their properties, e.g., density, hygroscopicity and vapor pressure. The element ratios and OA/OC ratios in OA obtained from seasonal observations in Beijing and at other urban and rural/suburban sites are listed in Table 2. During the campaigns, the average O/C and H/C ratios (in atomic number), and OA/OC ratios were in the range of 0.47–0.53, 1.52–1.63, and 1.77–1.88, respectively. In spring, the average OA/OC ratio in Beijing was lower than those determined in Mexico City, Bologna, and at Changdao Island (Table 2). In the summers of 2011–2012, the OA/OC ratios in Beijing were higher than those measured at urban sites in Shenzhen and Riverside, and rural/suburban sites in Jiaxing and Melpitz, indicating a high oxidation state of OA due to strong SOA formations via photochemical reactions in Beijing. However, in summers of 2008 in Beijing and 2010 in Shanghai, the OA/OC ratios were quite lower, maybe because the reduction of pollutant emissions reduced SOA formation during the Beijing Olympic Games and Shanghai World Expo, respectively. In autumn, the OA/OC ratio in Beijing was slightly higher than that in Shenzhen, but far lower than those obtained at rural/suburban sites, e.g., Kaiping, Heshan and Melpitz. The observed OA/OC ratio in Beijing in winter 2012 was higher than those in Fresno and in Beijing 2010, but comparable to or lower than those at rural/suburban sites such as Ziyang, Jiaxing and Melpitz. Overall, the OA/OC ratios in Beijing were higher among urban sites except for in spring, and lower among rural/suburban sites except for in summer.

The van Krevelen (VK) Diagram is an important tool to investigate the evolution and functional group alteration of OA (Heald et al., 2010). As shown in Table 3 and Fig. S36–S38, H/C and O/C ratios of OA exhibit good negative correlation (coefficient of determination r^2 = 0.70–0.79), with the slopes -0.57, -0.62 and -0.67, and intercepts 1.91, 1.94, 1.90 in the VK diagram in spring, summer and autumn, respectively. The slopes are flatter than those (-1.0–-0.7) obtained across the world (Chen et al., 2015), but are steeper than that determined in Ziyang (Table 3). The intercepts are slightly lower than those (2.1–2.2) at urban and downwind sites (Chen et al., 2015). However, the VK diagram in winter (Fig. 8 and Fig. S39) does not show any correlation (r^2 = 0.02) between H/C and O/C. The slope is nearly zero (-0.08). This is possibly caused by the more complex sources of OA in winter, e.g., CCOA was only resolved in winter.

Heald et al. (2010) concluded that OA trends to evolve along with a slope of -1 in the VK Diagram. Ng et al.

(2011) derived that the evolution from SV-OOA to LV-OOA is mainly along with a slope of approximately -0.5, and is associated with the replacement of carboxyl functional group (OH-(C=O)-). The identified reactions related to the alteration of functional groups are shown in Fig. 8. In spring, summer and autumn, the slopes fell between -1 (the addition of carboxyl functional groups without fragmentation or carbonyl and hydroxyl in different carbons) and -0.5 (carboxyl functionalization with fragmentation). In winter, the nearly zero slope of the VK Diagram suggests that hydroxylation and/or peroxidation processes (slope = 0) were likely to occur in Beijing during winter. On the other hand, carboxylation process might be unlikely to occur since the slope is higher than -0.5.

The average carbon oxidation state ($\overline{OS_C}$), approximated by 2×O/C–H/C, can also reflect the oxidation degree of OA (Kroll et al., 2011). The estimated $\overline{OS_C}$ of OA during seasonal observations are listed in Table 2 and the integrated Tri-VK-$\overline{OS_C}$ diagram is shown as Fig. 8. In summer and winter, the average carbon oxidation states were higher, with the average of -0.54±0.27 (in the range of -1.42–0.23) and -0.58±0.25 (-1.32–0.11), respectively. In spring and autumn, the average carbon oxidation states were -0.64±0.37 (-1.96–0.55) and -0.66±0.39 (-1.66–0.64). Compared with previous studies, in spring, the $\overline{OS_C}$ was significantly lower than those at Changdao Island and Bologna sites, but slightly higher than that in Mexico City. In summer, the $\overline{OS_C}$ was comparable to those in Beijing in 2011 and Melpitz, and much higher than those in Beijing in 2008, Shenzhen, Shanghai, Riverside, and Jiaxing. In autumn, it was higher than that in Shenzhen, lower than those in Kaiping and Melpitz, and close to that at Heshan site. The $\overline{OS_C}$ in winter was significantly higher than those in Beijing 2010, Fresno and Jiaxing, but lower than those in Ziyang and Melpitz. Compared with the oxidation states of SV-OOA, OOA and LV-OOA summarized by Canagaratna et al. (2015), the oxidation states of OOA, especially LO-OOA, in Beijing were generally higher than in other areas (Fig. 8). The oxidation states of MO-OOA in Beijing were only lower than those in very aged air masses in Ziyang in the basin (Hu et al., 2016b), over Mexico City (DeCarlo et al., 2010) and in Barcelona (Mohr et al., 2012). The oxidation states of LO-OOA were only slightly lower than those of MO-OOA in Beijing, and were comparable to those of MO-OOA in other urban areas (Fig. 8).

In summary, in urban Beijing, bulk organic aerosols were in a higher oxidation state in summer and in a medium oxidation state in other seasons, and were less oxygenated than at several rural/suburban sites. The possible reasons for relatively higher oxidation states of OA in Beijing could be the high hygroscopicity of aerosols and high OH radical concentration in air (Jimenez et al., 2009). The trend of increasing hygroscopicity with increasing O/C is robust based on field observations in Beijing and at several other sites (Jimenez et al., 2009; Wu et al., 2016). Xu et al. (2017) suggest a major role of aqueous-phase processes in increasing the oxidation degree of SOA in

Beijing based on the consistency of higher O/C of SOA and higher RH. Lim et al. (2010) suggest that reactions with OH radicals tend to be faster and form more SOA than non-radical reactions. High daily maximum concentrations ($0.4–1.7\times10^7$ cm^{-3}) for OH were observed in the North China Plain (Lu et al., 2013; Tan et al., 2017).

3.3.2 Evolution of OA along with the aging of air masses

The aging process of the air mass indicates that the physical and chemical changes occur and that secondary organics or inorganics form continuously, and the physicochemical properties of the air mass are modified during the transport of the air mass from source areas. In previous literatures, the ratio or standardized ratio of NO_x to NO_y concentrations, is used as a criterion to characterize the aging degree of air masses (Liang et al., 1998). Here the metric -log (NO_x/NO_y) is used to investigate the relationship between OA oxidation and the aging of air masses. The larger the metric is, the more aged the air mass is (Kleinman et al., 2008; Decarlo et al., 2008, 2010).

When -log (NO_x/NO_y) <0.1, the air plume is considered fresh (Liang et al., 1998). The maxima of the parameter -log (NO_x/NO_y) were about 0.4, 0.4, 0.2, and 0.2 during seasonal observations, in accordance with the photochemical reactions which were more active in spring and summer due to strong solar radiation, while in autumn and winter, the plumes of primary emissions had greater impacts. The urban Beijing was under the control of the relatively aged air masses during some periods (e.g., 23–24 Apr., 17–18 Aug., and 26–27 Oct. 2012). However, compared with the aerial results in Mexico City, where the highest -log (NO_x/NO_y) exceeded 1.4 (DeCarlo et al., 2010), the aging degree of air masses in urban Beijing were much lower.

The scatterplot of H/C vs. O/C ratios in Tri-VK-$\overline{\mathbf{OS_C}}$ diagram (Fig. 8) was colored with -log (NO_x/NO_y). There was a trend that the oxidation state of OA was higher (i.e., lower H/C ratio, and higher O/C ratio and $\overline{\mathbf{OS_C}}$) as the air mass aged more (from the upper left to the lower right). The OA factors resolved by the AMS-PMF analysis during seasonal campaigns are also marked in Fig. 8. In the order from POA (HOA, COA, CCOA and BBOA) to SOA (LO-OOA, OOA and MO-OOA), the factors evolved along with the direction to a higher oxidation state, which is consistent with the oxidation characteristics of the factors.

The OA/ΔCO ratio is used to evaluate the contribution of SOA formation, where ΔCO is CO subtracted the regional background concentration (0.1 ppmv) to exclude the influences of emitted and transported OA (de Gouw and Jimenez, 2009; DeCarlo et al., 2010). With the SOA formation, the OA/ΔCO ratio increases. The average of OA/ΔCO ratios (in the range of first and ninety-ninth percentile) were 37.0±30.7, 25.0±16.4, 20.3±16.5 and 15.1±8.1 μg m^{-3} $ppmv^{-1}$, respectively. The ratios were comparable to or higher than the urban ΔPOA/ΔCO ratios

(<15 μg m^{-3} $ppmv^{-1}$), but were much lower than the OA/ΔCO ratios (70±20 μg m^{-3} $ppmv^{-1}$) in aged urban air (de Gouw and Jimenez, 2009), implying that the contribution of POA was considerable in Beijing during seasonal campaigns, especially in autumn and winter.

Investigating the variations of OA/ΔCO ratios with the aging process of air masses can help reveal the formation rate of SOA and parameterize it in the model simulation (Dzepina et al., 2011). The scatterplots of OA/ΔCO ratios over O/C ratios during the seasonal observations in Beijing are shown in Fig. 9, colored with the metric -log (NO_x/NO_y). In laboratory and field studies on OA aging under strong oxidizing conditions, it was found that the OA/ΔCO ratios remain relatively stable at high O/C ratios with the increase of O/C ratios because organics obtain oxygen atoms but loss carbon atoms in the oxidation processes (DeCarlo et al., 2008, 2010). During seasonal campaigns in Beijing, the OA/ΔCO ratios showed different trends with the increase of O/C ratios as well as aging degrees of air masses (Fig. 9). Due to the intricate sources of OA in urban Beijing, the O/C ratios cannot reach higher values and the OA/ΔCO cannot remain an obviously stable level. In autumn, the OA/ΔCO ratios decreased with the increase of O/C ratios in more aged air masses, suggesting that reductive POA contributed substantially to high OA concentrations. An important reason for the decrease of OA/ΔCO ratios in aged air in autumn is the mixing of urban and biomass burning plumes with high CO content (DeCarlo et al., 2010). In summer and winter, along with the increase of O/C ratios and the aging degree of air masses, the OA/ΔCO ratios trended to increase, indicating the material contribution of SOA formation. Guo et al. (2014) concluded that photochemical oxidations of VOCs from urban traffic emissions are primarily responsible for the secondary formation during severe aerosol pollution events. Many studies reported the rapid increase of SOA significantly exceeding the initial POA emission ratios in urban atmosphere in a day in the absence of biomass burning (DeCarlo et al., 2010).

In mass spectra measured by the AMS, some relatively abundant fragment ions have certain representativeness. As mentioned above, *m/z* 43 and *m/z* 44, mainly as $C_2H_3O^+$ and CO_2^+, respectively, are predominant in the MS of OOA. While in the MS of HOA *m/z* 43 is mainly composed of alkyl fragment $C_3H_7^+$ (Ng et al., 2010). The difference between the relative contents of *m/z* 43 and *m/z* 44 in OA can reflect the oxidation degree, e.g., the abundance of *m/z* 44 in MO-OOA is higher than that in LO-OOA. The fragment *m/z* 60 (mainly $C_2H_4O_2^+$) is often used as a tracer of biomass burning (Alfarra et al., 2007; Cubison et al., 2011).

The scatterplots of f_{44} against f_{43}, and f_{44} against f_{60} during seasonal campaigns are shown in Fig. 10, colored with -log (NO_x/NO_y). The data points in the scatterplots of f_{44} vs. f_{43} substantially fell into the triangle derived by

Ng et al. (2010). As the aging degree of air masses increased, OA showed the evolution trends moving from the lower right to the upper left generally in the triangle. The POA factors (HOA, COA, CCOA and BBOA) are concentrated in the bottom of the triangle, LO-OOA with a higher oxidation state is in an intermediate location, and MO-OOA with the highest oxidation state is at the top of the triangle. Ng et al. (2010) found that with the enhancement of OA oxidation, data points gradually move upward from the lower half of the triangle through summarizing the results of chamber experiments and field observations.

In the scatterplots of f_{44} vs. f_{60}, the majority of the data points concentrated on the left side and presented in a band-shaped region (Fig. 10e-h). Cubison et al. (2011) found that in the f_{44} against f_{60} space, data from biomass burning appear in the lower right part, while data with negligible biomass burning influence are concentrated on the left side as a band shape. There are a part of data points appearing in the conceptual space for BBOA (Cubison et al., 2011), more obviously in spring, autumn and winter (Fig. 10e, g, h). In spring and autumn, a large number of data points are of higher f_{60} than in other seasons, and the aging degrees of air masses were low ($-\log(NO_x/NO_y) < 0.05$), which may be subject to biomass burning emissions as mentioned above. HOA, COA, CCOA, LO-OOA, MO-OOA and OOA are located on the left side, while BBOA appears in the right. With the increase of the aging degree of air masses, f_{60} did not trend to change dramatically, suggesting that the contribution of biomass burning to OA has no dependence on the aging degree of air masses.

4. Conclusions

We investigated the compositions of submicron aerosols during four seasons in urban Beijing with highly time-resolved HR-ToF-AMS measurements. These conclusions can be drawn:

(1) The submicron aerosol pollution in Beijing was serious. The average PM_1 was highest (82 μg m^{-3}) in winter, resulting from intense emissions due to adverse meteorological conditions and secondary formation, and lowest (38 μg m^{-3}) in summer due to frequent washout. Chemical compositions in PM_1 also showed seasonal dependence. Carbonaceous fraction (OA+BC) constituted more than 50% of PM_1 in autumn due to primary emissions, while SNA contributed 60% of PM_1 in other seasons.

(2) OA was identified as secondary fractions, MO-OOA and LO-OOA (or total OOA), and primary fractions COA, CCOA, BBOA, and HOA. In summer, OOA dominated OA (69%) due to the crucial contribution of SOA formation; while POA was almost equivalent (50–53%) to SOA in other seasons. SOA contributed to OA much

more significantly in winter (50%) than in previous studies (20–30%), which may be associated with stronger SOA formation under long-lasting static and heavy-polluted days.

(3) Secondary species (SNA+SOA) represented about 60–80% of PM_1 in four seasons, stressing the importance of measures targeting the reduction of gaseous precursor (NO_x, SO_2 and VOCs) emissions.

(4) OA was in a relatively high oxidation state in urban Beijing according to OA/OC and O/C ratios, and $\overline{\mathbf{OS_C}}$, especially in summer and winter. The $\overline{\mathbf{OS_C}}$ were -0.64, -0.54, -0.66 and -0.58 in four seasons, respectively. The evolution of OA was, along with the increase of oxidation state, from POA (HOA, COA, CCOA, and BBOA) to SOA (LO-OOA and MO-OOA). Meanwhile, higher oxidation states of OA were observed in more aged air masses.

In this study, the chemical compositions of PM_1 varied obviously in four seasons. Meteorological conditions and gaseous and particulate emissions determined the severity of atmospheric aerosol pollution. To prevent regional aerosol pollution effectively, further strengthening the control of primary particulate emissions is expected. In addition, the emissions of secondary species′ precursors must be reduced, especially in adverse meteorological conditions.

5. Data availability

The data presented in this article are available from the authors upon request (minhu@pku.edu.cn).

Acknowledgements

This work was supported by the National Natural Science Foundation of China (91544214, 41421064), the National Basic Research Program of China (2013CB228503) and National Key Research and Development Program of China (2016YFC0202003). The authors appreciate Prof. M. Shao and Dr. Y. Yang in Peking University for data of VOCs and Prof. J. Morrow in the Prefectural University of Kumamoto for his assistance in the word and grammar editing.

References

Alfarra, M. R., Prevot, A. S., Szidat, S., Sandradewi, J., Weimer, S., Lanz, V. A., Schreiber, D., Mohr, M., and Baltensperger, U.: Identification of the mass spectral signature of organic aerosols from wood burning emissions, Environ. Sci. Technol. 41, 5770-5777, 2007.

Aiken, A. C., Salcedo, D., Cubison, M. J., Huffman, J. A., DeCarlo, P. F., Ulbrich, I. M., Docherty, K. S., Sueper, D., Kimmel, J. R., Worsnop, D. R., Trimborn, A., Northway, M., Stone, E. A., Schauer, J. J., Volkamer, R. M., Fortner, E., de Foy, B., Wang, J., Laskin, A., Shutthanandan, V., Zheng, J., Zhang, R., Gaffney, J., Marley, N. A., Paredes-Miranda, G., Arnott, W. P., Molina, L. T., Sosa, G., and Jimenez, J. L.: Mexico City aerosol analysis during MILAGRO using high resolution aerosol mass spectrometry at the urban supersite (T0)–Part 1: Fine particle composition and organic source apportionment, Atmos. Chem. Phys., 9, 6633–6653, doi:10.5194/acp-9-6633-2009, 2009.

Allan, J. D., Williams, P. I., Morgan, W. T., Martin, C. L., Flynn, M. J., Lee, J., Nemitz, E., Phillips, G. J., Gallagher, M. W., and Coe, H.: Contributions from transport, solid fuel burning and cooking to primary organic aerosols in two UK cities, Atmos. Chem. Phys., 10, 647–668, doi:10.5194/acp-10-647-2010, 2010.

Bond, T. C., Doherty, S. J., Fahey, D. W., Forster, P. M., Berntsen, T., DeAngelo, B. J., Flanner, M. G., Ghan, S., Kärcher, B., Koch, D., Kinne, S., Kondo, Y., Quinn, P. K., Sarofim, M. C., Schultz, M. G., Schulz, M., Venkataraman, C., Zhang, H., Zhang, S., Bellouin, N., Guttikunda, S. K., Hopke, P. K., Jacobson, M. Z., Kaiser, J. W., Klimont, Z., Lohmann, U., Schwarz, J. P., Shindell, D., Storelvmo, T., Warren, S. G., and Zender, C. S.: Bounding the role of black carbon in the climate system: A scientific assessment, J. Geophys. Res. Atmos., 118, 5380-5552, doi:10.1002/jgrd.50171, 2013.

Budisulistiorini, S. H., Baumann, K., Edgerton, E. S., Bairai, S. T., Mueller, S., Shaw, S. L., Knipping, E. M., Gold, A., and Surratt, J. D.: Seasonal characterization of submicron aerosol chemical composition and organic aerosol sources in the southeastern United States: Atlanta, Georgia, and Look Rock, Tennessee, Atmos. Chem. Phys., 16, 5171-5189, doi:10.5194/acp-16-5171-2016, 2016.

Buseck, P. R., and Adachi, K.: Nanoparticles in the Atmosphere, Elements, 4, 389–394, doi:10.2113/gselements.4.6.389, 2008.

Canagaratna, M. R., Jimenez, J. L., Kroll, J. H., Chen, Q., Kessler, S. H., Massoli, P., Hildebrandt Ruiz, L., Fortner, E., Williams, L. R., Wilson, K. R., Surratt, J. D., Donahue, N. M., Jayne, J. T., and Worsnop, D. R.: Elemental ratio measurements of organic compounds using aerosol mass spectrometry: characterization, improved calibration, and implications, Atmos. Chem. Phys., 15, 253–272, doi:10.5194/acp-15-253-2015, 2015.

Carlton, A. G., Wiedinmyer, C., and Kroll, J. H.: A review of Secondary Organic Aerosol (SOA) formation from isoprene, Atmos. Chem. Phys., 9, 4987–5005, doi:10.5194/acp-9-4987-2009, 2009.

Chen, Q., Heald, C. L., Jimenez, J. L., Canagaratna, M. R., Zhang, Q., He, L.-Y., Huang, X.-F., Campuzano-Jost, P., Palm, B. B., Poulain, L., Kuwata, M., Martin, S. T., Abbatt, J. P. D., Lee, A. K. Y., and Liggio, J.: Elemental composition of organic aerosol: The gap between ambient and laboratory measurements, Geophys. Res. Lett., 42, 4182–4189, doi:10.1002/2015gl063693, 2015.

Cheng, Y., Zheng, G., Wei, C., Mu, Q., Zheng, B., Wang, Z., Gao, M., Zhang, Q., He, K., and Carmichael, G.: Reactive nitrogen chemistry in aerosol water as a source of sulfate during haze events in China, Sci. Adv., 2, e1601530, 2016.

Cubison, M. J., Ortega, A. M., Hayes, P. L., Farmer, D. K., Day, D., Lechner, M. J., Brune, W. H., Apel, E., Diskin, G. S., Fisher, J. A., Fuelberg, H. E., Hecobian, A., Knapp, D. J., Mikoviny, T., Riemer, D., Sachse, G. W., Sessions, W., Weber, R. J., Weinheimer, A. J., Wisthaler, A., and Jimenez, J. L.: Effects of aging on organic aerosol from open biomass burning smoke in aircraft and laboratory studies, Atmos. Chem. Phys., 11, 12049–12064, doi:10.5194/acp-11-12049-2011, 2011.

Dall'Osto, M., Paglione, M., Decesari, S., Facchini, M. C., O'Dowd, C., Plass-Duellmer, C., and Harrison, R. M.: On the origin of AMS "Cooking Organic Aerosol" at a rural site, Environ. Sci. Technol., 49, 13964–13972, 2015.

de Gouw, J., and Jimenez, J. L.: Organic aerosols in the Earth's atmosphere, Environ. Sci. Technol., 43, 7614–7618, 2009.

DeCarlo, P. F., Dunlea, E. J., Kimmel, J. R., Aiken, A. C., Sueper, D., Crounse, J., Wennberg, P. O., Emmons, L., Shinozuka, Y., Clarke, A., Zhou, J., Tomlinson, J., Collins, D. R., Knapp, D., Weinheimer, A. J., Montzka, D. D., Campos, T., and Jimenez, J. L.: Fast airborne aerosol size and chemistry measurements above Mexico City and Central Mexico during the MILAGRO campaign, Atmos. Chem. Phys., 8, 4027–4048, doi:10.5194/acp-8-4027-2008, 2008.

DeCarlo, P. F., Ulbrich, I. M., Crounse, J., de Foy, B., Dunlea, E. J., Aiken, A. C., Knapp, D., Weinheimer, A. J., Campos, T., Wennberg, P. O., and Jimenez, J. L.: Investigation of the sources and processing of organic aerosol over the Central Mexican Plateau from aircraft measurements during MILAGRO, Atmos. Chem. Phys., 10, 5257–5280, doi:10.5194/acp-10-5257-2010, 2010.

Docherty, K. S., Aiken, A. C., Huffman, J. A., Ulbrich, I. M., DeCarlo, P. F., Sueper, D., Worsnop, D. R., Snyder, D. C., Peltier, R. E., Weber, R. J., Grover, B. D., Eatough, D. J., Williams, B. J., Goldstein, A. H., Ziemann, P. J., and Jimenez, J. L.: The 2005 Study of Organic Aerosols at Riverside (SOAR-1): instrumental intercomparisons and fine particle composition, Atmos. Chem. Phys., 11, 12387–12420, doi:10.5194/acp-11-12387-2011, 2011.

Duan, F., Liu, X., Yu, T., and Cachier, H.: Identification and estimate of biomass burning contribution to the urban aerosol organic carbon concentrations in Beijing, Atmos. Environ., 38, 1275–1282, 2004.

Dyer, J. M., Stymne, S., Green, A. G., and Carlsson, A. S.: High-value oils from plants, Plant J., 54, 640-655, doi:10.1111/j.1365-313X.2008.03430.x, 2008.

Dzepina, K., Cappa, C. D., Volkamer, R. M., Madronich, S., DeCarlo, P. F., Zaveri, R. A., and Jimenez, J. L.: Modeling the multiday evolution and aging of secondary organic aerosol during MILAGRO 2006, Environ. Sci. Technol., 45, 3496–3503, 2011.

Ervens, B., Turpin, B. J., and Weber, R. J.: Secondary organic aerosol formation in cloud droplets and aqueous particles (aqSOA): a review of laboratory, field and model studies, Atmos. Chem. Phys., 11, 11069-11102, doi:10.5194/acp-11-11069-2011, 2011.

Fabian, P., Kohlpaintner, M., and Rollenbeck, R.: Biomass burning in the Amazon-fertilizer for the mountaineous rain forest in Ecuador, Environ. Sci. Pollut. Res., 12, 290–296, 2005.

Ge, X. L., Setyan, A., Sun, Y. L., and Zhang, Q.: Primary and secondary organic aerosols in Fresno, California during wintertime: Results from high resolution aerosol mass spectrometry, J. Geophys. Res.-Atmos., 117, D19301, doi:10.1029/2012jd018026, 2012.

Gong, Z., Lan, Z., Xue, L., Zeng, L., He, L., and Huang, X.: Characterization of submicron aerosols in the urban outflow of the central Pearl River Delta region of China, Front. Environ. Sci. Eng., 6, 725–733, 2012.

Gong, Z., Xue, L., Sun, T., Deng, Y., He, L., and Huang, X.: Online measurement of PM_1 chemical composition and size distribution using a high-resolution aerosol mass spectrometer during 2011 Shenzhen Universiade, Sci. Sinica Chim., 43, 363–372, doi:10.1360/032012-384, 2013.

Guo, S., Hu, M., Wang, Z., Slanina, J., and Zhao, Y.: Size-resolved aerosol water-soluble ionic compositions in the summer of Beijing: implication of regional secondary formation, Atmos. Chem. Phys., 10, 947–959, doi:10.5194/acp-10-947-2010, 2010.

Guo, S., Hu, M., Guo, Q., Zhang, X., Zheng, M., Zheng, J., Chang, C. C., Schauer, J. J., and Zhang, R.: Primary sources and secondary formation of organic aerosols in Beijing, China, Environ. Sci. Technol., 46, 9846-9853, 10.1021/es2042564, 2012.

Guo, S., Hu, M., Guo, Q., Zhang, X., Schauer, J. J., and Zhang, R.: Quantitative evaluation of emission controls on primary and secondary organic aerosol sources during Beijing 2008 Olympics, Atmos. Chem. Phys., 13, 8303–8314, doi:10.5194/acp-13-8303-2013, 2013.

Guo, S., Hu, M., Zamora, M. L., Peng, J., Shang, D., Zheng, J., Du, Z., Wu, Z., Shao, M., Zeng, L., Molina, M. J., and Zhang, R.: Elucidating severe urban haze formation in China, Proc. Natl. Acad. Sci. USA, 111, 17373–17378, 2014.

Hallquist, M., Wenger, J., Baltensperger, U., Rudich, Y., Simpson, D., Claeys, M., Dommen, J., Donahue, N., George, C., and Goldstein, A.: The formation, properties and impact of secondary organic aerosol: current and emerging issues, Atmos. Chem. Phys., 9, 5155–5236, doi:10.5194/acp-9-5155-2009, 2009.

He, L.Y., Huang, X.F., Xue, L., Hu, M., Lin, Y., Zheng, J., Zhang, R., and Zhang, Y.-H.: Submicron aerosol analysis and organic source apportionment in an urban atmosphere in Pearl River Delta of China using high-resolution aerosol mass spectrometry, J. Geophys. Res.-Atmos., 116, D12304, doi:10.1029/2010JD014566, 2011.

He, L. Y., Lin, Y., Huang, X. F., Guo, S., Xue, L., Su, Q., Hu, M., Luan, S. J., and Zhang, Y. H.: Characterization of high-resolution aerosol mass spectra of primary organic aerosol emissions from Chinese cooking and biomass burning, Atmos. Chem. Phys., 10, 11535–11543, doi:10.5194/acp-10-11535-2010, 2010.

Heald, C. L., Kroll, J. H., Jimenez, J. L., Docherty, K. S., DeCarlo, P. F., Aiken, A. C., Chen, Q., Martin, S. T., Farmer, D. K., and Artaxo, P.: A simplified description of the evolution of organic aerosol composition in the atmosphere, Geophys. Res. Lett., 37, L08803, doi:10.1029/2010gl042737, 2010.

Hu, W., Hu, M., Hu, W., Jimenez, J. L., Yuan, B., Chen, W., Wang, M., Wu, Y., Chen, C., Wang, Z., Peng, J., Zeng, L., and Shao, M.: Chemical composition, sources and aging process of sub-micron aerosols in Beijing: contrast between summer and winter, J. Geophys. Res.-Atmos., 121, 1955–1977, doi: 10.1002/2015JD024020, 2016a.

Hu, W., Hu, M., Hu, W. W., Niu, H., Zheng, J., Wu, Y., Chen, W., Chen, C., Li, L., Shao, M., Xie, S., and Zhang, Y.: Characterization of submicron aerosols influenced by biomass burning at a site in the Sichuan Basin, southwestern China, Atmos. Chem. Phys., 16, 13213–13230, doi:10.5194/acp-16-13213-2016, 2016b.

Hu, W. W., Campuzano-Jost, P., Palm, B. B., Day, D. A., Ortega, A. M., Hayes, P. L., Krechmer, J. E., Chen, Q., Kuwata, M., Liu, Y. J., de Sá, S. S., McKinney, K., Martin, S. T., Hu, M., Budisulistiorini, S. H., Riva, M., Surratt, J. D., St. Clair, J. M., Isaacman-Van Wertz, G., Yee, L. D., Goldstein, A. H., Carbone, S., Brito, J., Artaxo, P., de Gouw, J. A., Koss, A., Wisthaler, A., Mikoviny, T., Karl, T., Kaser, L., Jud, W., Hansel, A., Docherty, K. S., Alexander, M. L., Robinson, N. H., Coe, H., Allan, J. D., Canagaratna, M. R., Paulot, F., and Jimenez, J. L.: Characterization of a real-time tracer for isoprene epoxydiols-derived secondary organic aerosol (IEPOX-SOA) from aerosol mass spectrometer measurements, Atmos. Chem. Phys., 15, 11807-11833, doi:10.5194/acp-15-11807-2015, 2015.

Hu, W. W., Hu, M., Deng, Z. Q., Xiao, R., Kondo, Y., Takegawa, N., Zhao, Y. J., Guo, S., and Zhang, Y. H.: The characteristics and origins of carbonaceous aerosol at a rural site of PRD in summer of 2006, Atmos. Chem. Phys., 12, 1811–1822, doi:10.5194/acp-12-1811-2012, 2012.

Hu, W. W., Hu, M., Yuan, B., Jimenez, J. L., Tang, Q., Peng, J. F., Hu, W., Shao, M., Wang, M., Zeng, L. M., Wu, Y. S., Gong, Z. H., Huang, X. F., and He, L. Y.: Insights on organic aerosol aging and the influence of coal combustion at a regional receptor site of central eastern China, Atmos. Chem. Phys., 13, 10095–10112, doi:10.5194/acp-13-10095-2013, 2013.

Huang, X. F., Xue, L., Tian, X. D., Shao, W. W., Sun, T. L., Gong, Z. H., Ju, W. W., Jiang, B., Hu, M., and He, L.-Y.: Highly time-resolved carbonaceous aerosol characterization in Yangtze River Delta of China: Composition, mixing state and secondary formation, Atmos. Environ., 64, 200–207, 2013.

Huang, X. F., He, L. Y., Hu, M., Canagaratna, M. R., Sun, Y., Zhang, Q., Zhu, T., Xue, L., Zeng, L. W., Liu, X. G., Zhang, Y. H., Jayne, J. T., Ng, N. L., and Worsnop, D. R.: Highly time-resolved chemical characterization of atmospheric submicron particles during 2008 Beijing Olympic Games using an Aerodyne High-Resolution Aerosol Mass Spectrometer, Atmos. Chem. Phys., 10, 8933–8945, doi:10.5194/acp-10-8933-2010, 2010.

Huang, X. F., He, L. Y., Hu, M., Canagaratna, M. R., Kroll, J. H., Ng, N. L., Zhang, Y. H., Lin, Y., Xue, L., Sun, T. L., Liu, X. G., Shao, M., Jayne, J. T., and Worsnop, D. R.: Characterization of submicron aerosols at a rural site in Pearl River Delta of China using an Aerodyne High-Resolution Aerosol Mass Spectrometer, Atmos. Chem. Phys., 11, 1865–1877, doi:10.5194/acp-11-1865-2011, 2011.

Huang, X.-F., He, L.-Y., Xue, L., Sun, T.-L., Zeng, L.-W., Gong, Z.-H., Hu, M., and Zhu, T.: Highly time-resolved chemical characterization of atmospheric fine particles during 2010 Shanghai World Expo, Atmos. Chem. Phys., 12, 4897–4907, doi:10.5194/acp-12-4897-2012, 2012.

Huang, R.J., Zhang, Y., Bozzetti, C., Ho, K.F., Cao, J.J., Han, Y., Daellenbach, K.R., Slowik, J.G., Platt, S.M., Canonaco, F., Zotter, P., Wolf, R., Pieber, S.M., Bruns, E.A., Crippa, M., Ciarelli, G., Piazzalunga, A., Schwikowski, M., Abbaszade, G., Schnelle-Kreis, J., Zimmermann, R., An, Z., Szidat, S., Baltensperger, U., El Haddad, I., Prevot, A.S., 2014. High secondary aerosol contribution to particulate pollution during haze events in China. Nature 514, 218-222.

Jimenez, J. L., Canagaratna, M. R., Donahue, N. M., Prevot, A. S. H., Zhang, Q., Kroll, J. H., DeCarlo, P. F., Allan, J. D., Coe, H., Ng, N. L., Aiken, A. C., Docherty, K. S., Ulbrich, I. M., Grieshop, A. P., Robinson, A. L., Duplissy, J., Smith, J. D., Wilson, K. R., Lanz, V. A., Hueglin, C., Sun, Y. L., Tian, J., Laaksonen, A., Raatikainen, T., Rautiainen, J., Vaattovaara, P., Ehn, M., Kulmala, M., Tomlinson, J. M., Collins, D. R., Cubison, M. J., Dunlea, J., Huffman, J. A., Onasch, T. B., Alfarra, M. R., Williams, P. I., Bower, K., Kondo, Y., Schneider, J., Drewnick, F., Borrmann, S., Weimer, S., Demerjian, K., Salcedo, D., Cottrell, L., Griffin, R., Takami, A., Miyoshi, T., Hatakeyama, S., Shimono, A., Sun, J. Y., Zhang, Y. M., Dzepina, K., Kimmel, J. R., Sueper, D., Jayne, J. T., Herndon, S. C., Trimborn, A. M., Williams, L. R., Wood, E. C., Middlebrook, A. M., Kolb, C. E., Baltensperger, U., and Worsnop, D. R.: Evolution of Organic Aerosols in the Atmosphere, Science, 326, 1525-1529, doi:10.1126/science.1180353, 2009.

Kleinman, L. I., Springston, S. R., Daum, P. H., Lee, Y.-N., Nunnermacker, L., Senum, G., Wang, J., Weinstein-Lloyd, J., Alexander, M., and Hubbe, J.: The time evolution of aerosol composition over the Mexico City plateau, Atmos. Chem. Phys., 8, 1559–1575, doi:10.5194/acp-8-1559-2008, 2008.

Kroll, J. H., Donahue, N. M., Jimenez, J. L., Kessler, S. H., Canagaratna, M. R., Wilson, K. R., Altieri, K. E., Mazzoleni, L. R., Wozniak, A. S., Bluhm, H., Mysak, E. R., Smith, J. D., Kolb, C. E., and Worsnop, D. R.: Carbon oxidation state as a metric for describing the chemistry of atmospheric organic aerosol, Nat. Chem., 3, 133–139, 2011.

Lanz, V. A., Alfarra, M. R., Baltensperger, U., Buchmann, B., Hueglin, C., Szidat, S., Wehrli, M. N., Wacker, L., Weimer, S., Caseiro, A., Puxbaum, H., and Prevot, A. S. H.: Source attribution of submicron organic aerosols during wintertime inversions by advanced factor analysis of aerosol mass spectra, Environ. Sci. Technol., 42, 214–220, 2008.

Lee, A. K.: Haze formation in China: Importance of secondary aerosol, J. Environ. Sci., 33, 261-262, 2015.

Lee, S.-H., and Allen, H. C.: Analytical measurements of atmospheric urban aerosol, Anal. Chem., 84, 1196–1201, 2012.

Li, Y. J., Lee, B. P., Su, L., Fung, J. C. H., and Chan, C. K.: Seasonal characteristics of fine particulate matter (PM) based on high-resolution time-of-flight aerosol mass spectrometric (HR-ToF-AMS) measurements at the HKUST Supersite in Hong Kong, Atmos. Chem. Phys., 15, 37–53, doi:10.5194/acp-15-37-2015, 2015.

Liang, J., Horowitz, L. W., Jacob, D. J., Wang, Y., Fiore, A. M., Logan, J. A., Gardner, G. M., and Munger, J. W.: Seasonal budgets of reactive nitrogen species and ozone over the United States, and export fluxes to the global atmosphere, J. Geophys. Res.-Atmos., 103, 13435–13450, doi:10.1029/97JD03126, 1998.

Lim, Y. B., Tan, Y., Perri, M. J., Seitzinger, S. P., and Turpin, B. J.: Aqueous chemistry and its role in secondary organic aerosol (SOA) formation, Atmos. Chem. Phys., 10, 10521-10539, doi:10.5194/acp-10-10521-2010, 2010.

Lin, P., Hu, M., Deng, Z., Slanina, J., Han, S., Kondo, Y., Takegawa, N., Miyazaki, Y., Zhao, Y., and Sugimoto, N.: Seasonal and diurnal variations of organic carbon in $PM_{2.5}$ in Beijing and the estimation of secondary organic carbon, J. Geophys. Res.-Atmos., 114, D00G11, doi:10.1029/2008JD010902, 2009.

Lu, K. D., Hofzumahaus, A., Holland, F., Bohn, B., Brauers, T., Fuchs, H., Hu, M., Häseler, R., Kita, K., Kondo,

Y., Li, X., Lou, S. R., Oebel, A., Shao, M., Zeng, L. M., Wahner, A., Zhu, T., Zhang, Y. H., and Rohrer, F.: Missing OH source in a suburban environment near Beijing: observed and modelled OH and HO_2 concentrations in summer 2006, Atmos. Chem. Phys., 13, 1057-1080, doi:10.5194/acp-13-1057-2013, 2013.

Middlebrook, A. M., Bahreini, R., Jimenez, J. L., and Canagaratna, M. R.: Evaluation of Composition-Dependent Collection Efficiencies for the Aerodyne Aerosol Mass Spectrometer using Field Data, Aerosol Sci. Technol., 46, 258–271, 2012.

Mohr, C., Huffman, J. A., Cubison, M. J., Aiken, A. C., Docherty, K. S., Kimmel, J. R., Ulbrich, I. M., Hannigan, M., and Jimenez, J. L.: Characterization of primary organic aerosol emissions from meat cooking, trash burning, and motor vehicles with high-resolution aerosol mass spectrometry and comparison with ambient and chamber observations, Environ. Sci. Technol., 43, 2443–2449, 2009.

Mohr, C., DeCarlo, P. F., Heringa, M. F., Chirico, R., Slowik, J. G., Richter, R., Reche, C., Alastuey, A., Querol, X., Seco, R., Penuelas, J., Jimenez, J. L., Crippa, M., Zimmermann, R., Baltensperger, U., and Prevot, A. S. H.: Identification and quantification of organic aerosol from cooking and other sources in Barcelona using aerosol mass spectrometer data, Atmos. Chem. Phys., 12, 1649–1665, doi:10.5194/acp-12-1649-2012, 2012.

Murphy, B. N. and Pandis, S. N.: Simulating the formation of semivolatile primary and secondary organic aerosol in a regional chemical transport model, Environ. Sci. Technol., 43, 4722–4728, 2009.

Ng, N. L., Canagaratna, M. R., Zhang, Q., Jimenez, J. L., Tian, J., Ulbrich, I. M., Kroll, J. H., Docherty, K. S., Chhabra, P. S., Bahreini, R., Murphy, S. M., Seinfeld, J. H., Hildebrandt, L., Donahue, N. M., DeCarlo, P. F., Lanz, V. A., Prevot, A. S. H., Dinar, E., Rudich, Y., and Worsnop, D. R.: Organic aerosol components observed in Northern Hemispheric datasets from Aerosol Mass Spectrometry, Atmos. Chem. Phys., 10, 4625–4641, doi:10.5194/acp-10-4625-2010, 2010.

Ng, N. L., Canagaratna, M. R., Jimenez, J. L., Chhabra, P. S., Seinfeld, J. H., and Worsnop, D. R.: Changes in organic aerosol composition with aging inferred from aerosol mass spectra, Atmos. Chem. Phys., 11, 6465–6474, doi:10.5194/acp-11-6465-2011, 2011.

Ndiaye, P. M., Tavares, F. W., Dalmolin, I., Dariva, C., Oliveira, D., and Oliveira, J. V.: Vapor Pressure Data of Soybean Oil, Castor Oil, and Their Fatty Acid Ethyl Ester Derivatives, J. Chem. Eng. Data, 50, 330-333, doi:10.1021/je049898o, 2005.

Pye, H. O., R. W. Pinder, I. R. Piletic, Y. Xie, S. L. Capps, Y.-H. Lin, J. D. Surratt, Z. Zhang, A. Gold, and D. J. Luecken (2013), Epoxide pathways improve model predictions of isoprene markers and reveal key role of acidity in aerosol formation, Environ. Sci. Technol., 47(19), 11056-11064.

Poulain, L., Spindler, G., Birmili, W., Plass-Dulmer, C., Wiedensohler, A., and Herrmann, H.: Seasonal and diurnal variations of particulate nitrate and organic matter at the IfT research station Melpitz, Atmos. Chem. Phys., 11, 12579–12599, doi:10.5194/acp-11-12579-2011, 2011.

Robinson, A. L., Donahue, N. M., Shrivastava, M. K., Weitkamp, E. A., Sage, A. M., Grieshop, A. P., Lane, T. E., Pierce, J. R., and Pandis, S. N.: Rethinking organic aerosols: Semivolatile emissions and photochemical aging, Science, 315, 1259-1262, 2007.

Saarikoski, S., Carbone, S., Decesari, S., Giulianelli, L., Angelini, F., Canagaratna, M., Ng, N., Trimborn, A.,

Facchini, M., and Fuzzi, S.: Chemical characterization of springtime submicrometer aerosol in Po Valley, Italy, Atmos. Chem. Phys., 12, 8401–8421, doi:10.5194/acp-12-8401-2012, 2012.

Silva, P. J., Liu, D.-Y., Noble, C. A., and Prather, K. A.: Size and chemical characterization of individual particles resulting from biomass burning of local Southern California species, Environ. Sci. Technol., 33, 3068–3076, 1999.

Setyan, A., Zhang, Q., Merkel, M., Knighton, W. B., Sun, Y., Song, C., Shilling, J. E., Onasch, T. B., Herndon, S. C., Worsnop, D. R., Fast, J. D., Zaveri, R. A., Berg, L. K., Wiedensohler, A., Flowers, B. A., Dubey, M. K., and Subramanian, R.: Characterization of submicron particles influenced by mixed biogenic and anthropogenic emissions using high-resolution aerosol mass spectrometry: results from CARES, Atmos. Chem. Phys., 12, 8131-8156, doi:10.5194/acp-12-8131-2012, 2012.

Sun, J., Zhang, Q., Canagaratna, M. R., Zhang, Y., Ng, N. L., Sun, Y., Jayne, J. T., Zhang, X., Zhang, X., and Worsnop, D. R.: Highly time- and size-resolved characterization of submicron aerosol particles in Beijing using an Aerodyne Aerosol Mass Spectrometer, Atmos. Environ., 44, 131–140, 2010.

Sun, Y., Wang, Z., Dong, H., Yang, T., Li, J., Pan, X., Chen, P., and Jayne, J. T.: Characterization of summer organic and inorganic aerosols in Beijing, China with an Aerosol Chemical Speciation Monitor, Atmos. Environ., 51, 250–259, 2012.

Sun, Y., Wang, Z., Fu, P., Jiang, Q., Yang, T., Li, J., and Ge, X.: The impact of relative humidity on aerosol composition and evolution processes during wintertime in Beijing, China, Atmos. Environ., 77, 927–934, 2013a.

Sun, Y., Jiang, Q., Wang, Z., Fu, P., Li, J., Yang, T., and Yin, Y.: Investigation of the sources and evolution processes of severe haze pollution in Beijing in January 2013, J. Geophys. Res.-Atmos., 119, 4380–4398, 2014.

Sun, Y. L., Wang, Z. F., Du, W., Zhang, Q., Wang, Q. Q., Fu, P. Q., Pan, X. L., Li, J., Jayne, J., and Worsnop, D. R.: Long-term real-time measurements of aerosol particle composition in Beijing, China: seasonal variations, meteorological effects, and source analysis, Atmos. Chem. Phys., 15, 10149–10165, doi:10.5194/acp-15-10149-2015, 2015.

Sun, Y. L., Wang, Z. F., Fu, P. Q., Yang, T., Jiang, Q., Dong, H. B., Li, J., and Jia, J. J.: Aerosol composition, sources and processes during wintertime in Beijing, China, Atmos. Chem. Phys., 13, 4577–4592, doi:10.5194/acp-13-4577-2013, 2013b.

Tan, Z., Fuchs, H., Lu, K., Hofzumahaus, A., Bohn, B., Broch, S., Dong, H., Gomm, S., Häseler, R., He, L., Holland, F., Li, X., Liu, Y., Lu, S., Rohrer, F., Shao, M., Wang, B., Wang, M., Wu, Y., Zeng, L., Zhang, Y., Wahner, A., and Zhang, Y.: Radical chemistry at a rural site (Wangdu) in the North China Plain: observation and model calculations of OH, HO_2 and RO_2 radicals, Atmos. Chem. Phys., 17, 663-690, doi:10.5194/acp-17-663-2017, 2017.

Turpin, B. J., Saxena, P., and Andrews, E.: Measuring and simulating particulate organics in the atmosphere: problems and prospects, Atmos. Environ., 34, 2983–3013, 2000.

Ulbrich, I. M., Canagaratna, M. R., Zhang, Q., Worsnop, D. R., and Jimenez, J. L.: Interpretation of organic components from Positive Matrix Factorization of aerosol mass spectrometric data, Atmos. Chem. Phys., 9,

2891–2918, doi:10.5194/acp-9-2891-2009, 2009.

Wang, G., Zhang, R., Gomez, M. E., Yang, L., Levy Zamora, M., Hu, M., Lin, Y., Peng, J., Guo, S., Meng, J., Li, J., Cheng, C., Hu, T., Ren, Y., Wang, Y., Gao, J., Cao, J., An, Z., Zhou, W., Li, G., Wang, J., Tian, P., Marrero-Ortiz, W., Secrest, J., Du, Z., Zheng, J., Shang, D., Zeng, L., Shao, M., Wang, W., Huang, Y., Wang, Y., Zhu, Y., Li, Y., Hu, J., Pan, B., Cai, L., Cheng, Y., Ji, Y., Zhang, F., Rosenfeld, D., Liss, P. S., Duce, R. A., Kolb, C. E., and Molina, M. J.: Persistent sulfate formation from London Fog to Chinese haze, Natl. Acad. Sci. USA, 113, 13630-13635, 2016.

Wang, Q., Shao, M., Zhang, Y., Wei, Y., Hu, M., and Guo, S.: Source apportionment of fine organic aerosols in Beijing, Atmos. Chem. Phys., 9, 8573–8585, doi:10.5194/acp-9-8573-2009, 2009.

Weimer, S., Drewnick, F., Hogrefe, O., Schwab, J. J., Rhoads, K., Orsini, D., Canagaratna, M., Worsnop, D. R., and Demerjian, K. L.: Size-selective nonrefractory ambient aerosol measurements during the Particulate Matter Technology Assessment and Characterization Study–New York 2004 Winter Intensive in New York City, J. Geophys. Res.-Atmos., 111, D18305, doi:10.1029/2006JD007215, 2006.

Wu, Z. J., Cheng, Y. F., Hu, M., Wehner, B., Sugimoto, N., and Wiedensohler, A.: Dust events in Beijing, China (2004-2006): comparison of ground-based measurements with columnar integrated observations, Atmos. Chem. Phys., 9, 6915-6932, doi:10.5194/acp-9-6915-2009, 2009.

Wu, Z. J., Hu, M., Liu, S., Wehner, B., Bauer, S., Ssling, A. M., Wiedensohler, A., Petaja, T., Dal Maso, M., and Kulmala, M.: New particle formation in Beijing, China: Statistical analysis of a 1-year data set, J. Geophys. Res.-Atmos., 112, D09209, doi:10.1029/2006JD007406, 2007.

Wu, Z. J., Zheng, J., Shang, D. J., Du, Z. F., Wu, Y. S., Zeng, L. M., Wiedensohler, A., and Hu, M.: Particle hygroscopicity and its link to chemical composition in the urban atmosphere of Beijing, China, during summertime, Atmos. Chem. Phys., 16, 1123-1138, doi:10.5194/acp-16-1123-2016, 2016.

Xu, J., Zhang, Q., Chen, M., Ge, X., Ren, J., and Qin, D.: Chemical composition, sources, and processes of urban aerosols during summertime in northwest China: insights from high-resolution aerosol mass spectrometry, Atmos. Chem. Phys., 14, 12593-12611, doi:10.5194/acp-14-12593-2014, 2014.

Xu, W., Han, T., Du, W., Wang, Q., Chen, C., Zhao, J., Zhang, Y., Li, J., Fu, P., Wang, Z., Worsnop, D. R., and Sun, Y.: Effects of aqueous-phase and photochemical processing on secondary organic aerosol formation and evolution in Beijing, China, Environ. Sci. Technol., 51, 762-770, 2017.

You, C., and Xu, X.: Coal combustion and its pollution control in China, Energy, 35, 4467-4472, 2010.

Zhang, J. K., Sun, Y., Liu, Z. R., Ji, D. S., Hu, B., Liu, Q., and Wang, Y. S.: Characterization of submicron aerosols during a month of serious pollution in Beijing, 2013, Atmos. Chem. Phys., 14, 2887-2903, doi:10.5194/acp-14-2887-2014, 2014.

Zhang, Q., Alfarra, M. R., Worsnop, D. R., Allan, J. D., Coe, H., Canagaratna, M. R., and Jimenez, J. L.: Deconvolution and quantification of hydrocarbon-like and oxygenated organic aerosols based on aerosol mass spectrometry, Environ. Sci. Technol., 39, 4938-4952, 2005.

Zhang, Q., Jimenez, J. L., Canagaratna, M. R., Ulbrich, I. M., Ng, N. L., Worsnop, D. R., and Sun, Y.: Understanding atmospheric organic aerosols via factor analysis of aerosol mass spectrometry: a review, Anal.

Bioanal. Chem., 401, 3045–3067, 2011.

Zhang, Y., Sun, J., Zhang, X., Shen, X., Wang, T., and Qin, M.: Seasonal characterization of components and size distributions for submicron aerosols in Beijing, Sci. China Earth Sci., 56, 890–900, 2013.

Zhang, Y. M., Zhang, X. Y., Sun, J. Y., Hu, G. Y., Shen, X. J., Wang, Y. Q., Wang, T. T., Wang, D. Z., and Zhao, Y.: Chemical composition and mass size distribution of PM_1 at an elevated site in central east China, Atmos. Chem. Phys., 14, 12237-12249, doi:10.5194/acp-14-12237-2014, 2014.

Zheng, X., Liu, X., Zhao, F., Duan, F., Yu, T., and Cachier, H.: Seasonal characteristics of biomass burning contribution to Beijing aerosol, Sci. China Ser. B Chem., 48, 481–488, 2005.

Zhu, Q., He, L.-Y., Huang, X.-F., Cao, L.-M., Gong, Z.-H., Wang, C., Zhuang, X., and Hu, M.: Atmospheric aerosol compositions and sources at two national background sites in northern and southern China, Atmos. Chem. Phys., 16, 10283–10297, doi:10.5194/acp-16-10283-2016, 2016.

Table 1 Seasonal variations of main chemical components in PM_1 and gaseous pollutants, and meteorological conditions (temperature, T; relative humidity, RH; wind speed, WS; pressure, P). The data are listed in the form of "average±standard deviation". Units of particulate and gaseous pollutants are ppbv and μg m^{-3}, respectively.

	Spring Mar. 30–May 7 2012	Summer Jul. 29–Aug. 29 2012	Autumn Oct. 13–Nov. 13 2012	Winter Jan. 23–Mar. 2 2013
PM_1	45.1±45.8	37.5±31.0	41.3±42.7	81.7±72.4
OA	14.0±11.3	12.5±7.8	18.2±17.5	29.7±25.7
MO-OOA	6.8±6.8	3.3±2.9	8.6±8.4	9.8±8.5
LO-OOA		5.3±3.6		5.0±6.9
COA	2.6±2.6	2.5±2.1	5.2±7.3	4.3±4.4
HOA	2.8±2.8	1.4±1.1	2.5±2.9	5.5±5.7
BBOA	1.8±1.6		2.0±2.7	
CCOA				5.0±7.2
SO_4^{2-}	9.3±11.5	9.7±9.9	5.5±7.3	17.4±17.9
NO_3^-	10.2±13.6	6.4±8.2	7.9±10.3	16.2±15.4
NH_4^+	7.3±9.0	5.4±5.8	4.5±5.7	11.7±10.8
Cl^-	1.2±1.5	0.4±0.6	2.0±2.7	2.8±3.1
BC	3.1±2.3	3.2±2.0	3.2±2.8	3.9±3.6
LWC	17.3±28.5	18.8±24.9	12.8±27.3	25.2±32.8
SO_2	7.4±7.0	3.1±3.3	9.2±8.8	32.0±21.2
CO	636±568	671±317	1229±1139	2224±1844
NO	10.5±21.0	3.5±6.6	37.5±44.7	24.4±30.9
NO_2	29.3±17.7	23.2±10.4	33.8±19.4	36.8±19.3
O_3	28.3±20.6	41.6±34.7	11.6±11.5	13.1±13.0
T (°C)	16.8±4.8	26.8±4.0	11.2±4.8	-0.1±4.0
RH (%)	33.7±23.1	61.4±16.9	43.5±19.9	37.5±20.3
WS (m s^{-1})	2.3±1.5	1.8±0.9	1.0±0.9	2.0±1.5
P (hPa)	1004.2±5.6	1001.6±3.4	1012.6±3.8	1019.2±5.3

Table 2 Elemental ratios and OA/OC ratios in OA obtained from field observations at urban and rural/suburban sites. The ratios are corrected by the "improved-ambient" method (Canagaratna et al., 2015), except for Hu et al. (2013) and Gong et al. (2013).

Sites	Site types	Periods	O/C	H/C	$\overline{OS_C}$	OA/OC	References
Beijing (China)	Urban	Mar.–May 2012 (sp)	0.49	1.63	-0.64	1.81	This study
		Jul.–Aug. 2012 (su)	0.53	1.61	-0.54	1.88	
		Oct.–Nov. 2012 (a)	0.46	1.58	-0.66	1.77	
		Jan.–Mar. 2013 (w)	0.47	1.52	-0.58	1.79	
		Aug.–Sept. 2011 (su)	0.56	1.61	-0.49	1.91	Hu et al., 2016a
		Nov.–Dec. 2010 (w)	0.32	1.65	-1.01	1.58	
		Jul.–Sept. 2008 (su)	0.41	1.63	-0.80	1.69	Huang et al., 2010
Shenzhen (China)		Oct.–Dec. 2009 (a)	0.39	1.83	-1.04	1.71	He *et al.*, 2011
		Aug.–Sept. 2011 (su)	0.45[a]	1.74[a]	-0.84	1.81[a]	Gong et al., 2013
Shanghai (China)		May–Jun. 2010 (su)	0.40	1.92	-1.12	1.69	Huang *et al.*, 2012
Mexico City (Mexico)		Mar. 2006 (sp)	0.53	1.82	-0.77	1.86	Aiken *et al.*, 2009
Bologna (Italy)		Mar.–Apr. 2008 (sp)	0.59	1.64	-0.46	1.92	Saarikoski *et al.*, 2012
Fresno, CA (US)		Jan. 2010 (w)	0.35	1.75	-1.05	1.63	Ge et al., 2012
Riverside, CA (US)		Jul.–Aug. 2005 (su)	0.44	1.71	-0.82	1.73	Docherty et al., 2011
Kaiping (China)	Rural/Suburban	Oct.–Nov. 2008 (a)	0.60	1.64	-0.44	1.94	Huang et al., 2011
Heshan (China)		Nov.–Dec. 2010 (a)	0.50	1.63	-0.63	1.87	Gong et al., 2012
Changdao Island (China)		Mar.–Apr. 2011 (sp)	0.75[a]	1.48[a]	0.02	2.08[a]	Hu et al., 2013
Ziyang (China)		Dec. 2012–Jan. 2013 (w)	0.65	1.56	-0.26	2.02	Hu et al., 2016b
Jiaxing (China)		Jun.–Jul. 2010 (su)	0.36	1.94	-1.22	1.67	Huang et al., 2013
		Dec. 2010 (w)	0.43	1.73	-0.87	1.75	
Melpitz (Germany)		May–Jul. 2008 (su)	0.52	1.51	-0.47	1.83	Poulain et al., 2011
		Sept.–Nov. 2008 (a)	0.54	1.48	-0.40	1.84	
		Feb.–Mar 2009 (w)	0.53	1.48	-0.41	1.83	

[a] The O/C, H/C and OA/OC ratios were scaled up by 27, 11 and 7% (the average corrections for ambient OA; Canagaratna et al., 2015), respectively.

Table 3 Slopes in the van Krevelen diagram based on field observations at urban and background/suburban sites.

Sites	Site types	Periods	Slope	Intercept	r^2	O/C range	References
Beijing (China)	Urban	Mar.–May 2012	-0.57	1.91	0.74	0.12–0.95	This study
		Jul.–Aug. 2012	-0.62	1.94	0.79	0.20–0.83	
		Oct.–Nov. 2012	-0.67	1.90	0.70	0.15–0.92	
		Jan.–Mar. 2013	-0.08	1.56	0.02	0.18–0.77	
Mexico City (Mexico)		Mar. 2006	-0.69	2.19	0.99		Aiken et al., 2009
Fresno (US)		Jan. 2010	-0.95	2.08	0.77		Ge et al., 2012
Riverside (US)		Jul.–Aug. 2005	-0.96	2.13	0.81		Docherty et al., 2011
Lake Hongze (China)	Background /suburban	Mar.–Apr. 2011	-0.72	2.00	0.56		Zhu et al., 2016
Mount Wuzhi (China)		Mar.–Apr. 2015.	-0.69	1.99	0.54		
Ziyang (China)		Dec. 2012–Jan. 2013	-0.44	1.84	0.70	0.12–0.70	Hu et al., 2016b
Melpitz (Germany)		May–Jul. 2008	-0.69	1.83	0.91		Poulain et al., 2011

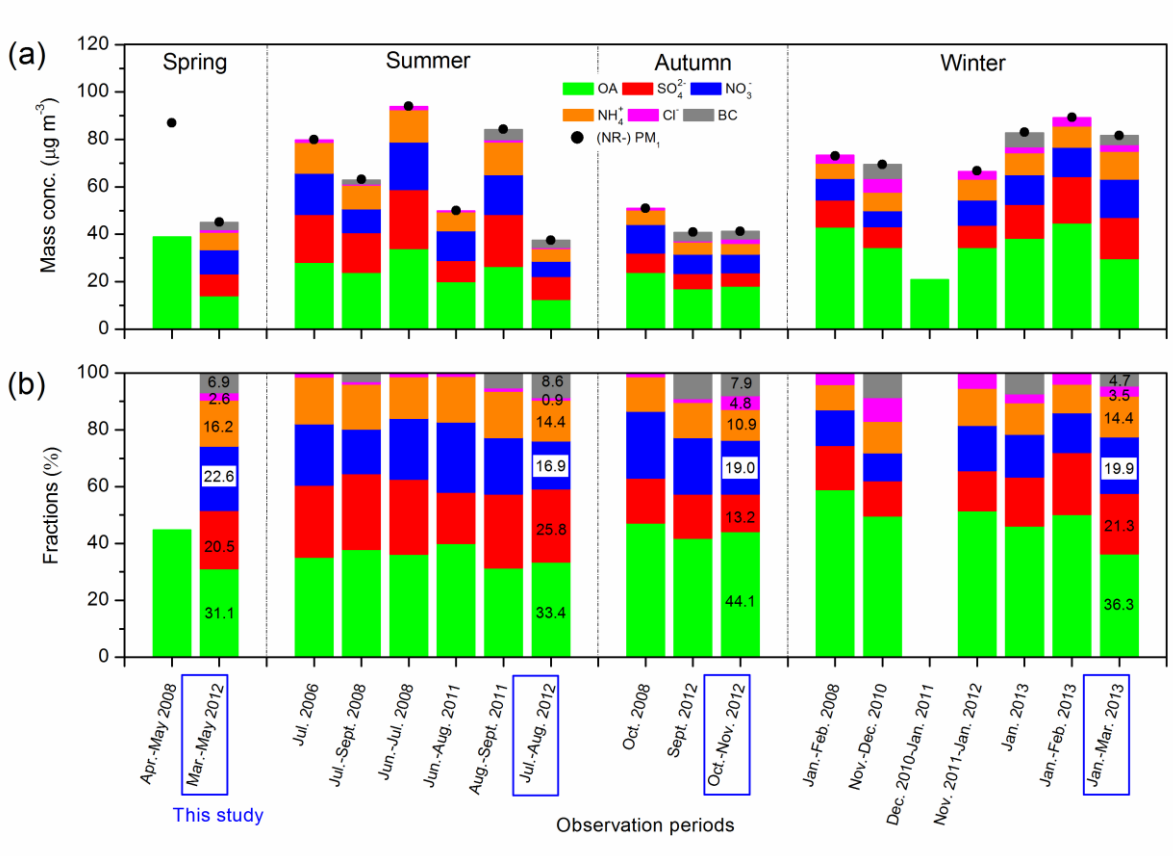

Figure 1. Concentrations (a) and fractions (b) of main chemical components in PM_1 during seasonal observations in Beijing in recent years. The data and references are available in Table S4 in the supplement.

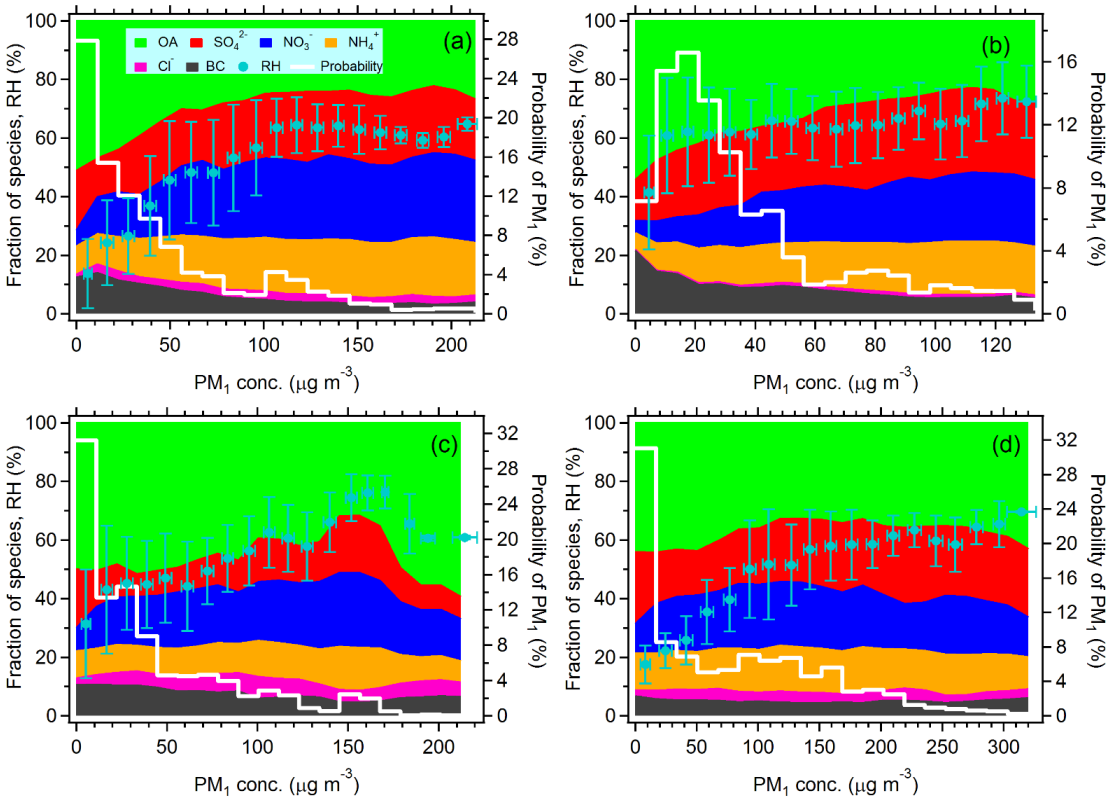

Figure 2. Fractions of main chemical compositions in submicron aerosols at different PM_1 levels, and the probability density of PM_1 (white curves) during the spring (a), summer (b), autumn (c) and winter (d) observations. The average RH values in each segment are illustrated and the error bars in the x- and y-axis were the standard deviations of PM_1 and RH, respectively.

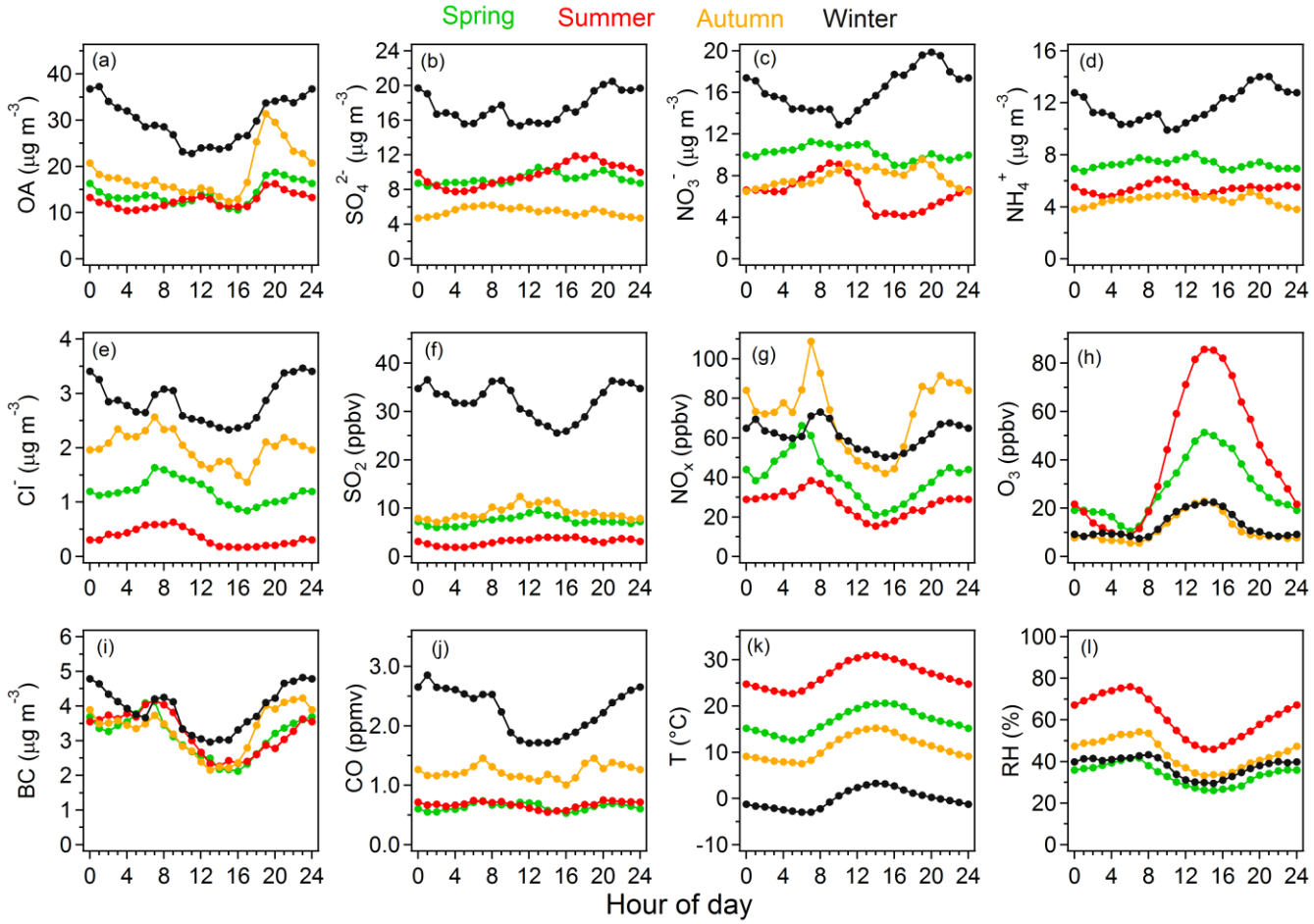

Figure 3. Diurnal patterns of chemical species of PM_1, gaseous pollutants, temperature (T) and relative humidity (RH) during seasonal observations. The ranges of diurnal variations for each season are shown in Fig S12–S15.

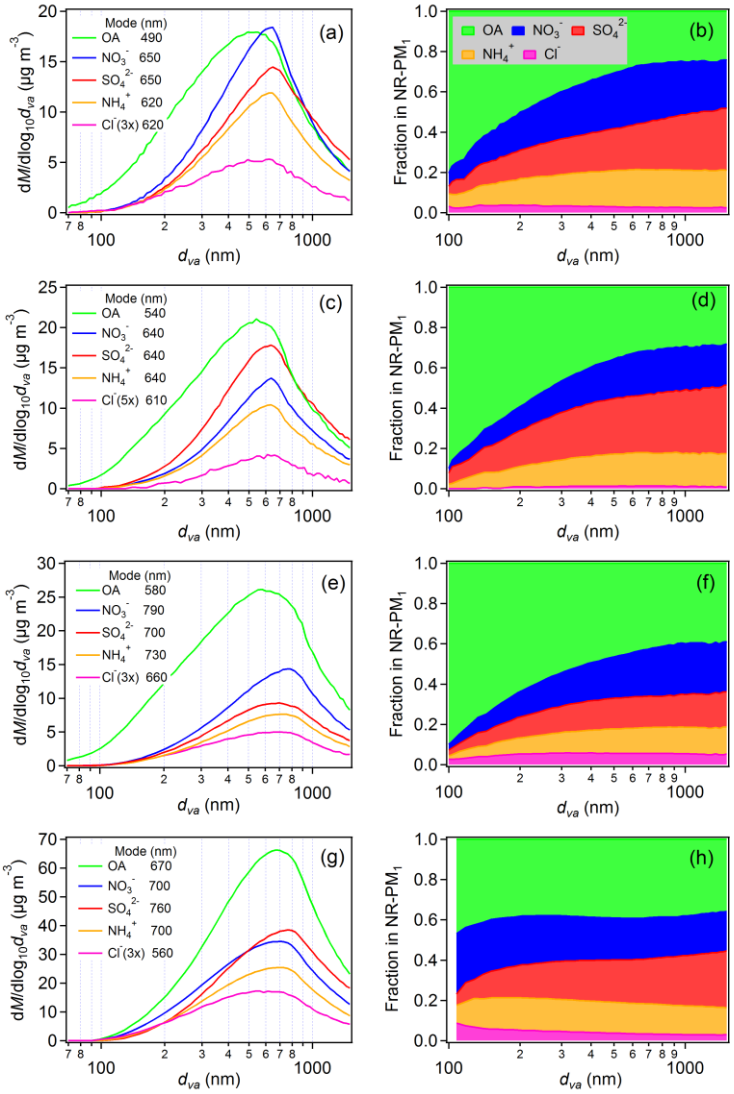

Figure 4. Mass size distributions of chemical compositions in NR-PM_1 during the spring (a, b), summer (c, d), autumn (e, f) and winter (g, h) observations.

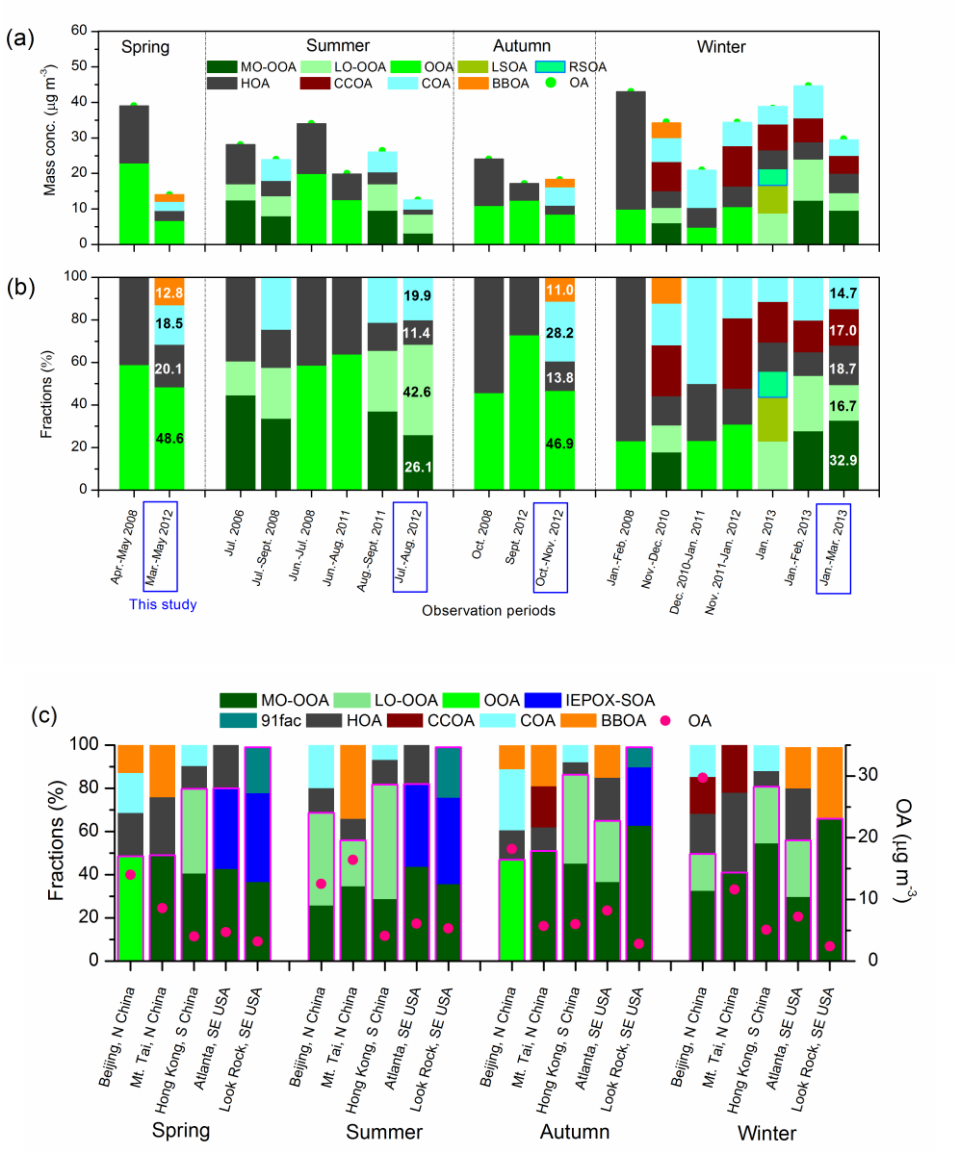

Figure 5. Resolved components of OA during seasonal observations in Beijing (a and b; data and references are listed in Table S8 in the supplement) and at other sites (c) in Mt. Tai (Zhang et al., 2014), Hong Kong (Li et al., 2015) and southeastern USA (Budisulistiorini et al., 2016) in recent years. LSOA, local SOA; RSOA, regional SOA; IEPOX-SOA, isoprene-epoxydiols-derived SOA; 91fac, a biogenically influenced factor characterized by distinct *m/z* 91. MO-OOA and LO-OOA are identified as LV-OOA and SV-OOA, respectively, except for during Aug.–Sept. 2011 and Nov.–Dec. 2010 (Hu et al., 2016a), and in this study.

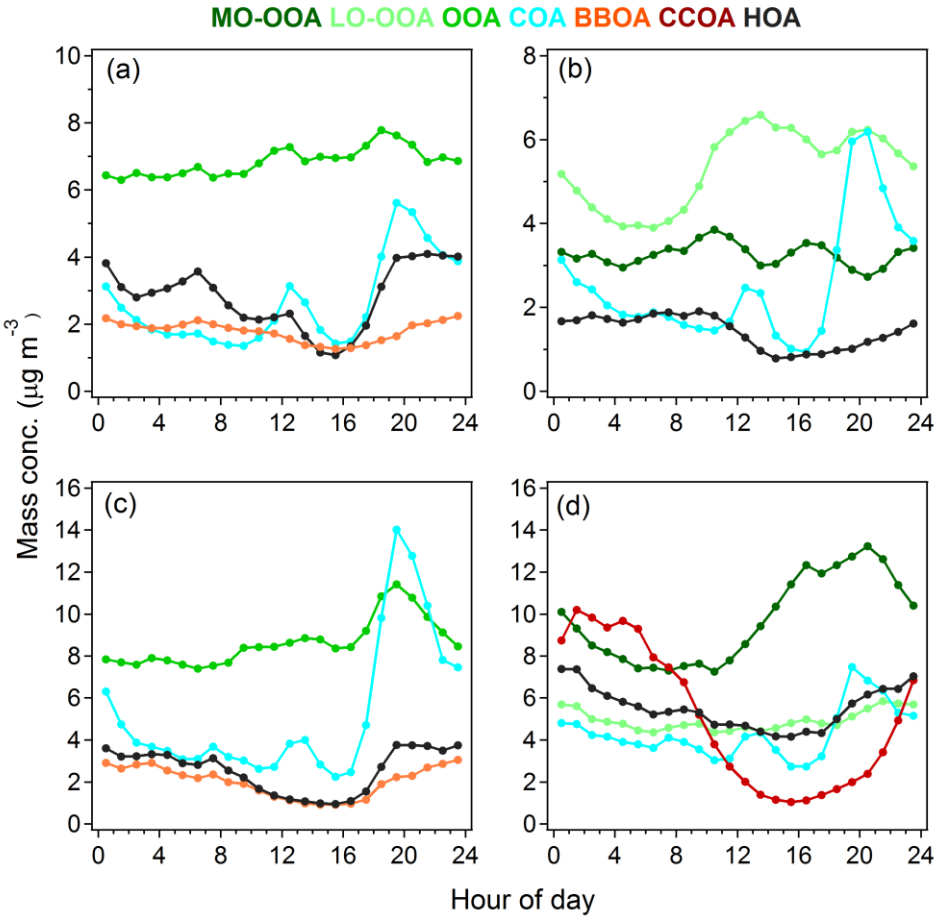

Figure 6. Diurnal variations of OA components in spring (a), summer (b), autumn (c) and winter (d) observations.

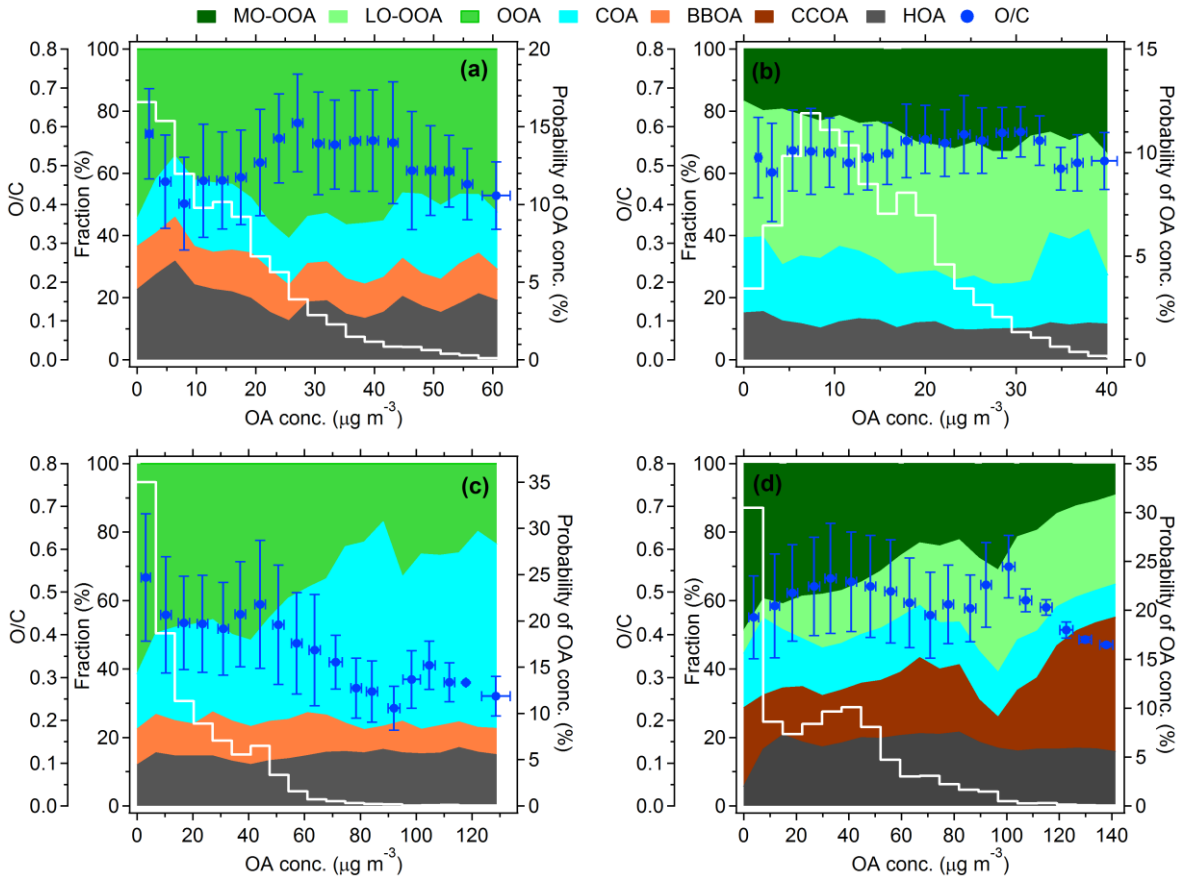

Figure 7. Fractions of OA components at different OA concentration levels and the probability distributions of OA concentrations (white curves) during the spring (a), summer (b), autumn (c) and winter (d) observations. The average O/C ratios in each segment are illustrated and the error bars in the x- and y-axis were the standard deviations of OA concentration and O/C ratios, respectively.

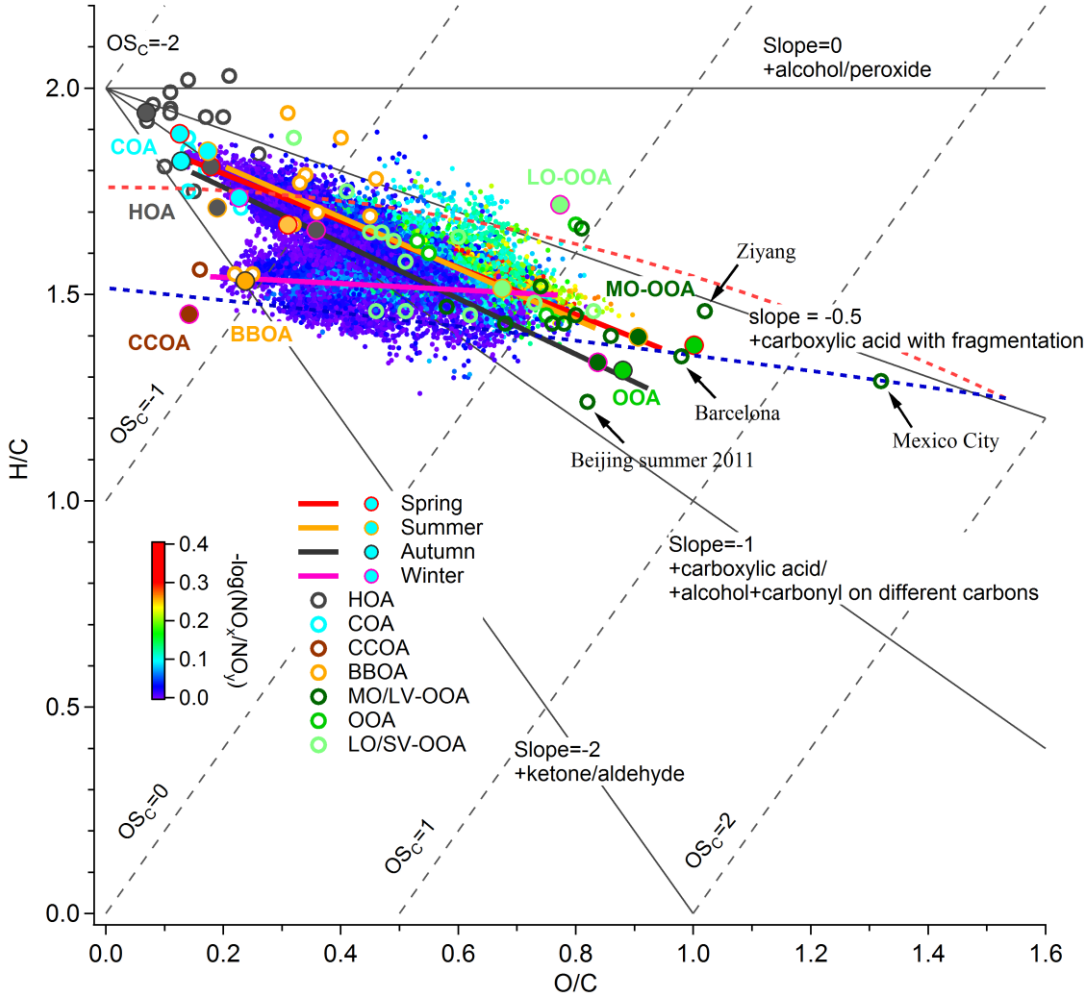

Figure 8. Tri-VK-$\overline{\mathbf{OS_C}}$ diagram based on seasonal observations. The scatterplot of H/C vs. O/C ratios is colored by the parameter -log (NO_x/NO_y). The OA factors resolved by the AMS-PMF analysis are also marked in the diagram. The majority of the data fall into colored triangle lines (Ng et al., 2011). Improved-ambient results for OA factors are from Hu et al. (2016a), Hu et al. (2016b) and the summarization of Canagaratna et al. (2015).

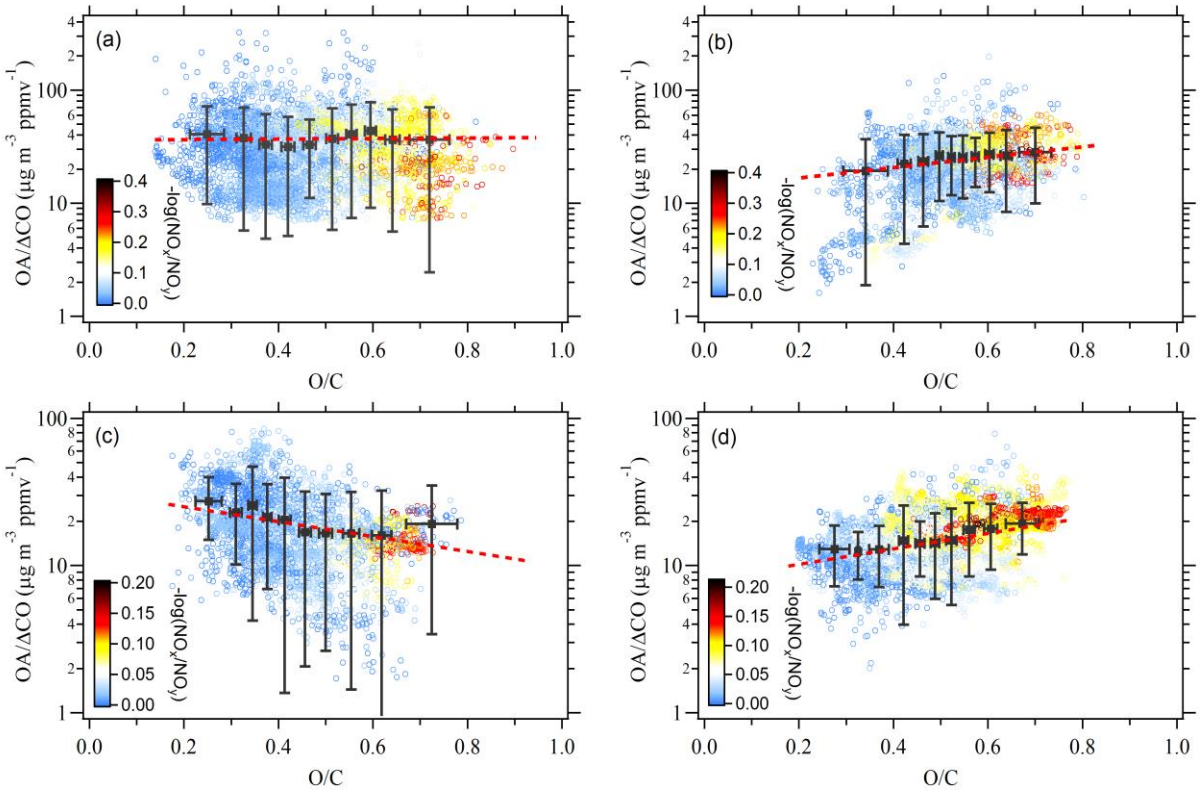

Figure 9. Scatterplots of OA/ΔCO (ΔCO=CO-0.1) ratios vs. O/C atomic ratios in OA during the (a) spring, (b) summer, (c) autumn and (d) winter observations. The OA/ΔCO ratios are in the range of first and ninety-ninth percentile. The scatterplots are colored by the parameter -log (NO_x/NO_y).

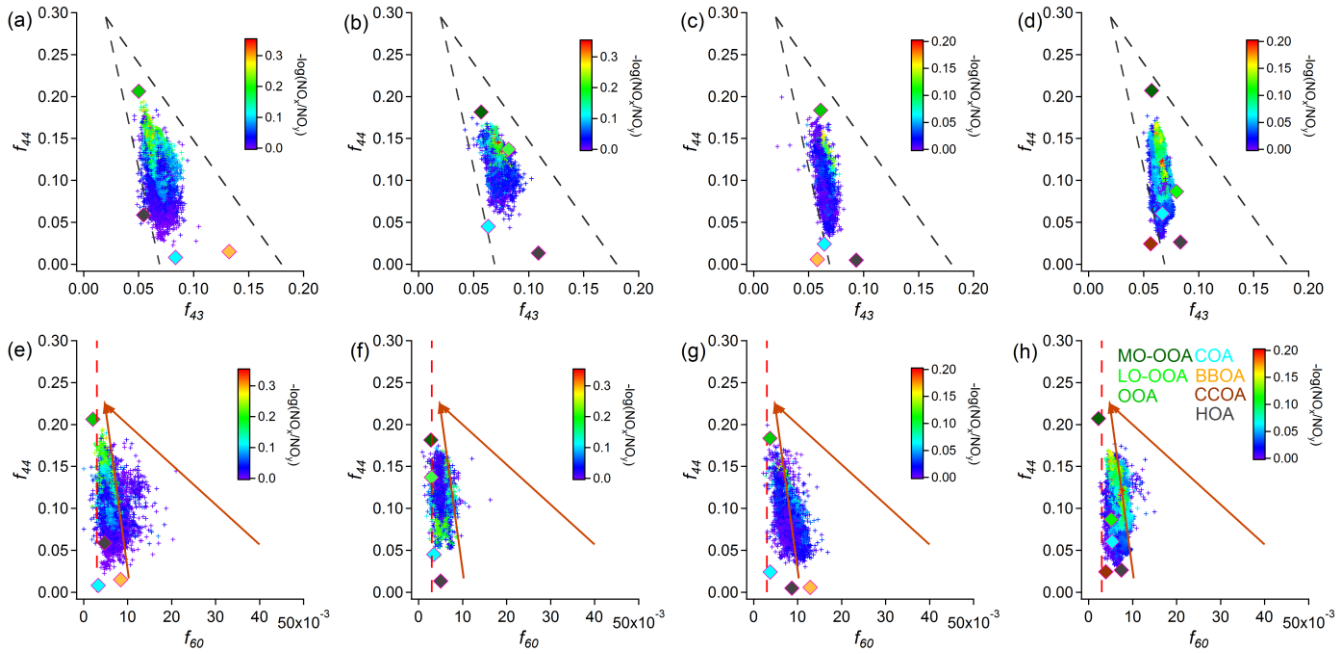

Figure 10. Scatterplots of f_{44} vs. f_{43} and f_{44} vs. f_{60} in OA during the spring (a, e), summer (b, f), autumn (c, g) and winter (d, h) observations. The triangle for f_{44} against f_{43} derived by Ng et al. (2010) is lineated. The conceptual space for BBOA and the nominal background value at 0.3% (Cubison et al., 2011) are marked by arrows and vertical dash lines, respectively. The scatterplots are colored by the metric -log (NO_x/NO_y). The OA factors resolved by the AMS-PMF analysis are also marked in all diagrams.

Supporting information for "Seasonal variations of high time-resolved chemical compositions, sources and evolution for atmospheric submicron aerosols in the megacity Beijing"

Wei Hu, Min Hu*, Wei-Wei Hu, Jing Zheng, Chen Chen, Yusheng Wu, Song Guo

State Key Joint Laboratory of Environmental Simulation and Pollution Control, College of Environmental Sciences and Engineering, Peking University, Beijing 100871, China
*Corresponding author: minhu@pku.edu.cn

S1 Sampling site and measurements

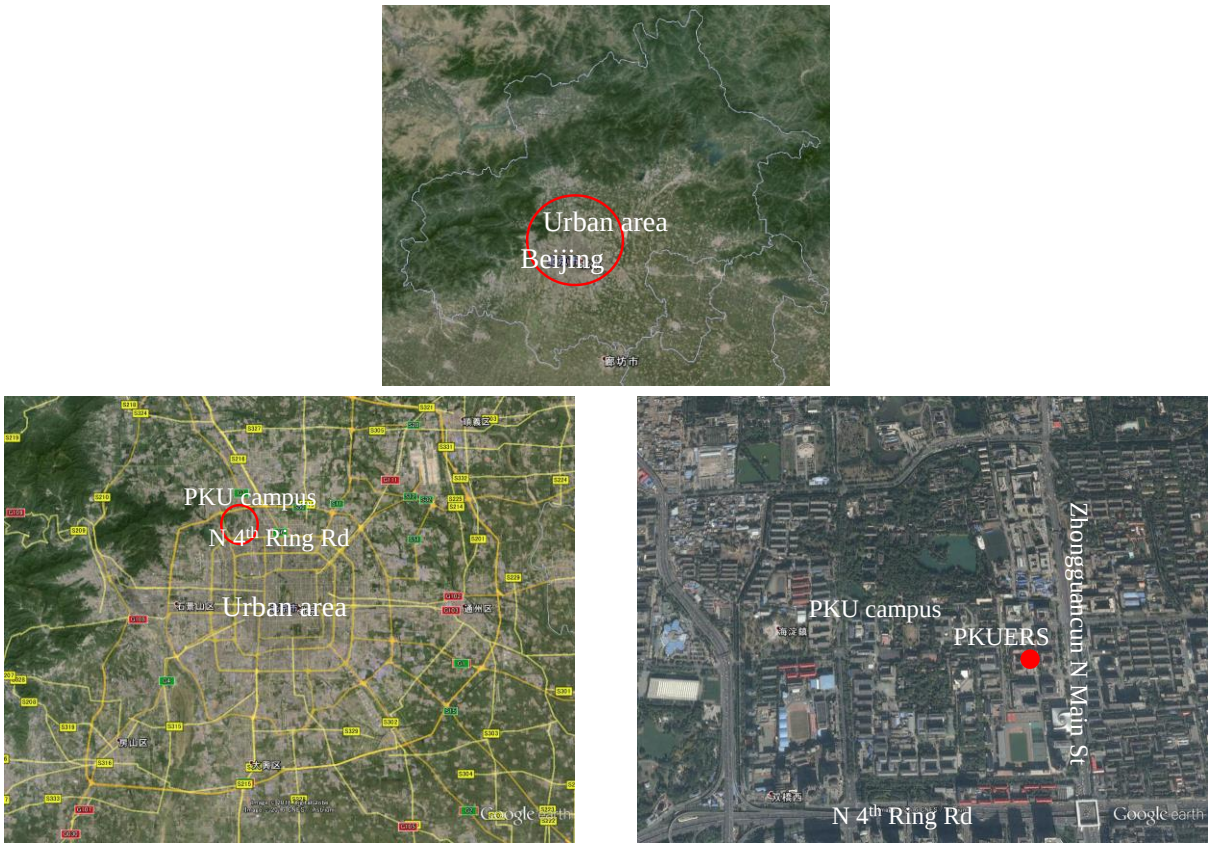

Figure S1. Location of observation site (PKUERS) and topographic map of Beijing.

Table S1 Measurement instrumentation for the campaigns.

Instrument	Parameters	Size	Time resolution	Manufacturer
HR-ToF-AMS	Mass concentrations size distributions of submicron non-refractory species	60~600 nm	4 min	Aerodyne Research Inc., USA
MAAP/Aethalometer	Particle absorption coefficient (BC)	2.5 μm	5 min	Thermo/Magee Scientific Co., USA
Semi-continuous EC/OC analyzer	Mass concentrations of OC and EC	2.5 μm	1 h	Sunset Lab Inc., USA
SMPS	Number concentrations of atmospheric particles	15~600 nm	5 min	TSI Inc., USA
TEOM 1400a, b	$PM_{2.5}$	2.5 μm	1 min	Thermo Scientific Co., USA
PTR-MS	Multiple volatile organic compounds (VOCs)		30 s	Ionicon Analytik, Austria
Gaseous pollutants	SO_2, NO_x, NO_y, CO, O_3		1 min	Ecotech Inc., USA
Meteorology	Wind speed and direction, temperature, relative humidity, atmospheric pressure		1 min	Met One Instruments Inc., USA

S2 Parameters of the AMS instrument

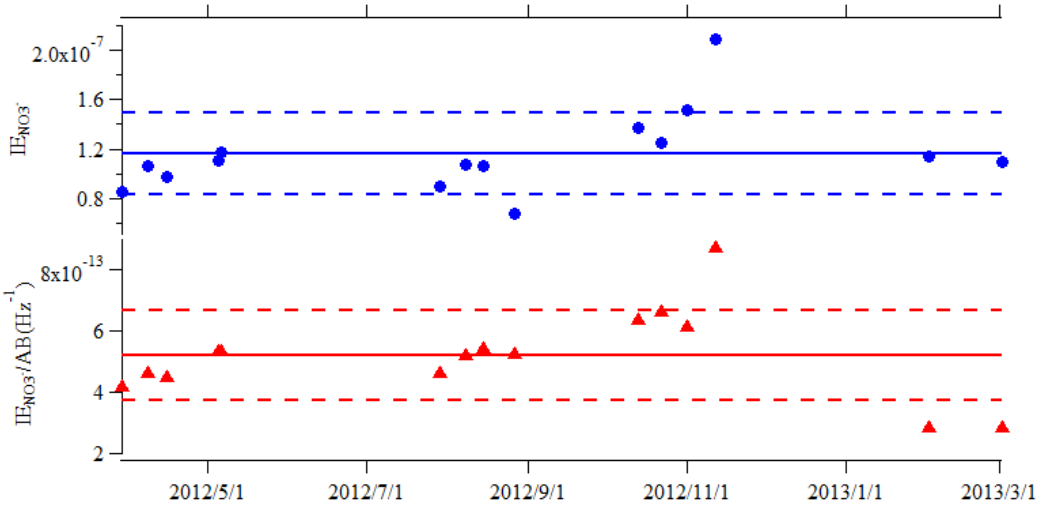

Figure S2. Ion efficiency (IE) and IE/air beam (AB) of the AMS in this study. The dashed line is the standard deviation of the average IE/AB (solid line).

Table S2 Detection limits (V-mode) of main components of aerosol detected by the AMS in this study. Units are μg m^{-3}. Detection limit of each species was determined by three times the standard deviations of detected signal of this species under particle-free condition.

Campaigns	OA	NO_3^-	SO_4^{2-}	NH_4^+	Cl^-
Spring	0.102	0.026	0.026	0.076	0.051
Summer	0.202	0.045	0.073	0.094	0.053
Autumn	0.337	0.019	0.017	0.068	0.025
Winter	0.072	0.016	0.022	0.043	0.014

S3 Comparison of results between AMS and other instruments, and ammonium balances

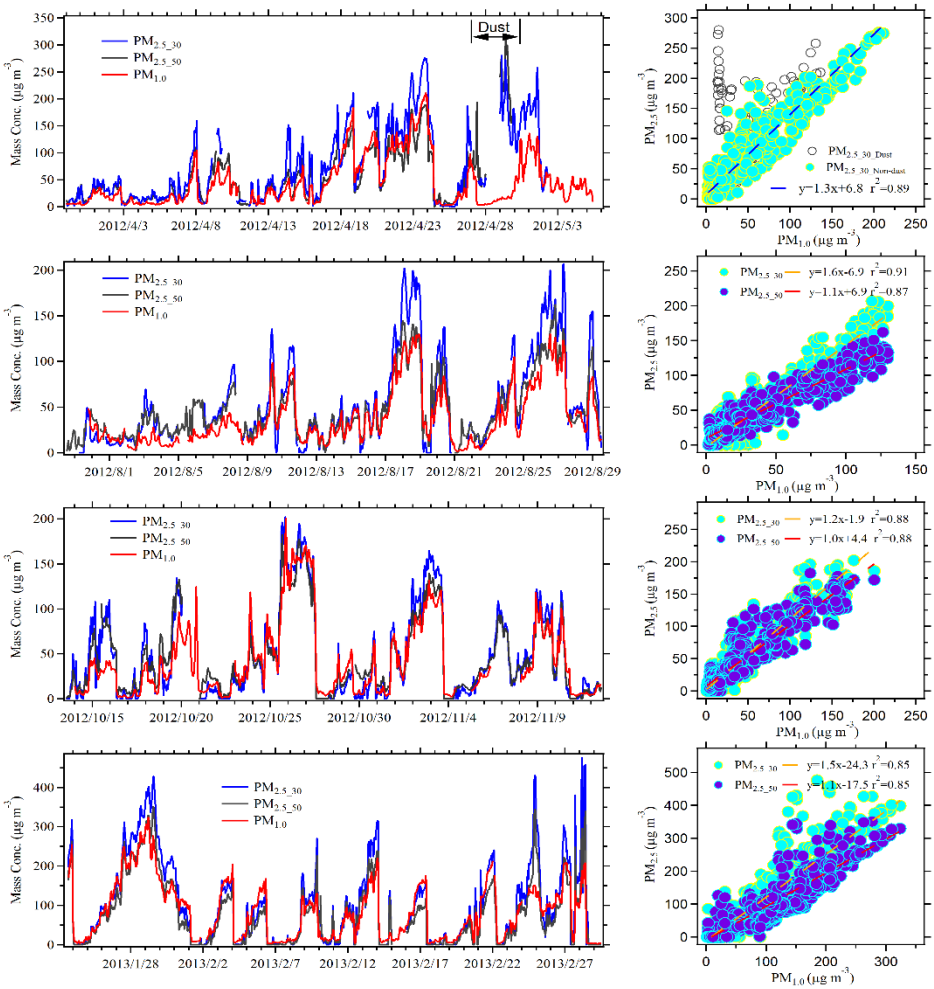

Figure S3. Time series and scatter plot of aerosol mass concentrations detected by the AMS plus BC vs. TEOM during seasonal observations. The size cut off for BC is $PM_{2.5}$. The size cut of TEOM is $PM_{2.5}$, which should be the main reason that lower concentration in AMS+BC observed. $PM_{2.5\_30}$ and $PM_{2.5\_50}$ mean the concentrations of fine particles with dehumidification at 30°C and 50°C, respectively.

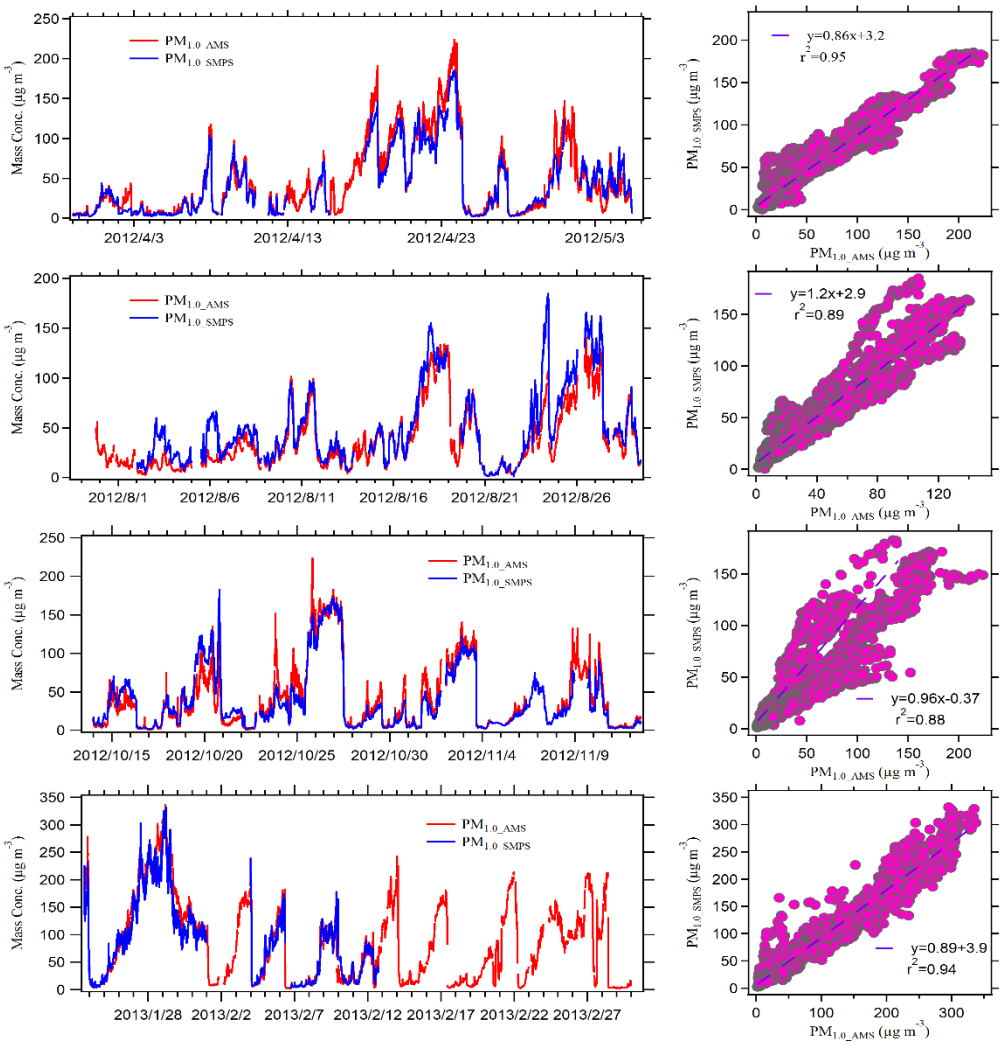

Figure S4. Time series and scatter plots of aerosol mass concentrations detected by the AMS plus BC vs. SMPS during seasonal observations. The aerosol density based on chemical composition of aerosols was used to convert SMPS volume concentrations to be mass concentrations (Middlebrook et al., 2012).

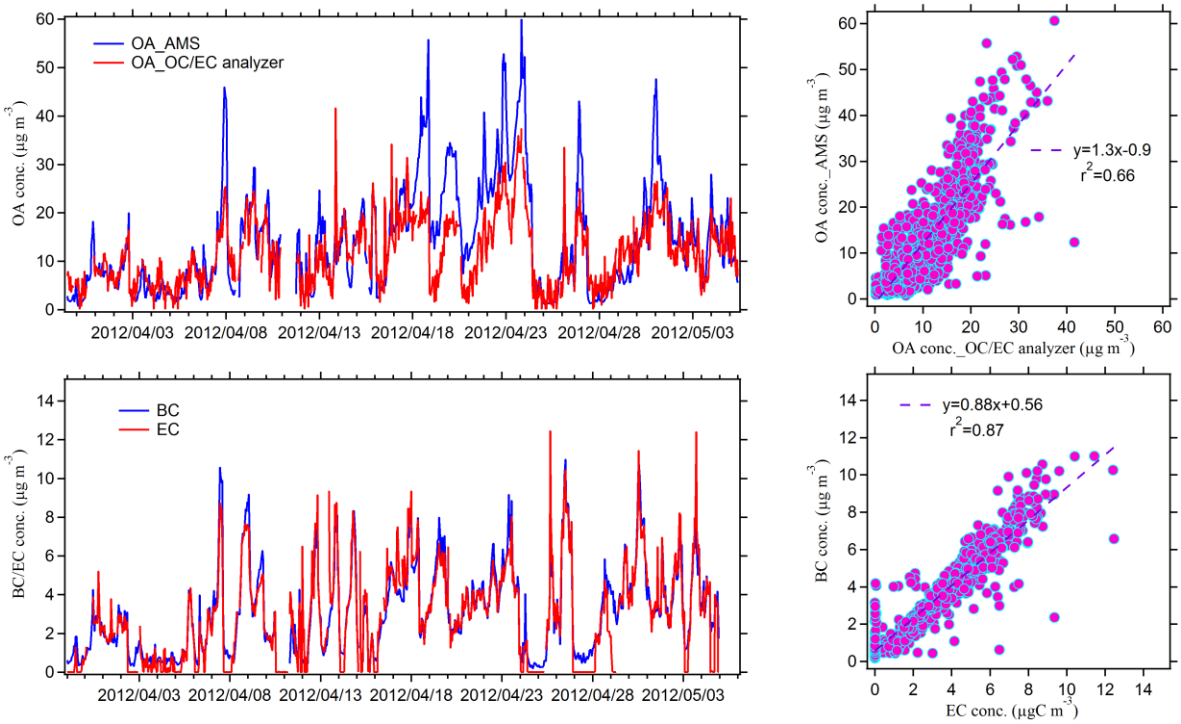

Figure S5. Time series and scatter plots of OA detected by the AMS vs. OA converted from OC measured by a semi-continuous OC/EC analyzer ($PM_{2.5}$ cutoff) using the OA/OC ratios measured by AMS, and BC vs. EC during the spring observation.

OA concentrations measured by the AMS showed tight correlation with the OC concentrations measured by a Sunset OC/EC Analyzer (r^2 =0.61). The linear regression slope of 2.4 is comparable to or within the range (2.0–2.7) of the previous results (Sun et al., 2011; Hu et al., 2013; Lan et al., 2011; Weimer et al., 2006), but is higher than the average OA/OC ratio of 1.81 determined via elemental analysis of the AMS. When the OM were at high concentration levels, the OA converted from OC measured by the OC/EC analyzer, using the OA/OC ratios measured by the AMS, deviated more from the OA time-series trends, consistent with the result of Lan et al. (2011). Possible reasons for this discrepancy include: (1) evaporative losses of semi-volatile organic species due to striking the balance of gas-particle partition after passing the activated-carbon denuder (Grover et al., 2008), and during the carbon analysis (Sun et al., 2011); (2) "over-calibration" of the OC data using the blank filter values (Bae et al., 2006).

S4 Variations of meteorological parameters and main compositions in PM_1

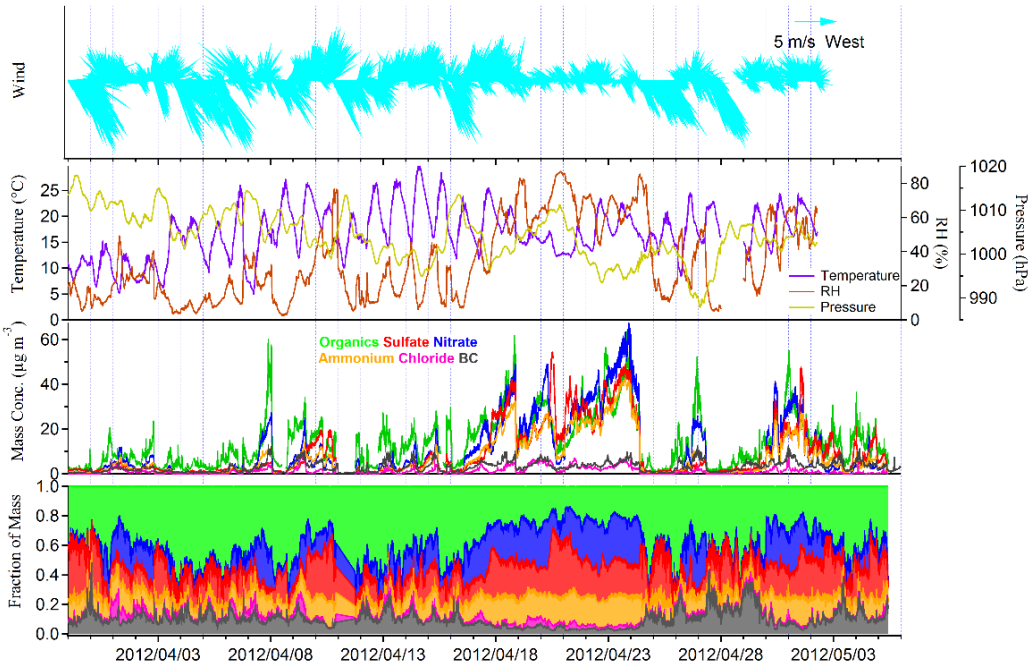

Figure S6. Time series of meteorological parameters (wind speed and direction, temperature, relative humidity (RH), and atmospheric pressure), and concentrations and fractions of main chemical compositions in submicron aerosols during the spring observation.

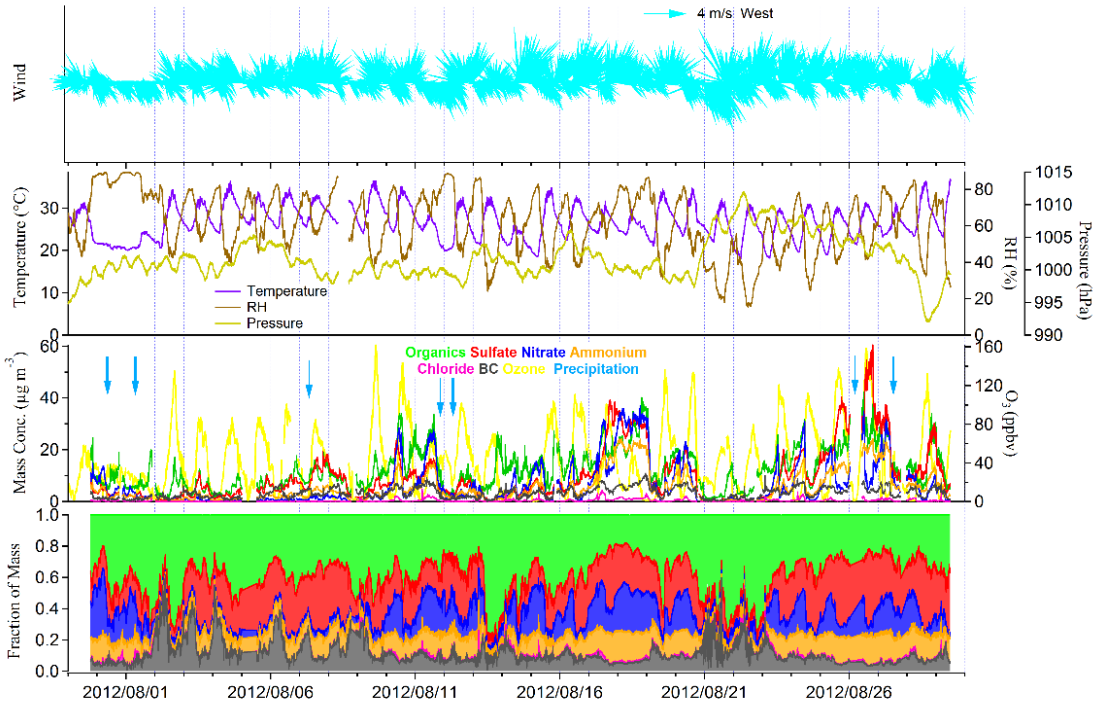

Figure S7. Time series of meteorological parameters (wind speed and direction, temperature, RH, and atmospheric pressure), and concentrations and fractions of main chemical compositions in submicron aerosols during the summer observation.

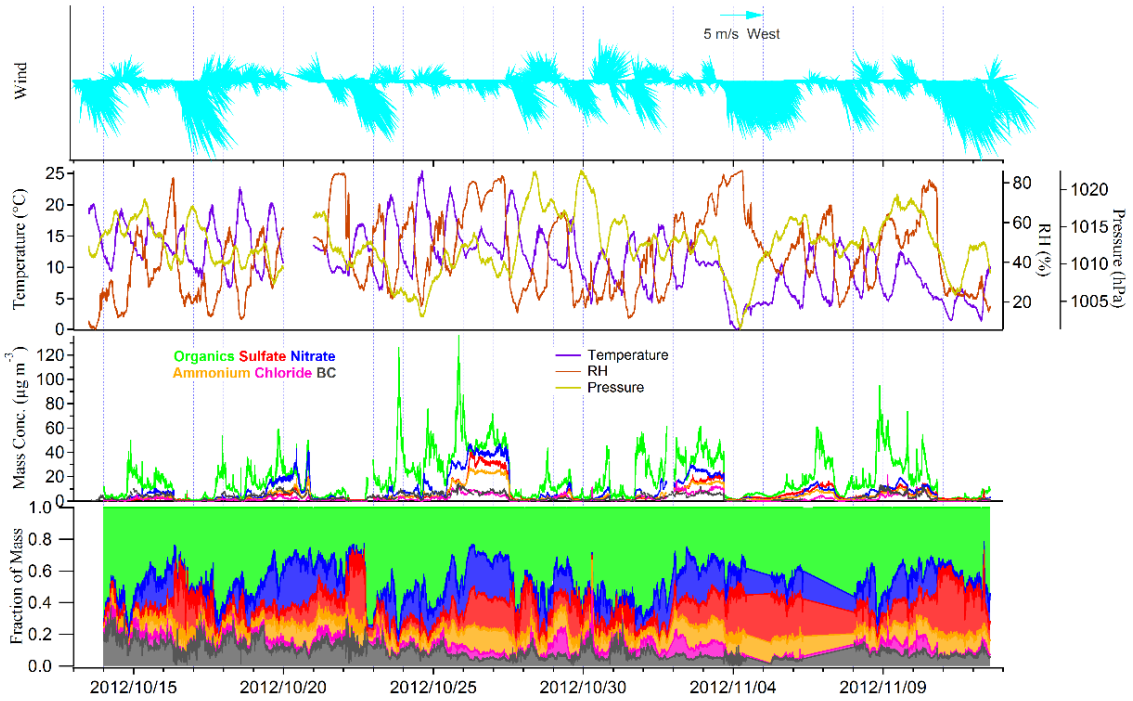

Figure S8. Time series of meteorological parameters (wind speed and direction, temperature, RH, and atmospheric pressure), and concentrations and fractions of main chemical compositions in submicron aerosols during the autumn observation.

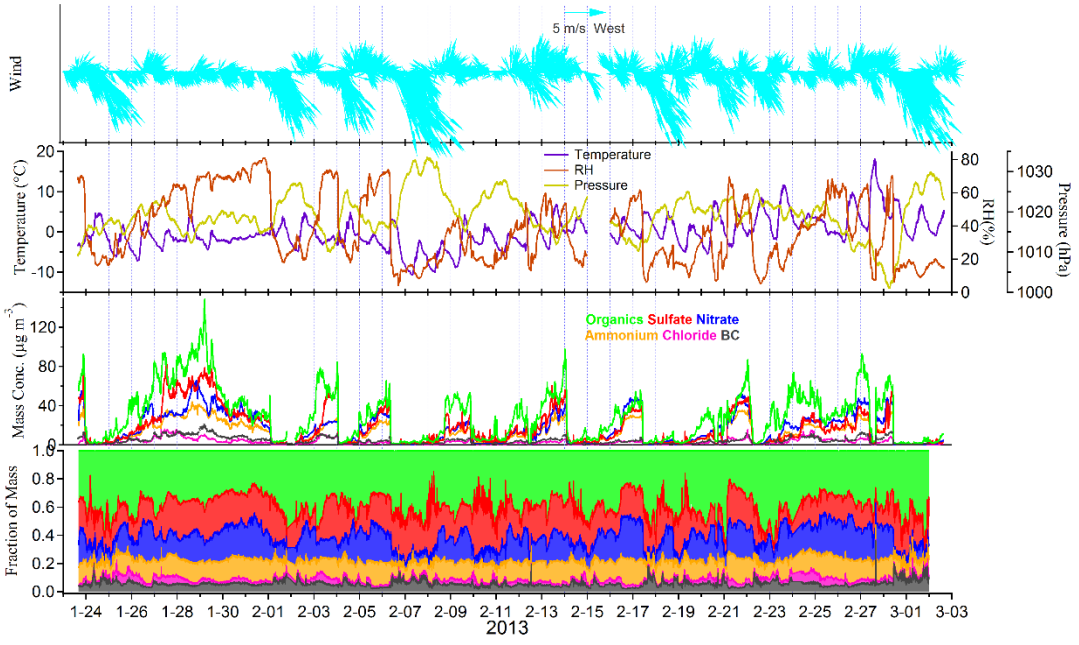

Figure S9. Time series of meteorological parameters (wind speed and direction, temperature, RH, and atmospheric pressure), and concentrations and fractions of main chemical compositions in submicron aerosols during the winter observation.

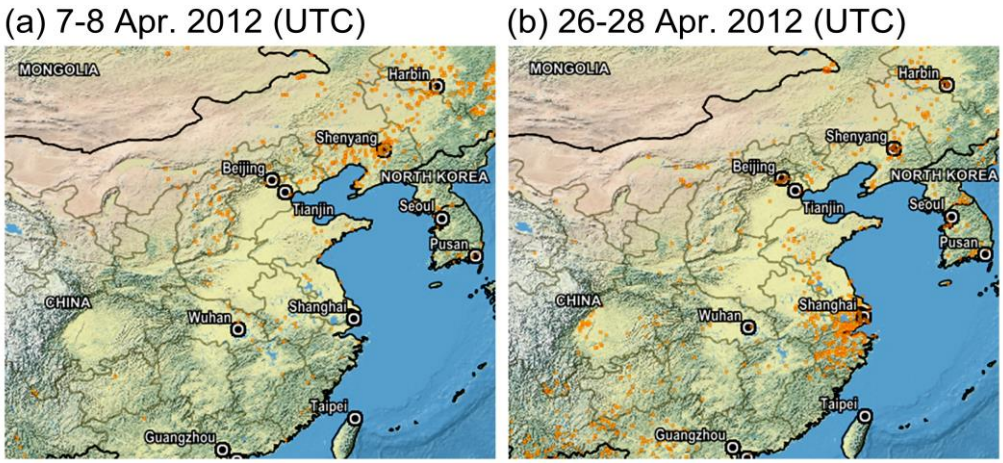

Figure S10. Fire points observed by satellites (https://firms.modaps.eosdis.nasa.gov/firemap) in Beijing and surrounding areas during 7–8 (a) and 26–28 (b) Apr. 2012.

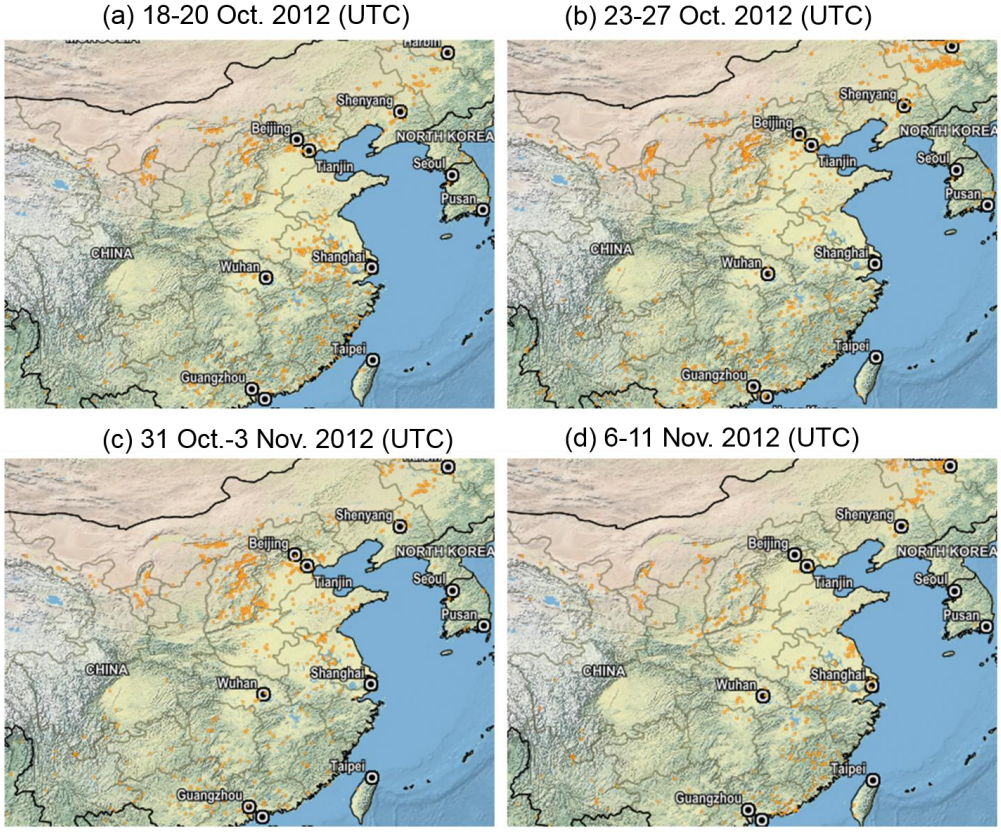

Figure S11. Fire points observed by satellites (https://firms.modaps.eosdis.nasa.gov/firemap) in Beijing and surrounding areas during the autumn observation.

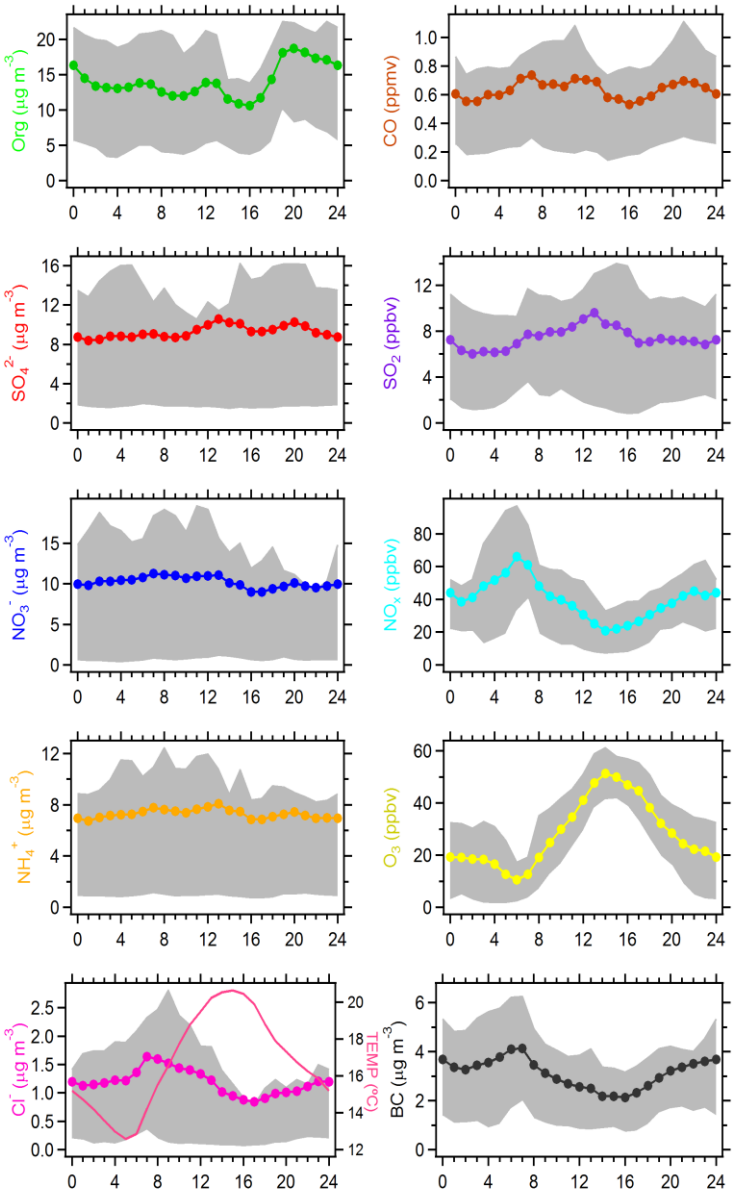

Figure S12. Diurnal patterns of chemical species of submicron particles and gaseous pollutants during the spring observation. The shaded area is between the 25% and 75% quantiles.

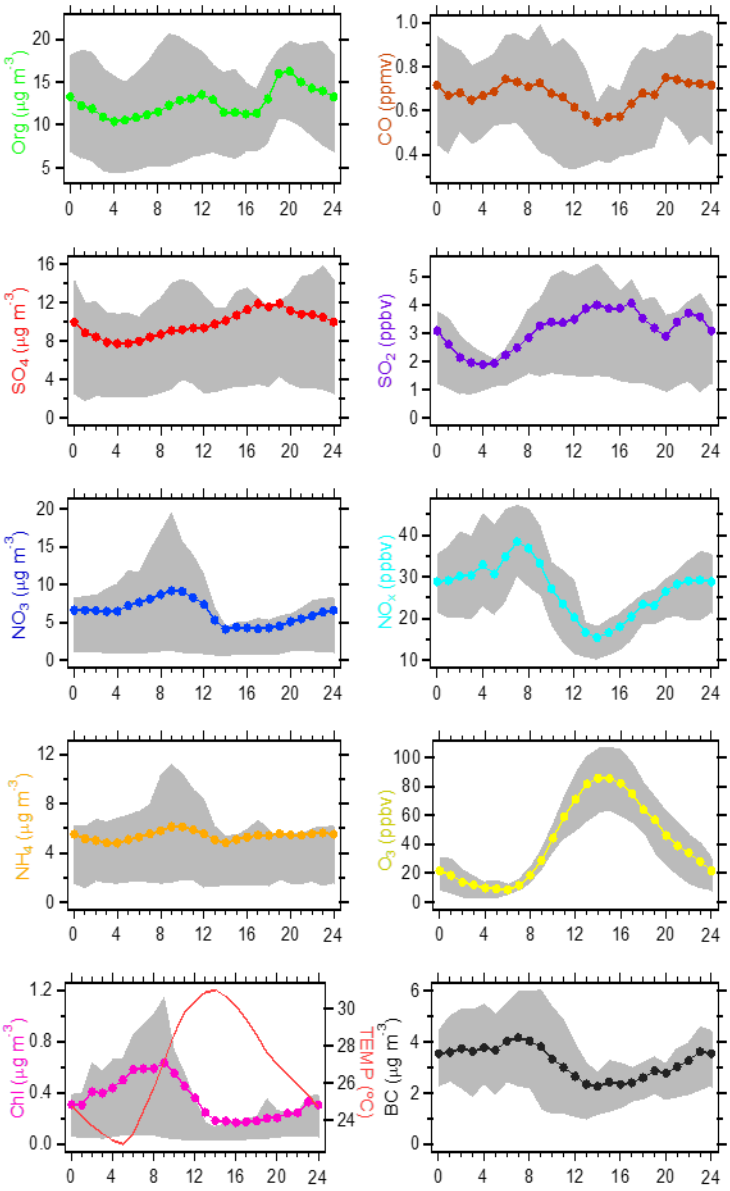

Figure S13. Diurnal patterns of chemical species of submicron particles and gaseous pollutants during the summer observation. The shaded area is between the 25% and 75% quantiles.

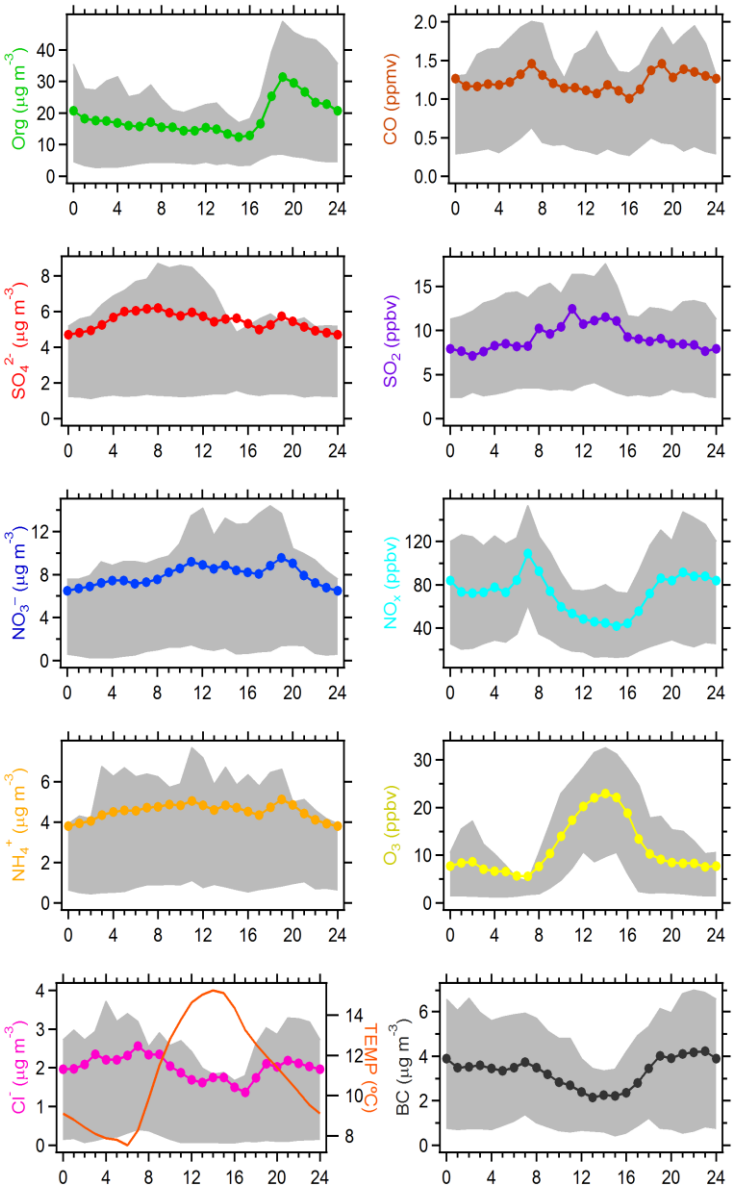

Figure S14. Diurnal patterns of chemical species of submicron particles and gaseous pollutants during the autumn observation. The shaded area is between the 25% and 75% quantiles.

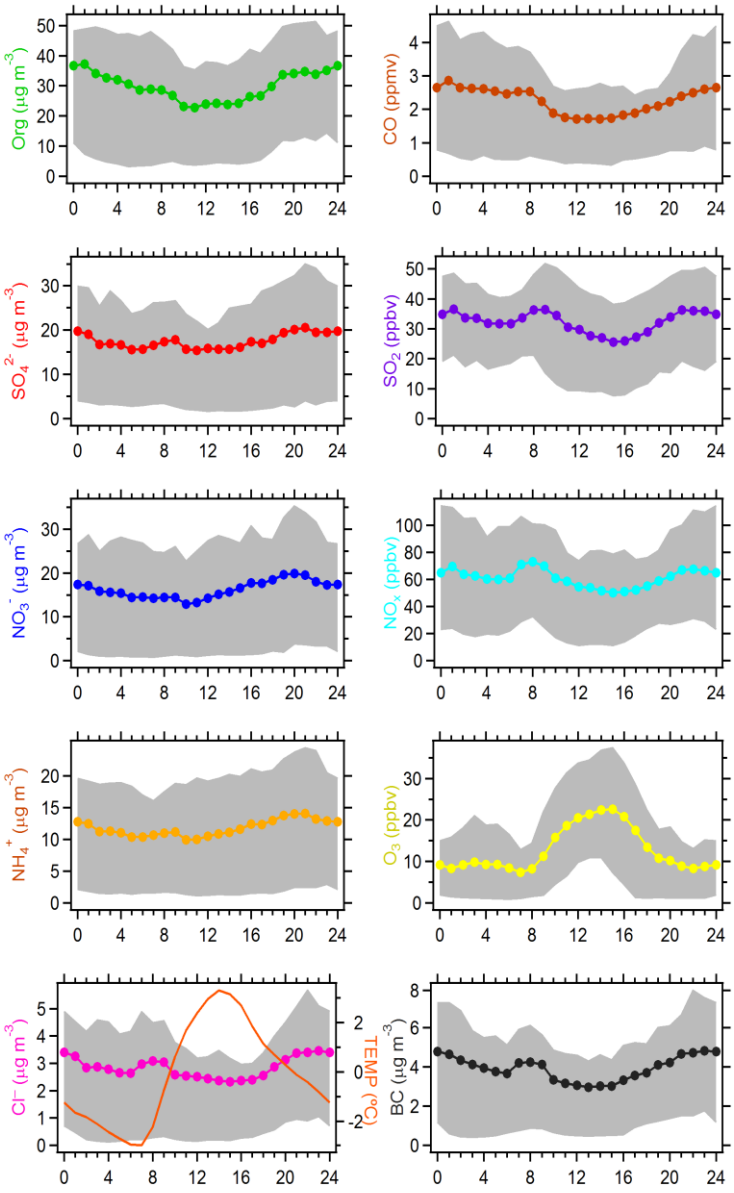

Figure S15. Diurnal patterns of chemical species of submicron particles and gaseous pollutants during the winter observation. The shaded area is between the 25% and 75% quantiles.

During four seasons, NOR ($\boldsymbol{n}$–NO_3^-/ ($\boldsymbol{n}$–NO_3^-+ $\boldsymbol{n}$–NO_2)) showed strong correlations with NH_4^+, indicating the main form of NO_3^- was NH_4NO_3. NH_4^+ also presented in the form of $(NH_4)_2SO_4$ and NH_4Cl. The predicted NH_4^+ was calculated assuming full neutralization of particulate anions of NO_3^-, SO_4^{2-}, and Cl^- in four seasons. The slopes of linear fitting of measured against predicted NH_4^+ in spring, summer, autumn and winter were 1.05, 1.02, 0.85, and 0.89, respectively. In autumn and winter, the relatively lower slopes implied that NH_4^+ was not enough to balance NO_3^-, SO_4^{2-} and Cl^-.

Field and emission studies have shown that a large fraction of KCl can exist in the fresh biomass burning plumes. As biomass burning plumes get aged, more S- and N- containing species (e.g., KNO_3 and K_2SO_4) in aerosol phase have been found (Li et al., 2003; Yokelson et al., 2009). It has also been reported that NaCl and NH_4Cl are important components in the aerosols directly emitted from biomass burning (Lewis et al., 2009; Levin et al., 2010). It was found that atmospheric aerosols were mostly acidic during heavy pollution episodes (Zhang et al, 2007; Sun et al, 2014.). During the heavy pollution periods in winter, SO_4^{2-} may exist in the form of NH_4HSO_4. Chloride existing in the form of KCl and NaCl in aerosol phase for coal combustion sources has been reported (McNallan et al., 1981; Doshi et al., 2009). Therefore, NO_3^-, SO_4^{2-}, and Cl^- may exist as other forms in addition to ammonium due to the influences of intense autumn biomass burning and coal combustion in autumn and winter, respectively.

Table S3. Concentrations of main chemical components in PM_1 during seasonal observations in Beijing in recent years. Unit: μg m^{-3}.

Seasons	Periods	PM_1	OA	SO_4^{2-}	NO_3^-	NH_4^+	Cl^-	BC	References
Spring	10 Apr.-4 May. 2008	87.0	39.0						Zhang et al., 2013
	30 Mar.-7 May. 2012	**45.1**	**14.0**	**9.3**	**10.2**	**7.3**	**1.2**	**3.1**	**This study**
Summer	9-21 Jul. 2006	80.0	28.1	20.3	17.3	13.1	1.1		Sun et al., 2010
	24 Jul.-20 Sept. 2008	63.1	23.9	16.8	10.0	10.0	0.5	1.8	Huang et al., 2010
	5 Jun.-3 Jul. 2008	94.0	34.0	24.8	20.1	13.7	1.4		Zhang et al., 2013
	26 Jun.-28 Aug. 2011	50.0	20.0	9.0	12.4	8.0	0.5		Sun et al., 2012
	4 Aug.-14 Sept. 2011	84.3	26.4	22.0	16.8	13.7	1.0	4.4	Hu et al., 2016
	29 Jul.-29 Aug. 2012	**37.5**	**12.5**	**9.7**	**6.4**	**5.4**	**0.4**	**3.2**	**This study**
Autumn	4-18 Oct. 2008	51.0	24.0	8.1	12.0	6.2	0.7		Zhang et al., 2013
	1-30 Sept. 2012	40.9	17.1	6.4	8.1	5.1	0.5	3.7	Jiang et al., 2013
	13 Oct.-13 Nov. 2012	**41.3**	**18.2**	**5.5**	**7.9**	**4.5**	**2.0**	**3.2**	**This study**
Winter	4 Jan.-3 Feb. 2008	73.0	43.0	11.4	9.2	6.4	3.5		Zhang et al., 2013
	22 Nov.-22 Dec. 2010	69.5	34.5	8.7	6.8	7.7	5.8	6.0	Hu et al., 2016
	14 Dec. 2010-15 Jan. 2011		20.9						Liu et al., 2012
	21 Nov. 2011-20 Jan. 2012	66.8	34.4	9.4	10.7	8.7	3.3		Sun et al., 2013
	1-17 Jan. 2013	83.0	38.3	14.3	12.5	9.2	2.6	6.0	Sun et al., 2014
	1 Jan.-1 Feb. 2013	89.3	44.7	19.6	12.5	8.9	3.6		Zhang et al., 2014
	23 Jan.- 2 Mar. 2013	**81.7**	**29.7**	**17.4**	**16.2**	**11.7**	**2.8**	**3.9**	**This study**

S5 Determination of the PMF solution

Factor number from 1 to 10 and the different seeds (0-50) were selected to run in the PMF model. For the spring observation, diagnostic plots of the PMF analysis are shown in Fig. S16. When OA was separated into four fractions, it included more oxidized (MO-OOA) and less oxidized OOA (LO-OOA), cooking OA (COA) and hydrocarbon-like OA (HOA). The performances of spectra and time series of the four factors at different f_{peak} are shown in Fig. S17. When OA was separated into five fractions, OOA was also split into two factors, but more information on the OA sources (BBOA) could be provided. When more than five factors, OOA decomposed into three or more factors. After comparing the performances of MS spectra and time series of five factors at different f_{peak}, the five factors, f_{Peak}=1 solution is chosen as the optimal solution for this PMF analysis because the signal of the characteristic ion fragment m/z is more obvious in one factor. In the five-factor solution, the mass spectra of two OOA factors are similar (r= 0.955), and the elemental ratios and OA/OC ratios (O/C: 0.99, 1.00; H/C: 1.50, 1.26; OA/OC: 2.51, 2.47) are close. It is unclear if the two OOA components represent distinct sources or chemical types. Thus, two OOA factors were combined into total OOA for further analysis (Hayes et al., 2013). Finally, four factors of OA were obtained, i.e., oxygenated OA (OOA), cooking OA (COA), hydrocarbon-like OA (HOA), and biomass burning OA(BBOA), as shown in Fig. S28. The detailed information on how to select the optimum PMF solution is available in Table S4.

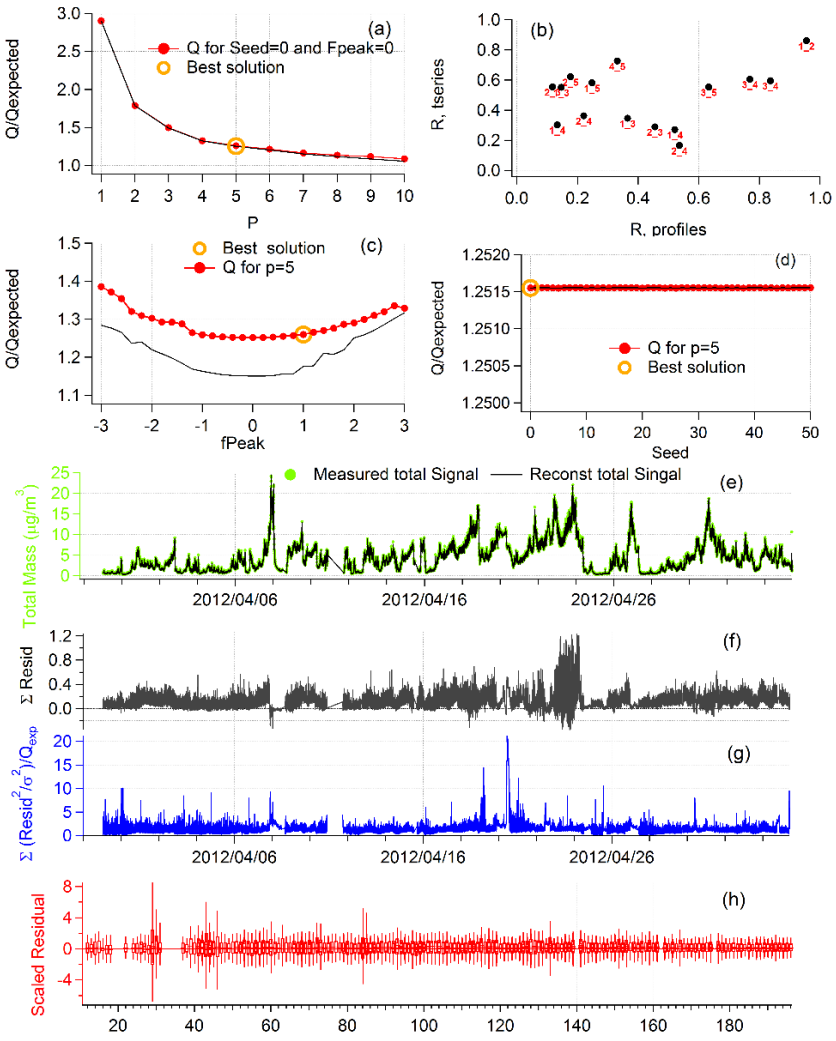

Figure S16. Diagnostic plots of the PMF analysis on OA mass spectral matrix for the spring observation.

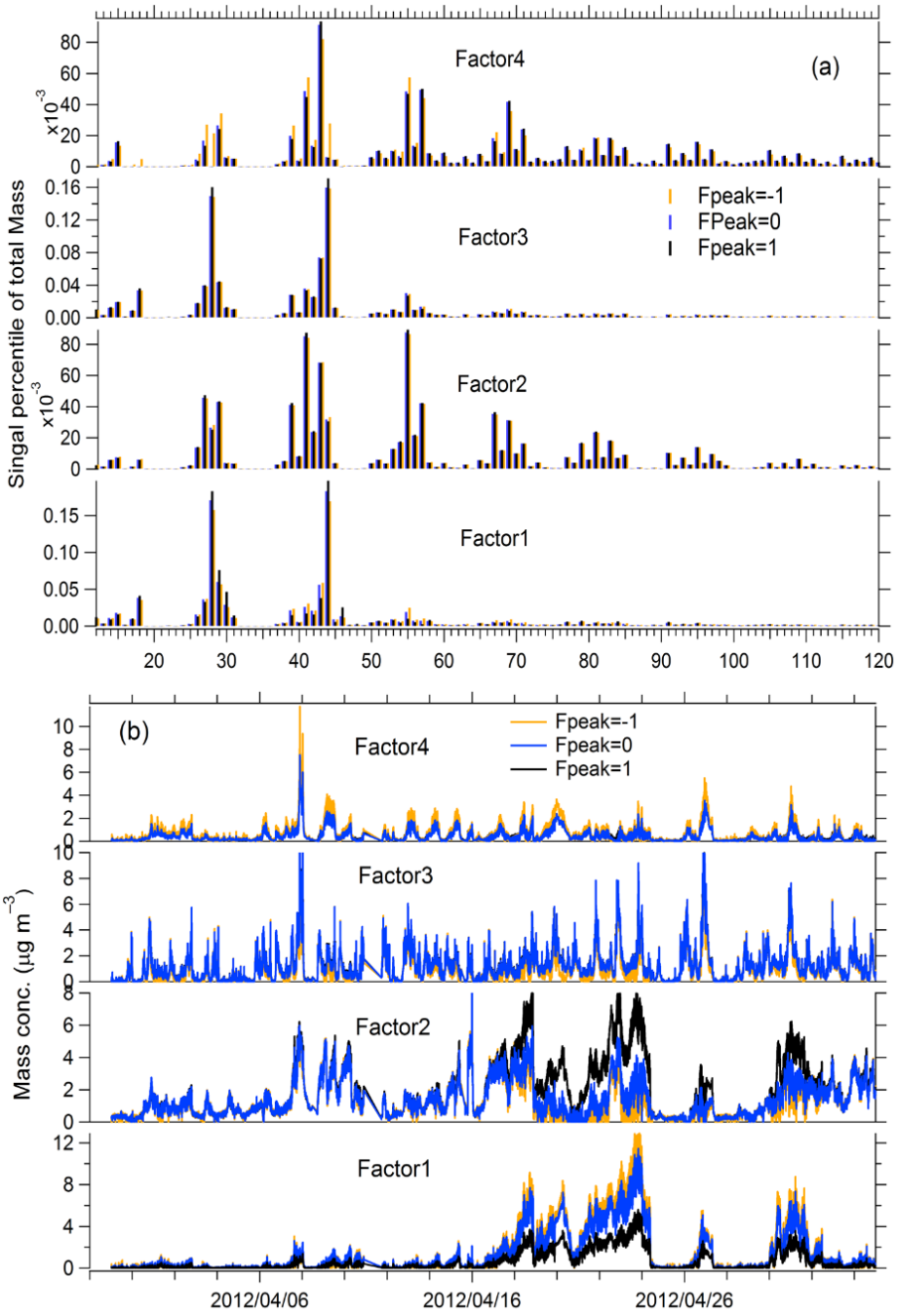

Figure S17. The spectra and time series of 4-factor solution at different f_{peak} values for the spring observation.

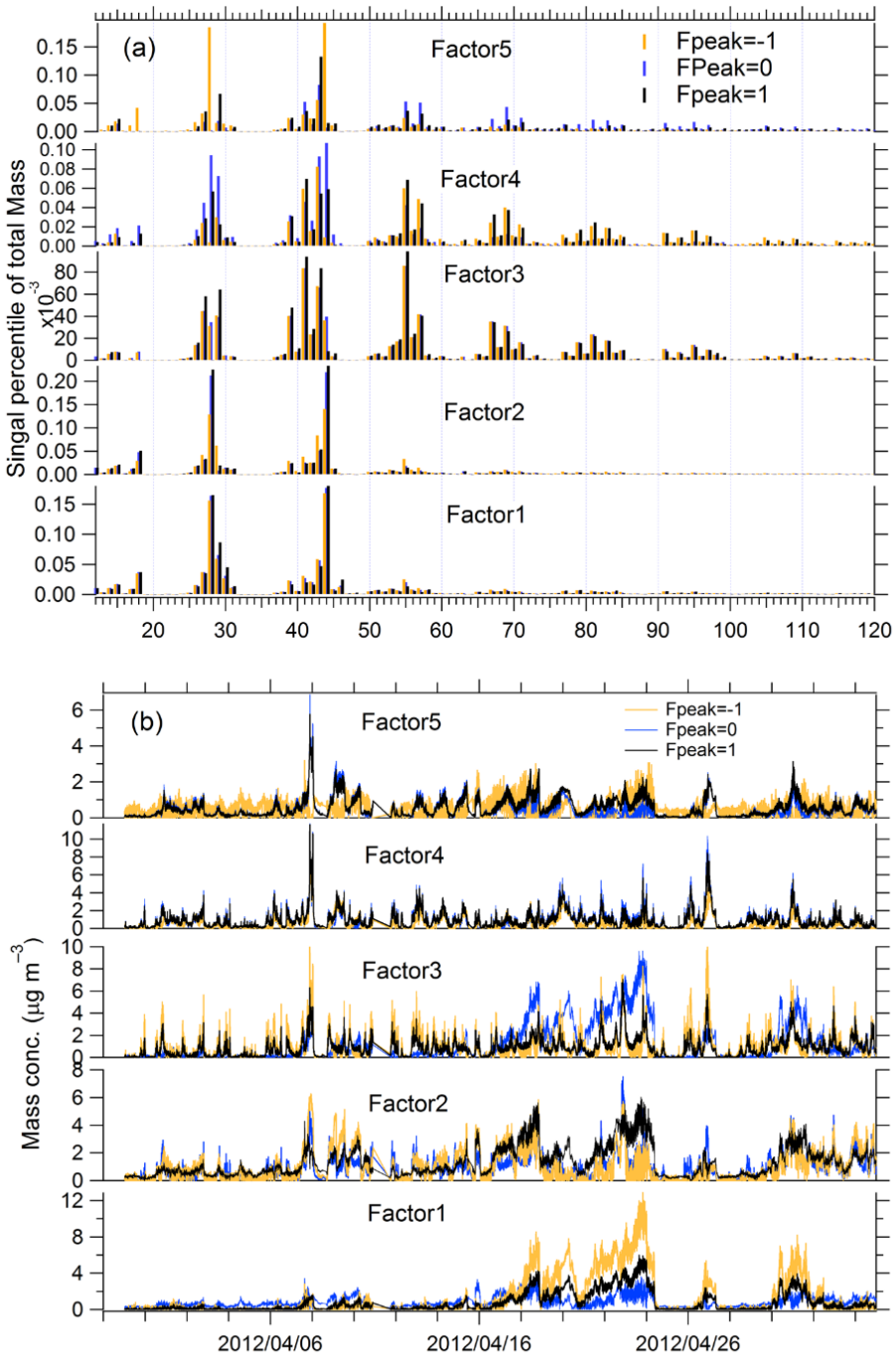

Figure S18. The spectra and time series of 5-factor solution at different f_{peak} values for the spring observation.

Table S4 Descriptions of PMF solutions for the spring observation in Beijing.

Factor number	**F_{peak}**	**Seed**	**Q/Q_{exp}**	**Solution Description**
1	0	0	2.90	Too few factors, large residuals at time periods and key *m/z*'s
2	0	0	1.79	Too few factors, large residuals at time periods and key *m/z*'s
3	0	0	1.49	Too few factors (OOA, HOA and COA). The Q/Q_{exp} at different seeds (0-50) are very unstable. Factors are mixed to some extent based on the time series and spectra.
4	0	0	1.32	OA factors could be identified as MO-OOA, LO-OOA, COA and HOA. Time series and diurnal variations of OA factors are consistent with the external tracers. But, the signal of characteristic ion *m/z* 60 biomass burning is strong in HOA factor.
5	**1**	**0**	**1.25**	**Final choice for the PMF solution. Two OOA factors, COA, HOA and BBOA are identified. Two similar OOA factors are combined for further analysis. Time series and diurnal variations of OA factors are consistent with the external tracers.**
6-10	0	0	1.20-1.06	Factor split. OOA was split into three or more factors with similar spectra, however, different time series.
5	-3 to 3	0	1.25-1.39	In f_{peak} range from −1.0 to 1.0, factor MS of OOA and COA are nearly identical, but there is a shift between HOA and BBOA for some ion fragments. The time series of OOA and HOA are nearly identical, but the other show some changes.

For the summer observation, the 4-factor, f_{peak}=0 solution was selected as the optimum solution. Four OA factors are more oxidized (MO-OOA) and less oxidized OOA (LO-OOA), cooking OA (COA) and hydrocarbon-like OA (HOA). The performances of spectra and time series of the four factors at different f_{peak} were also investigated. The detailed information on how to select the optimum PMF solution can be found in Figure S19-S21 and Table S5.

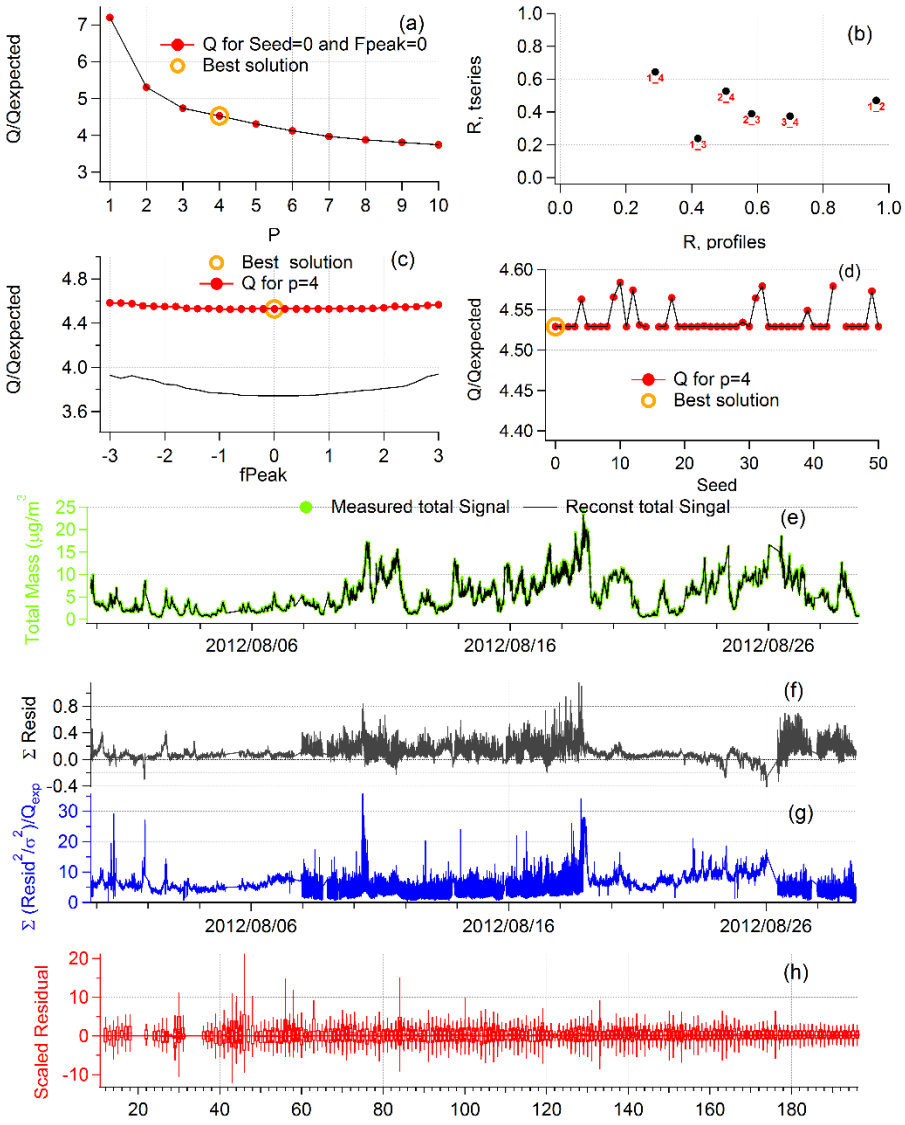

Figure S19. Diagnostic plots of the PMF analysis on OA mass spectral matrix for the summer observation.

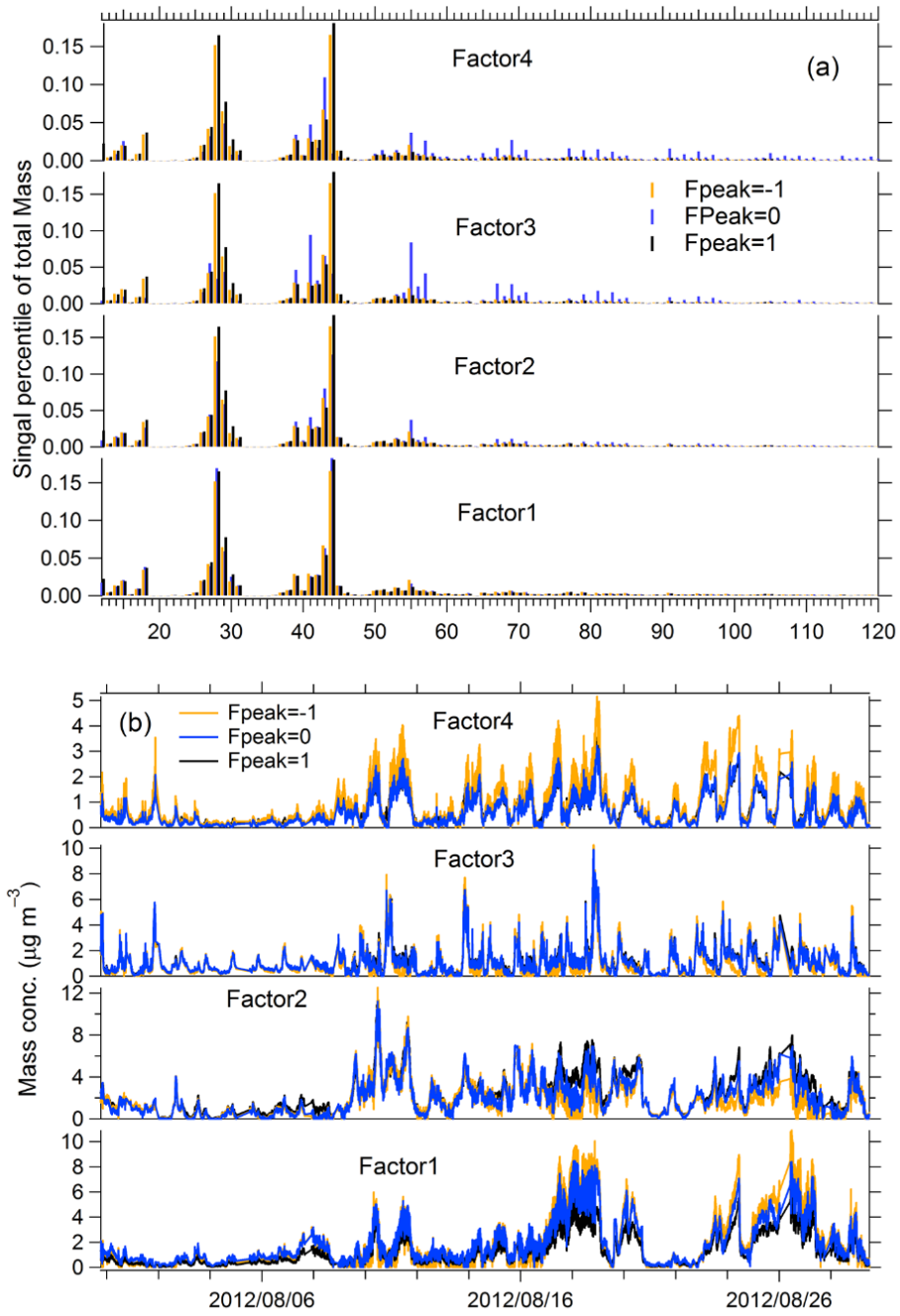

Figure S20. The spectra and time series of 4-factor solution at different f_{peak} values for the summer observation.

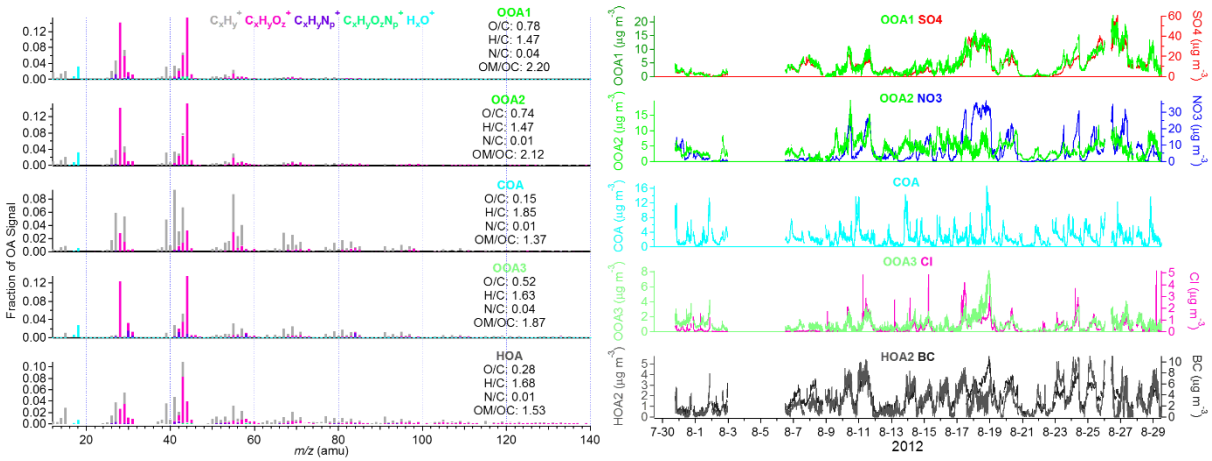

Figure S21. Unit mass spectra and time series of OA factors for 5-factor solution. The factors are marked as OOA1, OOA2, COA, OOA3 and HOA, respectively. OOA1, OOA2 and OOA3 show similar MS features (r=0.87–0.90). It is unclear if these OOA components represent distinct sources or chemical types. The elemental ratios and OA/OC ratios of each component are added.

Table S5 Descriptions of PMF solutions for the summer observation in Beijing.

Factor number	**Fpeak**	**Seed**	**Q/Q$_{exp}$**	**Solution Description**
1	0	0	7.20	Too few factors, large residuals at time periods and key *m/z*'s
2	0	0	5.31	Too few factors, large residuals at time periods and key *m/z*'s
3	0	0	4.73	Too few factors (OOA, HOA and COA). Factors are mixed to some extent based on the time series and spectra.
4	**0**	**0**	**4.53**	**Optimum solution for the PMF analysis (MO-OOA, LO-OOA, COA and HOA). Time series and diurnal variations of OA factors are consistent with the external tracers. The spectra of four factors are consistent with the source spectra in AMS spectra database.**
5-10	0	0	4.30-3.74	Factor split. Take 5 factor number solution as an example, OOA is likely split into three factors with similar mass spectra and different time series. However, it is difficult to explain if they represent distinct sources or chemical types.
4	-3 to 3	0	4.53-4.58	In f_{peak} range from −1.0 to 1.0, factor MS and time series are nearly identical.

The solution of the PMF analysis for the autumn observation is similar to that for the spring observation. When OA was separated into five fractions, OOA was also split into two factors, but a BBOA factor of distinct characteristics (f_{60}=1.3%) could be identified. When more than five factors, OOA decomposed into three or more factors. The performances of spectra and time series of the four factors at different f_{peak} are nearly identical. The five factors, f_{Peak}=0 and seed=0 solution is chosen as the optimal solution for this PMF analysis. In the five-factor solution, two OOA factors have similar MS characteristics (r= 0.976) and the elemental ratios and OA/OC ratios (O/C: 0.85–0.91; H/C: 1.24–1.40; OA/OC: 2.24–2.37) are close. It is unclear if the two OOA components represent distinct sources or chemical types. Thus, two OOA factors were combined into total OOA for further analysis (Hayes et al., 2013). Finally, four factors of OA were obtained, i.e., oxygenated OA (OOA), cooking OA (COA), hydrocarbon-like OA (HOA), and biomass burning OA(BBOA), as shown in Fig. S30. The detailed information on how to select the optimum PMF solution are given as Fig. S22-S24 and Table S6.

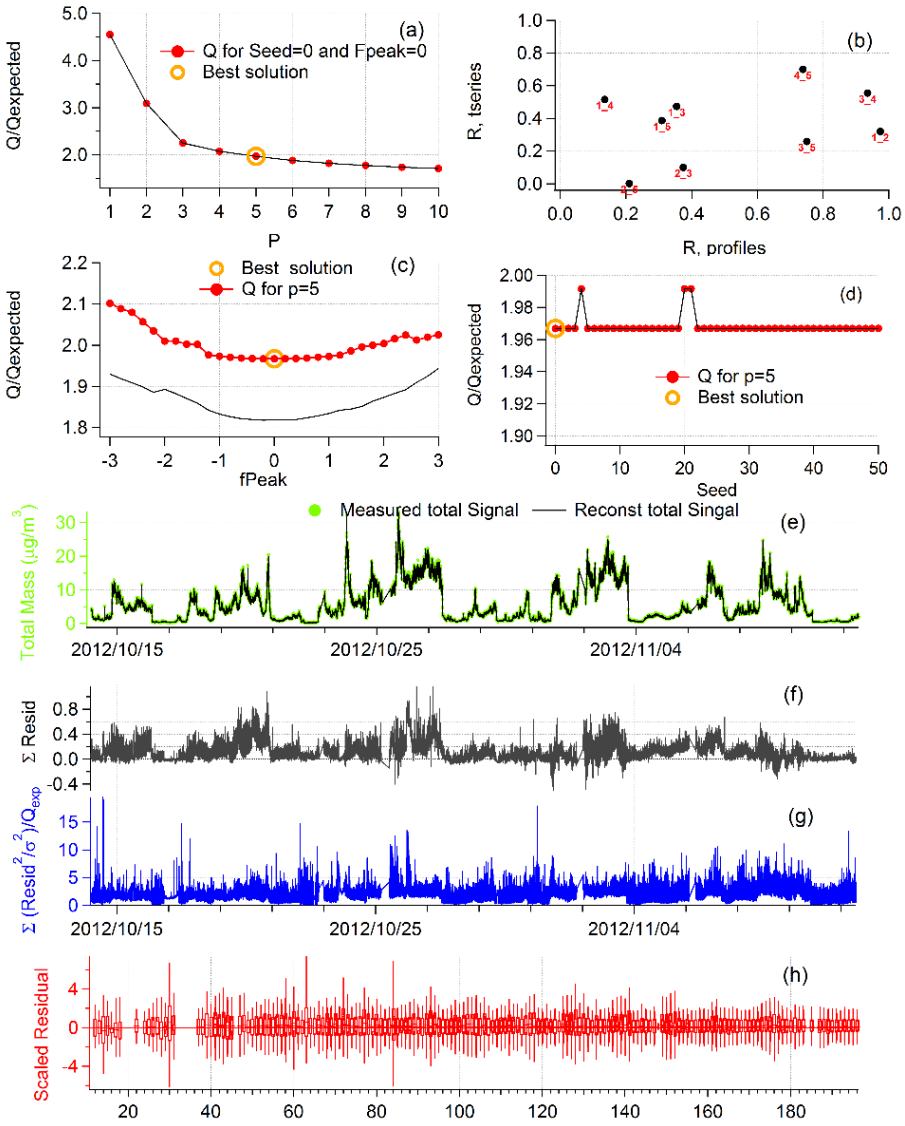

Figure S22. Diagnostic plots of the PMF analysis on OA mass spectral matrix for the autumn observation.

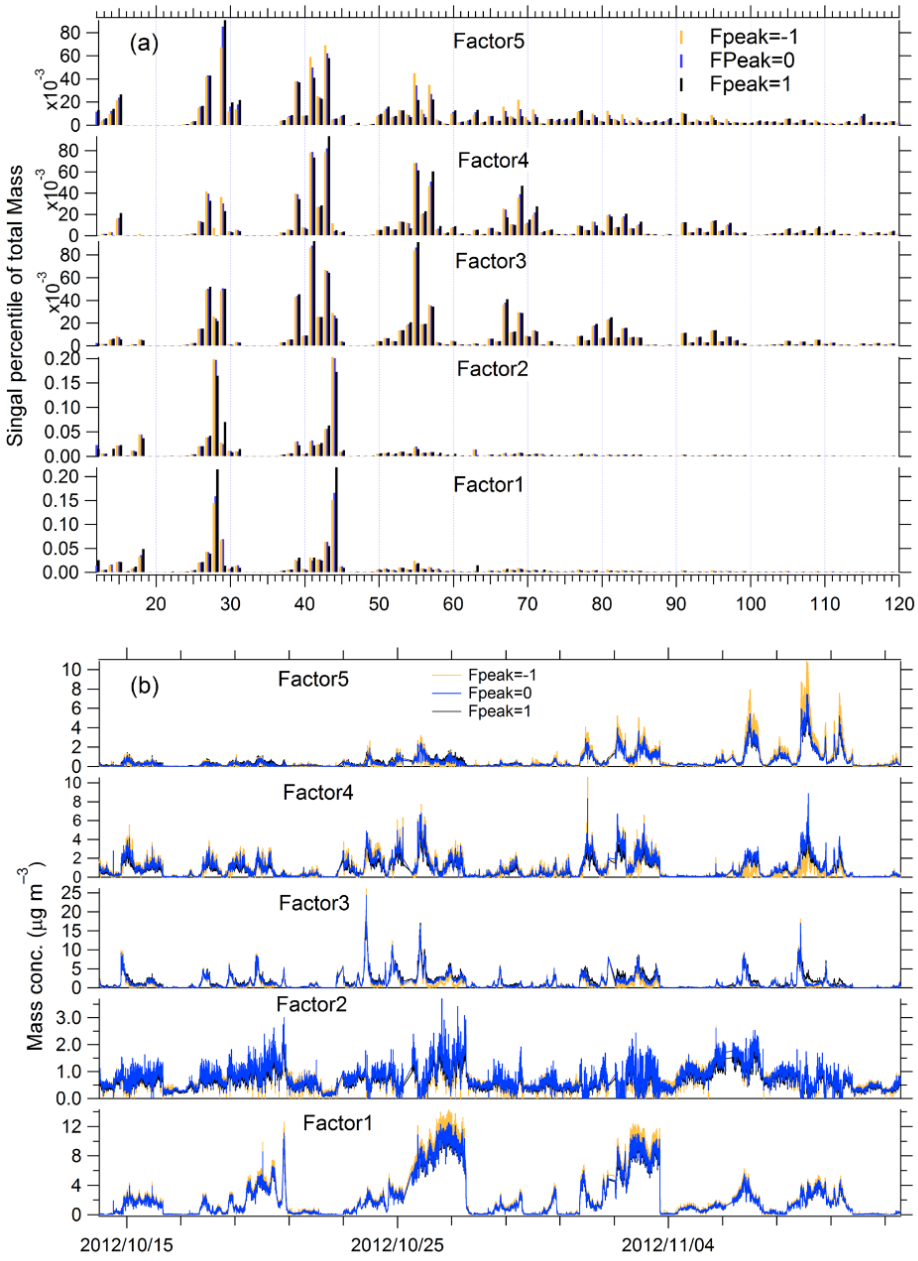

Figure S23. The spectra and time series of 5-factor solution at different f_{peak} values for the autumn observation.

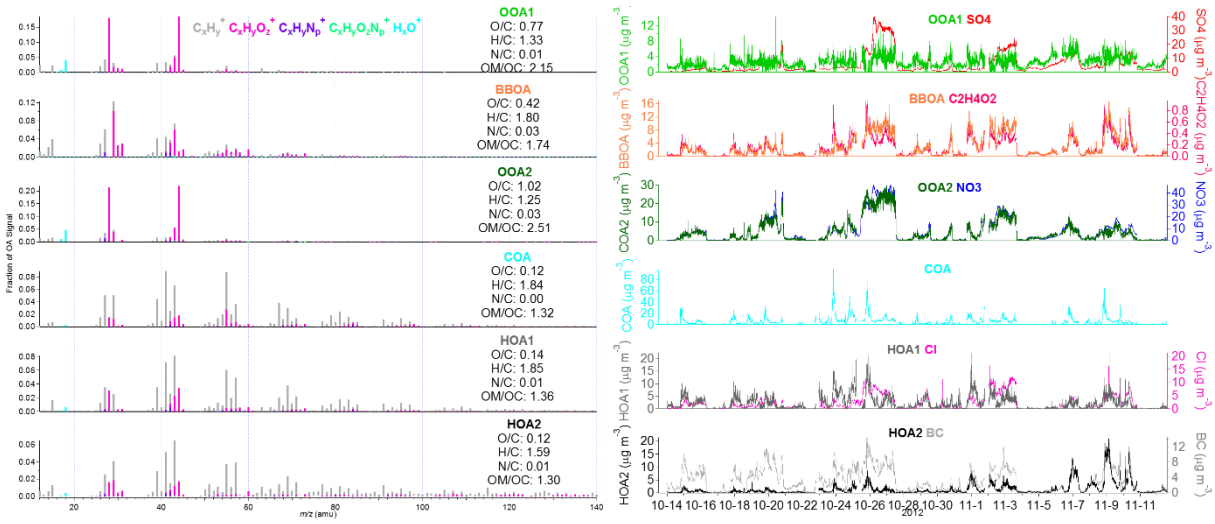

Figure S24. Unit mass spectra and time series of OA factors for 6-factor solution. The factors are marked as OOA1, BBOA, OOA2, COA, HOA1 and HOA2, respectively. The time series of BBOA and OOA2 trend well (r=0.78). HOA1 and HOA2 have similar MS (r=0.94) and diurnal variations (r=0.93). These factors appear mixed with each other.

Table S6 Descriptions of PMF solutions for the autumn observation in Beijing.

Factor number	**Fpeak**	**Seed**	**Q/Q$_{exp}$**	**Solution Description**
1	0	0	4.55	Too few factors, large residuals at time periods and key *m/z*'s
2	0	0	3.09	Too few factors, large residuals at time periods and key *m/z*'s
3	0	0	2.25	Too few factors (OOA, COA and HOA). The Q/Q$_{exp}$ at different seeds (0-50) are very unstable. The HOA factor contain high abundance (1.0%) of *m/z* 60.
4	0	0	2.07	Four factors include two similar OOA factors, COA and HOA. The HOA factor contain high abundance (1.1%) of *m/z* 60.
5	**0**	**0**	**1.97**	**Optimum solution for the PMF analysis (two OOA factor, COA, HOA and BBOA). Two similar OOA factors are combined for further analysis. Time series and diurnal variations of OA factors are consistent with the external tracers.**
6-10	0	0	1.88-1.71	Factor split. Some of the split factors have time series and MS that appear mixed.
5	-3 to 3	0	1.97-2.10	In f_{peak} range from −1.0 to 1.0, factor MS and time series are nearly identical.

For the winter observation, a 5-factor, f_{peak}=0 solution was selected as the optimum solution. Five OA factors are more oxidized (MO-OOA) and less oxidized OOA (LO-OOA), cooking OA (COA), coal combustion OA (CCOA) and hydrocarbon-like OA (HOA), respectively. The performances of spectra and time series of the five factors at different f_{peak} were also investigated. The detailed information on how to select the optimum PMF solution can be found in Fig. S25-S27 and Table S7.

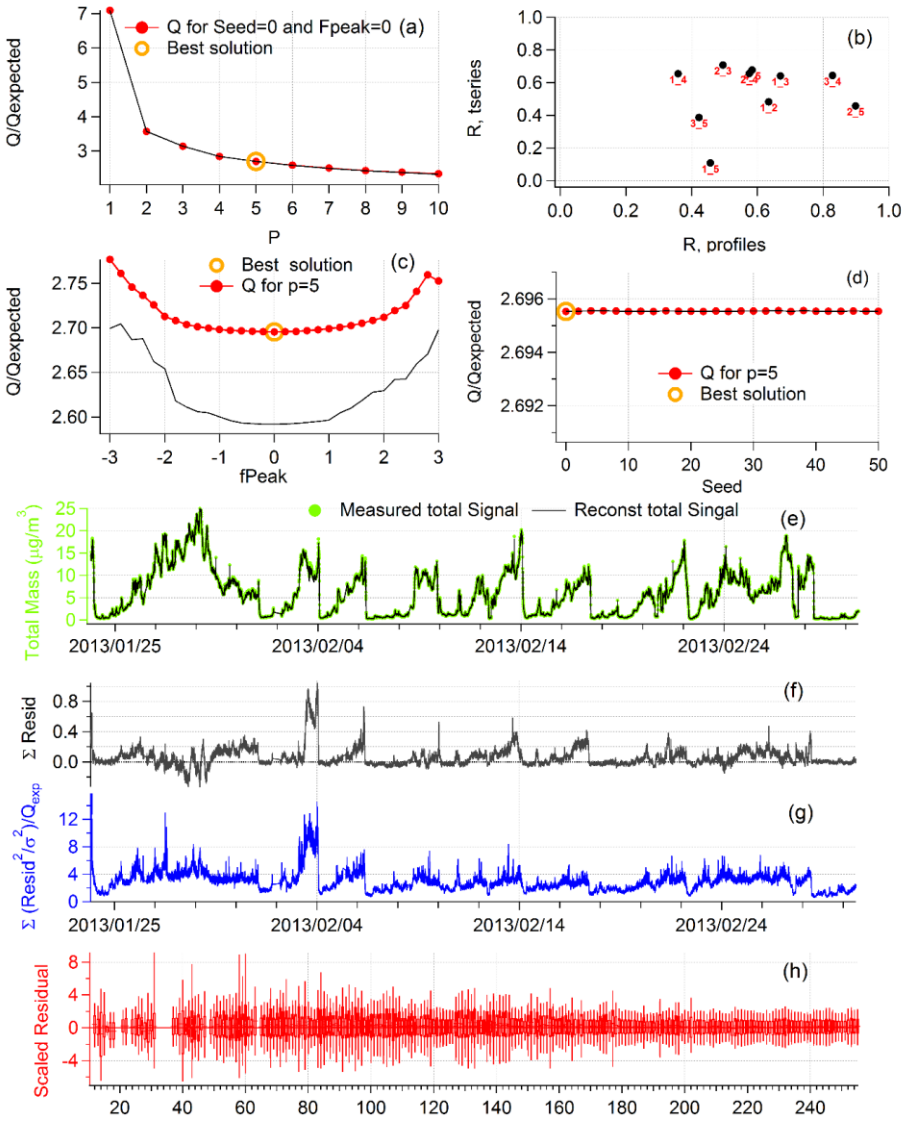

Figure S25. Diagnostic plots of the PMF analysis on OA mass spectral matrix for the winter observation.

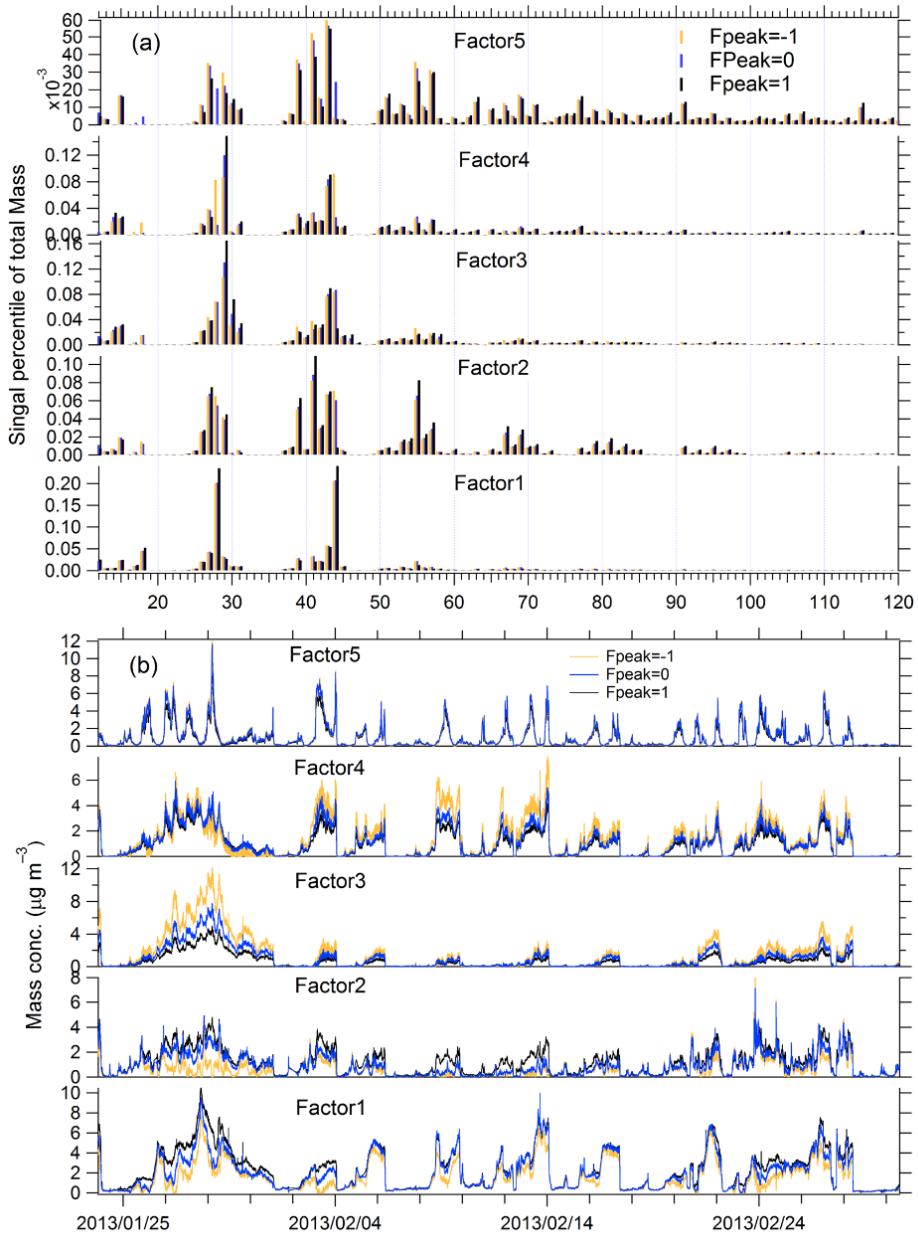

Figure S26. The spectra and time series of 5-factor solution at different f_{peak} values for the winter observation.

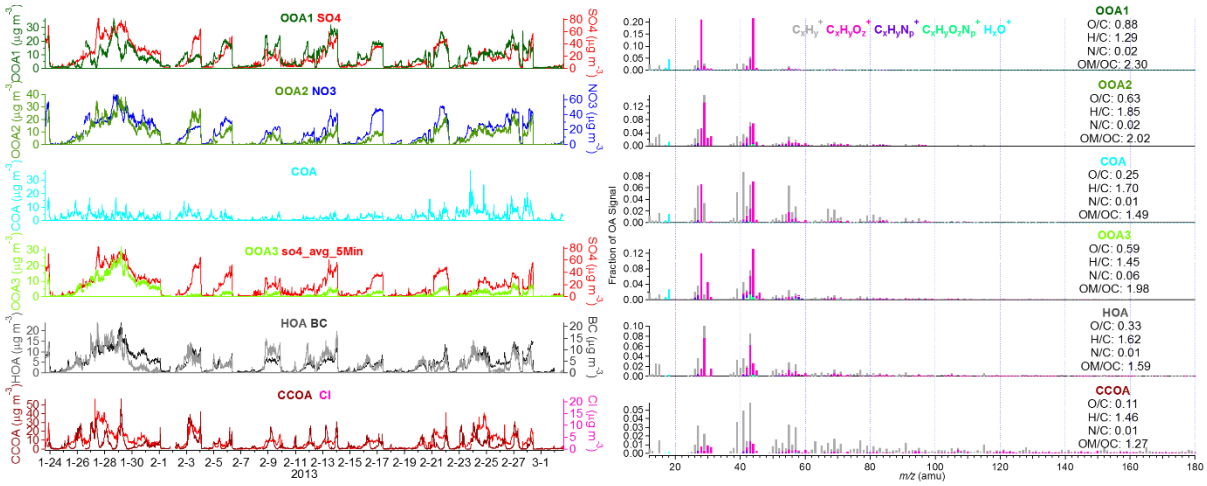

Figure S27. Unit mass spectra and time series of OA factors for 6-factor solution. The factors are marked as OOA1, OOA2, COA, OOA3, HOA and CCOA, respectively. OOA1, OOA2 and OOA3 show similar time series or MS features (r=0.56–0.95). The characteristics of OOA3 factor is not obvious. It is unclear if these factors represent distinct sources or chemical types.

Table S7 Descriptions of PMF solutions for the winter observation in Beijing.

Factor number	**Fpeak**	**Seed**	**Q/Q$_{exp}$**	**Solution Description**
1	0	0	7.09	Too few factors, large residuals at time periods and key *m/z*'s
2	0	0	3.57	Too few factors, large residuals at time periods and key *m/z*'s
3	0	0	3.14	Too few factors (OOA-, HOA- and COA-like). The Q/Q$_{exp}$ at different seeds (0-50) are very unstable. Factors are mixed to some extent based on the time series and spectra.
4	0	0	2.84	OA is split to two OOA factors, COA and HOA. It seems that HOA mixed with CCOA.
5	**0**	**0**	**2.70**	**Optimum choice for PMF factors (MO-OOA, LO-OOA, COA, HOA and CCOA). Time series and diurnal variations of OA factors are consistent with the external tracers. The spectra of four factors are consistent with the source spectra in AMS spectra database.**
6-10	0	0	2.59-2.33	Factor split. Take 6 factor number solution as an example, OOA was split into three factors with similar spectra and/or time series.
5	-3 to 3	0	2.70-2.78	In f_{peak} range from −1.0 to 1, factor MS and time series are nearly identical, but there is likely a shift of the time series for LO-OOA and COA during the heavy-pollution episodes.

S6 Concentration and mass spectra of OA factors

Table S8. Resolved fractions of OA during seasonal observations in Beijing in recent years. Unit: μg m^{-3}.

Seasons	Periods	LV-OOA[a]	SV-OOA[b]	OOA	LSOA	RSOA	HOA	CCOA	COA	BBOA	OOA/OA (%)	References
Spring	10 Apr.-4 May. 2008			23.0			16.0				59	Zhang et al., 2013
	30 Mar.-7 May. 2012			**6.8**			**2.8**		**2.6**	**1.8**	**49**	This study
Summer	9-21 Jul. 2006	12.6	4.5				11.0				61	Sun et al., 2010
	24 Jul.-20 Sept. 2008	8.1	5.7				4.3		5.8		58	Huang et al., 2010
	5 Jun.-3 Jul. 2008			20.0			14.0				59	Zhang et al., 2013
	26 Jun.-28 Aug. 2011			12.7			7.1				64	Sun et al., 2012
	4 Aug.-14 Sept. 2011	9.7	7.4				3.4		5.5		66	Hu et al., 2016
	29 Jul.-29 Aug. 2012	**3.3**	**5.3**				**1.4**		**2.5**		**69**	This study
Autumn	4-18 Oct. 2008			11.0			13.0				46	Zhang et al., 2013
	1-30 Sept. 2012			12.5			4.6				73	Jiang et al., 2013
	13 Oct.-13 Nov. 2012			**8.6**			**2.5**		**5.2**	**2.0**	**47**	This study
Winter	4 Jan.-3 Feb. 2008			10.0			33.0				23	Zhang et al., 2013
	22 Nov.-22 Dec. 2010	6.2	4.3				4.7	8.2	6.7	4.1	30	Hu et al., 2016
	14 Dec.2010-15 Jan. 2011			4.9			5.6		10.4		23	Liu et al., 2012
	21 Nov. 2011-20 Jan. 2012			10.7			5.8	11.4	6.5		31	Sun et al., 2013
	1-17 Jan. 2013		8.9		7.8	4.7	5.3	7.3	4.8		55	Sun et al., 2014
	1 Jan.-1 Feb. 2013	12.5	11.6				4.9	6.7	8.9		54	Zhang et al., 2014
	23 Jan.- 2 Mar. 2013	**9.8**	**5.0**				**5.5**	**5.1**	**4.3**		**50**	This study

Note: In Hu et al. (2016) and this study, [a] LV-OOA is defined as more-oxidized oxygenated OA (MO-OOA); [b] SV-OOA is defined as less-oxidized oxygenated OA (LO-OOA).

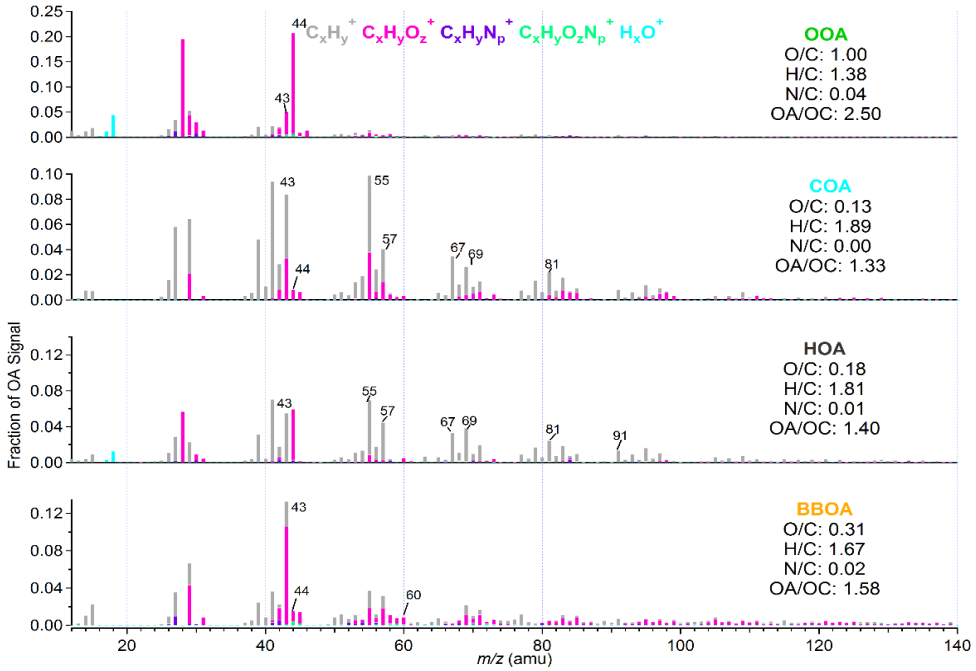

Figure S28. Unit mass spectra of OA factors resolved in the spring study: OOA, COA, HOA and BBOA. The elemental ratios and OA/OC ratios of each component are also shown in the legends. The ion fragments are classified into five categories to identify the mass spectra characteristics: $C_xH_y^+$, $C_xH_yO_z^+$, $C_xH_yN_p^+$, $C_xH_yO_zN_p^+$ and H_xO^+ represent the reductive alkyl fragments, the oxygenated fragments of carboxylic acid and aldehyde, the nitrogen-containing alkyl fragments, the oxygenated organonitrogen fragment ions, and fragmented H_2O and carboxyl, respectively.

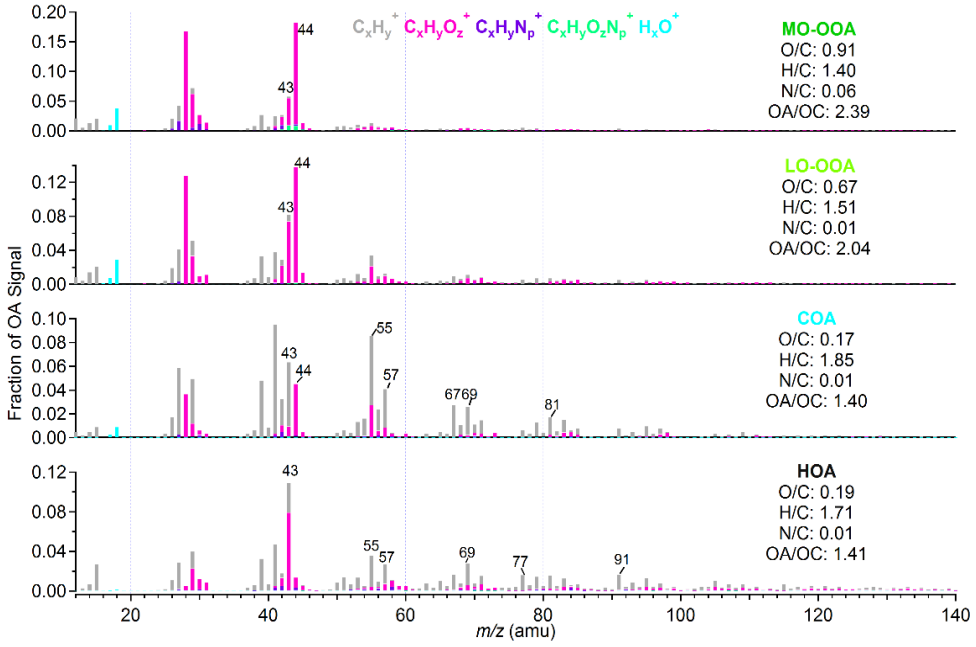

Figure S29. Unit mass spectra of OA factors resolved in the summer study: MO-OOA, LO-OOA, COA and HOA. The elemental ratios and OA/OC ratios of each component are also shown in the legends. The ion fragments are classified into five categories as described in Fig. S28.

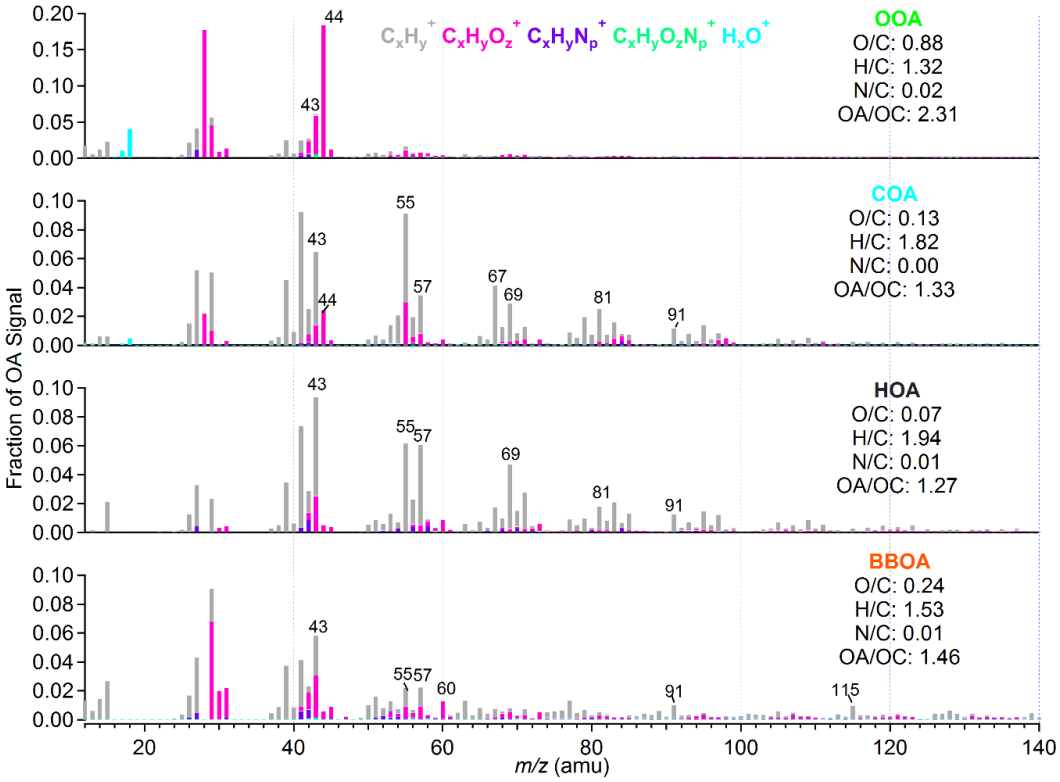

Figure S30. Unit mass spectra of OA factors resolved in the autumn study: OOA, COA, HOA, and BBOA. The elemental ratios and OA/OC ratios of each component are also shown in the legends. The ion fragments are classified into five categories as described in Fig. S28.

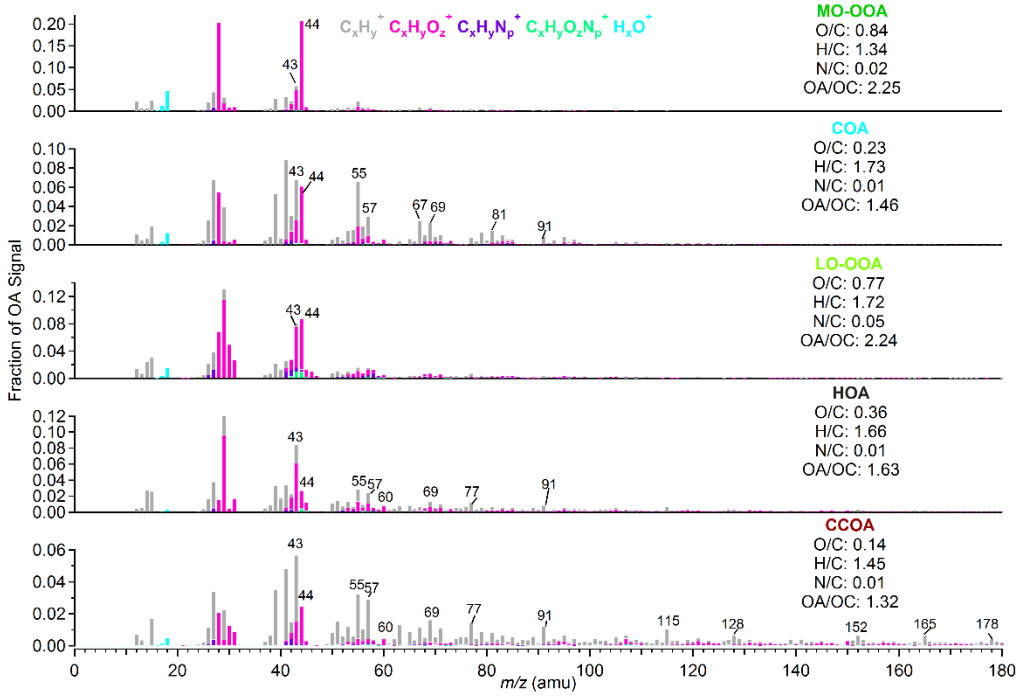

Figure S31. Unit mass spectra of OA factors resolved in the winter study: MO-OOA, LO-OOA, COA, HOA, and CCOA. The elemental ratios and OA/OC ratios of each component are also shown in the legends. The ion fragments are classified into five categories as described in Fig. S28.

S7 Time series of OA fractions

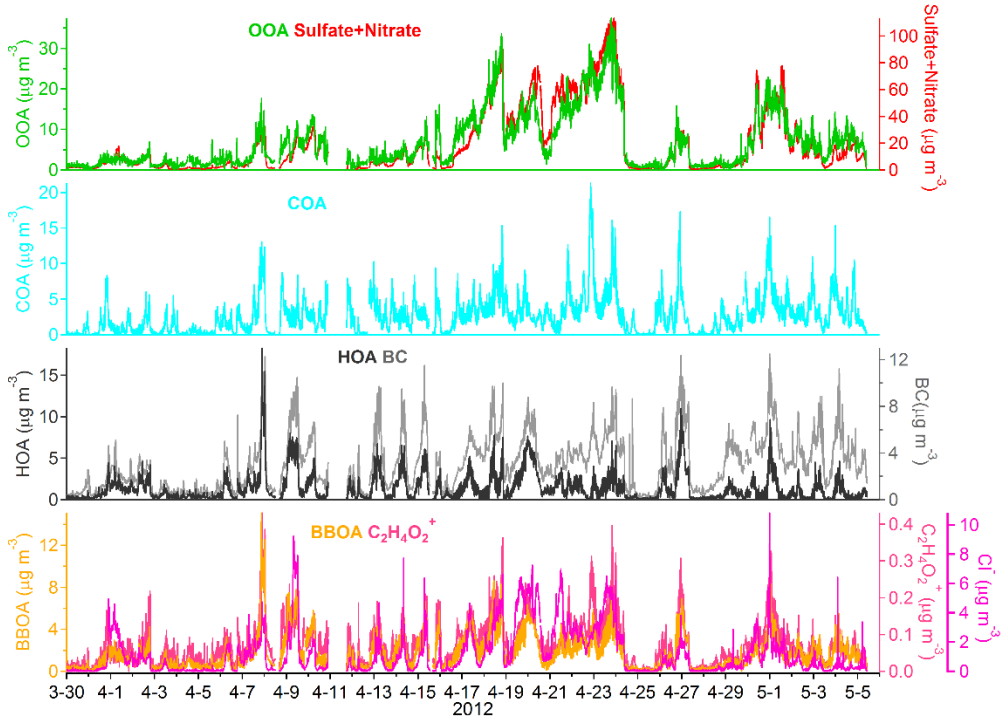

Figure S32. Time series of OA fractions and external tracers (sulfate, nitrate, chloride, BC, and $C_2H_4O_2^+$) during the spring observation.

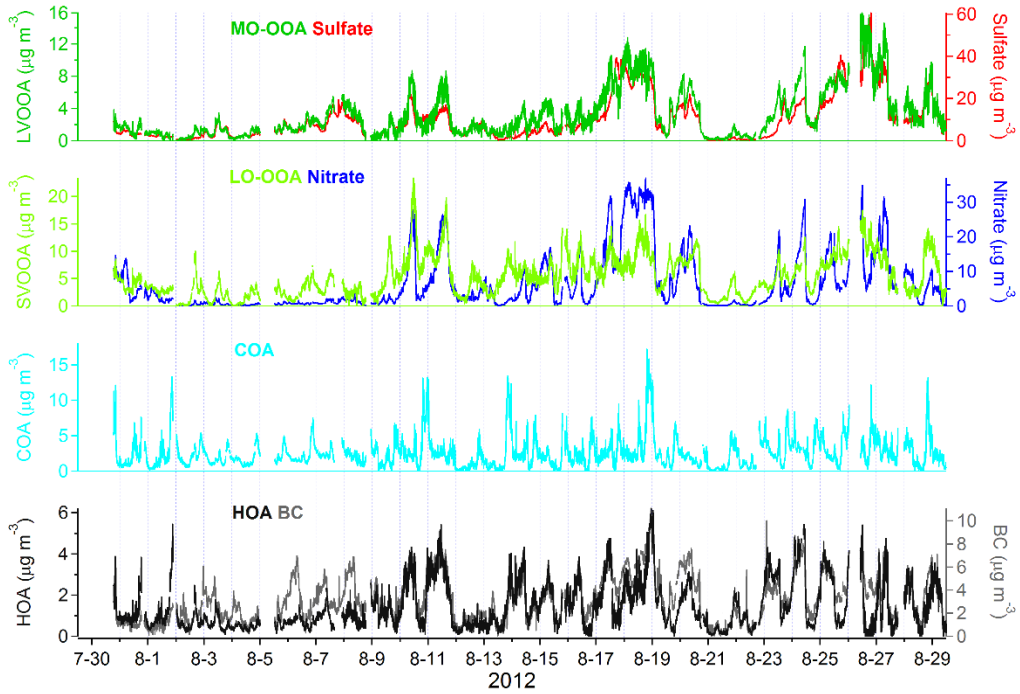

Figure S33. Time series of OA fractions and external tracers (sulfate, nitrate, and BC) during the summer observation.

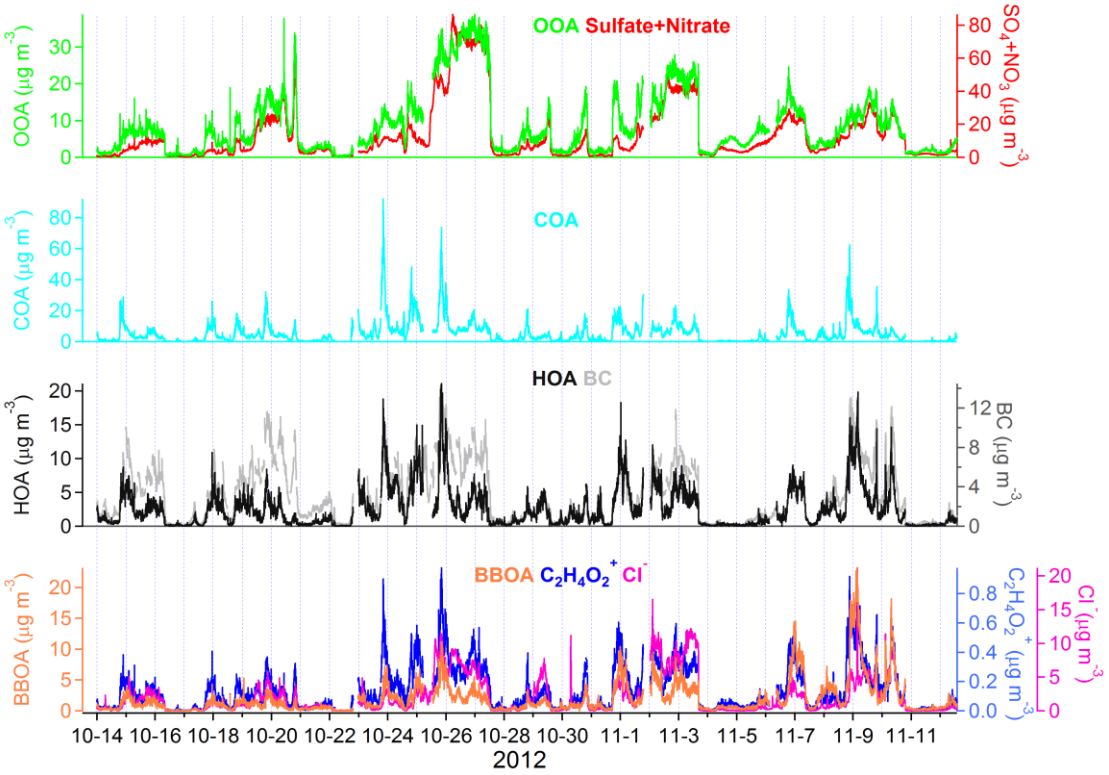

Figure S34. Time series of OA fractions and external tracers (sulfate+nitrate, BC, chloride and $C_2H_4O_2^+$) during the autumn observation.

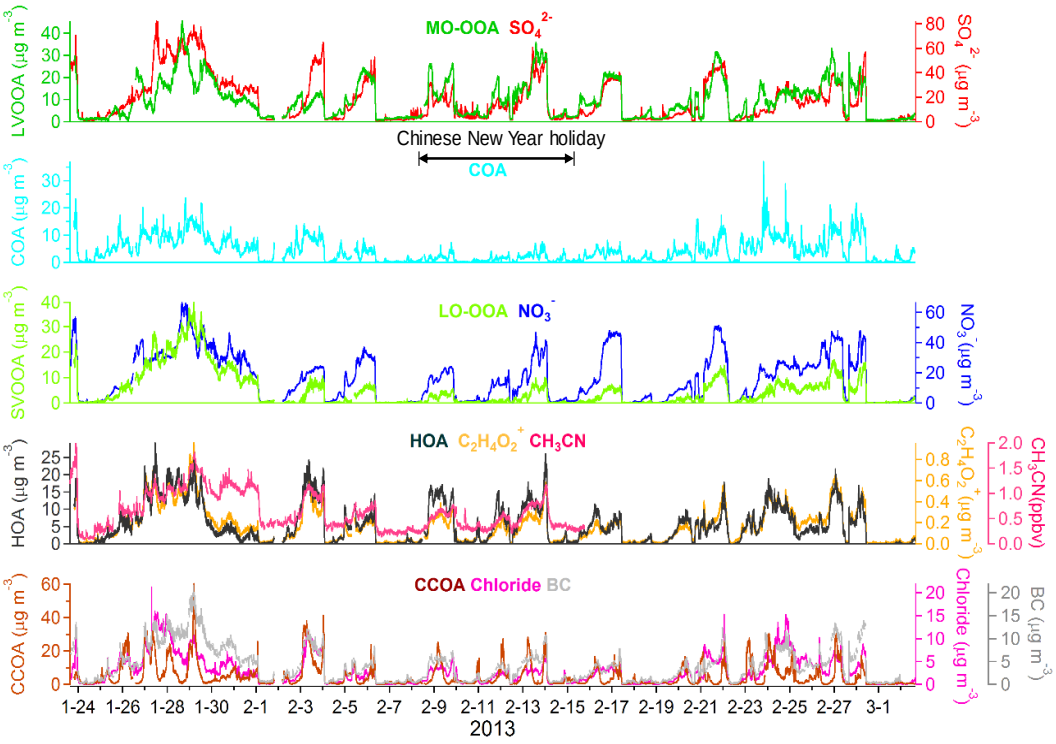

Figure S35. Time series of OA fractions and external tracers (sulfate, nitrate, $C_2H_4O_2^+$, acetonitrile, chloride and BC) during the winter observation.

S8 Elemental compositions of OA

The diurnal variations of element ratios (O/C, H/C) and OA/OC ratios were obvious during the seasonal observations in Beijing (Fig. S36-S39). The diurnal patterns of O/C and OA/OC ratios in the spring, summer and autumn were similar: during the daytime, the oxidation state of OA gradually increased due to the effect of photochemical reactions; the O/C and OA/OC ratios were peaked at about 16:00 in the afternoon, indicating that secondary formation is an important factor affecting the properties of OA. As the products of photochemical reactions, SOA gradually accumulated in the daytime, making an important contribution to OA. In the morning, the O/C and OA/OC ratios declined slightly at 7:00-8:00, which may be affected by reductive OA emitted from vehicles during the rush hour. They showed two valleys at noon (12:00-13:00) and in the evening (19:00-20:00), reflecting the impacts of cooking emissions during meal time (Huang et al., 2010). In the autumn, the oxidation state of OA (O/C and OA/OC ratio) maintained at a low level after the valley at 20:00, mainly caused by the biomass emissions at night. While in the summer, the O/C and OA/OC ratios rose after 20:00, indicating the aqueous oxidation processes may play a significant role under high humidity conditions at nighttime (Ervens et al., 2011). In the winter, the diurnal patterns of O/C and OA/OC ratios were close to those in other seasons, but the impacts of vehicular and cooking emissions were less significant than in other seasons; the oxidation state of OA kept to decrease after 20:00, which is mainly influenced by primary emissions (e.g., coal combustion and biomass burning) at night. Hydrogen mainly comes from the alkyl fragments. Along with oxidation of OA, alkyl functional groups are gradually substituted by oxygenated ones, the proportion of hydrogen in OA is gradually reduced. Therefore, the diurnal variations of H/C ratios always trended oppositely with those of O/C and OA/OC ratios.

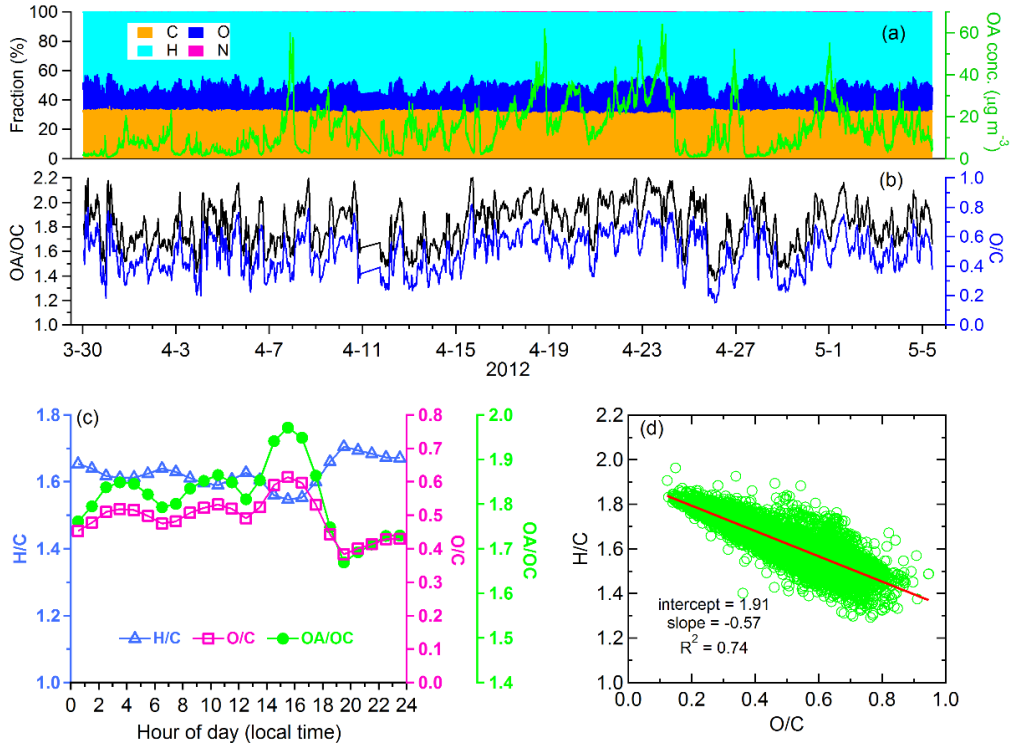

Figure S36. Time series of (a) elemental fractions and (b) OA/OC and O/C ratios in OA; (c) Diurnal patterns of OA/OC, H/C and O/C ratios; (d) van Krevelen diagram of OA during the spring observation.

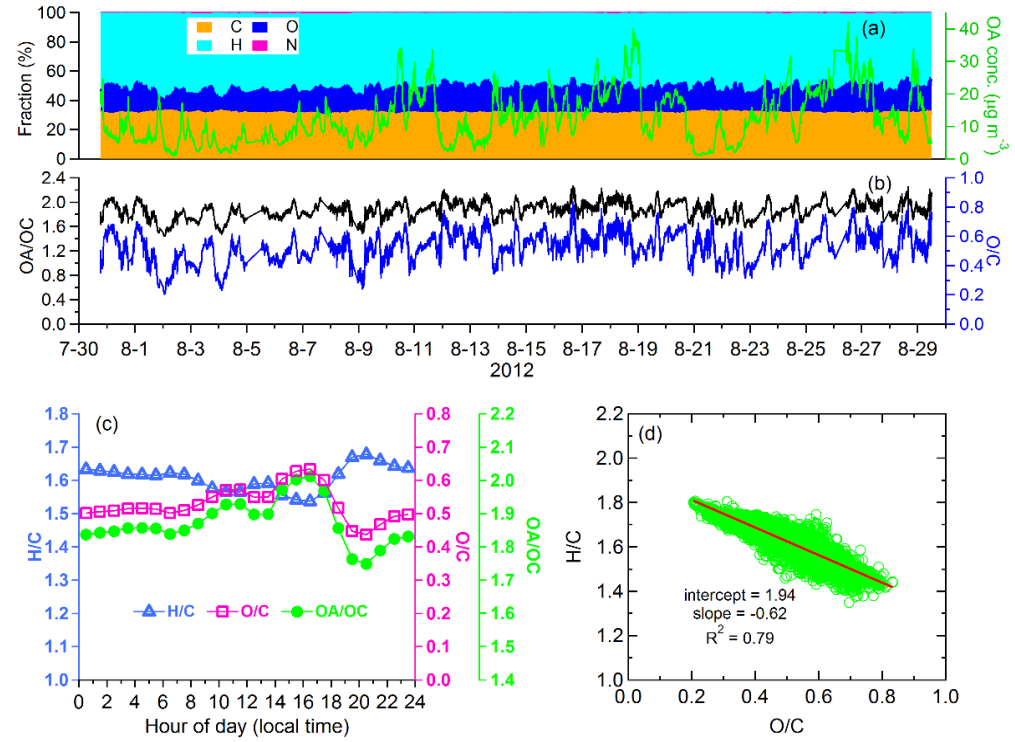

Figure S37. Time series of (a) elemental fractions and (b) OA/OC and O/C ratios in OA; (c) Diurnal patterns of OA/OC, H/C and O/C ratios; (d) van Krevelen diagram of OA during the summer observation.

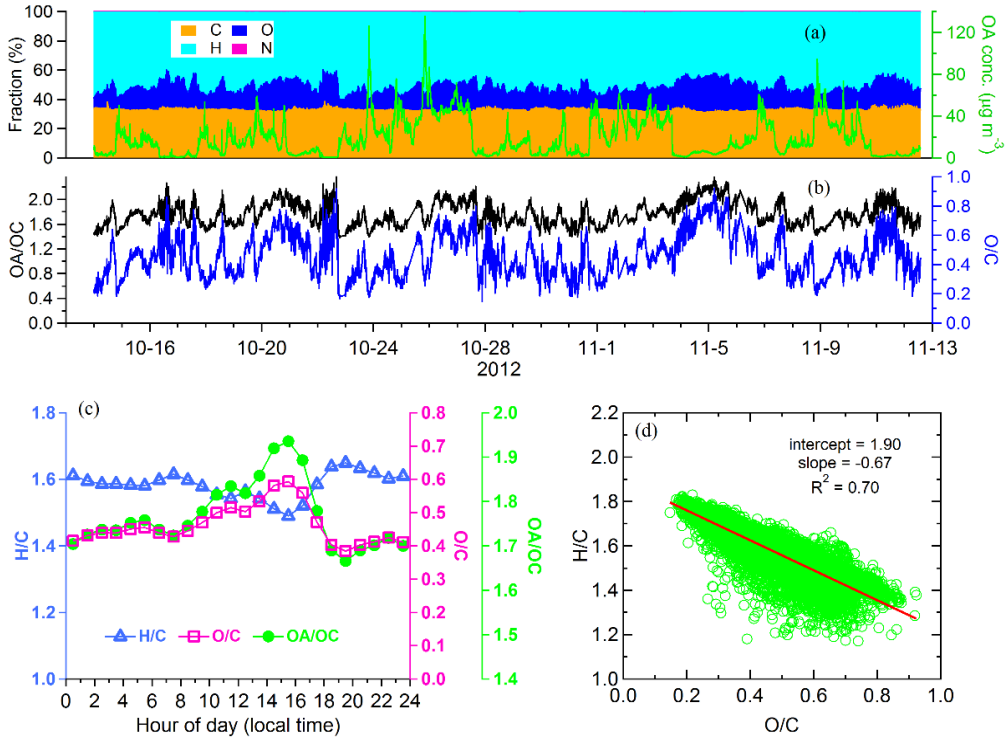

Figure S38. Time series of (a) elemental fractions and (b) OA/OC and O/C ratios in OA; (c) Diurnal patterns of OA/OC, H/C and O/C ratios; (d) van Krevelen diagram of OA during the autumn observation.

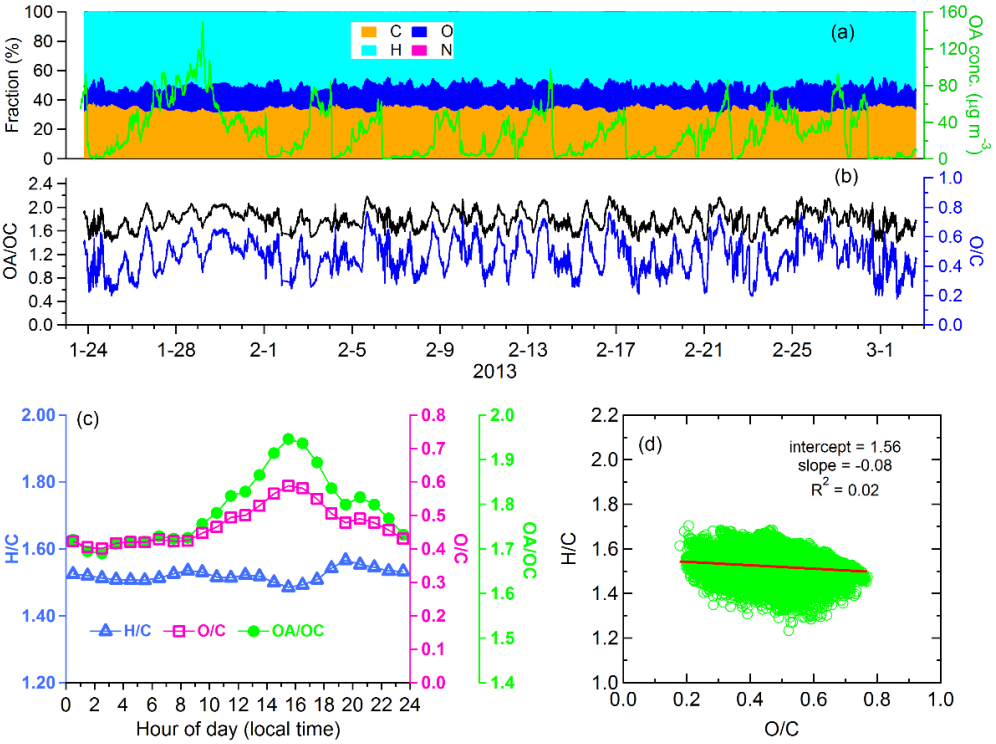

Figure S39. Time series of (a) elemental fractions and (b) OA/OC and O/C ratios in OA; (c) Diurnal patterns of OA/OC, H/C and O/C ratios; (d) van Krevelen diagram of OA during the winter observation.

S9 Correlation matrix of gaseous pollutants and particulate chemical compositions

Table S9 Correlation matrix of gaseous pollutants and particulate chemical compositions in submicron aerosols during the spring campaign.

	CO	NO_x	SO_2	O_3	O_x	SO_4^{2-}	NO_3^-	NH_4^+	Cl^-	BC	$C_2H_4O_2^+$	OOA	COA	HOA	BBOA
CO	1.000														
NO_x	.475	1.000													
SO_2	**.755**	.301	1.000												
O_3	-.376	-.679	-.051	1.000											
O_x	.219	.029	.485	.561	1.000										
SO_4^{2-}	**.758**	.189	.531	-.205	.186	1.000									
NO_3^-	**.773**	.361	.550	-.314	.258	**.871**	1.000								
NH_4^+	**.798**	.300	.577	-.282	.231	**.953**	**.973**	1.000							
Cl^-	**.764**	.480	.598	-.461	.094	**.667**	**.755**	**.771**	1.000						
BC	**.615**	**.826**	.513	-.532	.275	.454	**.635**	.580	**.676**	1.000					
$C_2H_4O_2^+$	.591	.580	.448	-.396	.342	.556	**.716**	**.670**	**.674**	**.822**	1.000				
OOA	**.704**	.274	.542	-.196	.346	**.881**	**.925**	**.936**	**.668**	.570	**.705**	1.000			
COA	.464	.439	.309	-.241	.429	.486	.537	.524	.371	.584	**.754**	**.603**	1.000		
HOA	.432	**.787**	.272	-.572	.106	.136	.325	.260	.497	**.728**	**.691**	.231	.560	1.000	
BBOA	.548	.596	.497	-.422	.285	.454	**.624**	.578	**.705**	**.819**	**.831**	**.652**	.538	**.695**	1.000

Table S10 Correlation matrix of gaseous pollutants and particulate chemical compositions in submicron aerosols during the summer campaign.

	CO	NO_x	SO_2	O_3	O_x	SO_4^{2-}	NO_3^-	NH_4^+	Cl^-	BC	$C_2H_4O_2^+$	LV-OOA	SV-OOA	COA	HOA
CO	1.000														
NO_x	.456	1.000													
SO_2	.354	-.027	1.000												
O_3	-.041	-.541	.382	1.000											
O_x	.124	-.310	.431	.957	1.000										
SO_4^{2-}	.620	.099	.644	.261	.351	1.000									
NO_3^-	.718	.334	.321	-.123	-.007	.657	1.000								
NH_4^+	.720	.213	.555	.098	.205	.932	.882	1.000							
Cl^-	.625	.441	.186	-.252	-.145	.463	.795	.668	1.000						
BC	.773	.672	.270	-.232	-.030	.604	.740	.715	.727	1.000					
$C_2H_4O_2^+$	.697	.469	.327	.030	.227	.667	.702	.737	.619	.773	1.000				
MO-OOA	.663	.260	.529	.129	.252	.912	.813	.946	.651	.756	.745	1.000			
LO-OOA	.601	.196	.320	.382	.543	.642	.626	.682	.449	.613	.816	.691	1.000		
COA	.428	.449	.100	-.135	.035	.266	.238	.274	.217	.415	.646	.222	.310	1.000	
HOA	.558	.741	.036	-.404	-.203	.255	.626	.443	.710	.787	.705	.498	.469	.423	1.000

Table S11 Correlation matrix of gaseous pollutants and particulate chemical compositions in submicron aerosols during the autumn campaign.

	CO	NO_x	SO_2	O_3	O_x	SO_4^{2-}	NO_3^-	NH_4^+	Cl^-	BC	$C_2H_4O_2^+$	OOA	COA	HOA	BBOA
CO	1.000														
NO_x	.639	1.000													
SO_2	.694	.379	1.000												
O_3	-.511	-.694	-.319	1.000											
O_x	.517	.371	.566	-.044	1.000										
SO_4^{2-}	.789	.334	.458	-.332	.335	1.000									
NO_3^-	.827	.447	.521	-.373	.541	.943	1.000								
NH_4^+	.838	.423	.522	-.379	.462	.976	.987	1.000							
Cl^-	.855	.532	.618	-.477	.367	.745	.753	.804	1.000						
BC	.833	.851	.516	-.636	.465	.595	.691	.676	.732	1.000					
$C_2H_4O_2^+$	.761	.741	.431	-.536	.383	.560	.631	.629	.743	.864	1.000				
OOA	.834	.526	.510	-.419	.567	.901	.969	.957	.775	.746	.733	1.000			
COA	.499	.671	.223	-.398	.430	.272	.393	.351	.391	.638	.798	.502	1.000		
HOA	.590	.812	.286	-.567	.236	.302	.383	.376	.578	.812	.908	.493	.785	1.000	
BBOA	.606	.573	.407	-.439	.156	.352	.359	.383	.613	.728	.827	.433	.487	.816	1.000

Table S12 Correlation matrix of gaseous pollutants and particulate chemical compositions in submicron aerosols during the winter campaign.

	CO	NO_x	SO_2	CH_3CN	O_3	O_x	SO_4^{2-}	NO_3^-	NH_4^+	Cl^-	BC	$C_2H_4O_2^+$	LV-OOA	COA	SV-OOA	HOA	CCOA
CO	1.000																
NO_x	.933	1.000															
SO_2	.682	.702	1.000														
CH_3CN	.914	.895	.669	1.000													
O_3	-.763	-.757	-.701	-.712	1.000												
O_x	.692	.755	.561	.723	-.404	1.000											
SO_4^{2-}	.852	.826	.635	.852	-.635	.727	1.000										
NO_3^-	.813	.790	.627	.844	-.651	.804	.898	1.000									
NH_4^+	.854	.824	.652	.861	-.668	.777	.971	.971	1.000								
Cl^-	.790	.795	.572	.733	-.623	.555	.801	.666	.778	1.000							
BC	.922	.917	.646	.899	-.696	.749	.911	.850	.902	.874	1.000						
$C_2H_4O_2^+$	.833	.826	.555	.807	-.634	.644	.847	.774	.835	.889	.945	1.000					
MO-OOA	.562	.504	.493	.593	-.461	.702	.783	.872	.855	.463	.644	.603	1.000				
COA	.806	.879	.539	.808	-.655	.690	.765	.753	.778	.797	.859	.830	.480	1.000			
LO-OOA	.842	.880	.590	.844	-.556	.833	.887	.857	.877	.747	.902	.819	.627	.817	1.000		
HOA	.699	.658	.509	.666	-.587	.514	.797	.695	.781	.839	.839	.916	.666	.670	.636	1.000	
CCOA	.618	.561	.317	.520	-.515	.151	.432	.318	.387	.648	.635	.751	.086	.527	.408	.667	1.000

Table S13 Uncentered coefficients between mass spectra of COA factors during the seasonal campaigns in Beijing and the average from previous studies.

	Spring	**Summer**	**Autumn**	**Winter**	**Average**
Spring	1.000				
Summer	0.956	1.000			
Autumn	0.924	0.888	1.000		
Winter	0.893	0.977	0.835	1.000	
Average	0.977	0.990	0.910	0.954	1.000

S10 Assessment of secondary formation pathways

In this study, the LWC in aerosols was roughly estimated with the ISORROPIAII model. The input data were the four species (sulfate, nitrate, ammonium and chloride) measured by the AMS, the RH and temperature of ambient air. The reverse mode and the metastable state of aerosols were selected. According to the results, the ambient aerosols were generally in aqueous phase. The average values of aerosol LWC in four seasons were 17.3±28.5, 18.8±24.9, 12.8±27.3 and 25.2±32.8 μg m^{-3}, respectively. During the heavy-polluted episodes, the LWC was frequently higher than 100 μg m^{-3}.

It is well known that most of aerosol sulfate are formed from heterogeneous or aqueous-phase/cloud processes (Kulmala et al., 2016). On a global scale, about 80% of the sulfate formation occurs within clouds. Ambient aerosol populations often show two distinct submicron modes (<0.2 μm and 0.5–1 μm) where the larger (droplet) mode is formed from the smaller (condensation) mode through volume-phase reactions in clouds and wet aerosols (Ervens et al., 2011). Based on this assumption, Guo et al. (2010) found that the gas-to-particle condensation process was important for aerosol pollution in the summer of Beijing. In urban Beijing, the formation of sulfate was mainly attributed to in-cloud or aerosol droplet process (80%) and gas condensation process (14%).

Table S14 shows the correlation coefficients between OOA and some indicators (RH, LWC, O_3 and O_x). As shown in Table S14, secondary inorganics (sulfate and nitrate) correlated well with RH and/or LWC in four seasons, indicating that the aqueous-phase reactions in aerosols played an important role in secondary inorganic formation in Beijing. The contributions of photochemical processes to the formation of sulfate and nitrate in four seasons were likely less than those of aqueous-phase reactions according to the weaker correlations between secondary inorganics and odd oxygen (O_x=O_3+NO_2). Especially, in summer nitrate showed no correlation with O_x. As shown in Fig. S40, when RH was higher than 40% (or 30% in winter), aqueous-phase processed likely played a dominant role in secondary inorganic formation.

Table S14 Pearson correlation coefficients between secondary organic and inorganic species and some indicators (RH, LWC, O_3 and O_x). Coefficients greater than 0.5 are in bold. Correlation is significant at the 0.01 level (2-tailed) except for those marked by #.

		RH	LWC	O_3	O_x
Spring	OOA	**.661**	**.754**	-.199	.345
	SO_4^{2-}	**.764**	**.901**	-.207	.186
	NO_3^-	**.705**	**.827**	-.318	.254
Summer	MO-OOA	.176	**.751**	.131	.264
	LO-OOA	.005#	.469	.360	**.527**
	SO_4^{2-}	.114	**.686**	.262	.359
	NO_3^-	.335	**.873**	-.123	.000#
Autumn	OOA	.483	**.803**	-.433	**.571**
	SO_4^{2-}	**.552**	**.919**	-.340	.338
	NO_3^-	.489	**.854**	-.379	**.548**
Winter	MO-OOA	**.624**	**.647**	-.504	**.640**
	LO-OOA	**.692**	**.840**	-.534	**.726**
	SO_4^{2-}	**.801**	**.899**	-.613	**.597**
	NO_3^-	**.785**	**.819**	-.637	**.655**

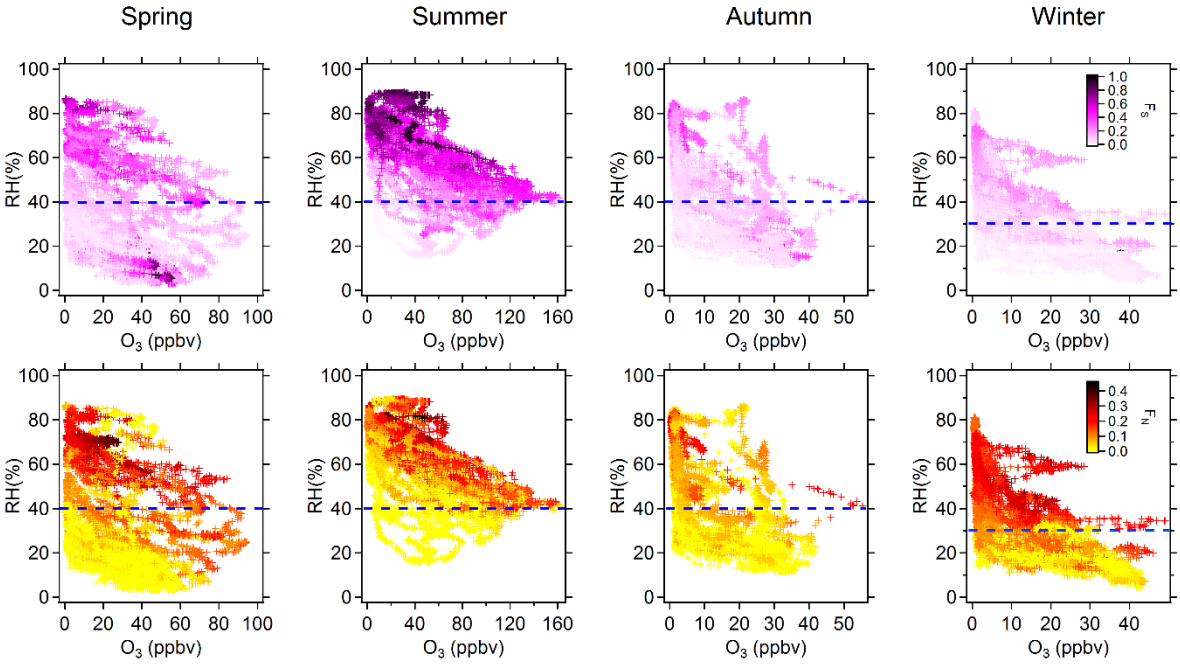

Figure S40. Influences of RH and O_3 concentrations on sulfate and nitrate formation.

Conversion ratios for sulfur and nitrogen (F_S and F_N) were calculated as follows:

$$F_S = \boldsymbol{n} - SO_4^{2-} / (\boldsymbol{n} - SO_4^{2-} + \boldsymbol{n} - SO_2) \quad (3)$$

$$F_N = \boldsymbol{n} - NO_3^- / (\boldsymbol{n} - NO_3^- + \boldsymbol{n} - NO_2) \quad (4)$$

where *n* means the amount of substance of the gaseous and particulate pollutants, mol m^{-3}.

The good correlation between F_N/F_S and RH/LWC also support that aqueous-phase reactions in aqueous aerosols and/or clouds could contribute to secondary inorganic formation remarkably in highly humid air.

Table S15 Pearson correlation coefficients between F_S and F_N with RH, LWC, O_3, O_x and NH_4^+.

	Spring		Summer		Autumn		Winter	
	F_S	F_N	F_S	F_N	F_S	F_N	F_S	F_N
RH	.339	**.722**	**.639**	.393	.432	**.574**	**.531**	**.744**
LWC	.475	**.816**	.464	**.816**	**.647**	**.874**	**.583**	**.676**
O_3	.024*	-.146	-.100	.024*	.035	-.321	-.268	-.518
O_x	-.166	.277	-.096	.052	-.122	.359	.342	.368
NH_4^+	.324	**.924**	.353	**.822**	.495	**.938**	**.598**	**.855**

Note: Coefficients greater than 0.5 are in bold. Correlation is significant at the 0.01 level (2-tailed) except for those marked with *.

Based on laboratory experiments and simulations, Ervens et al. (2011) suggest that SOA formed in cloud and aerosol water (aqSOA) might contribute almost as much mass as SOA formed in the gas phase to the SOA budget, with highest contributions from biogenic emissions of VOCs in the presence of anthropogenic pollutants (i.e., NO_x) at high RH and cloudiness. Xu et al. (2017) show that aqueous-phase processes have a dominant impact on the formation of MO-OOA, and the contribution of MO-OOA to OA increases substantially as a function of RH or liquid water content (LWC) in aerosols. In contrast, photochemical processing plays a major role in the formation of LO-OOA, as indicated by the strong correlations between LO-OOA and O_x during periods of photochemical production.

The good correlations between OOA and RH and/or LWC indicate that aqueous-phase reactions play a dominant role in OOA formation (Table S14). The slope of OOA against O_x steepened with the increase of RH and LWC (Figs. S41 and S42), also implying that the aqueous-phase oxidation was an important pathway of the OOA formation. The strong correlations between O_x and LO-OOA in summer, and between O_x and OOA in autumn and winter, suggesting photochemical processes also contributed substantially to OOA, especially LO-OOA, in these seasons.

It is difficult to give a quantitative result for the relative contribution of photochemical vs. aqueous-phase oxidation to the secondary formation based on field observation data only. Further studies including laboratory experiments, field observations and model simulations are needed to close the gaps in the current understanding of SOA formation pathways (Ervens et al., 2011).

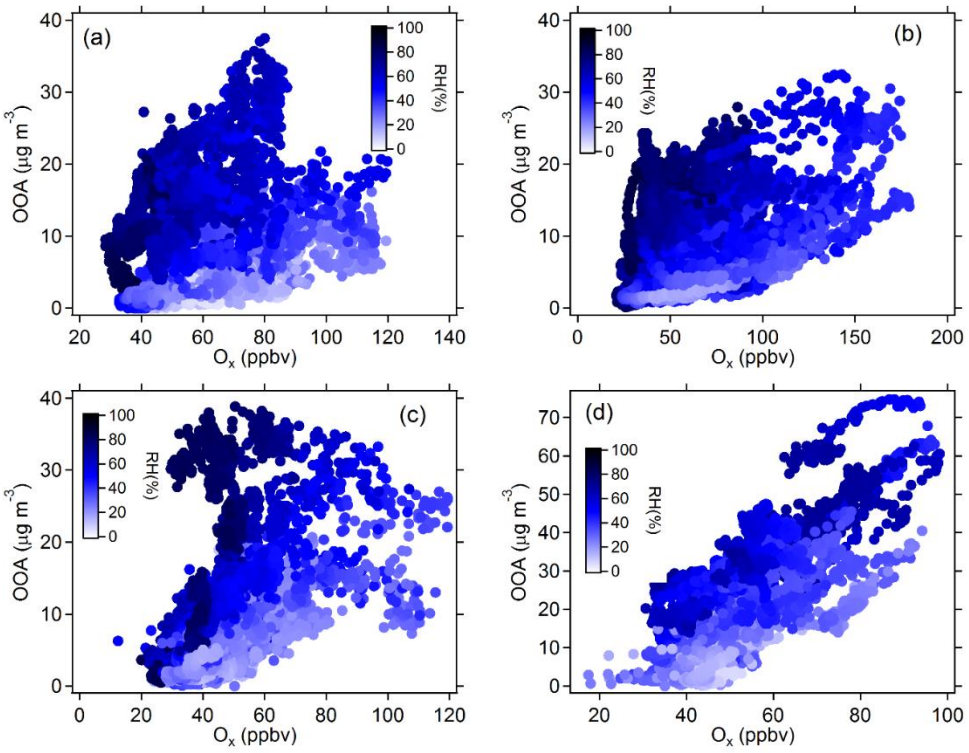

Figure S41. Scattering plots of OOA mass concentrations against O_x concentrations. (a) spring; (b) summer; (c) autumn and (d) winter. Data points are color coded by RH.

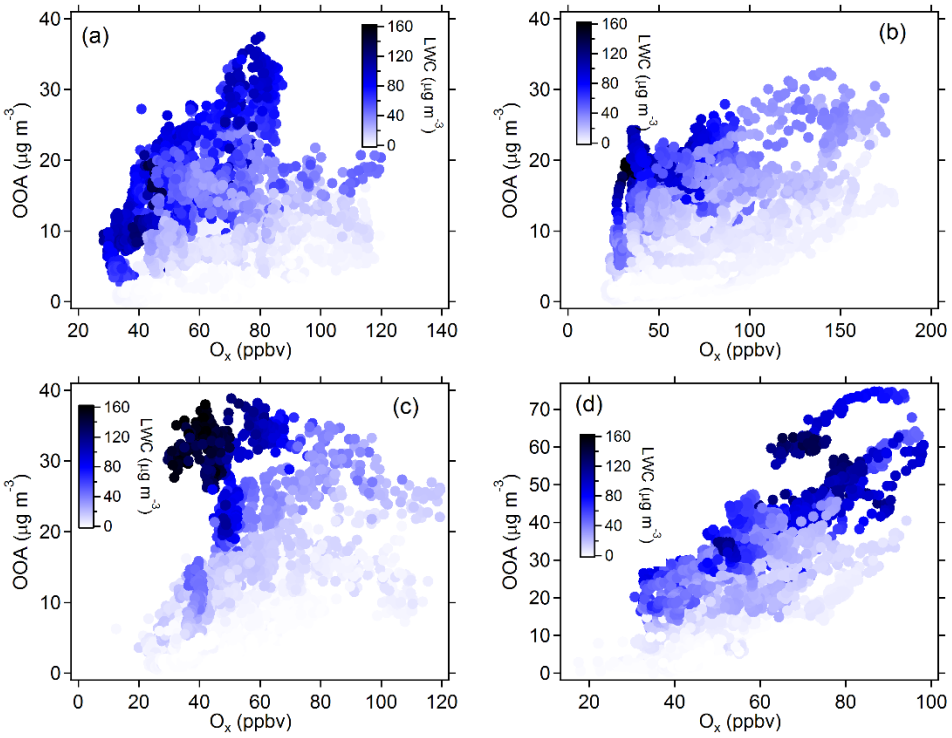

Figure S42. The same as above. Data points are color coded by estimated LWC in aerosols.

S11 Impacts of regional and long range transport on atmospheric aerosols

To give an insight into the impacts of regional/long-distance transport on atmospheric aerosols in Beijing, the backward trajectories of air parcels during the observation periods were calculated with the NOAA's HYSPLIT4 trajectory model (http://www.arl.noaa.gov/hysplit.html). A new 3-day backward trajectory was traced from the observation site at an altitude of 500 m above ground level every hour. Cluster analyses of backward trajectories were applied to reveal the major pathways during different campaigns (Fig. S43).

During the seasonal observations in Beijing, the pathways of dominant air masses are different. Both long-distance transported and regional/local air masses influenced Beijing. In summer, the transport distance of long-distance transported air masses was shorter than in other seasons. In general, with the decrease of transport distance, the concentration of PM_1 gradually increased. When Beijing was dominated by regional/local air masses, the fractions of secondary inorganic species (SNA) increased, while the contributions of carbonaceous components (OA+BC) decreased, which is consistent with the previous results in Beijing (Sun et al., 2010; Huang et al., 2010; Zhang et al., 2014). Higher concentrations of SNA and PM_1 under the control of regional/local air masses reflected the great contribution of secondary formation from the gaseous precursors (e.g., NO_x and SO_2) emitted by vehicles and coal combustion in urban areas.

During the observations in spring, summer and autumn, the contributions of OOA (MO-OOA+LO-OOA) increased when Beijing was dominated by regional or local air masses. In summer, the fractions of LO-OOA in OA were high (29–48%) regardless of the different trajectories, signifying that the secondary formation from photochemical oxidations probably made an important contribution to OA. During the winter observation, POA and OOA contributed equally to OA in most cases due to the long-lasting stable weather conditions, indicating that both primary pollutants and regional secondary formation made important contributions to OA. When Beijing was dominated by long-distance transported air masses from north polar regions in winter, OOA contributed more significantly to OA, implying that organic aerosols were fully aged during long-distance transport.

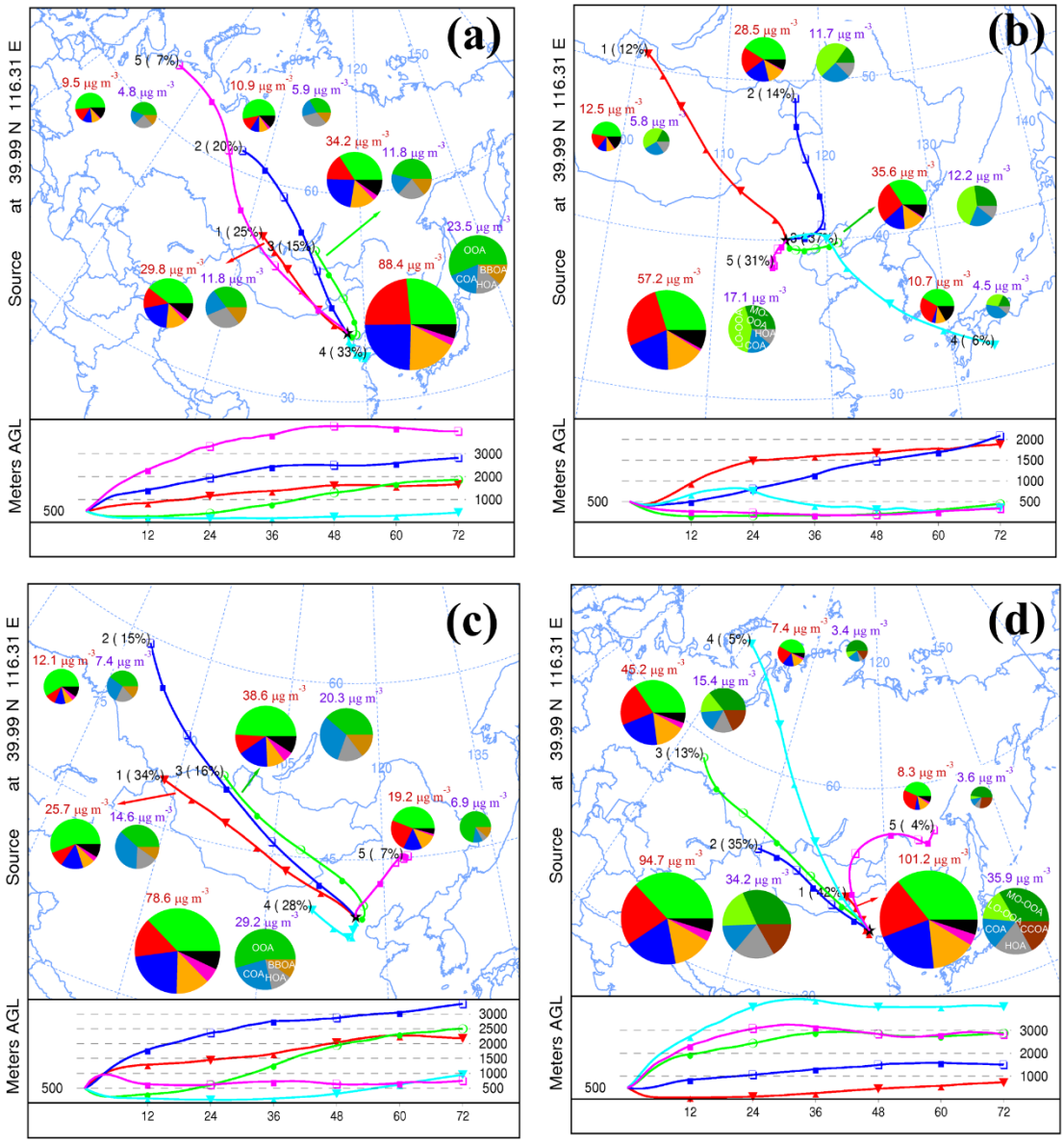

Figure S43. Back trajectories for each of the identified clusters and corresponding average main components of PM_1 and OA in PM_1 during the seasonal campaigns. (a) spring; (b)summer; (c) autumn and (d) winter. The filling color of main chemical species in PM_1 is the same with other figures.

References

Bae, M.-S., Demerjian, K. L., and Schwab, J. J.: Seasonal estimation of organic mass to organic carbon in $PM_{2.5}$ at rural and urban locations in New York state, Atmos. Environ., 40, 7467–7479, 2006.

Doshi, V., Vuthaluru, H. B., Korbee, R., and Kiel, J. H. A.: Development of a modeling approach to predict ash formation during co-firing of coal and biomass, Fuel Process Technol, 90, 1148-1156, doi: 10.1016/j.fuproc.2009.05.019, 2009.

Ervens, B., Turpin, B., and Weber, R.: Secondary organic aerosol formation in cloud droplets and aqueous particles (aqSOA): a review of laboratory, field and model studies, Atmos. Chem. Phys., 11, 11069-11102, 2011.

Grover, B. D., Eatough, N. L., Woolwine, W. R., Cannon, J. P., Eatough, D. J., and Long, R. W.: Semi-continuous mass closure of the major components of fine particulate matter in Riverside, CA, Atmos. Environ., 42, 250-260, 2008.

Guo, S., Hu, M., Wang, Z., Slanina, J., and Zhao, Y.: Size-resolved aerosol water-soluble ionic compositions in the summer of Beijing: implication of regional secondary formation, Atmos. Chem. Phys., 10, 947–959, doi:10.5194/acp-10-947-2010, 2010.

Hayes, P. L., Ortega, A. M., Cubison, M. J., Froyd, K. D., Zhao, Y., Cliff, S. S., Hu, W. W., Toohey, D. W., Flynn, J. H., Lefer, B. L., Grossberg, N., Alvarez, S., Rappenglück, B., Taylor, J. W., Allan, J. D., Holloway, J. S., Gilman, J. B., Kuster, W. C., de Gouw, J. A., Massoli, P., Zhang, X., Liu, J., Weber, R. J., Corrigan, A. L., Russell, L. M., Isaacman, G., Worton, D. R., Kreisberg, N. M., Goldstein, A. H., Thalman, R., Waxman, E. M., Volkamer, R., Lin, Y. H., Surratt, J. D., Kleindienst, T. E., Offenberg, J. H., Dusanter, S., Griffith, S., Stevens, P. S., Brioude, J., Angevine, W. M., and Jimenez, J. L.: Organic aerosol composition and sources in Pasadena, California, during the 2010 CalNex campaign, J. Geophys. Res. Atmos., 118, 9233-9257, 2013.

Hu, W. W., Hu, M., Yuan, B., Jimenez, J. L., Tang, Q., Peng, J. F., Hu, W., Shao, M., Wang, M., Zeng, L. M., Wu, Y. S., Gong, Z. H., Huang, X. F., and He, L. Y.: Insights on organic aerosol aging and the influence of coal combustion at a regional receptor site of central eastern China, Atmos. Chem. Phys., 13, 10095-10112, doi:10.5194/acp-13-10095-2013, 2013.

Hu, W. W., Hu, M., Hu, W., Jimenez, J. L., Yuan, B., Chen, W., Wang, M., Wu, Y., Chen, C., Wang, Z., Peng, J., Yang, K., Zeng, L., and Shao, M.: Chemical composition, sources and aging process of sub-micron aerosols in Beijing: contrast between summer and winter, J. Geophys. Res.-Atmos., 121, 1955–1977, doi:10.1002/2015JD024020, 2016.

Huang, X. F., He, L. Y., Hu, M., Canagaratna, M. R., Sun, Y., Zhang, Q., Zhu, T., Xue, L., Zeng, L. W., Liu, X. G., Zhang, Y. H., Jayne, J. T., Ng, N. L., and Worsnop, D. R.: Highly time-resolved chemical characterization of atmospheric submicron particles during 2008 Beijing Olympic Games using an Aerodyne High-Resolution Aerosol Mass Spectrometer, Atmos. Chem. Phys., 10, 8933-8945, 2010.

Jiang, Q., Sun, Y., Wang, Z., Yin, Y.: Real-time online measurements of the inorganic and organic composition of haze fine particles with an Aerosol Chemical Speciation Monitor (ACSM). Chin. Sci. Bull., 58, 3818-3828, 2013.

Kulmala, M., Petäjä, T., Kerminen, V.-M., Kujansuu, J., Ruuskanen, T., Ding, A., Nie, W., Hu,

M., Wang, Z., Wu, Z., Wang, L., and Worsnop, D. R.: On secondary new particle formation in China, Front. Environ. Sci. Eng., 10, doi:10.1007/s11783-016-0850-1, 2016.

Lan, Z., Huang X., He, L., Hu, M., Xue, L., Sun, T., Hu, W., Lin, Y., Zhang Y. Comparison of measurement results of several online carbonaceous aerosol monitoring techniques. Acta Scientiarum Naturalium Universitatis Pekinensis, 47, 159-165, 2011.

Levin, E. J. T., McMeeking, G. R., Carrico, C. M., Mack, L. E., Kreidenweis, S. M., Wold, C. E., Moosmüller, H., Arnott, W. P., Hao, W. M., Collett, J. L., and Malm, W. C.: Biomass burning smoke aerosol properties measured during Fire Laboratory at Missoula Experiments (FLAME), J. Geophys. Res. Atmos., 115, doi: 10.1029/2009jd013601, 2010.

Lewis, K. A., Arnott, W. P., Moosmuller, H., Chakrabarty, R. K., Carrico, C. M., Kreidenweis, S. M., Day, D. E., Malm, W. C., Laskin, A., Jimenez, J. L., Ulbrich, I. M., Huffman, J. A., Onasch, T. B., Trimborn, A., Liu, L., and Mishchenko, M. I.: Reduction in biomass burning aerosol light absorption upon humidification: roles of inorganically-induced hygroscopicity, particle collapse, and photoacoustic heat and mass transfer, Atmos. Chem. Phys., 9, 8949-8966, 2009.

Li, J., Pósfai, M., Hobbs, P. V., and Buseck, P. R.: Individual aerosol particles from biomass burning in southern Africa: 2, Compositions and aging of inorganic particles, J. Geophys. Res. Atmos., 108, D13, 8484, 2003.

Liu, Q., Sun, Y., Hu, B., Liu, Z., Akio, S., and Wang, Y.: In situ measurement of PM1 organic aerosol in Beijing winter using a high-resolution aerosol mass spectrometer, Chin. Sci. Bull., 57, 819-826, 2011.

McNallan, M. J., Yurek, G. J., and Elliott, J. F.: The formation of inorganic particulates by homogeneous nucleation in gases produced by the combustion of coal, Combustion and Flame, 42, 45-60, doi:10.1016/0010-2180(81)90141-3, 1981.

Middlebrook, A. M., Bahreini, R., Jimenez, J. L., and Canagaratna, M. R.: Evaluation of Composition-Dependent Collection Efficiencies for the Aerodyne Aerosol Mass Spectrometer using Field Data, Aerosol Sci. Technol., 46, 258-271, doi:10.1080/02786826.2011.620041, 2012.

Sun, J., Zhang, Q., Canagaratna, M. R., Zhang, Y., Ng, N. L., Sun, Y., Jayne, J. T., Zhang, X., Zhang, X., and Worsnop, D. R.: Highly time- and size-resolved characterization of submicron aerosol particles in Beijing using an Aerodyne Aerosol Mass Spectrometer, Atmos. Environ., 44, 131-140, 2010.

Sun, Y., Wang, Z., Dong, H., Yang, T., Li, J., Pan, X., Chen, P., and Jayne, J. T.: Characterization of summer organic and inorganic aerosols in Beijing, China with an Aerosol Chemical Speciation Monitor, Atmos. Environ., 51, 250-259, 2012.

Sun, Y., Jiang, Q., Wang, Z., Fu, P., Li, J., Yang, T., and Yin, Y.: Investigation of the sources and evolution processes of severe haze pollution in Beijing in January 2013, J. Geophys. Res. Atmos., 119, 4380-4398, 2014.

Sun, Y. L., Wang, Z. F., Fu, P. Q., Yang, T., Jiang, Q., Dong, H. B., Li, J., and Jia, J. J.: Aerosol composition, sources and processes during wintertime in Beijing, China, Atmos. Chem. Phys., 13, 4577-4592, 2013.

Sun, Y. L., Zhang, Q., Schwab, J. J., Demerjian, K. L., Chen, W. N., Bae, M. S., Hung, H. M., Hogrefe, O., Frank, B., Rattigan, O. V., and Lin, Y. C.: Characterization of the sources and processes of organic and inorganic aerosols in New York city with a high-resolution time-

of-flight aerosol mass apectrometer, Atmos. Chem. Phys., 11, 1581-1602, 10.5194/acp-11-1581-2011, 2011.

Xu, W., Han, T., Du, W., Wang, Q., Chen, C., Zhao, J., Zhang, Y., Li, J., Fu, P., Wang, Z., Worsnop, D. R., and Sun, Y.: Effects of Aqueous-Phase and Photochemical Processing on Secondary Organic Aerosol Formation and Evolution in Beijing, China, Environ. Sci. Technol., 51, 762-770, doi:10.1021/acs.est.6b04498, 2017.

Yokelson, R. J., Crounse, J. D., DeCarlo, P. F., Karl, T., Urbanski, S., Atlas, E., Campos, T., Shinozuka, Y., Kapustin, V., Clarke, A. D., Weinheimer, A., Knapp, D. J., Montzka, D. D., Holloway, J., Weibring, P., Flocke, F., Zheng, W., Toohey, D., Wennberg, P. O., Wiedinmyer, C., Mauldin, L., Fried, A., Richter, D., Walega, J., Jimenez, J. L., Adachi, K., Buseck, P. R., Hall, S. R., and Shetter, R.: Emissions from biomass burning in the Yucatan, Atmos. Chem. Phys., 9, 5785-5812, 2009.

Zhang, J. K., Sun, Y., Liu, Z. R., Ji, D. S., Hu, B., Liu, Q., and Wang, Y. S.: Characterization of submicron aerosols during a month of serious pollution in Beijing, 2013, Atmos. Chem. Phys., 14, 2887-2903, 2014.

Zhang, Q., Jimenez, J. L., Canagaratna, M. R., Allan, J. D., Coe, H., Ulbrich, I., Alfarra, M. R., Takami, A., Middlebrook, A. M., Sun, Y. L., Dzepina, K., Dunlea, E., Docherty, K., DeCarlo, P. F., Salcedo, D., Onasch, T., Jayne, J. T., Miyoshi, T., Shimono, A., Hatakeyama, S., Takegawa, N., Kondo, Y., Schneider, J., Drewnick, F., Borrmann, S., Weimer, S., Demerjian, K., Williams, P., Bower, K., Bahreini, R., Cottrell, L., Griffin, R. J., Rautiainen, J., Sun, J. Y., Zhang, Y. M., and Worsnop, D. R.: Ubiquity and dominance of oxygenated species in organic aerosols in anthropogenically-influenced Northern Hemisphere midlatitudes, Geophys. Res. Lett., 34, 2007.

Zhang, Y., Sun, J., Zhang, X., Shen, X., Wang, T., and Qin, M.: Seasonal characterization of components and size distributions for submicron aerosols in Beijing, Sci. China Earth Sci., 56, 890-900, 2013.

Bae, M.-S., Demerjian, K. L., and Schwab, J. J.: Seasonal estimation of organic mass to organic carbon in PM2.5 at rural and urban locations in New York state, Atmos. Environ., 40, 7467–7479, 2006.

Grover, B. D., Eatough, N. L., Woolwine, W. R., Cannon, J. P., Eatough, D. J., and Long, R. W.: Semi-continuous mass closure of the major components of fine particulate matter in Riverside, CA, Atmos. Environ., 42, 250-260, 2008.

Hu, W. W., Hu, M., Yuan, B., Jimenez, J. L., Tang, Q., Peng, J. F., Hu, W., Shao, M., Wang, M., Zeng, L. M., Wu, Y. S., Gong, Z. H., Huang, X. F., and He, L. Y.: Insights on organic aerosol aging and the influence of coal combustion at a regional receptor site of central eastern China, Atmos. Chem. Phys., 13, 10095-10112, 10.5194/acp-13-10095-2013, 2013.

Lan, Z., Huang X., He, L., Hu, M., Xue, L., Sun, T., Hu, W., Lin, Y., Zhang Y. Comparison of measurement results of several online carbonaceous aerosol monitoring techniques. Acta Scientiarum Naturalium Universitatis Pekinensis, 47, 159-165, 2011.

Sun, Y. L., Zhang, Q., Schwab, J. J., Demerjian, K. L., Chen, W. N., Bae, M. S., Hung, H. M., Hogrefe, O., Frank, B., Rattigan, O. V., and Lin, Y. C.: Characterization of the sources and processes of organic and inorganic aerosols in New York city with a high-resolution time-of-flight aerosol mass apectrometer, Atmos. Chem. Phys., 11, 1581-1602, 10.5194/acp-11-1581-2011, 2011.

Weimer, S., Drewnick, F., Hogrefe, O., Schwab, J. J., Rhoads, K., Orsini, D., Canagaratna, M., Worsnop, D. R., and Demerjian, K. L.: Size-selective nonrefractory ambient aerosol measurements during the Particulate Matter Technology Assessment and Characterization Study–New York 2004 Winter Intensive in New York City, J. Geophys. Res., 111, D18305, doi:10.1029/2006JD007215, 2006.